ACTA UNIVERSITATIS SZEGEDIENSIS

ACTA MINERALOGICA-PETROGRAPHICA

Tomus XXXIX.

SZEGED, HUNGARIA
1998

NOTE TO CONTRIBUTORS

General

The Acta Mineralogica–Petrographica publishes original studies on the field of geochemistry mineralogy and petrology, first of all studies Hungarian researches, papers resulted in by cooperation of Hungarian researches and those of other countries and, in a limited volume, papers from abroad on topics of global interest.

Manuscripts should be written in English and submitted to the Editor-in-chief, Institute of Mineralogy, Geochemistry and Petrography, Attila József University, H–6701 Szeged, Pf. 651 Hungary.

The authors are responsible for the accuracy of their data, references and quotations from other sources.

Manuscript

Manuscript should be typewritten with double spacing, 25 lines on a page and space for 50 letter in a line. Each new paragraph should begin with an indented line. Underline only words that should be typed in italics.

Manuscript should be generally be organized in the following order:

Title
Name(s) of author(s) and their affiliations, in foot-note the address of the author to whom the correspondence should be sent
Abstract
Introduction
Methods, techniques, material studied, description of the area investigated, etc.
Results
Discussion or conclusions
Acknowledgement
Explanation of plates (if any)
Tables
Captions of figures (drawings, photomicrographs, etc.)

Abstract

The abstract cannot be longer than 500 words.

Tables

The tables should be typewritten on separate sheets and numbered according to their sequence in the text, which refers to all tables.

The title of the table as well as the column headings must be brief, but sufficiently explanatory.

The tables generally should not exceed the type-area of the journal, i.e. 12,5x18,5 cm. Foldouts can only exceptionally be accepted.

(continuation on the inner side of verso)

ACTA UNIVERSITATIS SZEGEDIENSIS

ACTA MINERALOGICA-PETROGRAPHICA

Tomus XXXIX.

SZEGED, HUNGARIA
1998

HU ISSN 0365–8006
HU ISSN 0324–6523

SERIES NOSTRA AB ISNSTITUTIS MINERALOGICIS, GEOCHEMICIS PETROGRAPHICS UNIVERSITATUM HUNGARICUM ADIUVATUR

Institut Mineralogicum, Geochemicum et Petrographicum
Universitatis Szegediensis de Attila József nominatae

Nota

Acta Miner. Petr., Szeged

Kiadja

a József Attila Tudományegyetem Ásványtani, Geokémiai és Kőzettani Tanszéke
H-6722 Szeged, Egyetem u. 2–6.

Kiadványunk címének rövidítése
Acta Miner. Petr., Szeged

SOROZATUNK A MAGYARORSZÁGI EGYETEMEK ROKON TANSZÉKEINEK TÁMOGATÁSÁVAL JELENIK MEG

Printed in JUHÁSZ NYOMDA, Szeged

CONTENTS

Acta Mineralogica-Petrographica, Szeged, XXXIX, 5–12, 1998

NA-SANIDINE MEGACRYSTS FROM THE SHAVARIN CARAM VOLCANO, MONGOLIA

J. ULRYCH, E. PIVEC, P. POVONDRA*, G. BUDA**

* Geological Institute, Academy of Sciences of the Czech Republic
** Department of Mineralogy, Eötvös University

ABSTRACT

Na-sanidine crystals, their fragments and corroded relicts occur in scoria of leucite trachyte from the Shavarin Caram volcano, NW Mongolia. Opalescent perfect crystals of gem quality (up to 40 mm size) of moderate Or contents (46-49) reveal the following unit cell parameters: $a = 0.8334(9)$nm, $b = 1.2997(6)$, $c = 0.7159(6)$, $\beta = 116.17^\circ(5)$, $V = 0.6949(15)$ nm^3. Na-sanidine together with garnet (Pyr-Alm), Al-clinopyroxene, Ti-phlogopite megacrysts represent a very strange, mostly high-pressure near-liquidus phenocryst association of high-potassic magma. Na-sanidine megacrysts, however, would crystallize probably from a Fe and fluid rich melt at lower pressure in near-solidus regions.

INTRODUCTION

The Shavarin-Caram volcano (2,450 m a.s.l.) occurs in the Khangai Mts. 650 km, W of the capital of Ulan Bator, 17 km SE of the district centre of Tariat Somon on 48°00' N and 99°59' E. Crystalline basement and Paleozoic volcano-sedimentary sequences are frequently pierced by Plio-Pleistocene sills, dykes, plugs, pipes and rare volcanoes. Earlier differentiates are represented by subalkaline olivine basalts and hawaiites, the younger ones belong to an alkali basalt suite (leucite tephrite to melanephelinite). The Cenozoic volcanism is associated with the deep-seated Tariat Fault limiting the Tariat depression (rift?) active since the Early Paleozoic in the Khangai volcanic area. The Shavarin-Caram volcano lies in the intermonate valley with exposed Devonian quartzites just near the volcano (ULRYCH and ŠEVČIK 1986).

Products of the Shavarin-Caram volcano (volcanic bombs, lapilli sand, ash, as well as welded eruptive breccia and scoria) have unusual compositions. Most of them are of leucite trachyte to leucite basanite, and only rarely of melanephelinite composition (KEPEZHINSKAS 1979). The common accessories are represented by monazite, zircon and rare moissanite. According to the chemical classification of LE MAITRE ed. (1989) they, however, plot mostly into the field of phonotephrite (cf. the analysis of parental rock of the sanidine in Table 1). The rock corresponds to leucite tephrite and has clastic-porphyritic texture, with matrix enriched in K-rich glass and microlites of olivine, clinopyroxene and plagioclase.

* CZ-165 02 Prague 6, Rozvojová 135, Czech Republic
** H-1088 Budapest, Múzeum krt. 4/A, Hungary

ANALYTICAL METHODS

Wet chemical analyses of all reported minerals were made by the routine procedures used in the laboratory of the Department of Geochemistry, Mineralogy and Mineral Resources, Charles University. Rock forming minerals were analysed in polished sections using a JEOL JXA 50A electron microprobe, equipped with EDAX 711 (Geological Institute, Academy of Sciences of the Czech Republic), operating at 15 kV, beam currents of 30 nA, a beam diameter of 2μm and a counting time of 30s. Used standards are natural minerals (jadeite, diopside, leucite, apatite, barite) and synthetic phases.

Sanidine phenocryst was extracted manually in the form of single crystal from the host rock. Crystal was crushed to pass a 120 mesh sieve and powdered. The X-ray procedure (Dron 3 diffractometer at 40 kV, 20 mA using CuK_α filtered radiation) is esentially the same as that of WRIGHT and STEWART (1968). The sample was rotated during the step counting (0.5°/min). Cell parameters were computed using modified version of the program of BURNHAM (1962). Final cell parameters were computed from 18 peaks, the indices of which were carefully checked and found to match those recommended by WRIGHT and STEWART (1.c.)

The IR investigation was made by using the SPECORD IR 75 instrument and the powdered feldspar sample mixed with KBr was pressed into tablets. The obtained infrared absorption spectra were studied in the 6.25–32.25 μm region. Absorption bands 16.50–16.66 μm and 18.18–20.00 μm, recommended by HAFNER and LAVES (1957) and KUZNETSOVA (1971) as important for the study of ordering of Si and Al in the structure of the crystal lattice, were used. The obtained data are shown in a modified diagram (*Fig. 2*, SMITH 1974). Sanidines of liparites and trachyliparites from Central Caucasus (KUZNETSOVA, 1971) are also plotted for comparison.

XENOLITHS AND PHENOCRYSTS OF ERUPTIVE BRECCIA

Homogenous dunite to spinel lherzolite mantle xenoliths attaining the size up to several tens of cm are homogenously disseminated in the Shavarin-Caram eruptiva breccia, together with individual mineral components originated by their disintegration (IONOV and BORISOVSKII 1987). Xenoliths reveal following modal composition: olivine Fo_{91} (80–100 vol.%), enstatite (0–15%), Cr-diopside (0–5%), Cr, Al-spinel (0–2%). KEPEZHINSKAS (1979) mentioned more rare xenoliths of garnet lherzolite, garnet harzburgite, garnet websterite, clinopyroxenite, eclogite and granulite.

High-magnesium (Fo_{90-91}) isometrical olivine grains (5–8 mm) originate from disintegrated peridotitic xenoliths, cf. analyses in Table 1. However, low magnesium (Fo_{79-82}) magmatically corroded subhedral phenocrysts of olivine (1–15 mm) occur genetically associated with early crystallization phases of the parental rock, see Table 2.

Garnet (Pyr-Alm), Al-clinopyroxene, Ti-phlogopite (and Na-sanidine) megacrysts from Shavarin-Caram represent a very strange, mostly high-pressure near-liquidus phenocrysts association of high-potassic magma. Na-sanidine megacrysts, however, would crystallize probably from a Fe and fluid rich melt at lower pressure in near-solidus regions (cf. KAPEZHINSKAS 1979).

Garnets of a pyrope-(almandine) composition (see Table 1 and 2), cf. ULRYCH and ŠEVČIK (1986), sometimes in a monomineral garnetolite aggregates (mostly 5–20 mm, up to 10 cm in size) belong to the best known megacrysts (5–50 mm) of the site. The garnets

Wet chemical analyses of parental rock and megacrysts from Shavarin-Caram volcano (wt. %)

	Rock	Ol	Gar	Cpx	Fsp
SiO_2	48.09	40.09	40.82	48.6	65.46
Al_2O_3	15.68	0.31	17.82	9.5	19.63
TiO_2	1.11	–	1.48	1.95	–
Cr_2O_3	–	0.24	–	–	–
Fe_2O_3	1.64	0.52	6.02	2.95	0.05
FeO	7.36	8.76	12.77	5.69	–
MnO	0.16	0.12	0.41	0.15	tr.
MgO	6.98	48.55	14.72	12.57	0.5
NiO	–	0.39	–	–	–
Na_2O	5.39	0.03	0.05	2.47	5.81
K_2O	4.17	0.05	0.48	0.12	7.69
Li_2O	–	–	–	–	0.004
CaO	6.61	0.02	5.12	16.53	0.8
BaO	n.d.		n.d.	n.d.	0.18
P_2O_5	1.23	–	–	–	–
H_2O^+	1.05	–	–	–	–
Total	99.47	99.08	99.69	100.53	100.124
Recalculated to		8 (O)	24 (O)	6 (O)	32 (O)
Si		1.986	6.088	1.777	11.776
Al^{IV}		0.014	–	0.223	4.160
Al^{VI}		0.005	3.133	0.438	–
Ti		–	0.166	0.054	–
Cr		0.010	–	–	–
Fe^{3+}		0.019	0.674	0.081	0.010
Fe^{2+}		0.363	1.597	0.174	–
Mn		0.006	0.052	0.005	–
Mg		3.578	3.270	0.658	0.134
Ni		0.016	–	–	–
Na		0.002	0.144	0.175	2.025
K		0.002	0.096	0.005	1.764
Ca		0.002	0.188	0.648	0.155
Ba		–	–	–	–
X		2.000	6.088	2.000	15.936
Y		4.001	9.950	2.014	4.091
		Fo 90.4	Pyr 52.2	Wo 41.9	Or 51.2
		Fa 9.6	Alm 33.9	En 43.3	Ab 44.9
			And 4.3	Fs 14.8	An 3.9
			Grs 8.8		
			Sps 0.8		

Rock – parental phonotephrite
Gar – garnet
Cpx – clinopyroxene
Ol – olivine
Fsp – Na-sanidine
n.d. – not determined

Na-SANIDINE

The most interesting phenocrysts of the Shavarin Caram volcano are represented by alkali feldspar. They form colourless to whitish (i) perfect tabular crystals (up to 40 mm) of gem quality with opalescence found in cavities of scoriaceous facies of the tephritic rock, (ii) mechanical fragments of the above mentioned crystals, and (iii) magmatically corroded crystals (up to 20 mm) with narrow clinopyroxene reaction rims in more homogenous facies of the parental rock. We had only the first type (i) at disposal in a satisfactory amount. The chemical composition of the megacrysts (see Table 1 and 2) reveal their pertinence to Na-sanidine (Or_{46-49}) in the sense of SMITH (1974) with midly increased Na contents. KEPEZHINSKAS and ANTIPIN (1975) data on sanidine (Or_{71}) from the same locality pointed to the substantial variation in megacrysts chemical composition. KEPEZHINSKAS (1979) presented very broad array of Or contents (22–71) from the potassic alkaline province of the Tariat depression. SALTYKOVSKII and GENSHAFT (1985) report megacrysts of Na-rich alkali feldspars with low Or contents (4–56) from Cenozoic basalts of the Dariganga plateau in SE Mongolia. Nevertheless, the Dolina Ozer volcanic area in western Mongolia characterized by the limited range of composition of sanidine autolits (Or_{71-76}). A similar chemical composition was reported from megacrysts of alkali feldspars of volcanites of New Mexico (An_{22-32}) by HOFFER & HOFFER (1973), New South Wales (Or_{12-18}) by BINNS et al. (1970) and Victoria (Or_{18-33}) by IRVING (1974), cf. in *Fig. 1.*

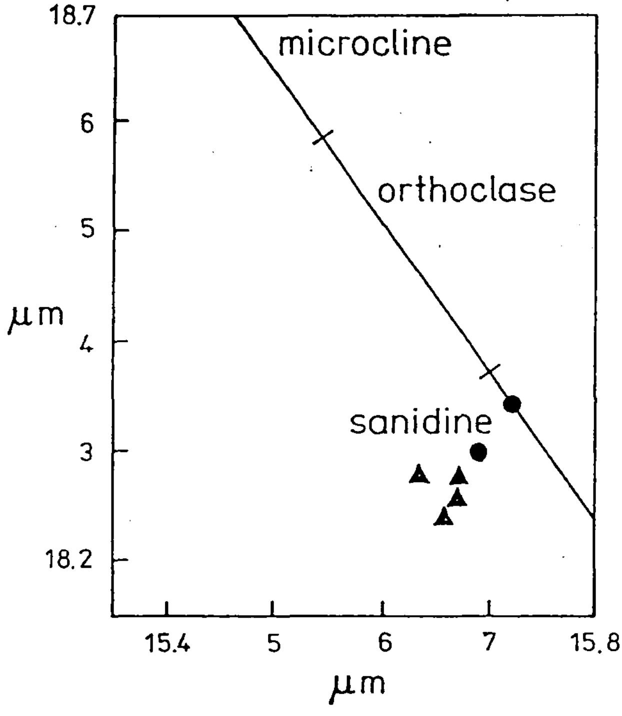

Fig. 2. Relation between two chosen absoption wave length for the studied alkali feldspars in diagram modified after SMITH (1974a). Studied feldspars (full circles), sanidines from liparites and trachyliparites (full triangles), Central Caucasus (KUZNETSOVA, 1971) for comparison.

The BaO contents (0.3–0.6 wt.%) show homogenous distribution of Ba in the Na-sanidine megacrysts. SMITH (1974a) reports Ba contents in phenocrysts of volcanic rocks in K-feldspars up to 10,000 ppm.

Then Na-sanidine has the following unit cell data: a = 0.8334(9) nm, b = 1.2997(6), c = 0.7159(6), β = 116.17°(5), V = 0.6949(15) nm^3. The results of X-ray investigations reveal the following characteristics: (i) high albite-sanidine structural state, (ii) presence of normal unit-cell parameters, and (iii) 42 mol. % of Or component by equation of WRIGHT and STEWART (1968); 44.0 % Or component follows from the average of chemical analyses (Table 2).

The obtained IR data correspond to sanidine (*Fig. 2.*). The 2Vx optical angle is substantially low and fluctuate in array of 25–30°, which is characteristic for the series sanidine – anorthoclase (DEER et al. 1963).

DISCUSSION

BAHAT (1979) has suggested that feldspars megacryst commonly appearing with rounded or subrounded partially rounded shapes show no recognizable crystal forms. On the other hand feldspars that crystallize from host melts in plutonic pegmatites under equilibrium conditions, or terminate the magmatic differentiation in sölvsbergites under shallow conditions are often euhedral. According to BAHAT (1979) there are two possible interpretations of the rounded morphology: either the relative growth rate of the planes involved did not remain constant, or these crystals suffered from chemical solution or mechanical attrition prior to eruption under low water pressure and at shallow depth.

The assignment and genesis of Na-sanidine in alkaline volcanic rocks remains to be limited owing to the lack of high-pressure experiments concerning triclinic feldspars and sanidines. However, the stability of sanidine in high-pressure conditions in coesite-sanidine grospydite from kimberlite was confirmed by SMYTH and HATTON (1977). Deep crustal fractionation of high-pressure Al-rich augite–pyrope–Ti-rich phlogopite–Na-sanidine megacrysts association in the parental high-magnesium K-rich basaltic magma, ascertained in the Shavarin-Caram volcano, lead to a specific differentiation trend in the whole Khangai potassic volcanic province. Together with the results of BAHAT (1979), STOSH et al. (1986) and PRESS et al. (1986) our results may serve an argument in the debate on asthenospheric vs. continental lithospheric potassic magma generation and on heterogeneity of upper mantle regions, respectively.

ACKNOWLEDGEMENT

Authors are indebted to J. ŠEVČIK, Geoindustria Prague for providing rare materials from the Shavarin Caram Volcano.

REFERENCES

BAHAT, B. (1979): Anorthoclase megacrysts: physical conditions of formation. – Miner. Mag., 43, 287–294.

BARTH, T. F. W. (1969): Feldspars. Wiley-Interscience 261 pp. New York–London–Toronto–Sydney.

BINNS, R. A., DUGGEN, M. B. and WILKINSON, J. F. G. (1970): High pressure megacrysts in alkaline lavas from northeastern New South Wales. – Amer. J. Sci., 269, 132–168.

BURNHAM, Ch. W. (1962): Lattice constant refinement. – Carnegie Inst. Washington, Year Book, 61, 132–135.
DEER, W. A., HOWIE, R. A. and ZUSSMANN, J. (1963): Rock-forming minerals, vol. 4. Framework silicates. – Longmans 481 pp, London.
HAFNER, S. and LAVES, F. (1957): Ordnung / Unordnung und Ultrarotabsorption II. Variation der Lage und Intensität einiger Absorptionen von Feldspäten. Zur Struktur von Orthoklas und Adular. – Z. Kristallogr., 109, 204–225. Frankfurt a. M.
HOFFER, J. M. and HOFFER, R. Z. (1973): Compositional and structural state of feldspar inclusions from alkali olivine basalt, Potrillo basalt, Southern New Mexico. – Bull. Geol. Soc. Amer., 84, 2139–2142.
IONOV, D. A. and BORISOVSKII, S. E. (1987): Complex xenoliths of the Shavarin-Caram volcano in Mongolia. – Study of high-pressure minerals, 94–107. Acad Sci. USSR, Institute of Physics of the Earth, Moscow (in Russian).
IRVING, A. J. (1974): Megacrysts from the Newer basalt and other basaltic rocks of Southeastern Australia. – Bull. Geol. Soc. Amer., 85, 1503–1514.
JAKEŠ, P. and KLOMÍNSKÝ, J. (1979): Garnet peridotite inclusions from Bulgan-Mongolia. – Čas. Mineral. Geol., 24, 1–8.
KEPEZHINSKAS, V. V. (1979): Cenozoic alkaline basaltoids of Mongolia and related deep inclusions. The Joint Soviet-Mongolian Scientific Research Geological Expedition, Transactions, Vol. 25. Nauka, Moscow (in Russian).
KEPEZHINSKAS, V. V. and ANTIPIN, V. S. (1975): Sanidine megacrysts of Cenozoic alkali basalt from Mongolia. – Geol. i geofiz., 2, 138–144. (in Russian).
KUZNETSOVA, L. G. (1971): The application of infra-red spectrometry in defining the degree in the order of K-Na feldspars. – Mineral. Sbor. 18–26. L'vov (in Russian).
LEMAITRE, R. W. ed. (1989): A classification of igenous rocks and glossary of terms. Blackwell Sci. Publ., Oxford.
MORIMOTO, N. ed. (1988): Nomenclature of pyroxenes. – Mineral. Mag., 52, 535–550.
PRESS, S., WITT, G. and SECK, H. A. (1986): Spinel peridotite xenoliths from the Tariat Depression, Mongolia I: Major element chemistry and mineralogy of a primitive mantle xenolith suite. – Geochim. Cosmochim. Acta, 50, 2587–2600.
SALTYKOVSKII, A. JA. and GENSHAFT JU. S. (1985): Cenozoic geodynamics of volcanism of the south-east Mongolia. The Joint Soviet-Mongolian Scientific Research Geological Expedition, Transactions, Vol. 42. Nauka, Moscow (in Russian).
SMITH, J. V. (1974): Feldspar minerals I. Crystal structure and physical properties. Springer Verlag 627 pp. Berlin–Heidelberg–New York.
SMITH, J. V. (1974a): Feldspar minerals II. Chemical and textural properties. Springer Verlag 690 pp. Berlin–Heidelberg–New York.
SMYTH, J. R. and HATTON, C. J. (1977): A coesite-grospydite from the Roberts Victor kimberlite. – Earth Planet. Sci. Lett., 34, 284–290.
SOBOLEV, N. V. and NIXON, P. H. (1987): Xenoliths from the USSR and Mongolia: a selective and brief review, 159–167. In P. H. Nixon: Mantle xenoliths. Wiley & Sons, Chichester etc.
STOSH, H. G., LUGMAIR, G. W. and KOVALENKO, V. I. (1986): Spinel peridotite xenoliths from the Tariat Depression, Mongolia II: Geochemistry and Nd and Sr isotopic composition and their implications for the evaluation of the sub-Continental lithosphere. – Geochim. Cosmochim. Acta., 50, 2601-2614.
ULRYCH, J. and ŠEVČIK, J. (1986): Garnet from the Shavarin-Caram deposit, Mongolia. – Geol. Zbor. Geologica Carpath., 37, 387–395.
WRIGHT, T. L. and STEWART, D. B. (1968): X-ray and optical study of alkali feldspar: I. Determination of composition and structural state from refined unit-cell parameters and 2V. – Amer. Mineralogist, 53, 38–87.

Manuscript received 10 June, 1998.

Acta Mineralogica-Petrographica, Szeged, XXXIX, 13–20, 1998

CHALCOSTIBITE: A NEW MINERAL FROM FELSŐBÁNYA (BAIA SPRIE, ROMANIA)

B. KÓBOR, E. PÁL MOLNÁR*

Department of Mineralogy, Geochemistry and Petrology, Attila József University

ABSTRACT

Crystals macroscopically reminding of chalcostibite were found in mineral group from Felsőbánya (Baia Sprie, Romania) in summer 1988. Studies performed in the Department of Mineralogy, Geochemistry and Petrology warranted this inference.

Number of sulphide minerals from Felsőbánya (Baia Sprie) increased to 40 by identification of chalcostibite.

INTRODUCTION

Felsőbánya (Baia Sprie) is perhaps the most varied mining area of the mine region near Nagybánya (Baia Mare) in the Gutin Mountains from a mineralogical point of view. Andorite, semseyite, felsőbanyite, dietrichite, klebelsbergite, monsmedite and szmikite were first described here.

Chalcostibite was known as a mineralogical rarity in the three other mining areas (Kapnikbánya - Cavnic, Herzsabánya - Herja, Erzsébetbánya - Baiuţ) of the Nagybánya (Baia Mare) mining region, although it was not proved in every case (Lapis, 7-8./1996).

During the last decade, mining activity removed from the 'Bányahegy' to the pit 5 located in 2-3 km from and ENE of there. Veins produced here have similar genetics to those of the Bányahegy, and many of them are their continuations. Mineral assemblages occurring in the veins in a certain depth are absolutely similar to each other in some cases. Locality of the 'new' chalcostibite occurrence is a druse in a 40-90 cm wide polymetallic vein produced at the level XI (cca. -580 m) of the pit 5.

MINERALOGICAL CHARACTERISATION OF CHALCOSTIBITE

Name of this mineral cames from the Greek χαλκοζ (copper) and σΥιβι (antimony) words.

Zinken was the first who mentioned $CuSbS_2$ as 'Kupferantimonglanz' (ZINKEN, 1835), however, it was called as chalcostibite as early as 1847 (GLOCKER, 1847). After its German locality, Nicol called it as wolfsbergite (NICOL, 1849), and Cumenge named it as guejarite after its occurrence in Spain (CUMENGE, 1879). It can be found as chalcostibite again in Dana's mineralogical system (1868), the most accepted system at that time.

* H-6701 Szeged, P.O.Box 651, Hungary

Chalcostibite is an ABX_2 (A:B ~ 1:1) type complex copper-antimony sulphide, a sulfosalt as it was called earlier, and it is the denominative member of the chalcostibite group (PALACHE, 1944).

It is often ranged among the 'copper-bismuth sulfosalts' ($xCu_2S+y(BiSb)_2S_2$ in the mineralogical literature (KOCH, SZTRÓKAY, 1994).

The new mineralogical systems (WEISS, HOCHLEITNER, 1994) mention it as a copper-containing and (S:As,Sb,Bi=x; x=2.0) type sulfosalt, member of the chalcostibite-hodrushite series. However, hodrushite as an independent mineral is not absolutely accepted.

Chalcostibite often contains lead and iron less than 1 %.

$CuSbS_2$ is a rhombic holohedral mineral. It crystalises in the form of long acicular or short rhombic prisms (Bolivia and Peru: Huanchaca, Oruro, Machacamarca, Almona, Bustillos, etc.). The classic European localities are Wolfsberg (Harz Mountains, Germany) and Guejara (Granada, Spain), where chisel- and blade-like tabular crystals // (010) with strongly fibrous prisms are characteristic (wolfsbergite and guejarite types).

Mean size of the chalcostibite crystals is 1-2 mm, but prismatic crystals of 6-9 cm also occur in some localities, e.g., Oruro and France (Le Régne Mineral, 5./1998). However, it can be found as disseminated or massive grainy mass in the most occurrences.

Hardness of chalcostibite is 3-4, its cleavage is perfect along (010), its fracture surface is uneven and has high lustre.

The chalcostibite crystals have metallic lustre, and they are lead-grey or dark blackish grey. They are fibrous parallel to the c-axis. Their surface is often plated by metallescent blue or bluish green cover.

The $CuSbS_2$ is a non-frequent mineral of the hydrothermal polymetallic Pb-Zn-Cu-Ag-Sb mineral deposits. In general, it is formed under epithermal conditions together with bournonite, andorite, antimonite, berthierite, stannite, chalcopyrite, pyrite, sphalerite, galena and quartz.

RESULTS

The chalcostibite from Felsőbánya is a crystal aggregate which macroscopically has high lustre, and lead-grey or dark grey colour. A steel-blue cover can often be observed on it.

In general, the crystals are 1-2 x 0.2-0.4 mm elongated tables or chisel-like crystals of 0.1-0.2 mm width; some of them are 0.5 cm long (*Fig. 1.*). Crystals of this type are similar to the crystals found in Guejara (Spain), the face (010) is much more developed, therefore, these crystals have a well-developed thin tabular or blade-like habit. On the basis of the German analogy, crystals from Felsőbánya have a wolfsbergite-type morphology (*Fig. 2.*).

There are long, elongated prismatic, almost acicular chalcostibite crystals of Felsőbánya, too.

It is characteristic for both types that crystals do not have too many faces, and even the ends of the crystals did not crystalise, and faces parallel to the c-axis can be distinguished. Moreover, strong fibrous structure can be observed on these faces (*Fig. 3.*).

Mineral paragenesis occurs together with chalcostibite is also interesting and remarkable.

Fig. 1. Chalcostibite from Felsőbánya (15x)

Fig. 2. Chalcostibite crystal from Felsőbánya (25x)

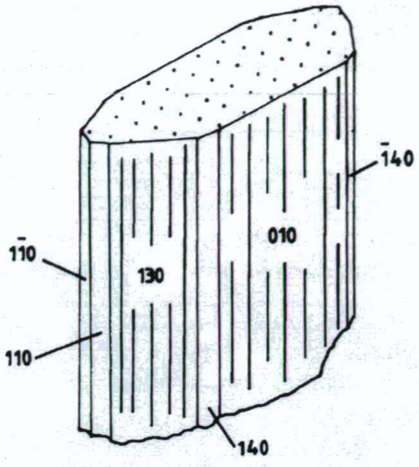

Fig. 3. Chalcostibite crystal from Felsőbánya

Fig. 4. Sheaf-like crystal group of chalcostibite on chalcopyrite (10x)

From an economic geological point of view, the ore deposit near Felsőbánya is a subvolcanic meso- and epithermal ore mineralisation that dominantly has the so-called Pulacayo-type Pb-Zn veins (SCHNEIDERHÖHN, 1962). The ore deposit is in connection with rhyolitic volcanism; it is quite uncommon in this mining area.

The ore veins were formed by pulsating phases thus they have striped-banded and often telescope structure. As depth increases as Au-Ag rich epithermal paragenesis is changed by mesothermal Cu-Zn-(Pb) mineralisation. Veins ramify in the 200 m zone near the surface.

The exact locality of chalcostibite is an exhausting but druse- and hole-rich end of a side vein at the level XI of the pit 5. The vein is dominantly of chalcopyrite and quartz in banded disposal, and subordinately of pyrite and sphalerite.

Amongst the minerals occurring on the wall of the druse of the vein pyrite and chalcopyrite represents the earliest phase. A metallescent, tobacco-coloured cover can be observed on the chalcopyrite crystals which often reach 2 cm. Further study is necessary to identify it.

Sheaf-like, or sometime acicular, aggregates of chalcostibite grew up on the chalcopyrite crystals (*Fig. 4.*).

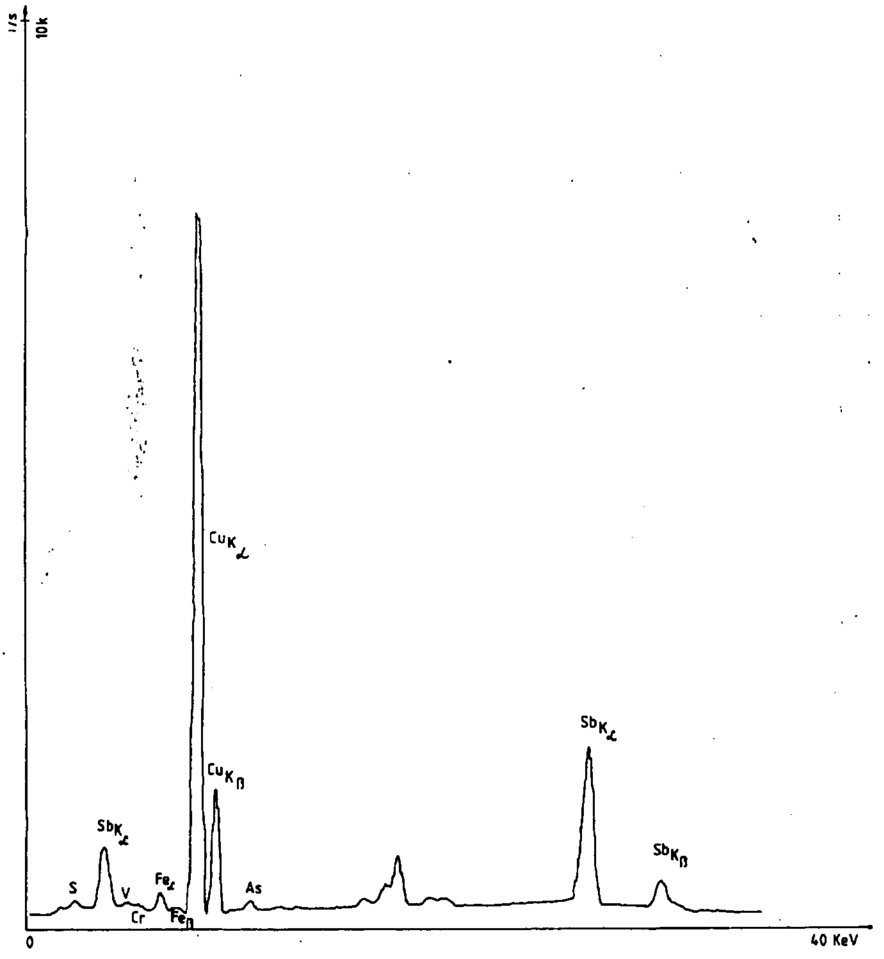

Fig. 5. XRF pattern of chalcostibite from Felsőbánya

The final phase is represented by dolomite perimorphs of calcite or dolomite rhombohedrons. The rhombohedrons and the discoidal crystal groups of rhombohedrons are spongy, and a cover of quartz crystals of smaller than 0.2 mm can be found on the lower and upper surface of the dolomite crust forming the rhombohedrons. The perimorphs and the larger quartz crystals might be formed at the same time because building of the carbonate perimorphs in the quartz crystals can also be observed almost everywhere.

The XRF study of the chalcostibite shows that beside Sb, Cu and S the studied sample contains some iron and arsenic, too. Unfortunately, chalcostibite crystals can not totally be separated from the associated minerals (mainly from the chalcopyrite), and this can also result in contaminating element content (*Fig. 5.*).

By XRD studies, our samples were compared with standard chalcostibite samples from Bolivia (9-143/ SMITH, J. V. ed., 1966) and from an unknown locality (200/ MICHEEV, V. I., 1957). Results also suggest presence of chalcopyrite contamination (Table 1).

TABLE 1

Result of XRD studies on chalcostibite samples

Standard 9-143 **Index of the powder diffraction file** **Editor: Smith, J.V.** **1966**	**Standard 200** **Micheev, V.I.:** **Rentgenometritseskij Opredelitel Mineralov** **Moszkva 1957**	**Sample from Felsőbánya (Baia Sprie)** **Attila József University** **Department of Mineralogy, Geochemistry and Petrology** **1998**
d(Å)	**d(Å)**	**d(Å)**
7.38	-	7.24165
4.67	-	4.62231
3.65	3.63	3.61931
3.13	-	3.13583
-	3.10	3.10374
3.00	2.98	3.00953
2.79	-	2.98744
2.56	2.54	2.94914
2.31	2.29	2.30493
2.24	2.23	2.24229
2.12	2.11	2.11910
1.895	1.888	1.89877
1.831	-	1.83050
1.817	1.818	1.81234
1.762	1.751	1.75704

REFERENCES

Annalen der Physik (1835): 35./1835 Halle, Leipzig.
BARNES, H. L.(1967): Geochemistry of hydrothermal ore deposits, by Holt.
Bulletin, Société mineralogique de France, 1879.
GLOCKER, T.(1847): Generum et specierummineralium secundum ordines naturales digestorum synopsis. Halle.
KOCH, S., SZTRÓKAY, K. I.(1994): Ásványtan II., 5.kiadás, 519.p. Budapest.
Lapis - Mineralienzeitschrift (6-8/1996), Weise-München, 1996.
Le Régne Mineral, 5./1998, Paris, 1998.
MICHEEV, V.I.(1957): Rentgenometrocheskij opredelitel mineralov, Moscow.
NICOL, J.(1849): Manual of Mineralogy, Edinburgh.
PALACHE, C., BERMAN, H., FRONDEL, C.(1944): Dana's System of Mineralogy. Harvard University, 7. ed.
RIBBE, P. H. (Editor) (1976): Sulfide Mineralogy, vol.1. in Reviews in Mineralogy.
RAHMDOHR, P.(1960): Die Erzmineralien und ihre Verwachsungen, Berlin.
SCHNEIDERHÖHN, H.(1941): Lehrbuch der Erzlagerstätten, Jena.
SCHNEIDERHÖHN, H.(1962): Erzlagerstätten, 4.Aufl., Fischer Verlag.
SMITH, J. V. (Editor) (1966): Index of the powder diffraction file.
WEISS, S., HOCHLEITNER, R.(1994): Das grosse Lapis-Mineralienverzeichnis, Weise-München.

Manuscript received 12 July, 1998.

Acta Mineralogica-Petrographica, Szeged, XXXIX, 21–34, 1998

MINERALOGICAL-PETROLOGICAL STUDY ON ORE VEIN PENETRATED BY THE KEY-BOREHOLE BAKSA NO. 2 SE TRANSDANUBIA, HUNGARY

T. TARNAI[1]

Department of Mineralogy, Geochemistry and Petrology
Attila József University, Szeged, Hungary

ABSTRACT

In 1995/96 complex study on ore minerals occurring in a 7 cm thick vein traversed in the drilling Baksa 2 at 186.4 m depth was made in the Department of Mineralogy, Geochemistry and Petrology of the Attila József University (Szeged, Hungary) to determine their mineralogical and genetic features. In this paper, results of ore microscopic study and those of the inclusion analyses are published.

The ore vein is massive sulphide one (almost its 60 % is composed by sulphide ore). Two phases can be distinguished in the vein by both ore microscopy and inclusion analysis. The outer ore phase is quantitatively subordinate. Its mineral paragenesis: chalcopyrite, galena, sphalerite, pyrite (marcasite). The inner ore phase represents the main mass of the vein; its minerals: pyrite (marcasite), sphalerite, chalcopyrite, pyrrhotite. Pyrite (marcasite) and sphalerite are the quantitatively most dominant minerals. The dominant non-ore minerals are quartz and carbonate minerals.

Possibly, the vein was formed in closed system at low pressure in a temperature interval ranging from 250 to 310 C°. A two-phase formation can be supposed. It is most likely that fluids forming the ore vein are differentiates of a real magmatic melt. Identification of the regional connection is quite difficult, however, it can be brought into connection with either the Permian volcanism in the Villány Mountains or an unknown independent volcanic activity.

INTRODUCTION

Aim of the key borehole Baksa 2 deepened in 1978/79 was to reveal crystalline rocks of Baksa Complex. Hydrothermal ore indications were found in several places in the rock beds traversed in great thickness. The most important of them was the 7 cm thick massive sulphide ore vein traversed at a depth of 186.4 m (*Fig. 1*).

Preliminary studies of the ore minerals found in the key borehole Baksa 2 were performed by SZEDERKÉNYI T. (1979) and GRASSELLY GY. (1979) in the József Attila University in Szeged. A detailed ore economic geological study on the formation traversed by the borehole was accomplished in 1996 (TARNAI T., 1996).

In this paper, results of the ore microscopic and inclusion studies on the vein traversed at a depth of 186.4 m are published by data that have not been published yet. Since geological setting of the exposed formations and formations traversed by the borehole was reviewed in a previous paper (TARNAI T., 1997), only the direct neighbourhood and host rocks of the ore vein will be characterised in this publication.

[1]H-6701 Szeged, P.O.Box 651, Hungary

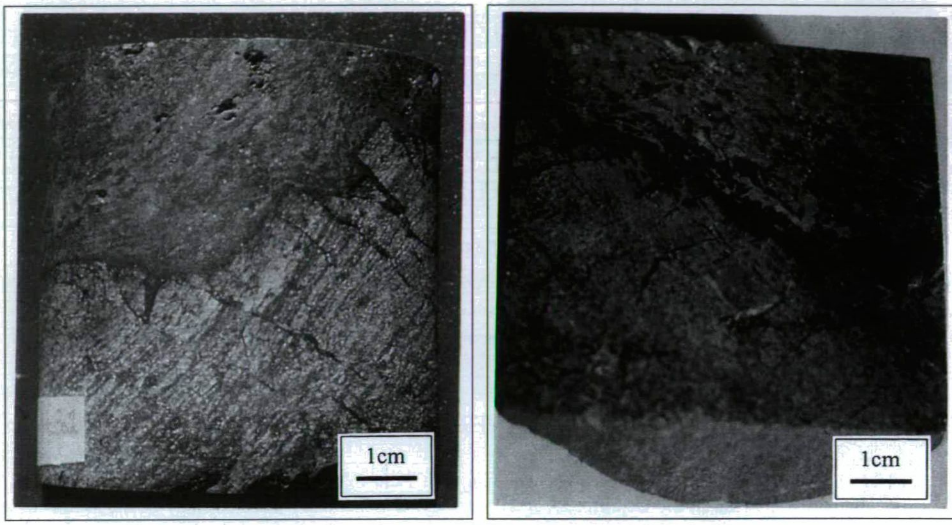

Fig. 1. Key borehole Baksa 2. Core sample of the ore vein traversed at 186.4 m depth (convex side and polished slab of the core)

CHARACTERISATION OF THE ORE VEIN FROM A DEPTH OF 186.4 M AND ITS ENCLOSING ROCK

The vein can be found in the Upper Márványos Member (57.1-223.7 m) and in the two-mica schist 'bed' occurring from 178.9 to 187.6 m. Its direct enclosing rock is chloritic gneiss (SZEDERKÉNYI T., 1979). Metamorphic schistosity of the enclosing rock can well be seen. Its polished sections excellently show that the intruded hydrothermal products well permeated and highly impregnated the enclosing rock along veinlets and apophyses. These veins have quite dark, almost totally black colour. In the host rock, glittering ore minerals, which crystalised along the thin veins, can be observed even 4 cm from the contact of the vein. Contact of the vein and the enclosed rock is sharp and outlined. The chloritic gneiss broke and cracked in a zone of some cm (*Fig. 2*).

The hydrothermal veins are 7 cm thick. In its neighbourhood, there are more smaller veins of some mm (or at most one cm) thick parallel to it. The ore vein is massive sulphide, non-ore minerals occasionally occur in it, only. Size and frequency of free spaces and gapes increase toward the centre. They are not filled by secondary material. Except of some rare crystals, the ore minerals are absolutely xenomorphic, and they are strongly interfingered. It can be seen that formation of the ores is striped, and their orientation is more or less parallel to running and sides of the vein. Bordering the vein and fitting to the side, a dark, almost black (similar to the veinlets in the enclosing rock), varying wide (1-4 mm) phase with the same orientation can be observed both in the polished and unpolished surface of the sample. It seems to be independent. Sulphides of the vein seem to be fresh, disregarding the superficial oxidation cover resulted by two decades storing in the open air. Pyrite can easily identified by eyes just as well as the glittering galena in the polished samples, however sphalerite can only be supposed. By single microscope, greenish golden yellow chalcopyrite and sphalerite (together with its inclusions) as disseminated grains can also be seen in the black zone fitting to the vein (*Fig. 1* and *2*).

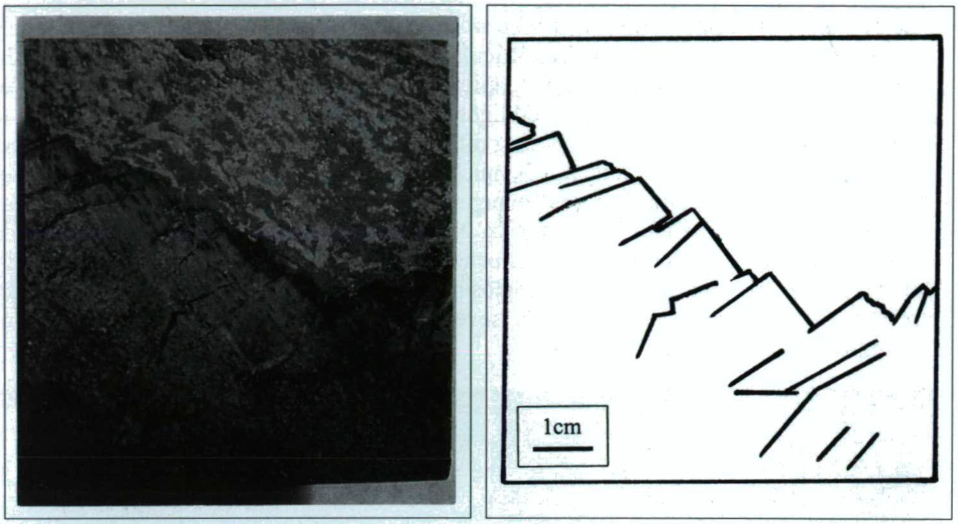

Fig. 2. Key borehole Baksa 2. Polished slab and main fracture lines of the core sample of the ore vein traversed at 186.4 m depth

ANALYSES

1. MICROSCOPIC STUDIES

A NIKON MICROPHOT-FXA polarizing microscope was used for the microscopic studies. Ore and non-ore minerals were identified in polished slabs and thin sections, respectively. Preparations for analyses were made by the usual way.

1.1. STUDIES IN REFLECTED LIGHT

The following minerals were identified in the course of study on the ore phase: pyrite, sphalerite, marcasite, pyrrhotite, chalcopyrite, galena. There was no other ore mineral that can be identified by a light microscope. Of the non-ore minerals, quartz can be determined on the basis of its idiomorphic shape, and presence of carbonate minerals can be supposed because of their high pseudoadsorption.

The ore veins are not homogeneous, there are two definitely separated parts having quite different ore mineral paragenesis. Hence, outer and inner (main) ore phases are distinguished. At the same time, however, there is no consistent difference between non-ore minerals occurring in the two phases. On the basis of the study on the polished slabs, therefore, it can not surely be determined wether two successive stages of the vein formation or a simple differentiated ore formation happened.

1.1.1. ANALYSIS OF THE OUTER ORE PHASE

Ore mineral paragenesis of the outer phase is the following: chalcopyrite, galena, sphalerite, pyrite (marcasite). Characteristic picture of the outer phase is shown by *Fig. 3.* As it has been mentioned in the macroscopic description, there is 1-4 mm wide black zone at the border of the vein and the enclosing rock, which is separated from the quantitatively more dominant main phase. It is more difficult to mark a border between the outer and the inner phase microscopically than macroscopically because the black colour visible by eyes can not been noticed. Studies in reflected light demonstrate the matrix of the two phases to be the same formation. It is an eye-striking difference, however, that, contrary to the inner ore phase, quantity of the ore minerals is much more subordinated comparing with that of the non-ore minerals, and the ore minerals occur as big independent crystals or disseminated grains or groups in the matrix. Non-ore material of the outer phase intruded into the cracks of the enclosing rock, and penetrated and impregnated it along apophyses. Although, sulphide content of the enclosing rock is generally more subordinated, somewhere – in some cases as far as several cm from the vein – ore minerals of considerable size were also crystalised.

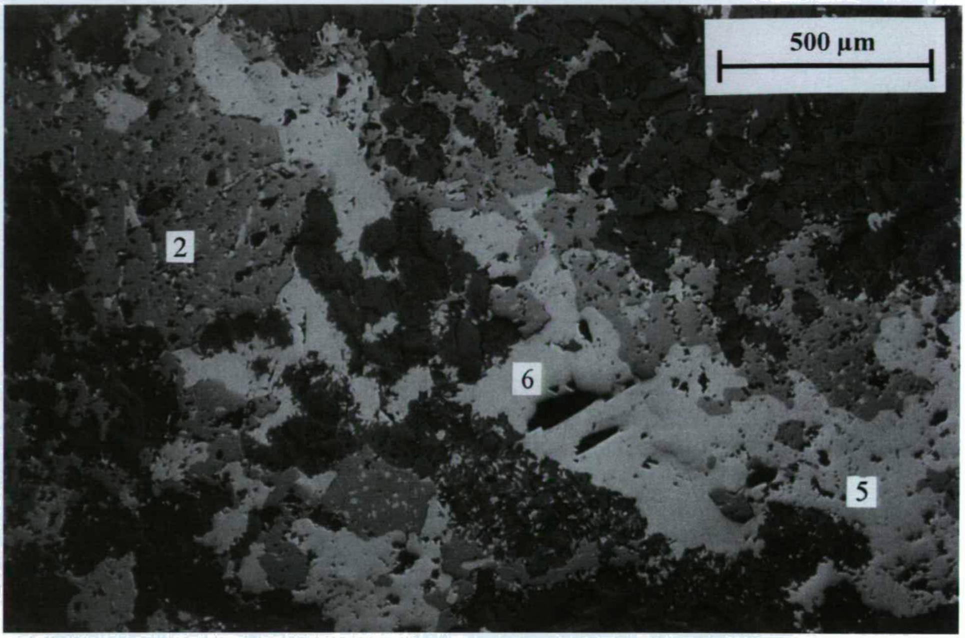

Fig. 3. Key borehole Baksa 2. Characteristic textural pattern of the outer ore phase of the ore vein traversed at 186.4 m depth. (Reflected light, 40x, 1 N). Legend: 2. sphalerite; 5. chalcopyrite; 6. galena

Chalcopyrite can be found as independent crystals in this phase, only; it occurs only as inclusions of sphalerite in the inner phase. It mainly appears as disseminated grains or bigger independent crystals. It is mainly accompanied by sphalerite, galena and pyrite. They can be intergrown, and can also occur as inclusions of each other. It frequently contains non-ore minerals, pores and gaps. Its quantity is quite small regarding the whole vein, however, it is significant in the outer ore phase; of the sulphide minerals it has the highest quantity in this phase. It is xenomorphic, its colour is the usual slightly greenish yellow. Size of its crystals is varying, therefore, it is not characteristic. The biggest crystal what I saw was 2.4 mm long.

As chalcopyrite, ***galena*** also occurs in the outer phase, only. It also has xenomorphic appearance, and, similar to chalcopyrite, it occurs as disseminated grains or bigger independent crystals. It is accompanied by minerals of the paragenesis in varied forms, and, similar to them, it has variable size. It can be found at the border of the inner main and the outer phases as well as along a veinlet in the enclosing rock 6 cm from the vein. The characteristic arrow-head-like 'cracklings' coming from cleavage can be observed very well. Length of the biggest studied crystal was almost 2 mm. Quantity of galena is also subordinated, it is half or two-thirds of that of chalcopyrite.

Galena was not mentioned by GRASSELLY GY. (in SZEDERKÉNYI T., 1979) in his ore optic study on the sample ÁGK-362. Galena occurs in the margins of the vein (i.e., in the outer phase), and it is probable that the sample studied by him was cut from the centre part of the vein where, as I mentioned, this mineral does not occur. It is characteristic, however, that galena is frequent in apophyses and veinlets intruding into the enclosing rock. For example, there is galena crystal of 1 mm intergrown with chalcopyrite 6cm from the ore vein in quartziferous groundmass.

Pyrite crystals in the outer phase are paler yellow, much smaller and more subordinated than in the inner phase. Studying them by two nicols, they also have paler colour. In some cases they are idiomorphic appearance (triangular and quadratic shape). On the basis of a cut, wideness of a face of a hexahedron was 0.25 mm. Pyrite occurs as independent crystals, inclusion in sphalerite and chalcopyrite, and intergrowing with sphalerite, chalcopyrite and galena. It size is variable, but it is smaller than the above mentioned three minerals. Its quantity is much lower than that of galena, sphalerite and chalcopyrite. The pyrite crystals are strongly marcasitized, fresh ones occur besides the idiomorphic crystals, only.

Sphalerite of the outer phase has similar features to that of the inner phase; therefore, it is characterised in details in that chapter. The difference between them is that size of crystals and inclusions found in them is smaller (size of inclusions in the outer phase 1 μm or hardly bigger). Moreover, sphalerite in the outer phase contains only chalcopyrite inclusions (but it does not contain pyrrhotite inclusions), and occurs as independent crystals or together with galena and chalcopyrite. The sharp differences between the two ore phases in the cases of the other three minerals (pyrite, chalcopyrite, galena) can not be observed for sphalerite. Feature of sphalerite crystal gradually changes from the border to the centre of the vein: size of its inclusions and quantity of its pyrrhotite inclusion increases.

1.1.2. ANALYSIS OF THE INNER ORE PHASE

Its ore mineral paragenesis is the following: pyrite (marcasite), sphalerite (with chalcopyrite and pyrrhotite inclusions), pyrrhotite. It is massive sulphide. It is mainly composed by pyrite, sphalerite and non-ore minerals. Pyrite has pyrrhotite inclusions, and it is marcasitized in several places. Sphalerite frequently has pyrrhotite and chalcopyrite inclusions. The characteristic formation of inner (main) ore phase is shown by *Fig. 4*.

Microscopic studies support the macroscopic description on its texture. Although, orientation parallel with the wall of the vein and zonality is less visible on a microscopic scale, however, it can be observed everywhere, and is quite characteristic in some cases. Its texture can hardly be characterised by the general terminological terms. Its texture is dominated by pyrite, sphalerite and non-ore minerals. The mineral grains are intergrown, or they displace each other, but there are absolutely linear contact borders, too. Ore minerals can occur as inclusions, fine dissemination or small flakes in non-ore minerals, and vice versa, ore grains also contain inclusions of non-ore minerals. Presence of pores and bigger continuous gaps also belongs to the complex textural pattern.

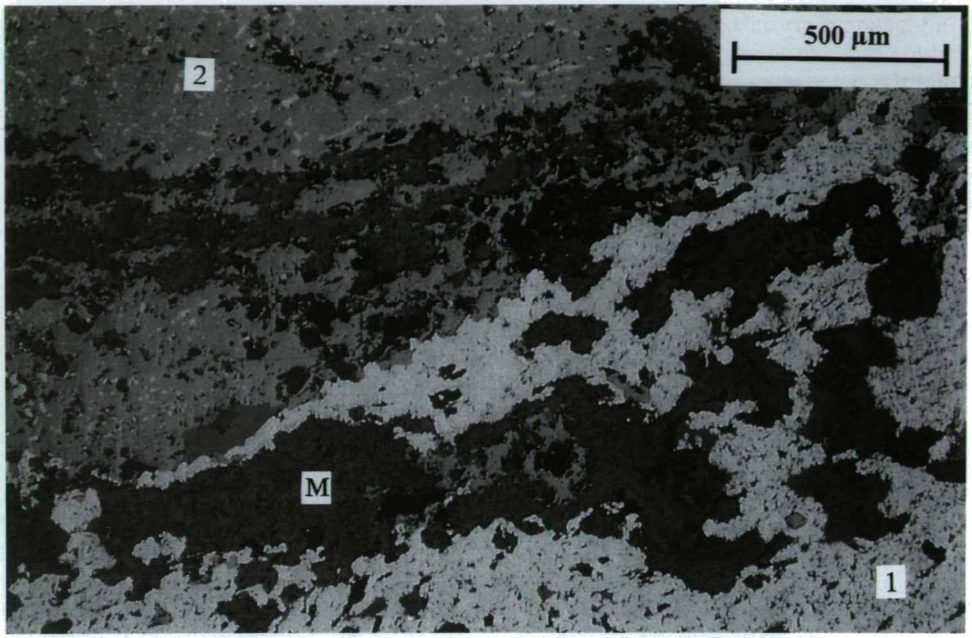

Fig. 4. Key borehole Baksa 2. Characteristic textural pattern with zonal formation of the inner (main) ore phase of the ore vein traversed at 186.4 m depth. (Reflected light, 40x, 1 N.)
Legend: 1. pyrite (marcasitized); 2. sphalerite; M: non-ore material

It seems to be a regularity that relative quantity of the pore space increases toward the centre of the vein, while that of sphalerite decreases. Change in quantity of pyrite and non-ore minerals does not show this kind of characteristics.

Non-ore minerals have no forms in most cases, however, quartz grains are frequently hypidiomorphic, and sometimes idiomorphic. Probably, quartz played a role in the vein formation as the first crystallisation product. Beside quartz, carbonate minerals can be identified by their characteristic pseudoadsorption under ore microscope.

Ore minerals are absolutely allotriomorphic (xenomorphic), and they are intergrown at their borders in most case. Independent crystals can hardly be found, they are arranged as complex groups or irregular net according to the manner mentioned in the textural description.

Pyrite (marcasite) is the most important mineral of the main phase. Its quantity (together with marcasite) reaches almost the one-third part of the ore vein. It is always xenomorphic; isometric faces can very rarely be found at its border to the pores, only. It is very slightly anisotropic at crossed nicols. This brownish-blueish anisotropy is hardly visible even in the freshest part of the crystals. The most characteristic feature is that it appears as tabular crystals of 1-2 or 5 mm and inclusions of some 10μm in other minerals. Absolutely fresh samples having intact border, and crumble, resorbed and slightly weathered parts also occur. Many fissures cutting up the vein are secondarily filled by pyrite. These fissures are younger than the vein, and they cut through both the inner phase and the enclosing rock.

Marcasitisation of pyrite is a quite characteristic process. All in all, it can be stated that weathered or partly weathered pyrite gives almost the half part of the vein. Marcasitisation is easily identified by crossed nicols. However, separation of the marcasitized area from the fresh part is difficult. Therefore, pyrite and marcasite can not absolutely be separated from each other. This is the reason why these two minerals are not separated from each other in the identification of mineral composition.

Pyrite has many groundmass inclusions and unfilled pores, very few and sporadic sphalerite and about 1% pyrrhotite inclusions. Presence of pyrrhotite inclusions are the most characteristic for them. This will be discussed in details later.

Sphalerite is the other main mineral in the ore vein. Its quantity is similar to that of pyrite: it gives about 25 % of the ore vein. Its position in the ore vein and its role in the determination of the textural character is the same what was mentioned above and written in the case of pyrite. Its size is similar to that of pyrite, borders of its grains are just like those of pyrite, however, sphalerite is always xenomorphic. It has no isometric face even at its side at the pores. Sphalerite appears at first in the interface of the inner and the outer phase; pyrite can hardly be found in this zone. It seems that sphalerite would have crystalised first during formation of the zonal arrangement. (Apart from this, every feature of this part of the zone, such as habit of sphalerite, is just like that of the main phase, therefore, it was not separated as a third phase.)

It is very characteristic that sphalerite is extraordinarily rich in **chalcopyrite** and **pyrrhotite inclusions** (2.2 and 1.3 %, respectively). These inclusions appear as oriented drops, lamellas, sometime spindles, or non-oriented drops and lamellas. Sphalerite of the outer phase contains only chalcopyrite inclusions which are much smaller than those of sphalerite in the inner phase. However, sphalerite in the main phase contains both chalcopyrite and pyrrhotite inclusions. It also contains non-ore material, pore and pyrite inclusions in subordinated quantity. In the cases of the oriented inclusions, chalcopyrite and pyrrhotite drops, lamellas, spindles alternate with each other many times even within the members situated in a line. There are inclusions, mainly among the smaller ones, which are composed of both minerals. Two fractions (a smaller and a bigger) of the inclusions can be distinguished. It is probable that the former is a product of intergrowth, while the later is that of exsolution. The bigger are 50-150 μm, and pyrrhotite is more frequent among them. Size of the smaller ones ranges from the smallest size to 10-15 μm, and chalcopyrite is more frequent among them. The bigger pyrrhotite inclusions are quite similar to which occur in pyrite, however, these are bigger by an order, and never weathered. Appearance and composition of the inclusions may also suggest that the vein was formed at high temperature. Temperature of the fluid must at least be supposed so high that it made formation of proper mixture of copper, iron, zinc and sulphur possible. Then sphalerite crystalised together with chalcopyrite and pyrrhotite mainly in the form of oriented intergrowth. Presumably, pyrite enclosing pyrrhotite crystalised in the same stage, which is suggested by intergrowth of pyrite and sphalerite. Sphalerite still had high iron an copper content. For this reason, another, although much smaller, inclusion association unmixed from sphalerite as exsolution inclusions.

Beside its appearance characterised at sphalerite, **pyrrhotite** can be found in pyrite as inclusion in a quantity of 1.3 %. Its size is quite variable, it ranges from some μm to almost 1 mm. Pyrite always surrounds it together with non-ore minerals and pores at the border, in this way this kind of pyrrhotite never contacts other ore minerals. Fresh, slightly and totally altered (which can be identified by its alteration product) pyrrhotite occurs, too. Consequently, the pyrrhotite-pyrite contact border is quite variable: there are both linear contact formed by identifiable crystal faces and altered pattern displacing pyrrhotite. Its main alteration product is marcasite, subordinately pyrite. Marcasitisation of pyrrhotite has an effect on pyrite surrounding it, because this pyrite also suffers this alteration.

1.1.3. IDENTIFICATION OF THE MINERAL COMPOSITION

The mineral composition was also identified by reflected light. Only the main phase was analysed. Area of the outer phase was not analysed either together with or separately from the main phase since it has only diagnostic importance because of its small quantity. Consequently, the following results do not concern the outer phase. Three big sections of the ore vein were used for identification. These preparations (sections 1, 2 and 3) were made from the whole halved core.

First, percentage of pyrite, sphalerite, pyrrhotite, non-ore minerals and pores was determined (Table 1). Marcasite and pyrite is summed up because they can not quantitatively be distinguished. Magnified forty times and a grid of 400 was applied for the analysis. In the second step, percentage of chalcopyrite and pyrrhotite inclusions in sphalerite was determined by a grid of 400 at a magnified 400 times (Table 2). Finally, the real modal composition was calculated by a comparison of the results of these measurements, i.e., inclusions of sphalerite were considered (Table 3).

TABLE 1

Key borehole Baksa 2. Mineral composition of the 7 cm thick massive sulphide vein found at 186.4 m depth (Inclusions of sphalerite are left out of consideration.)

Percentage modal composition of the inner (main) phase of the ore vein (inclusions of sphalerite are left out of consideration)						
Fraction or mineral	*section 1 mean*	*section 2 mean*	*section 3 mean*		*'gross mean'*	*'net mean'*
Pore	6.59	2.12	4.28		4.33	-
Non-ore minerals	39.98	39.14	37.99		39.05	40.81
Pyrite (marcasite)	29.39	34.35	30.61		31.46	32.88
Sphalerite	23.70	24.04	26.90		24.86	25.99
Pyrrhotite	0.34	0.36	0.22		0.31	0.32
Total	100.00	100.01	100.00		100.01	100.00

TABLE 2

Key borehole Baksa 2. Inclusions of sphalerite in the 7 cm thick massive sulphide vein found at 186.4 m depth.

Percentage modal composition of sphalerite found in the inner (main) ore phase of the ore vein					
Fraction or Mineral	*section 1 mean*	*section 2 mean*	*section 3 Mean*		*Mean*
Sphalerite	96.08	96.87	96.48		96.45
Chalcopyrite	2.52	1.90	2.08		2.20
Pyrrhotite	1.40	1.22	1.44		1.36
Total	100.00	99.99	100.00		100.01

On the basis of the measurements, the total percentage of the sulphides is 56.5 % in the vein. Pyrite (marcasite) (31.5 %) and sphalerite (24 %) are the main components, and pyrrhotite (0.5 %) and chalcopyrite (0.5 %) are the accessory ore minerals. Besides non-ore minerals (39 %), gaps and pores can also be found in considerable quantity (4.5 %) in the vein. The 24 % of the sphalerite represents a remarkable Zn-accumulation in the vein.

Key borehole Baksa 2. Mineral composition of the 7 cm thick massive sulphide ore vein found at 186.4 m depth (Inclusions of sphalerite are taking into consideration.)

Percentage modal composition of the inner (main) phase of the ore vein (Inclusions of sphalerite are taking into consideration)			
Fraction or mineral		*'gross mean'*	*'net mean'*
Pore		4.33	-
Non-ore minerals		39.05	40.81
Pyrite (marcasite)		31.46	32.88
Sphalerite		23.98	25.06
Pyrrhotite		0.65	0.67
Chalcopyrite		0.55	0.57
Total		100.02	99.99
Sulphide ore minerals		56.64	59.18

1.2. ANALYSES IN TRANSMITTED LIGHT

Ore minerals excepting sphalerite are opaque, therefore they can not be studied in transmitted light. In general, they xenomorphic, but there are some hypidiomorphic and idiomorphic grains, too (*Fig. 5*).

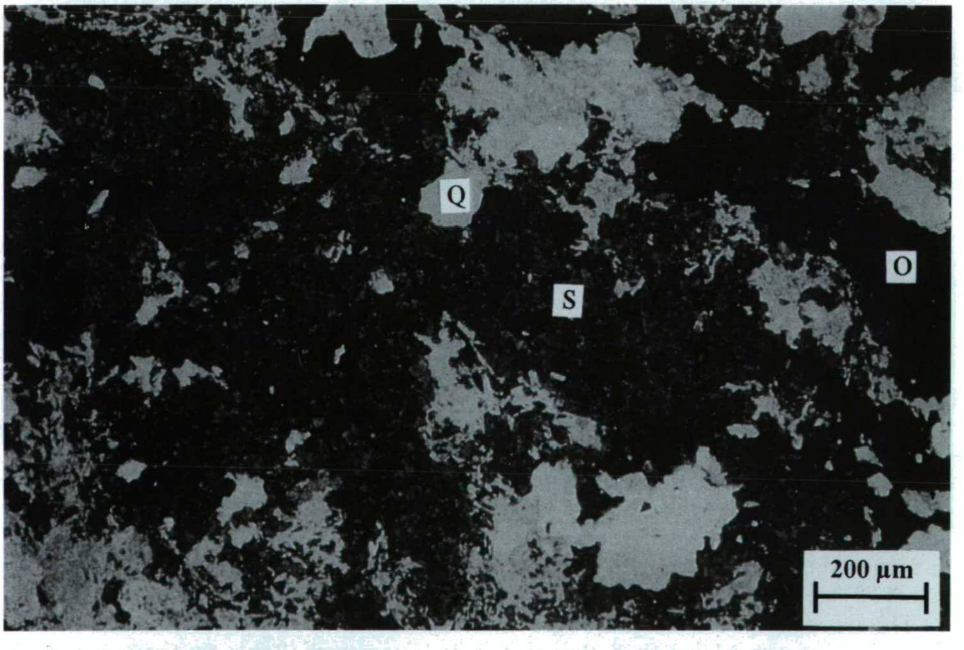

Fig. 5. Key borehole Baksa 2. Characteristic textural pattern of the inner (main) ore phase of the ore vein traversed at 186.4 m depth. (Transmitted light, 100x, +N)
Legend: O: opaque mineral; S: sphalerite; Q: quartz

Sphalerite is reddish brown and totally translucent at one nicol. Polysynthetic twins and chalcopyrite and pyrite inclusions can well be seen. The bigger (50-150 μm) and the smaller (5-15 μm) chalcopyrite and pyrrhotite inclusions occur at the border of the twins and inside of sphalerite, respectively (see at the ore microscopic description). These inclusions have sharp border line, this way, they can easily be recognised. Probably, the bigger ones are product of epitaxy, while the smaller ones come from exsolution. Some kind of zonality of sphalerite can also be observed on the basis of the oriented inclusions. Thin section explains the phenomenon that the biggest pyrrhotite inclusions are always inside of the sphalerite, which seems to be homogeneous on the polished slabs. Borders of sphalerite can be seen on thin sections, and it can be observed that big pyrrhotite inclusions fill the gaps between contacts of more sphalerite crystals. Sphalerite shows moderate anisotropy at crossed nicols, i.e., birefractive. This property is quite interesting because it belongs to the isometric system. The interference colour is dwarfed by its own colour.

Non-ore minerals were not studied in details, only the two most important components, quartz and calcite(carbonate), are described.

Quartz is the dominant non-ore mineral (at least 50-70 % of the non-ore material). Most of them occur as xenomorphic crystals of hexagonal section. The mean size is 2-400 μm. On the basis of some section parallel to the axis c, it can be stated that the characteristic width:length ratio is approximately 1:3-1:4, and there are pyramids on both ends of the crystals. Subordinately, hypidiomorphic and xenomorphic crystals also occur.

Quantity of ***calcite*** is also considerable. It occurs as xenomorphic crystals, only. It mainly fills the residual space, however, in some cases it covers opaque minerals and quartz as a thin layer. This suggests that it was formed in later crystallisation phase than quartz. Calcite represents approximately 10-20 % of non-ore minerals of the sample.

2. INCLUSION ANALYSES

Analysis of fluid inclusions in quartz grains of the vein was used for determination of thermal and pressure conditions during formation of the sulphide ore vein in the key borehole Baksa 2 at 186.4 m depth. It was eye-striking even microscopically that there are many fluid inclusions in the quartz grains found between the ore minerals. Both one-phase (fluid or gas) and two-phase (fluid + gas) inclusions occur. ZEISS JENA AMPLIVAL polarizing microscope equipped with CHAIXMECA heat-stage was used. The range of the equipment is from -180 C° to +600 C°, its accuracy is +/- 0.2 and 0.1 C° at homogenization (400 C°) and freezing, respectively (GATTER I., 1983). The results are listed in Table 4.

First, two-phase (gas + fluid) inclusions were analysed. Fluids in the inclusions were frozen by liquid nitrogen, and then heated at room-temperature; meanwhile, the initial (Te) and the final or total (T2) melting signs as well as temperatures belonging to them were detected. When the inclusions were heated to high temperature, homogenization temperature was observed. Results of the analyses and the values corrected because of instrumental constant are listed in table 4. Salinity values calculated from the final melting point (T2) are also shown by Table 4.

The second step was analysis of gas inclusions in which CO_2-phase could be detected in the form of non-mixing fluid phases at room-temperature (Table 5). Frequency of the inclusions containing CO_2 is subordinated in the ore vein.

TABLE 4

*Key borehole Baksa 2. Results of the inclusion analyses. *NaCl equivalent weight % (Calculation was by Flincor program.)*

Number of the inclusion	Measured Te (C°)	Calculat. Te (C°)	Measured T2 (C°)	Calculat. T2 (C°)	Calculat. Salinity*	Measured Th (C°)	Calculat. Th (C°)
1.	-47	-48	-2.6	-3.1	5.09 %	295	284.3
2.	-47	-48	-2.6	-3.1	5.09 %	295	284.3
3.	-47	-48	-2.4	-2.9	4.79 %	291	280.7
4.	-47	-48	-2.4	-2.9	4.79 %	291	280.7
5.	-47	-48	-2.2	-2.7	4.48 %	286	276.1
6.			-2.2	-2.7	4.48 %	286	276.1
7.	-47	-48	-2.1	-2.8	4.32 %	278	268.7
8.			-2.1	-2.8	4.32 %	278	268.7
9.			-1.6	-2.1	3.53 %	272	261.4
10.	-45	-46	-2.8	-3.3	5.04 %	265	256.8
11.	-47	-48	-2.1	-2.6	4.22 %	245	238.2
12.			-2.2	-2.7	4.48 %	245	238.2
13.	-45	-46	-2.4	-2.9	4.79 %	240	233.5
14.			-1.6	-2.1	3.53 %	235	228.3

TABLE 5

Key borehole Baksa 2. Results of preliminary analyses of the inclusions containing CO_2. Ratio of H_2O and CO_2 was calculated by Flincor program.

Number of the inclusion	H_2O content of the inclusion (mol %)	CO_2 content of the inclusion (mol %)	Homogenization temperature of the CO_2
1.	38.8 %	61.2 %	-21.0 °C
2.	40.3 %	59.7 %	-19.5 °C
3.	64.2 %	35.8 %	-13.2 °C
4.	36.1 %	63.9 %	-23.6 °C
5.	40.4 %	59.6 %	-19.4 °C

A T/P diagram based on isochrons calculated from the measurement data by the Flincor program is shown by *Fig. 6*. A Th-salinity diagram was also compiled (*Fig. 7*).

CONCLUSIONS

The most important hydrothermal activity explored by the key borehole Baksa 2 is a 6-7 cm thick sulphide vein found at 186.4 m depth. Its ore paragenesis is the following: pyrite (FeS_2), marcasite (FeS_2), sphalerite (ZnS), pyrrhotite (FeS), chalcopyrite ($CuFeS_2$), galena (PbS). Conditions of the formation of the ore vein (band) were approximately reconstructed by ore optical and preliminary fluid inclusion analyses. On the basis of these studies, the vein was formed in closed system but at not too high pressure (150-300 bar) which does not mean too thick covering layer (60-120 or, at most, some hundreds m). Salinity of the fluid forming the vein is 4-5 % (in term of NaCl equivalent weight percent),

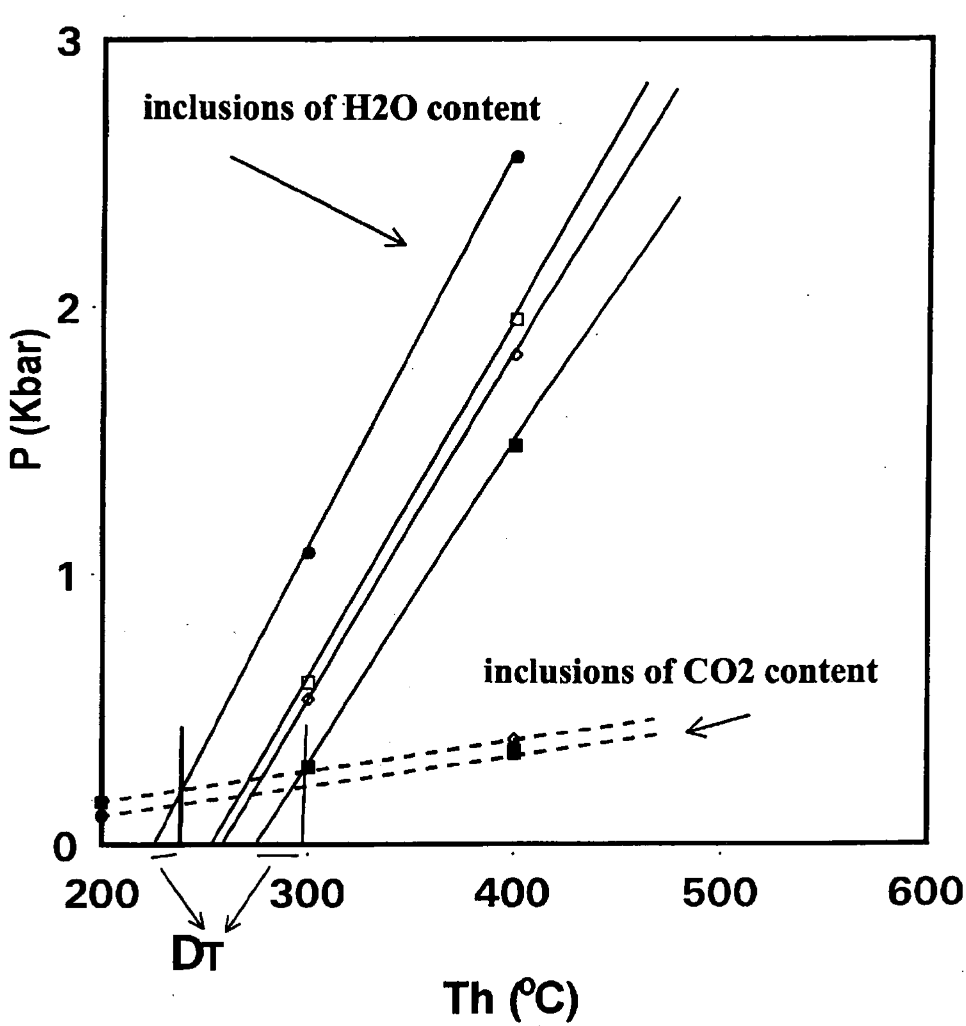

Fig. 6. Key borehole Baksa 2. Ore vein traversed at 186.4 m depth. T/P diagram based on the inclusion analyses and isochrons calculated by the Flincor program.

which is moderate, and suggests that considerable meteoritic water was not added to the ascending solutions. Both inclusion and ore microscopical analyses suggest that two phases can be distinguished in the formation of the vein. Paragenesis of the first one is galena, sphalerite, pyrite (marcasite), and it was formed at lower temperature (250-270 C°). This outer phase can be found at the margins of the vein in a thickness of 3-4 mm, and in apophyses and veinlets along the vein. Ore paragenesis of the main or inner phase is pyrite, marcasite, sphalerite, pyrrhotite, chalcopyrite. It was formed at a higher temperature (290-310 C°). The ore vein is a massive sulphide one with an ore content of almost 60 %. It is a genetic matter, however, whether there are two successive phases of the vein formation or it is one ore mineral formation differentiated by temperature from each other.

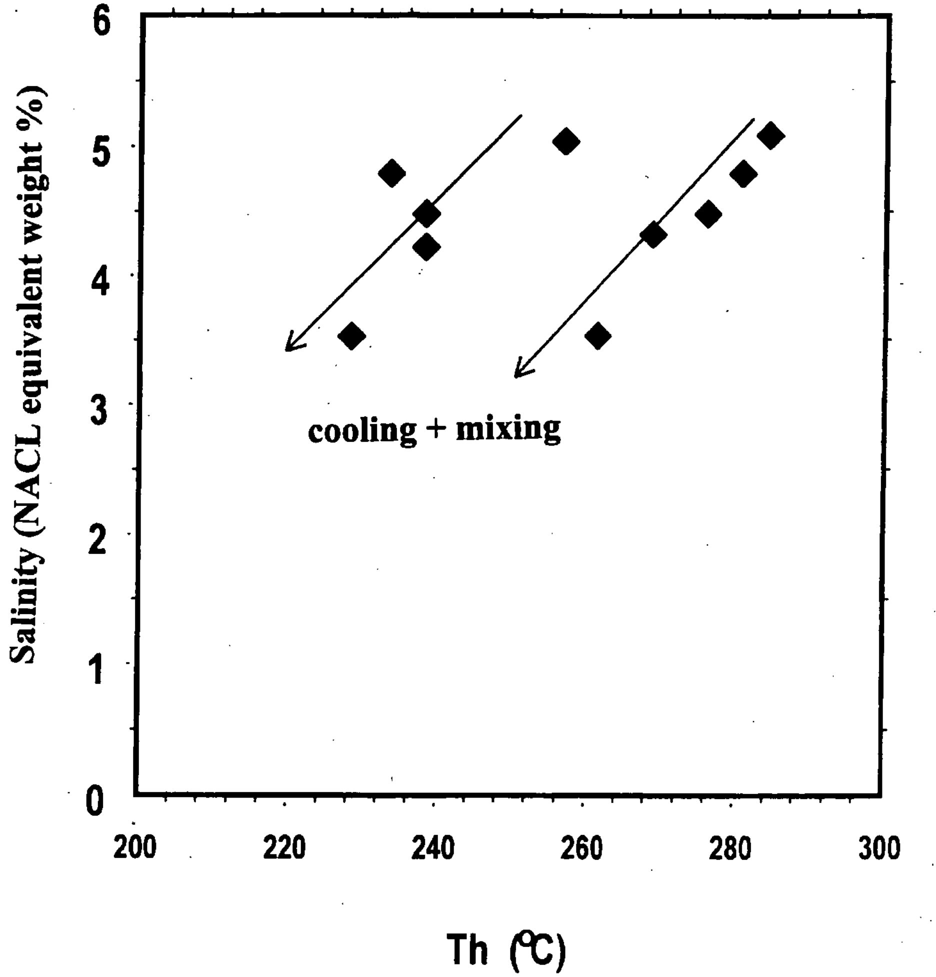

Fig. 7. Key borehole Baksa 2. Ore vein traversed at 186.4 m depth. Th-salinity diagram based on inclusion analyses.

Besides the values measured by fluid inclusion analyses, regular appearance of pyrrhotite and chalcopyrite and their exsolution in the inclusions also suggest a relative high temperature of the fluids forming the ore mineralisation.

The ore mineral paragenesis, results of the inclusion analyses, presence and habit of the main non-ore minerals (quartz, calcite, feldspar), their association with the variable ore minerals of relative high concentration can be resulted by a magmatic process. The ore vein may be in connection with the rhyolitic volcanism found in the basement in foreground of the Villány Mountains (FAZEKAS V.-VINCZE J., 1991), however, it is also possible that the ore vein of the crystalline formations of the Baksa Complex explored by the borehole Baksa 2 was formed by an absolutely new volcanic activity which has never known up till now.

ACKNOWLEDGEMENT

I would like to thank DR. ISTVÁN GATTER for making the inclusion analyses and interpretation of the results. I also express my thanks to DR. TIBOR SZEDERKÉNYI and TIBOR ZELENKA for choosing this topic for me and following my work with attention.

REFERENCES

BALLA Z. (1981): Plate tectonics interpretation of the south transdanubian ultramafics. - Acta Mineral. Petrogr. Szeged 25/1, pp. 3-24.

BARABÁS A., JÁMBOR Á., SZÉNÁS GY. et al. (1964): A Mecsek és a Villányi-hegység geofizikai kutatásának eredményei. - MÁELGI Évk. 1.

FAZEKAS V., VINCZE J., (1991): Hidrotermás Ércindikációk a Villányi-hegység északi előtere mélyfúrásaiban. - Földtani Közlöny 91/1-4, pp. 23-56.

GATTER I. (1983): Folyadék-gáz zárvány vizsgálatok a nyugat-mátrai érces képződményekben. Doktori értekezés. ELTE, Ásványtani Tanszék, Budapest.

GRASSELY GY. (1979): in: A mecseki ópaleozoós-prekambriumi alapszelvények komplex földtani feldolgozása (SZEDERKÉNYI T). Kézirat. JATE, Ásványtani, Geokémiai és Kőzettani Tanszék, Szeged. pp. 113-124.

HAJDÚ L. (1987): A telkibányai ércesedés vizsgálata korszerű anyagvizsgálati módszerekkel. Szakdolgozat. ELTE, Ásványtani Tanszék, Budapest.

HARANGI SZ. & ÁRVÁNÉ SÓS E. (1993): A Mecsek hegység alsókréta vulkáni kőzetei I. Ásvány- és kőzettan. - Földtani Közlöny 93/2, pp. 129-165.

JANTSKY B. (1979): A mecseki gránitosodott kristályos alaphegység földtana. - MÁFI Évk. LX.

KOVÁCS S. et al. (1996): Report of IGCP project. No. 276. Athenes (In press)

RAVASZNÉ BARANYAI L. (1969): Eclogite from the Mecsek Mountains, Hungary. - Acta Geol. Acad. Sci.13, pp. 315-322.

SZEDERKÉNYI T. (1974): Paleozoic magmatism and tectogenesis in Southeast Transdanubia, Hungary. Acta Geol. Sci. Hung., 18, 3-4, 305-313,

SZEDERKÉNYI T. (1977): Geological evolution of South Transdanubia (Hungary) in Paleozoic time. - Acta Mineral. Petrogr. Szeged 23/1.

SZEDERKÉNYI T. (1979): A mecseki ópaleozoós-prekambriumi alapszelvények komplex földtani feldolgozása. Kézirat. JATE, Szeged.

SZEDERKÉNYI T. (1983): Origin of amphibolites and metavolcanics of crystalline complexes of South Transdanubia, Hungary. - Acta Geol. Acad. Sci. Hung. 26/1-2, pp. 103-136.

SZEDERKÉNYI T., ÁRKAI P., LELKESNÉ FELVÁRI GY. (1991): Crystalline groundfloor of the Great Hungarian Plain and South Transdanubia, Hungary. Serbian Acad. Sci. and Arts Acad. Conf. 4, pp. 261-273.

TARNAI T. (1996) A Baksa-2. sz. földtani alapfúrásban feltárt ércásványok ásványtani és genetikai jellemzőinek vizsgálata. – Diplomamunka. JATE Ásványtani, Geokémiai és Kőzettani Tanszék, Szeged.

TARNAI T. (1997) Ore minerals from the key section of the Baksa Complex (W. Baranya Hills, Hungary). Acta. Mineral. Petrogr. Szeged 38. Supplementum, pp. 119–133.

VÁRSZEGI K. (1978): Série cristalline de Görcsöny. In FÜLÖP J. (Ed.): Lexique stratigraphique international. Vol 1. Europe. Fasc. 9. Hongrie. (pp. 223-224). - Centre Nat. de la Rech. Sci.

VÖRÖS I. (1970): Ércmikroszkópiai határozó. Tankönyvkiadó, Budapest.

Manuscript received 21 September, 1998.

Acta Mineralogica-Petrographica, Szeged, XXXIX, 35–48, 1998

PETROGRAPHICAL CHARACTERISTICS OF DITRÓ (OROTVA) GRANITES, EASTERN CARPATHIANS, TRANSYLVANIA, ROMANIA: A PRELIMINARY DESCRIPTION

G. KOVÁCS, E. PÁL MOLNÁR*

Department of Mineralogy, Geochemistry and Petrology, Attila József University

ABSTRACT

One of the most important rock groups outcropping in the NE part of the Ditró Massif, north of the Orotva (Nagyág) creek and from the Török creek to the crystalline schists is the group of the granitic rocks. On the basis of their modal composition and textural features, this rock group can be divided into the following rock types: 1. syeno- and monzogranites with equigranular texture; with potassium feldspar megacrystalline texture, alkaline granites. 2. syenites, quartz syenites, alkaline syenites, foidic monzosyenites. 3. monzonites, quartz monzonites. 4. cataclasites.

On the geological maps of 1:10.000 scale the granitoid formations were shown as a homogeneous body. Our studies have revealed that petrography of this area is much more complex than it was interpreted by the former studies. On the basis of the textural studies, it has been concluded that secondary textural patterns of the rock types are similar, and it can be attributed to endomagmatic effect, weathering processes and tectonic deformation.

INTRODUCTION

The Syenite Massif of Ditró is situated in the S-SW part of the Gyergyó Alps belonging to the Eastern Carpathians. Diameter of its surface is 19 km in NW-SE and 14 km in SW-NE directions, respectively; its area is 225 km, including the bordering zones as well (PÁL MOLNÁR, 1994a). This intrusion intruded into the central crystalline rock massif of the Eastern Carpathians is petrologically very complicated allochtonous body divided into tectonic units of E-NE dip, and it has a complex form (PÁL MOLNÁR, 1994b). The granitod rocks occur in many points of the Ditró Massif, and they can be found in the largest extent in the northern part of the massif, east of the Török creek and north of the Orotva-Nagyág creek as far as the crystalline rocks (*Fig. 1.*).

Aim of our study is a petrographical classification of this granitoid body, and the collection of the basic knowledge for the further detailed analyses. Structure and origin of the massif have been studied by several authors (STRECKEISEN, 1954; ANASTASIU, CONSTANTINESCU, 1977, 1981; JAKAB et al., 1987), however, a comprehensive classification has not been published, although, any further analysis would be inconsequent without this kind of study.

In this paper, we summarize the results of the petrographic study on rocks of this area described as granite.

* H-6701 Szeged, P. O. Box 651, Hungary

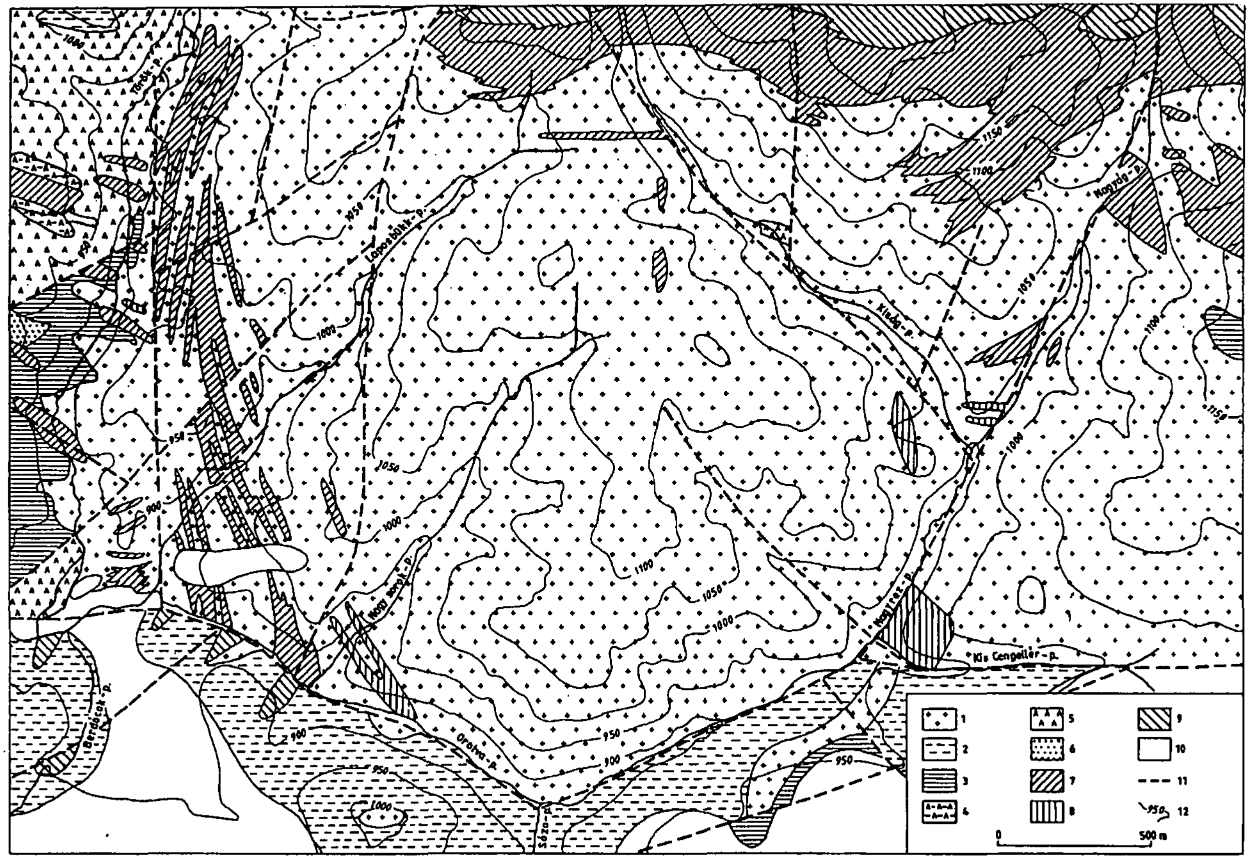

Fig. 1. Geological map of the NE part of the Ditró Syenite Massif (JAKAB et al., 1987)
1. granite; 2. syenite; 3. alkaline feldspar syenite with hornblende; 4. microcrystalline syenite; 5. monzonite; 6. microcrystalline alkaline feldspar syenite; 7. quartz-feldspar schists ; 8. quartzite; 9. sericite - graphite schists; 10. unknown area; 11. tectonic line; 12. contour line.

PETROGRAPHICAL CHARACTERIZATION OF THE 'GRANITOID ROCKS'

In this study, we intended to collect characteristic and common features that made the classification of the granitoid rocks possible. Moreover, textural and microstructural characters indicating the rock forming processes were observed. Of course, these studies themselves do not make reaching remote conclusions possible; a petrographical description only serves as a source for the genetic studies.

Granitoid rocks of the study area was described as red and grey coarse or fine grained granites (JAKAB et al., 1987). By macroscopic studies the following rock types could be distinguished:

- hypidiomorphic-granular 'granite' with potassium feldspar megacrystals;
- medium grained, hypidiomorphic-equigranular 'granite';
- cataclasites (tectonometamorphic rocks).

These rocks are dominantly leucocratic, pale grey, withish yellow, pink, pale red. Results of volume percentage composition measured in thin section (Table 1) are figured in diagrams (*Fig. 2.*) accepted by the IUGS (LE MAITRE, 1989). Rock analyses are in nine fields of the QAP diagram: alkaline granite, syenogranite, monzogranite, (alkaline) quartz syenite, quartz monzonite, (alkaline) syenite, monzonite and foidic monzosyenite (1 specimen). Results of the modal analyses show that petrography of the study area is more complex than it could have been expected on the basis of its geological map or the concerning literature.

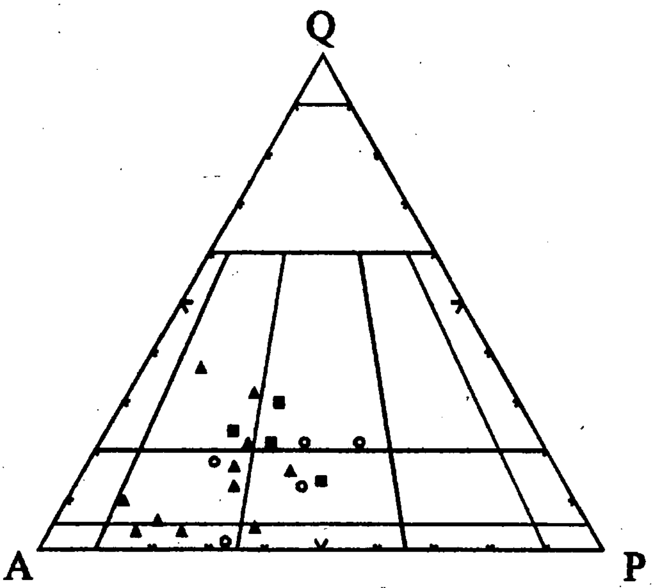

Fig. 2. Modal composition of the studied samples (LE MAITRE, 1989)

By the modal analyses and the textural studies, rocks of the Ditró Massif described as granites can be divided into the following groups:

1. syeno- and monzogranites
   a, with equigranular texture;

b, with potassium felspar megacrystalline texture;
c, alkaline granites.
2. syenites, quartz syenites, alkaline syenites, foidic monzosyenites
3. monzonites, quartz monzonites
4. cataclasites

Further on, petrographic features of the main groups are shown.

TABLE I

Results of the modal analyses for the QAP diagram

locality	sample number	A[2] (%)	P[3] (%)	Q[4] (%)	felsic constituents (%)	mafic index (%)	rock name
1. Török creek	ÁGK-6824	60	22	18	87	13	quartz syenite
	ÁGK-6826	47	40	13	92	8	quartz monzonite
	ÁGK-6827	32	46	22	75	25	monzogranite
	ÁGK-6829	66	32	2	90	10	syenite
	ÁGK-6831	42	35	22	91	9	monzogranite
2. Laposbükk creek	ÁGK-6835	48	30	22	84	16	monzogranite
	ÁGK-6836	67	21	F[5]11	79	21	foidic monzosyenite
	ÁGK-6838-B	43	43	14	87	13	quartz monzonite
	ÁGK-6839	54	22	24	92	8	monzogranite
	ÁGK-6842	53	22	24	995	5	syenogranite
3. Nagyág creek	ÁGK-6845	80	15	4	97	3	alkaline syenite
	ÁGK-6846	63	38	5	92	8	monzonite
	ÁGK-6847	53	10	37	98	2	syenogranite
	ÁGK-6848	72	23	4	89	11	syenite
	ÁGK-6849	76	18	6	92	8	quartz syenite
	ÁGK-6850	57	26	17	98	2	alkaline quartz syenite
	ÁGK-6851	59	28	13	90	10	quartz syenite
	ÁGK-6852	47	36	16	99	1	quartz monzonite
	ÁGK-6853	46	22	32	97	3	syenogranite
	ÁGK-6854	80	10	10	94	6	alkaline quartz syenite
	ÁGK-6856	51	27	22	98	2	syenogranite

1. Main textural features of the granites

The main felsic rock-forming minerals are as it follows: microcline, orthoclase, plagioclase of albite-oligoclase composition, quartz. Microcline and plagioclase often occur as hypidiomorphic megacrystal of 0.25-4 mm. Quartz is xenomorphic, its size ranges from 0.25 to 1.5 mm. The felsic components are in special microtextural relation to each other. In most cases, microcline is the most frequent felsic component. Their megacrystals are perthitic because of the albite ribbons (*Fig. 3.*). In many cases, it has a poikilitic texture, and contains quartz, plagioclase and (rarely) biotite as inclusions. Distribution of the inclusion is not equal in the crystal, but they can be found along the

[2] A: odal (volume percentage) ratio of potassium feldspars and An<5% (albite) in the Streckeisen diagram
[3] P: Modal (volume percentage) ratio of An>5% plagioclase feldspar in the Streckeisen diagram
[4] Q: Amount of the modal quartz in the Streckeisen diagram
[5] F: Modal amount of the feldspathoids in the Streckeisen diagram

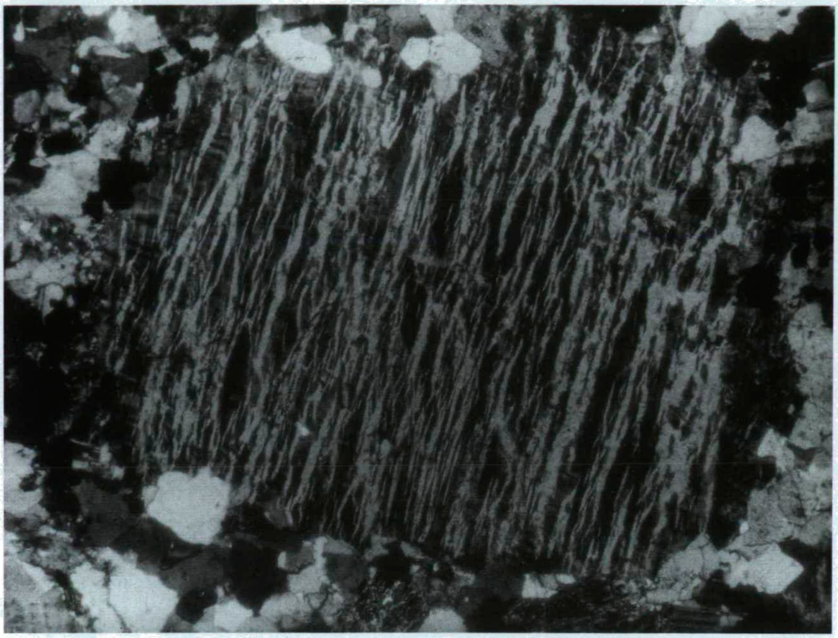

Fig. 3. ÁGK-6906 Microcline with perthite ribbons, 45x, +N

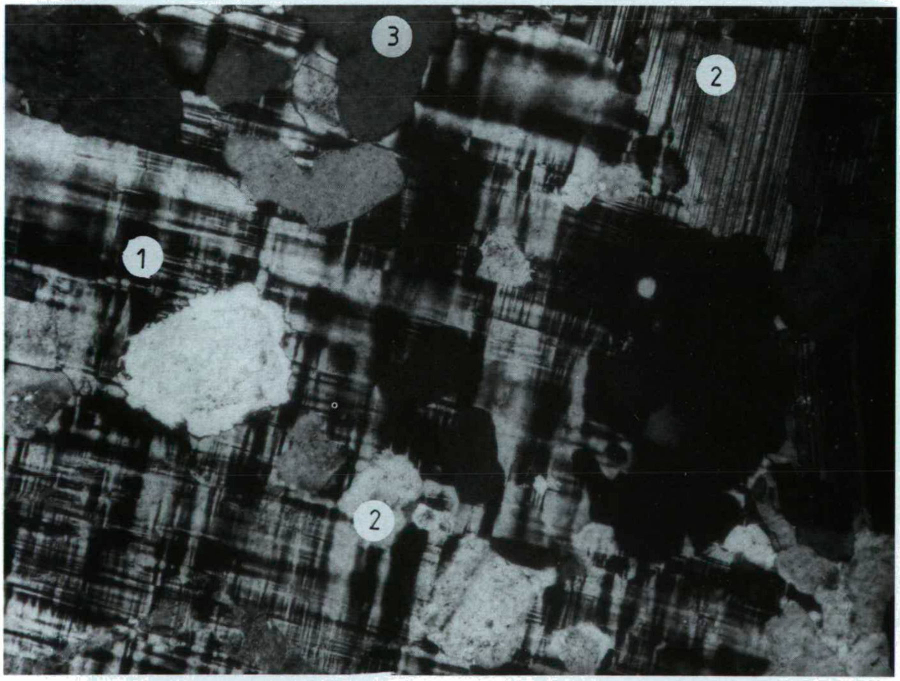

Fig. 4. ÁGK-6831 Microcline with plagioclase and quartz inclusions, 90x, +N
1. microcline; 2. plagioclase; 3. Quartz

Fig. 5. ÁGK-6842 Resorption embayment between microcline and quartz, 180x, +N
1. microcline; 2. Quartz

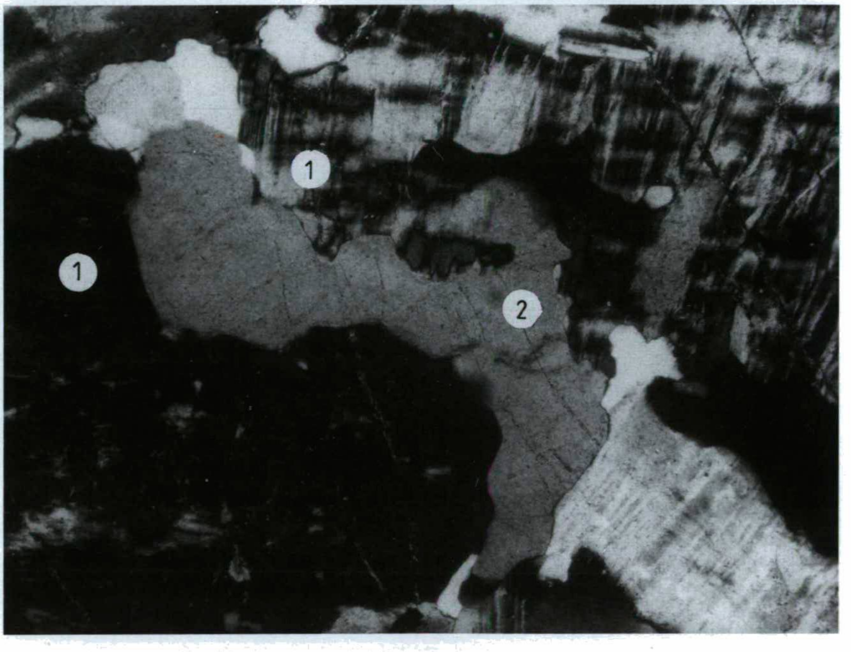

Fig. 6. ÁGK-6851 Resorption embayment between microcline and quartz, 90x, +N
1. microcline; 2. Quartz

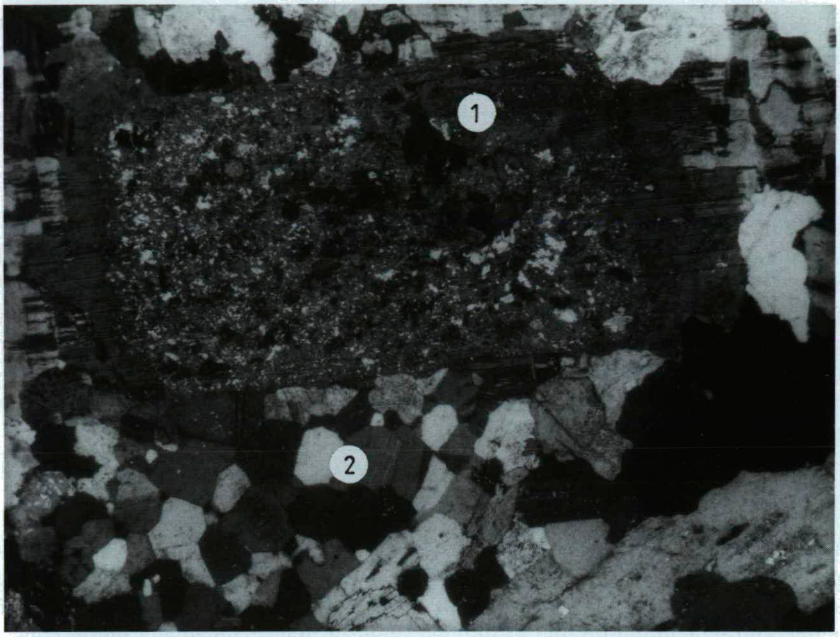

Fig. 7. ÁGK-6831 Primary sericitic plagioclase and secondary myrmekitic plagioclase, 45x, +N
1. plagioclase of first generation; 2. myrmekitic plagioclase of second generation

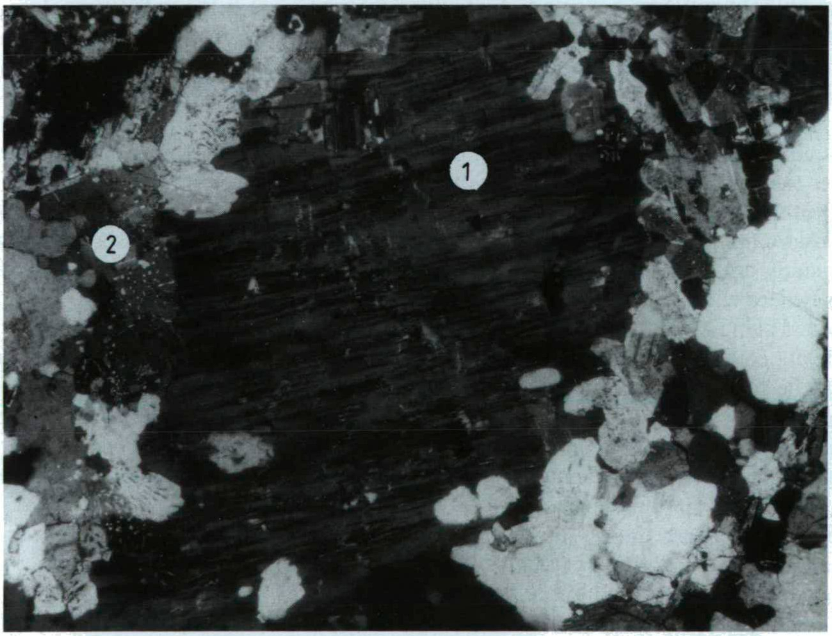

Fig. 8. ÁGK-6831 Microcline megacrystal and myrmekitic plagioclase, 45x, +N
1. microcline megacrystal; 2. myrmekitic plagioclase

margin as an inclusion belt (*Fig. 4.*). It is quite common that the much smaller quartz and feldspar grains are crowded between the big microcline megacrystals. The inclusions are embayed; it indicates gaining ground the host mineral (*Fig. 5.* and *6.*). These signs suggest that poikilitic texture of the microcline is not syngenetic with the other felsic constituents (i.e., it did not form during the crystallization) but it is a result of a secondary endomagmatic effect. Plagioclase feldspars have two generations. In general, the first has a megacrystalline habit, it is zoned, sericitic and slightly saussuritic (*Fig. 7.*); the second is smaller and often myrmekitic (*Fig. 8.*).

The dominant mafic rock-forming minerals are biotite, hornblende and alkaline amphiboles. Biotite can occur as single mafic constituent in the granites, while hornblende can occur only together with the biotite. The hornblende is generally weathered, relict, and associated with biotite, epidote and opaque grains (*Fig. 9.*). In some cases, the biotite is weathered, chloritized, and secondary rutile and titanite aggregates can be found along the cleavage faces (*Fig. 10.*). Its accessory minerals are apatite, zircon, orthite and primary opaque grains (magnetite).

2. Petrographic features of the syenites

In this part textural features of syenite, quartz syenites and alkaline syenites are summarised. It is true that volume percentage ratio of the felsic constituents is varying, however, their texture is similar to that of the granites in many respects. Dominance of microcline and its gaining ground to the detriment of that of felsic and mafic constituents can be found in the syenites of the study area. Compared to the granites, the special alteration of the amphiboles (hornblende and alkaline amphibole) is a new phenomenon. The amphibole structure became to be porous, the pores are filled with microcline grains, and an advance of microcline can be found at the margins, too (*Fig. 11.*). These xenomorphic amphiboles of perforated habit suggest secondary processes. A mineral association of alkali amphiboles and aegirine is quite frequent. The aegirine seems to be relict, and turned into alkaline amphibole (*Fig. 12.*). The alkaline amphibole can hardly be identified by optical way; they may belong to the arfvedsonite-eckermannite series and/or have a riebeckite composition. Accurate determination of their composition demands further mineral chemical analyses.

A foidic monzosyenite sample should also be mentioned here. This is a unique sample in the study area, however, its occurrence is known along the Török and the Laposbükk creeks where the foidic rocks attach to granites. This sample differs from the above mentioned samples in the higher volume percentage ratio of the mafic constituents (21 %) and the appearance of feldspathoids. It contains many idiomorhic, primary titanite crystals that can be found in lower amount in the above mentioned samples. The feldspathoids are altered; pseudomorphs of zoisite, muscovite and sericite aggregates after them can be seen. Possibly, they are liebneritized nepheline grains, and the isometric ones can be of sodalite origin. Of the mafic constituents, biotite and hornblende are fresh, augite is altered and surrounded by an amphibole crown.

Textural characterization of monzonites and quartz monzonites is not mentioned because, beside the volume percentage ratio of the QAP constituents, their microscopic features do not differ from those of the granites.

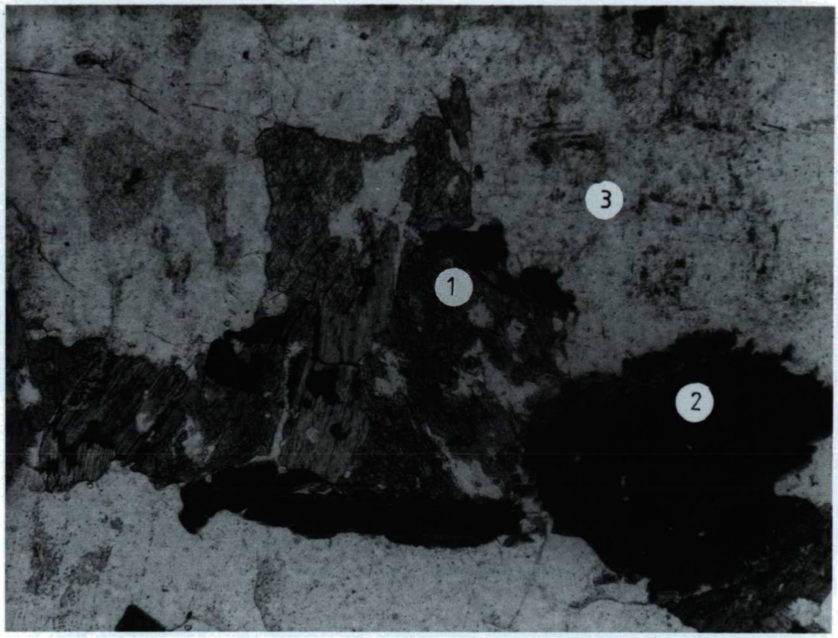

Fig. 9. ÁGK-6827 Biotite-amphibole-chlorite mineral association, 90x, 1N
1. hornblende; 2. chloritized biotite; 3. Microcline

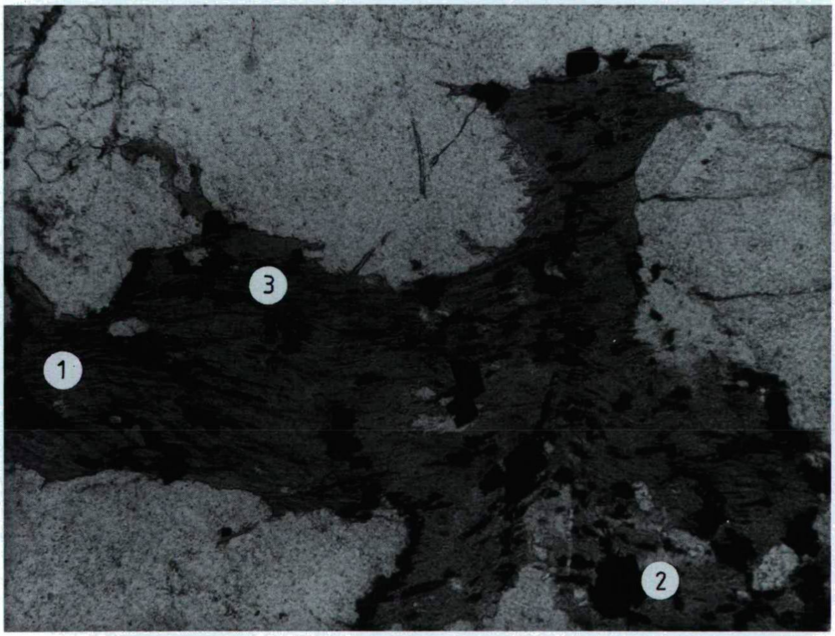

Fig. 10. ÁGK-6838-b Chloritized biotite with secondary rutile and opaque grains, 90x, 1N
1. chlorite pseudomorph after biotite; 2. opaque grain (magnetite); 3. secondary rutile

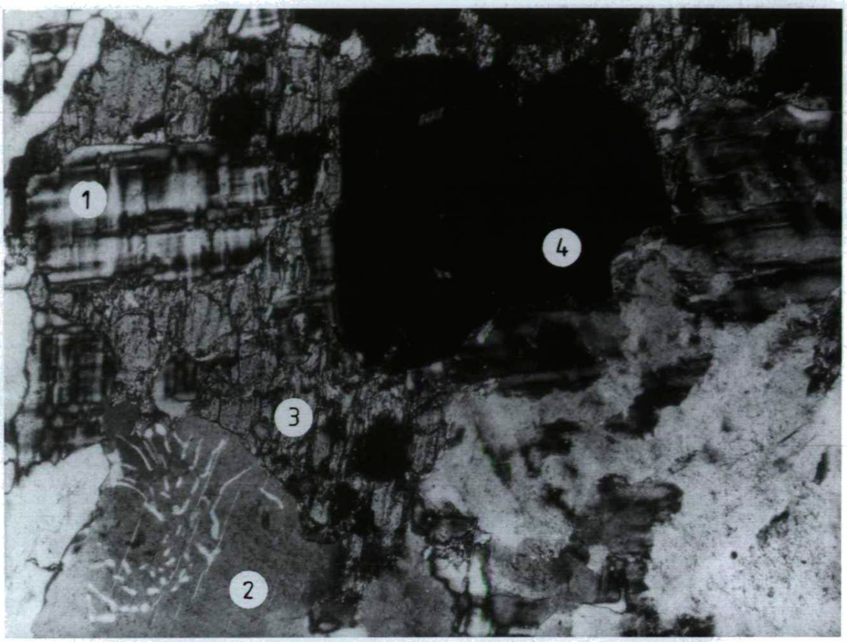

Fig. 11. ÁGK-6851 Myrmekite and microcline in altered amphibole, 90x, +N
1. microcline; 2. myrmekitic plagioclase; 3. hornblende; 4. opaque grain

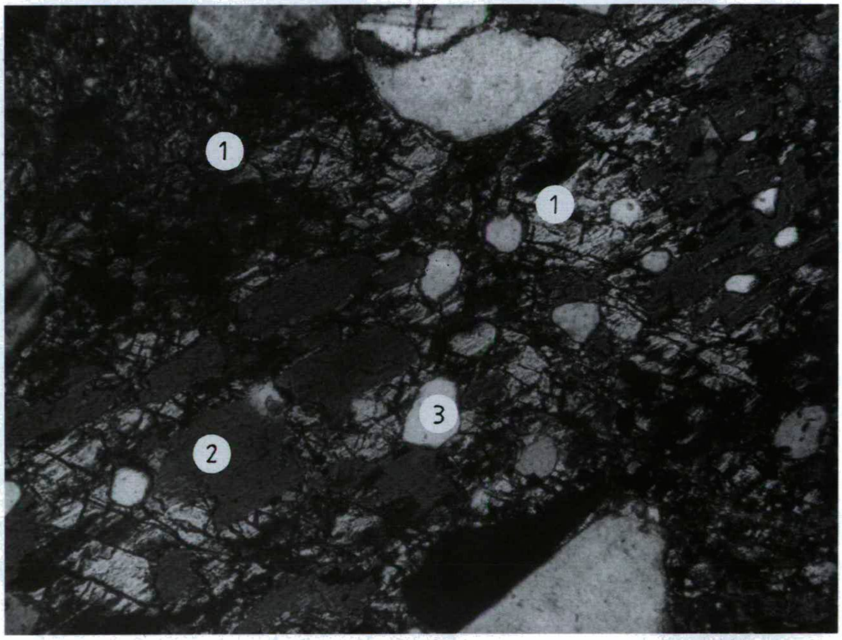

Fig. 12. ÁGK-6845 Aegirine of perforated texture and alkaline amphibole, 180x, +N
1. aegirine; 2. alkaline amphibole; 3. Microcline

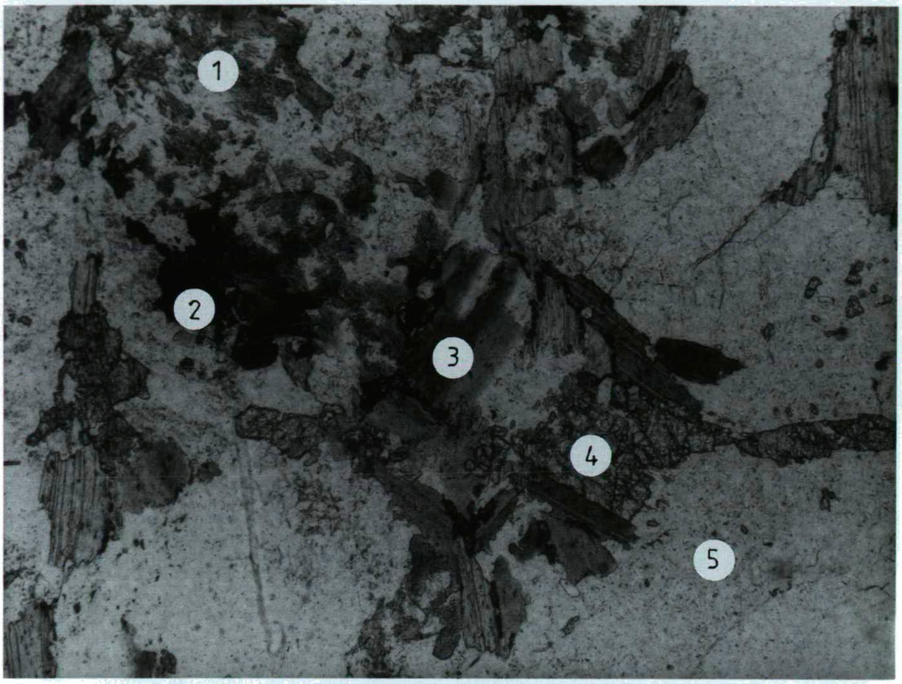

Fig. 13. ÁGK-6827 Amphibole-biotite-epidote mineral association, 90x, +N
1. hornblende; 2. opaque grain; 3. chloritized biotite; 4. epidote; 5. microcline

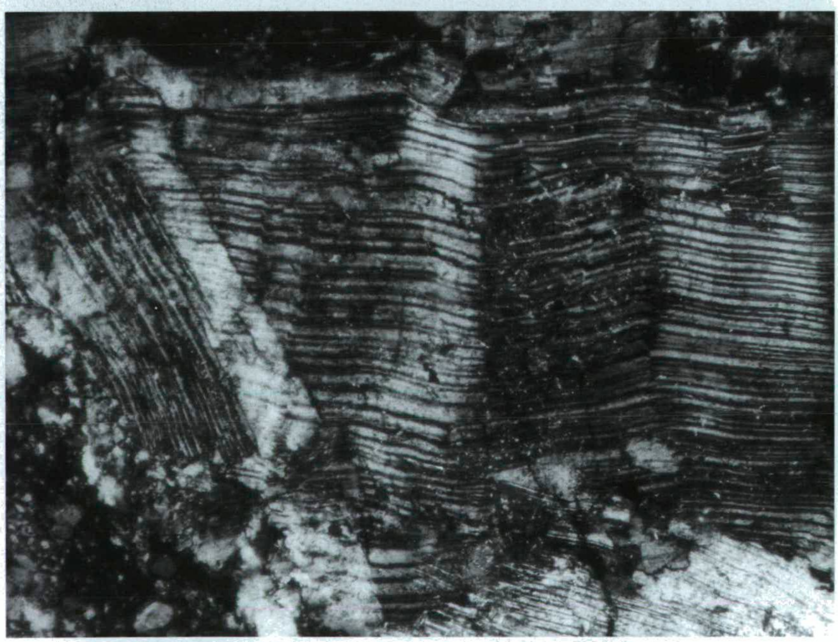

Fig. 14. ÁGK-6838-a Plagioclase with undulatory twins (kink-band), 90x, +N

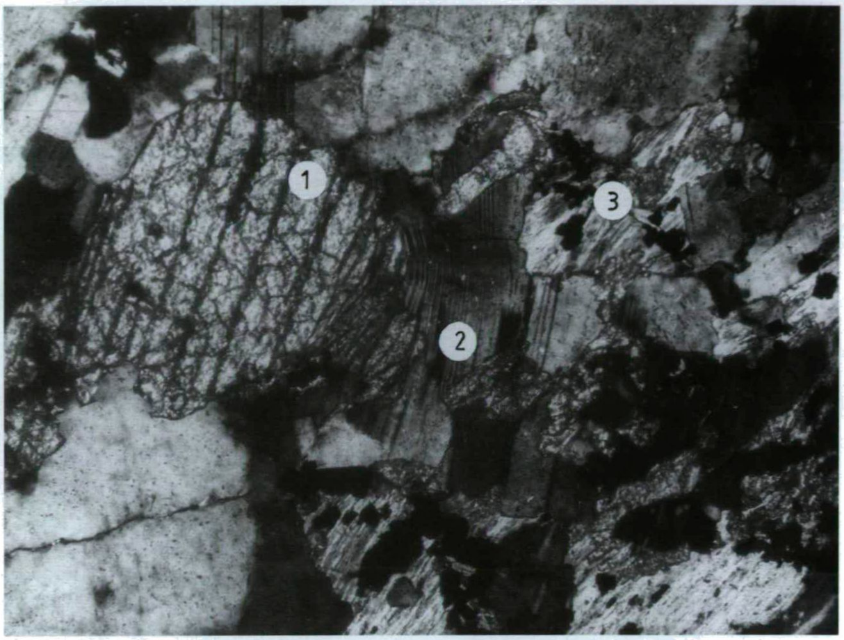

Fig. 15. ÁGK-6839 Deformed titanite and plagioclase, 90x, +N
1. titanite; 2. plagioclase; 3. chloritized biotite

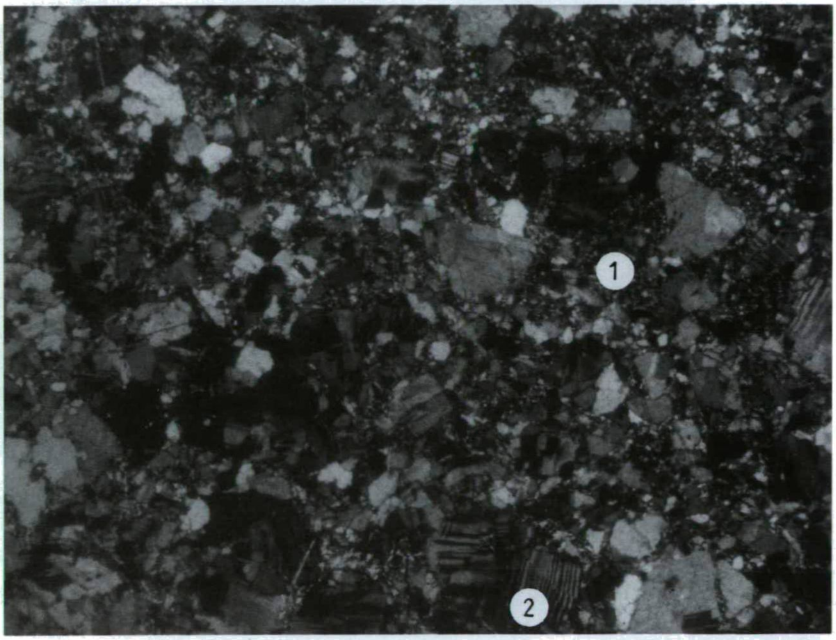

Fig. 16. ÁGK-6841 Fine-grained matrix of cataclasite, 45x, +N
1. matrix; 2. deformed plagioclase

3. Secondary textural features

Three processes can change the primary magmatic texture. These are: endomagmatic processes, weathering and tectonic deformation (MACKENZIE et al., 1984). Signs indicating *endomagmatic processes* have been mentioned above. One of them is the subsequent growth of the microcline to the detriment of the quartz and plagioclase crystals. Perforated structure of the alkaline amphibole can also be explained by these processes. Alteration of aegirine into alkaline amphibole, and that hornblende into biotite and epidote (*Fig. 13.*) can be resulted by an endomagmatic process, too. Mineral pseudomorphs of secondary, fibrous biotite can also be attributed to it. Microscopic studies alone do not make it possible to identify these secondary effects, and to distinguish them from the deuteric processes.

Weathering processes is suggested by several mineral associations. Of the mafic constituent, biotite is chloritized, bayeritized and opacitized. Pseudomorphs of biotite contain secondary rutile that can be found at the margin of the grains and along the cleavage faces. The amphibole turned into limonite and chlorite, and opaque minerals can often be found in the altered mineral associations. These alterations are resulted by meteoric water at low temperature (SHELLEY, 1993) (*Fig. 9., 10. ,13.*).

Third type of the textural alteration is resulted by *tectonic deformation.* It is often associated with weathering processes since continuity of the rocks is ceased by the deformation, and the meteoric water may induce more intensive weathering processes along the faults. In the study area, cataclasites indicate the tectonic effects. During a deformation under low temperature grains do not recrystallise but go to pieces and form a matrix around the intact grains. Rocks of the study area represent different grades of the tectonic metamorphism. Lower pressure results in deformation of the mineral grains: quartz grains show undulatory extinction, and the polysynthetic twins of the plagioclase are wavy (*Fig. 14.* and *15.*). Due to the increasing deformation effect the constituents become smaller and smaller, and form fine-grained matrix. On the basis of the ratio of the matrix, protocataclasite and cataclasite can be distinguished (*Fig. 16.*). The felsic constituents are dominant in the tectonometamorphic rocks because the mafic ones, which can be found in low (2-25) volume percentage as well, altered, and remained as chlorite-limonite aggregates and veins.

CONCLUSION

Previous classification of the granitoid rocks of the Ditró Massif was subjective and sketchy. The rock types were figured in too simplified way on the geological maps. It is a fact, however, that mapping of the granites and syenites is difficult, and changes of the modal composition may not be registered in many times.

Rocks described as granites could be divided into exact groups by more objective studies. On the basis of textural analyses, it has been shown that primary texture of the different rock types was transcribed by endomagmatic activity and weathering processes. Gaining ground of the microcline minerals to the detriment of plagioclase and quartz grains has been interpreted as an endomagmatic phenomenon since it is possible that their particular poikilitic texture and appearance in resorption embayments are results of potassium metasomatism. Dominance of the microcline is a general feature – it is characteristic for most of the petrographic groups. Alteration of mafic constituents, mainly that of hornblende, alkaline amphibole and biotite, is also frequent. Most cases, origin of these alteration processes is not known. A characteristic transcription of the primary texture of the rocks was resulted by tectonic deformation forming protocataclasites and cataclasites.

General occurrence of processes transcribing the primary texture of the studied rock types suggests that these rocks had similar development. This rock genetic problem requires other analyses; the results are to be published soon.

ACKNOWLEDGEMENTS

The authors wish to thank GYÖRGY SZAKMÁNY for his helpful discussions.

REFERENCES

ANASTASIU, N., CONSTANTINESCU, E. (1977): Feldspaţii potasici din Masivul alcalin de la Ditrău. (Potash Feldspars of the Ditrău Alkaline Massif). Dări de Seamă ale Şedinţelor Inst. Geol. Geofiz., LXIV, 13-36, Bucureşti.

ANASTASIU, N., CONSTANTINESCU, E. (1981): Feldspaţii plagioclazi din Masivul alcalin de la Ditrău. (Plagioclase feldspars from the Alkaline Massif of Ditrau). Stud. Cerc. Geol. Geofiz. Geogr. Ser. Geol.,.26/1, 83-95, Bucureşti.

IANOVICI, V. (1932): Le granite alcalin provenant de Magasbükk, Ditrău, district Ciuc (Transylvanie). Ann. Scient. Univ. Jassy, 18, 113-119.

JAKAB, GY., GARBAŞEVSCHI, N., BALLA, Z., ZAKARIÁS, L., PÉTER, J., STRUNGARU, T., HEREDEA, N., SILEANU, T., ARONESCU, M., POSTOLACHE, C., MOCANU, V., TEULEA, G., HANNICH, D., TIEPAC, I. (1987): Sinteza datelor obţinute prin prospecţiuni geologice complexe, lucrări miniere şi foraje, executate pentru minereuri de metale rare şi disperse, feroase şi neferoase în masivul de roci alcaline de la Ditrău, jud. Harghita. (Synthesis of informations from complex geological mapping, concerning especially the rare elements, ferrous and non ferrous minerals in the alkaline massif of Ditró, Hargita county). Doc. Dept. of IPEG "Harghita", Miercurea-Ciuc, Manuscript.

LE MAITRE, R. W. (1989): A Classificatiobn of Igneous Rocks and Glossary Terms, Blackwell, Oxford

MACKENZIE, W. S., DONALDSON, C. H. and GUILFORD, C. (1984): Atlas of igneous rock and their textures, Longman.

PÁL MOLNÁR, E. (1992): Petrographical characteristics of Ditró (Orotva) hornblendites, Eastern Charpathians, Transylvania (Romania): a Preliminary describtion. Acta Min. Petrol., Szeged, 33, 67-80.

PÁL MOLNÁR, E. (1994a): Petrographical characteristics of Ditró (Orotva) diorites, Eastern Charpatians, Transylvania (Romania). Acta Min. Petr., Szeged, **34**, 95-109.

PÁL MOLNÁR, E. (1994b): Adalékok a Ditrói szienitmasszívum szerkezeti és kőzettani ismeretéhez (Contributions on structural and petrological knowledge of Ditró Syenite Massif.), MTA SZAB Competition, Manuscript, 2-45.

SHELLEY, D.(1993): Igneous and Metamorphic rocks under the Microscope, Chapman & Hall.

STRECKEISEN, A. (1954): Das Nephelinsyenit-Massiv von Ditro (Siebenbürgen), II. Teil. Schweiz. Min. Petr. Mitt., 34, 336-409.

Manuscript received 9 August, 1998.

Acta Mineralogica-Petrographica,.Szeged, XXXIX, 49–76, 1998

GEOCHEMISTRY, TECTONIC SETTING AND CLASSIFICATION OF SOME GRANITOIDS, GEBEL ABU EL-HASAN, NORTH EASTERN DESERT, EGYPT

M. S. ATIA*, M. L. KABESH** and M. DAWOUD*

* Geology Dept., Faculty of Science, Menoufia University
** Earth Sciences Dept., National Research Centre, Cairo

ABSTRACT

Fifty six new chemical analyses for major and selected trace and REE of some granitoid rocks from Abu El-Hasan pluton, North Eastern Desert are presented. The petrochemical and geochemical characters of these granitoids. The studied rocks have a calc-alkaline to rather alkaline nature. Their chemical features reveal that they are well differentiated with an average THORNTON and TUTTLE D. I. 95. 83. These granitoids are low-calcium somewhat potassic rather than sodic and peraluminous. According to the different chemical classifications, Abu El-Hasan granitoids fall in the fields of granite, alkali granite, alkali feldspare granite, syenogranite and monzogranite. Variation and discrimination diagrams of major, selected trace and REE suggest that Abu El-Hasan granitoids are derived from partial fusion of the upper mantle with some crustal melt contribution. The source magma was subjected to high fractionation during successive pulses. The studied granitoids mostly pertain to the syn-and late-to post-orogenic highly fractionated calc-alkaline-granite suite. The younger granitoids (late-to post-orogenic) formed under extensional enviroment, while the older (synorogenic) are comparable with the compessional suite of PETRO et al., (1979).

INTRODUCTION

Abu El-Hasan pluton constitutes an igneous province characterized by high relief. It lies in the northern part of the Eastern Desert of Egypt rising to 1558 m above the sea level. The granitoids of Abu-Hasan are intruded into an older igneous-metamorphic sequence including meta-sediments and meta-volcanics, serpentinites and metagabbros. (*Fig. 1.*)

Broadly, the granitoid rocks constitute about 40% of the Egyptian Basement. They are classified into two major groups, víz.: Older Granites and Younger Granites (EL-RAMLY, 1972; EL-GABY, 1975; HASHAD, 1980; HUSSEIN ET AL., 1982; EL-GABY et al., 1988; HASAN and HASHAD, 1990). The Older granitoids (850-630 Ma, HASAN and HASHAD, 1990) cover about 26.7% of the total basement area. They are synorogenic (EL-SHAZLY, 1964), syntectonic (SABET, 1972) and calc-alkaline mesozonal (STERN et al., 1984). HUSSEIN et al., (1982) classified them into G-I-(subdection-related) and G-II-(suturerelated).

The younger granites constitute about 16.2% of the Basement in the Eastern Desert (STERN, 1979) and are mainly concentrated in its northern part. They are late to postorogenic (620-530 Ma, HASAN and HASHAD, 1990). These granites are late-orogenic (EL-SHAZLY, 1964), late to post-tectonic (EL-RAMLY, 1964), late to post-tectonic (EL-RAMLY, 1972), epizonal (STERN et al., 1984) and alkaline to peralkaline intraplate anorogenic (G-II granites), according to HUSSEIN et al., (1982).

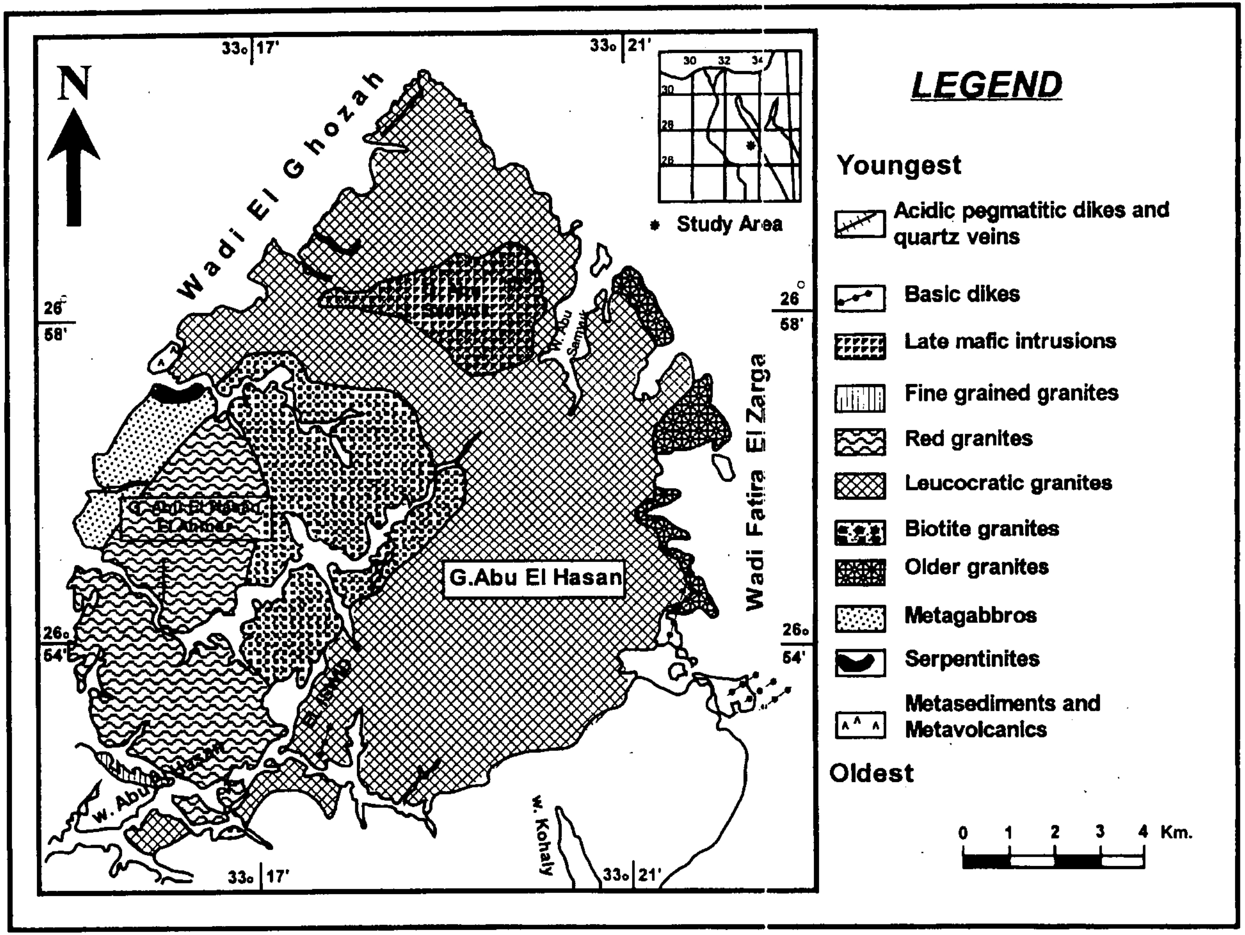

Fig. 1. Geological Map of Abu El-Hasan Pluton

The present study deals with the petrography, geochemistry, tectonic setting and classification of Abu El-Hasan granitoid pluton in the northern part of the Pan-African belt (*Fig. 1.*)

The granite in the present area were considered as Lower Gattarian on Schurmann's map (1966) of the Precambrian along the Gulf of Suez and the northern part of the Red Sea.

SABET et al., (1972) and ZALATA (1972) studied the geology of the basement rocks in the northern parts of Gebel El-Shayeb and Safaga sheets, Eastern Desert. According to their map, the present area comprises mainly calc-alkaline granite and alkaline granite. These authors did not give any chemical analyses of the granites in the present area. ZALATA (op. cit), gave only the modal analysis of one sample of Abu El-Hasan pluton. Eastern and South Western Desert of Egypt to the scale of 1:1.000.000, the present area was recorded as younger granitoids. According to the geological map of the Quena quadrangle published by the Geological Survey of Egypt in scale of 1:500.000, the present area is covered by younger granitoids.

HILMY et al., (1997) gave a petrological study of Abu El-Hasan area, Eastern Desert, Egypt, with special emphasis of the origin of the granitic rocks. According to Hilmy et al., (op. cit) the present area includes mesozonal granites (granodiorites – quartz diorite) and epizonal granites (phase II, phase III). These authors presented the chemical analyses of 19 granitic samples and 11 biotites for their major and some trace elements. More recently, TAKLA et al. (1997), Studied the Precambrian rock units of Wadi Safaga area, south-east the present area. These rock units comprise meta-volcanics, older granitoids, younger gabbros and younger granites. According to these authors (op. cit), the older granitoids are essentially calc-alkaline, island arc granites, while the younger granites represent alkaline post-organic type. They further added that the older granitoids pertain to the I-type granites and were formed in an arc environment, while the younger granites could be comparable with the I-type granite and with the extensional suites of PETRO et al., (1979).

Details of field observations, fracture analysis and modal classification of the granitoids of the present area are given by DAWOUD (1995).

CHARACTERIZATION OF THE GRANITOIDS

The present study deals with the petrography, geochemistry, tectonic setting and classification of the granitoids of Abu El-Hasan pluton.

PETROGRAPHY OF THE GRANITOID ROCKS

The granitoid rocks of Abu El-Hasan pluton include older and younger groups. The older granitoids occur in the eastern part of the pluton as minor outcrops. They are represented by biotite-hornblended granodiorite. Under the microscope the granodiorite is composed mainly of plagioclase, biotile, k-feldspar, with minor quartz and hornblende. Accessory minerals are opaques, apatite, zircon, sphene and allanite. Plagioclase occurs as subhedral to anhedral laths and shows wide variation in composition from ablite, oligoclase to sodic andesine (An_{6-35}). It also shows well-developed zoning and twinning (Carlsbad, albite, combined albite-Carlsbad, pericline and Baveno are present).

Plagioclase phenocrysts, up to 1.5 cm across may be corroded by quartz and microcline. Micrographic and myrmekitic textures are produced as a result of interaction between plagioclase, quartz and K-feldspar. Plagioclase may be rimmed and replaced by K-feldspar.

K-feldspars occur as xenomorphic crystals of orthoclase or microline. They show different types of perthitic textures (as string, vein and patch). Biotite is the main mafic mineral. It shows strong pleochroism from straw yellow to dark brown, some may exhibit grene colour. It may be chloritized and epidotized. Hornblende is found in small amount. It occurs in large crystals about 0.7 cm in length and shows pleochroism from yellowish green to bluish green and brown.

The younger granitoids occupy the major part of Abu El-Hasan pluton. Broadly, they comprise the following types: biotite granite, leucocratic granite, fine-grained granite and red granite. Petrographically biotite granites consist of K-feldspar, plagioclase, quartz and biotite. Accessory minerals are zircon, sphene, opaques, allanite and apatite. K-feldspar usually occurs as perthitic orthoclase which may be string, patch or braid perthite. K-feldspar may show carlsbad twinning. Plagioclase varies in composition from albite to oligoclase (An_{0-18}). They show albite, combined albite-Carlsbad and pericline twinning, also zoning may be present with more saussuritized core. The contact between K-feldspar and plagioclase may show fine blebs and vermicules directed to the plagioclase forming the myrmekitic texture. Biotite is the sole mafic. It suffered from tearing, chloritization, and vermiculitization. It shows brown colour and strong pleochroism from straw yellow to dark brown, but green and reddish brown flakes may be present.

Leucocratic granites microscopically are formed by K-feldspar, quartz and plagioclase with negligible amounts of biotite and hornblende. K-feldspar occurs as perthitic orthoclase. Plagioclase ranges in composition from albite to oligoclase and it occurs as perthitic orthoclase. Plagioclase in composition ranges from albite to oligoclase (An4-14) with albite, Carlsbad and albite-Carlsbad twinning. Accessories are mainly opaques, apatite, allanite and zircon.

Red granites are microscopically formed of K-feldspar, quartz, plagioclase and minor biotite. Accessories include opaques, zircon and apatite. K-feldspar occurs as perthitic orthoclase. It is usually intergrown with albite giving patch, vein, string and braid perthite.

Plagioclase in composition ranges from albite to oligoclase (An_{6-16}). Biotite is pleochroic from greenish yellow, pale yellow to dark brown. It is frequently altered to chlorite and iron oxides.

Fine-grained granites are microscopically formed by K-feldspar, plagioclase and biotite. K-feldspars are represented by altered orthoclase and perthite. Plagioclase is albite to oligoclase (An_{8-16}). It is usually saussuritized and exhibits albite, Carlsbad and combined albite-Carlsbad twinning, Biotite forms scattered delicate flakes suffering from severe tearing and alteration to chlorite and iron osides. Accessories are zircon, allanite and apatite.

MAJOR ELEMENTS CHEMISTRY

Microprobe analyses for major elements were carried out on the JEOL probe JXA-800 of Institute für Mineralogie and Institute für Geologie and Palaontologie, Salzburg University, Austria.

Table 1 presents the chemical analyses of the studied granitoids for major elements.

TABLE 1

Chemical analyses of Abu El Hasan granitoids. Major Elements (WT%)

S. No.	1. R.G.	2. R.G.	3. R.G.	4. R.G.	5. R.G.	6. R.G.	7. R.G.	8. R.G.	9. R.G.	10. F.G.G.	11. F.G.G.
D.I.	95.84	95.79	94.73	93.04	94.01	96.96	94.63	97.04	94.19	92.38	95.61
SiO_2	76.07	75.62	72.81	73.98	74.77	79.09	74.04	77.25	75.03	73.93	75.74
TiO_2	0.10	0.11	0.10	0.16	0.09	0.11	0.09	0.08	0.10	0.15	0.06
Al_2O_3	12.40	12.69	13.30	13.30	12.46	12.17	12.61	12.52	12.08	12.66	12.80
Fe_2O_3	0.94	1.64	1.22	1.35	1.66	1.36	1.32	1.14	0.86	1.55	0.55
MnO	0.01	0.03	0.01	0.02	0.05	0.02	0.03	0.02	0.01	0.04	0.01
MgO	0.02	0.03	0.05	0.13	0.00	0.08	0.04	0.04	0.05	0.07	0.08
CaO	0.16	0.34	0.29	0.53	0.50	0.38	0.29	0.19	0.24	0.64	0.40
Na_2O	3.87	4.50	4.31	3.99	3.62	3.36	4.30	3.93	3.84	4.36	4.29
K_2O	4.72	4.30	5.36	4.68	5.13	4.72	4.71	4.72	4.58	3.99	4.55
P_2O_5	0.03	0.03	0.02	0.04	0.02	0.03	0.03	0.01	0.02	0.03	0.01
LOI	0.81	0.86	0.77	1.44	0.83	0.67	0.88	0.92	0.67	1.08	0.74
Total	99.13	100.15	98.34	99.62	99.13	101.99	98.34	100.82	97.48	98.50	99.23

S. No.	12. F.G.G.	13. F.G.G.	14. F.G.G.	15. F. G.G.	16. L. G.	17. L.G.	18. L.G.	19. L.G.	20. L. G.	21. L.G.	22. L.G.
D.I.	96.10	94.36	94.07	96.29	98.08	91.93	93.44	97.80	95.11	95.16	97.56
SiO_2	76.84	74.47	75.35	77.27	78.43	72.70	74.00	79.39	78.81	75.60	79.06
TiO_2	0.06	0.13	0.04	0.08	0.07	0.11	0.10	0.09	0.10	0.12	0.07
Al_2O_3	12.74	12.81	12.47	12.90	13.25	12.87	12.80	12.09	11.37	12.37	11.48
Fe_2O_3	0.81	2.02	0.65	0.94	0.99	1.44	1.22	1.34	1.06	1.42	0.31
MnO	0.01	0.05	0.00	0.01	0.02	0.02	0.03	0.01	0.02	0.03	0.01
MgO	0.07	0.11	0.07	0.06	0.02	0.15	0.04	0.05	0.11	0.14	0.12
CaO	0.54	0.45	0.53	0.36	0.38	0.74	0.49	0.31	0.55	0.24	0.19
Na_2O	4.07	3.45	4.06	4.08	3.81	4.25	3.99	3.37	3.36	3.98	3.31
K_2O	4.66	5.68	4.42	4.34	4.97	4.57	4.76	4.89	4.15	4.63	4.93
P_2O_5	0.02	0.02	0.01	0.02	0.02	0.03	0.03	0.02	0.04	0.04	0.02
LOI	0.97	1.16	1.21	0.71	0.62	0.74	0.84	0.70	1.55	0.78	0.65
Total	100.81	100.34	98.81	100.77	102.58	97.62	98.30	102.26	101.12	99.35	100.15

S. No.	23. L.G.	24. L. G.	25. L. G.	26. L. G.	27. L. G.	28. L. G.	29. L. G.	30. L. G.	31. L. G.	32. L. G.	33. L. G.
D.I.	96.45	96.57	97.13	94.49	97.59	96.53	95.37	94.03	93.43	95.50	94.21
SiO_2	78.43	76.04	76.04	74.28	77.53	76.10	76.36	75.36	74.19	76.82	74.42
TiO_2	0.07	0.05	0.05	0.05	0.07	0.05	0.12	0.14	0.19	0.12	0.07
Al_2O_3	12.27	12.73	12.55	12.35	12.37	13.08	11.88	11.76	12.79	12.50	12.66
Fe_2O_3	1.20	1.12	1.04	0.48	0.83	0.94	2.12	0.96	1.28	1.15	0.65
MnO	0.05	0.00	0.02	0.01	0.01	0.05	0.02	0.01	0.02	0.02	0.02
MgO	0.04	0.08	0.00	0.00	0.05	0.05	0.00	0.00	0.00	0.06	0.04
CaO	0.44	0.10	0.07	0.22	0.13	0.23	0.39	0.23	0.54	0.40	0.36
Na_2O	3.87	4.29	4.55	4.30	4.06	4.20	4.40	3.74	3.93	3.74	4.06
K_2O	4.19	4.53	4.04	4.46	4.63	4.72	3.86	4.41	4.71	4.65	4.72
P_2O_5	0.02	0.03	0.01	0.01	0.01	0.02	0.02	0.03	0.07	0.02	0.02
LOI	0.92	0.60	0.91	1.49	0.70	0.70	0.84	0.87	1.32	1.07	0.91
Total	101.50	99.57	97.65	97.65	100.39	100.14	100.01	97.51	99.04	100.55	97.93

S. No.	34. L.G.	35. L.G.	36. B.G.	37. B.G.	38. B.G.	39. B.G.	40. B.G.	41. B.G.	42. B.G.	43. B.G.	44. B.G
D.I.	95.62	95.52	91.10	93.87	90.12	90.14	93.56	92.19	90.24	91.59	92.05
SiO_2	76.13	76.43	72.88	73.99	71.72	70.27	74.42	75.53	73.12	74.28	73.26
TiO_2	0.07	0.13	0.21	0.12	0.15	0.14	0.06	0.16	0.14	0.16	0.15
Al_2O_3	13.01	13.85	13.18	13.57	13.14	13.45	12.08	12.59	12.86	12.75	13.57
Fe_2O_3	1.06	1.13	2.32	1.20	1.50	1.72	0.72	1.64	1.47	1.72	1.57
MnO	0.02	0.01	0.05	0.02	0.04	0.04	0.03	0.04	0.05	0.04	0.04
MgO	0.07	0.13	0.15	0.10	0.21	0.27	0.05	0.17	0.17	0.22	0.19
CaO	0.35	0.26	0.81	0.46	0.90	0.75	0.51	0.92	0.82	0.91	0.90
Na_2O	4.03	3.69	4.19	3.69	3.95	4.28	3.71	3.76	3.66	4.00	3.98
K_2O	4.62	4.79	4.33	5.35	4.81	4.95	4.94	4.24	4.48	4.26	4.98
P_2O_5	0.02	0.04	0.03	0.04	0.04	0.05	0.02	0.04	0.04	0.05	0.04
LOI	1.07	1.28	0.74	0.75	0.73	1.28	0.47	0.75	0.81	0.46	0.98
Total	100.45	101.74	98.89	99.29	97.19	97.20	97.01	99.84	97.62	98.85	99.66

S. No.	45. B.G.	46. B.G.	47. B.G.	48. O.G.	49. O.G.	50. O.G.	51. O.G.	52. O.G.	53. O.G.	54. O.G.	55. O.G.	56. O.G.
D.I.	92.01	92.33	92.71	86.95	87.49	88.36	73.84	90.38	90.00	90.23	87.68	90.63
SiO_2	74.78	73.54	74.07	69.94	70.58	72.59	67.63	73.28	72.44	73.68	70.69	72.78
TiO_2	0.15	0.13	0.16	0.49	0.35	0.39	0.65	0.23	0.20	0.20	0.22	0.15
Al_2O_3	13.19	13.06	13.81	14.37	14.68	14.13	14.93	13.91	13.75	13.59	14.23	13.47
Fe_2O_3	1.37	1.41	1.63	2.49	1.92	2.06	3.34	1.66	1.50	1.60	1.58	1.51
MnO	0.04	0.04	0.04	0.08	0.05	0.06	0.09	0.05	0.03	0.05	0.03	0.03
MgO	0.20	0.15	0.28	0.63	0.58	0.60	1.00	0.37	0.32	0.35	0.31	0.19
CaO	0.92	0.71	0.84	1.33	1.52	1.48	2.04	0.98	0.87	1.10	1.26	0.89
Na_2O	3.80	3.78	4.17	5.11	4.59	4.15	5.20	3.86	3.87	3.77	3.83	3.68
K_2O	4.47	5.01	4.67	3.75	4.16	4.11	3.36	4.50	4.55	4.46	4.70	4.87
P_2O_5	0.05	0.04	0.04	0.12	0.08	0.11	0.22	0.06	0.07	0.06	0.08	0.06
LOI	0.60	0.96	0.73	0.74	0.52	0.94	0.84	1.36	1.43	0.95	0.78	0.78
Total	99.57	98.83	100.44	99.05	99.03	100.62	99.30	100.26	99.03	99.81	97.71	98.41

Late-to post-orogenic granites:

Red granites	R.G.	1-9
Fine-grained granites	F.G.G.	10-15
Leucoeratic granites	L.G.	16-35
Biotite quanites	B.G.	36-47

Syn-orogenic granites

Biotite-Hornblende-granodiorite

	O.G.	48-56
Average	D.I.	95-83

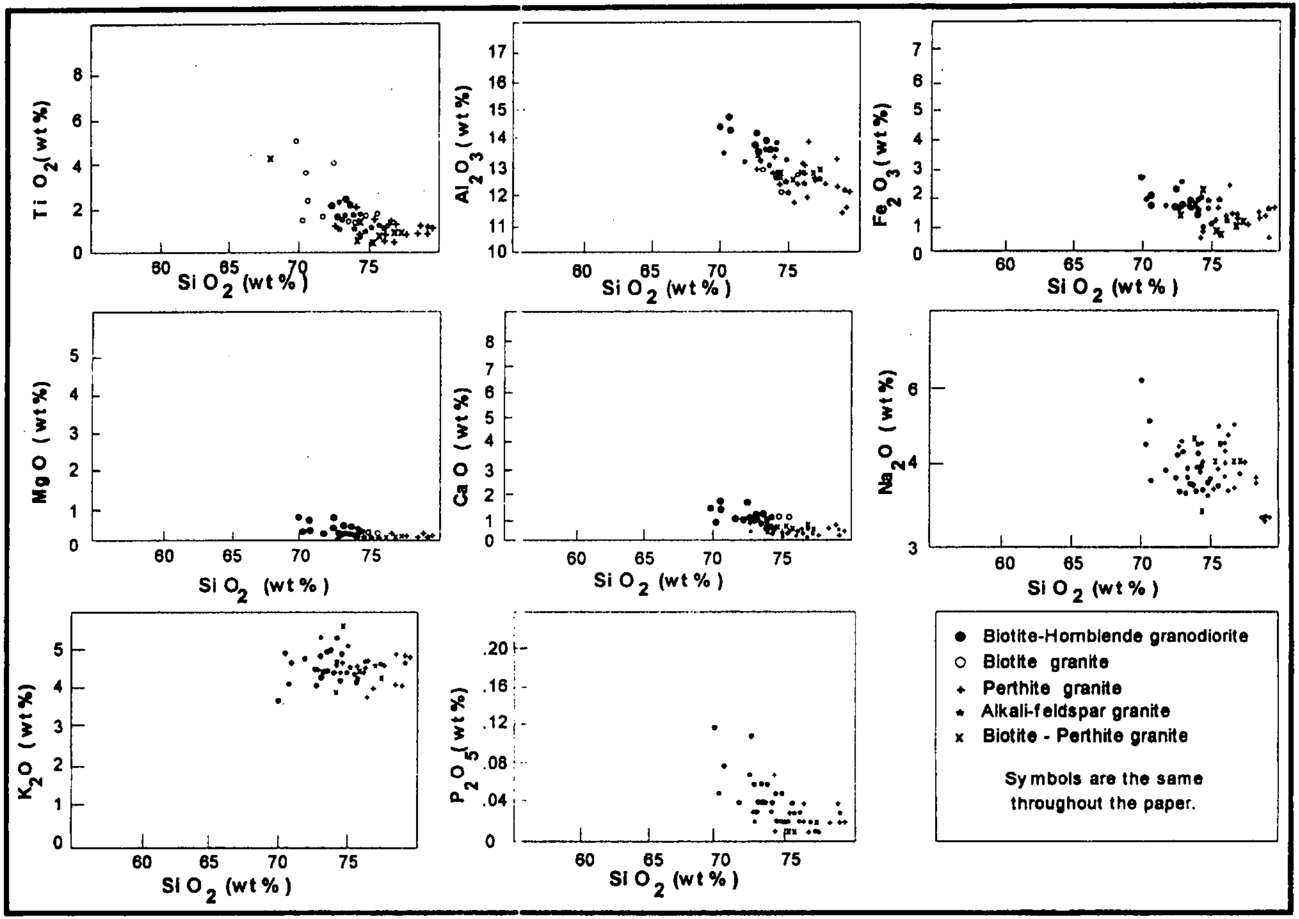

Fig. 2. Harker Variation Diagrams

MAJOR ELEMENT CHEMISTRY

Harker Variation Diagrams: The major elements are routinely plotted against silica (*Fig. 2*). It is clear that alumina, titania, magnesia, iron and calcium oxides show more or less well defined negative relations with silica, while sodium and phosphorous show a rough negative correlation. Potassium shows well-defined positive correlation with silica.

CaO-Na_2O-K_2O triangular diagram: shows that the studied granitoids are somewhat potassic rather than sodic (*Fig. 3.*). Fe_2O_3-(t)-MgO-CaO trianglar diagram shows that most of the samples plot near the Fe_2O_3-CaO side line and close to Fe_2O_3 apex (*Fig. 4.*)

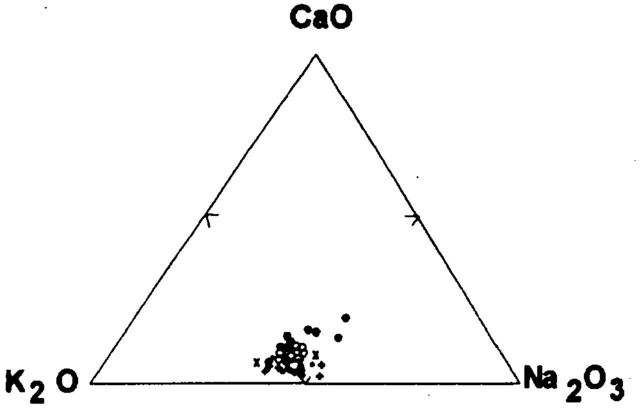

Fig. 3. CaO-Na_2O-K_2O Diagram

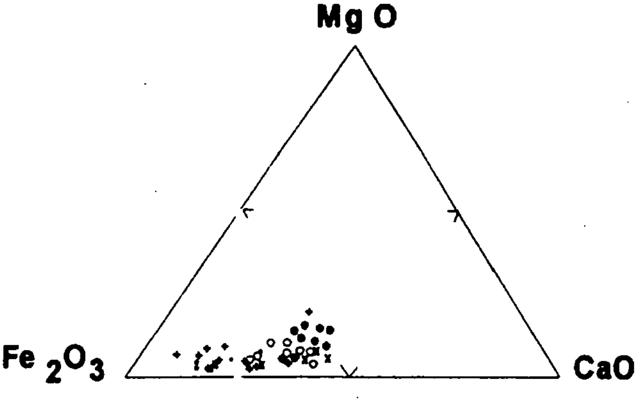

Fig. 4. Fe_2O_3+-MgO-CaO Diagram

Molecular Al_2O_3-CaO-Alkalis triangular diagram proposed by SHAND (1951) distinguished between peraluminous, metaluminous and peralkaline rocks. The studied granitoids plot in the field of peraluminous rocks close to the border with the metaluminous (*Fig. 5.*).

Calc-alkaline/alkaline nature: On the diagram of WRIGHT (1969), is obvious that the studied granitoids plot in the calc-alkaline and alkaline fields (*Fig. 6.*)

CIPW norm values are calculated by Newpet computer program and listed in Table 2.

S. No.	Rock Un.	Qz.	Cor.	Or.	Ab.	An.	Diop.	Woll.	Hyp.	Mag.	Chrom.	Hem.	Ilm.	Sphene	Rutile	Apatite
36	B.G.	30.06	0.2	25.59	35.45	3.82	0	0	0.37	0	0	2.32	0.11	0	0.15	0.07
37		31.03	0.96	31.62	31.22	2.02	0	0	0.25	0	0	1.2	0.04	0.12	0.1	0.09
38		28.27	0	28.43	33.42	3.92	0	0	0.52	0	0	1.5	0.09	0.2	0.02	0.09
39		24.67	0	29.26	36.21	2.87	0.15	0	0.6	0.	0	1.72	0.09	0.23	0	0.12
40		32.97	0	29.2	31.39	1.72	0.27	0.1	0	0	0	0.72	0.06	0.06	0	0.05
41		35.32	0.24	25.06	31.81	4.3	0	0	0.42	0	0	1.64	0.09	0	0.11	0.09
42		32.79	0.6	26.48	30.97	3.81	0	0	0.42	0	0	1.47	0.11	0	0.08	0.09
43		32.57	0.03	25.18	33.84	4.19	0	0	0.55	0	0	1.72	0.09	0	0.11	0.12
44		28.95	0.09	29.43	33.67	4.2	0	0	0.47	0	0	1.57	0.09	0	0.1	0.09
45		33.44	0.55	26.42	32.15	4.24	0	0	0.5	0	0	1.37	0.09	0	0.1	0.12
46		30.74	0.22	29.61	31.98	3.26	0	0	0.37	0	0	1.41	0.09	0	0.08	0.09
47		29.83	0.47	27.6	35.28	3.91	0	0	0.7	0	0	1.63	0.09	0	0.11	0.09
48	O.G.	22.55	0	22.16	43.24	5.2	0	0	1.57	0	0	2.49	0.17	0	0.22	0.28
49		24.06	0.06	24.59	38.84	7.02	0	0	1.44	0	0	1.92	0.11	0	0.29	0.19
50		28.96	0.43	24.29	35.11	6.62	0	0	1.49	0	0	2.06	0.13	0	0.32	0.26
51		19.54	0	19.86	44	7.48	0	0	2.39	0	0	3.34	0.19	0.85	0.2	0.52
52		31.12	1.05	26.6	32.66	4.47	0	0	0.92	0	0	1.66	0.11	0	0.17	0.14
53		30.37	1.05	26.89	32.74	3.86	0	0	0.8	0	0	1.5	0.06	0	0.17	0.17
54		31.97	0.71	26.36	31.9	5.07	0	0	0.87	0	0	1.6	0.11	0	0.14	0.14
55		27.49	0.74	27.78	32.41	5.73	0	0	0.77	0	0	1.58	0.06	0	0.19	0.19
56		30.71	0.67	28.78	31.14	4.02	0	0	0.47	0	0	1.51	0.06	0	0.12	0.14

S. No.	Rock Un.	Qz.	Cor.	Or.	Ab.	An.	Diop.	Woll.	Hyp.	Mag.	Chrom.	Hem.	Ilm.	Sphene	Rutile	Apatite
16	L.G.	36.46	0.96	29.38	32.24	1.75	0	0	0.05	0	0	0.99	0.04	0	0.05	0.05
17		28.96	0	27.01	35.96	2.55	0.49	0	0.15	0	0	1.44	0.04	0.12	0	0.07
18		31.55	0.27	28.13	33.76	2.24	0	0	0.1	0	0	1.22	0.06	0	0.07	0.07
19		40.39	0.74	28.9	28.51	1.41	0	0	0.12	0	0	1.34	0.02	0	0.08	0.05
20		42.15	0.45	24.53	28.43	2.74	0	0	0.27	0	0	1.06	0.04	0	0.08	0.09
21		34.12	1.37	27.37	33.67	0.93	0	0	0.35	0	0	1.42	0.06	0	0.09	0.09
22		40.41	0.4	29.14	28.01	0.81	0	0	0.3	0	0	0.31	0.02	0	0.06	0.05
23		38.94	0.62	24.77	32.74	2.05	0	0	0.1	0	0	1.2	0.11	0	0.01	0.05
24		33.5	0.66	26.77	36.3	0.3	0	0	0.2	0	0	1.12	0	0	0.05	0.07
25		34.75	0.59	23.88	38.5	0.28	0	0	0	0	0	1.04	0.04	0	0.02	0.02
26		31.75	0.07	26.36	36.38	1.03	0	0	0	0	0	0.48	0.02	0	0.04	0.02
27		35.87	0.47	27.37	34.35	0.58	0	0	0.12	0	0	0.83	0.02	0	0.06	0.02
28		33.09	0.69	27.9	35.54	0.01	0	0	0.12	0.02	0	0.93	0.09	0	0	0.05
29		35.33	0	22.81	37.23	1.27	0	0.08	0	0	0	2.12	0.04	0.24	0	0.05
30		36.32	0.49	26.07	31.64	0.95	0	0	0	0	0	0.96	0.02	0	0.13	0.07
31		32.34	0.41	27.84	33.25	2.22	0	0	0	0	0	1.28	0.04	0	0.17	0.17
32		36.38	0.64	27.48	31.64	1.85	0	0	0.15	0	0	1.15	0.04	0	0.1	0.05
33		31.96	0.27	27.9	34.35	1.66	0	0	0.1	0	0	0.65	0.04	0	0.05	0.05
34		34.21	0.79	27.31	34.1	1.61	0	0	0.17	0	0	1.06	0.04	0	0.05	0.05
35		35.99	2.22	28.31	31.22	1.03	0	0	0.32	0	0	1.13	0.02	0	0.12	0.09

S. No.	Rock Un.	Qz.	Cor.	Or.	Ab.	An.	Diop.	Woll.	Hyp.	Mag.	Chrom.	Hem.	Ilm.	Sphene	Rutile	Apatite
36	B.G.	30.06	0.2	25.59	35.45	3.82	0	0	0.37	0	0	2.32	0.11	0	0.15	0.07
37		31.03	0.96	31.62	31.22	2.02	0	0	0.25	0	0	1.2	0.04	0.12	0.1	0.09
38		28.27	0	28.43	33.42	3.92	0	0	0.52	0	0	1.5	0.09	0.2	0.02	0.09
39		24.67	0	29.26	36.21	2.87	0.15	0	0.6	0.	0	1.72	0.09	0.23	0	0.12
40		32.97	0	29.2	31.39	1.72	0.27	0.1	0	0	0	0.72	0.06	0.06	0	0.05
41		35.32	0.24	25.06	31.81	4.3	0	0	0.42	0	0	1.64	0.09	0	0.11	0.09
42		32.79	0.6	26.48	30.97	3.81	0	0	0.42	0	0	1.47	0.11	0	0.08	0.09
43		32.57	0.03	25.18	33.84	4.19	0	0	0.55	0	0	1.72	0.09	0	0.11	0.12
44		28.95	0.09	29.43	33.67	4.2	0	0	0.47	0	0	1.57	0.09	0	0.1	0.09
45		33.44	0.55	26.42	32.15	4.24	0	0	0.5	0	0	1.37	0.09	0	0.1	0.12
46		30.74	0.22	29.61	31.98	3.26	0	0	0.37	0	0	1.41	0.09	0	0.08	0.09
47		29.83	0.47	27.6	35.28	3.91	0	0	0.7	0	0	1.63	0.09	0	0.11	0.09
48	O.G.	22.55	0	22.16	43.24	5.2	0	0	1.57	0	0	2.49	0.17	0	0.22	0.28
49		24.06	0.06	24.59	38.84	7.02	0	0	1.44	0	0	1.92	0.11	0	0.29	0.19
50		28.96	0.43	24.29	35.11	6.62	0	0	1.49	0	0	2.06	0.13	0	0.32	0.26
51		19.54	0	19.86	44	7.48	0	0	2.39	0	0	3.34	0.19	0.85	0.2	0.52
52		31.12	1.05	26.6	32.66	4.47	0	0	0.92	0	0	1.66	0.11	0	0.17	0.14
53		30.37	1.05	26.89	32.74	3.86	0	0	0.8	0	0	1.5	0.06	0	0.17	0.17
54		31.97	0.71	26.36	31.9	5.07	0	0	0.87	0	0	1.6	0.11	0	0.14	0.14
55		27.49	0.74	27.78	32.41	5.73	0	0	0.77	0	0	1.58	0.06	0	0.19	0.19
56		30.71	0.67	28.78	31.14	4.02	0	0	0.47	0	0	1.51	0.06	0	0.12	0.14

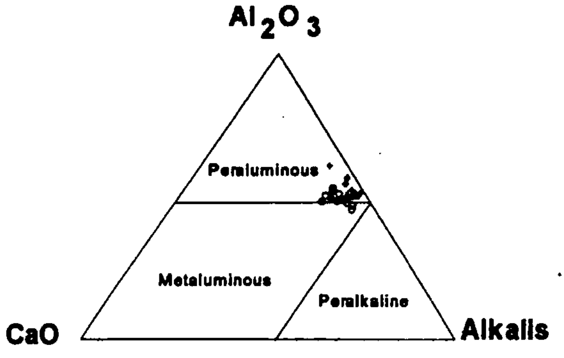

Fig. 5. Molecular Al_2O_3-CaO-Alkalis diagram

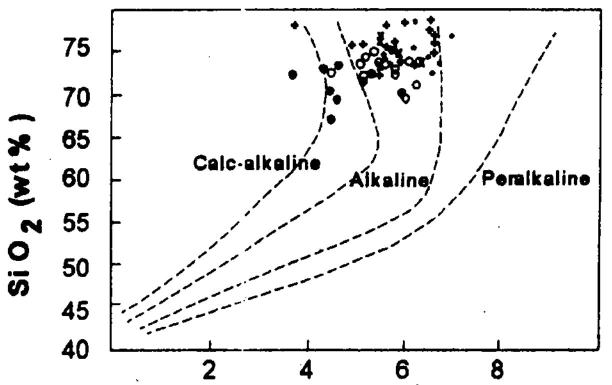

Fig. 6. Wright's Alkalinity diagram

An-Ab-Or diagram: IRVINE and BARAGAR (1971) proposed a classification of igneous rocks based on normative anorthite, albite and orthoclase proportions. The studied rocks plot in the field of average rocks close to the potassic series boundary rather than the sodic series (*Fig. 7.*).

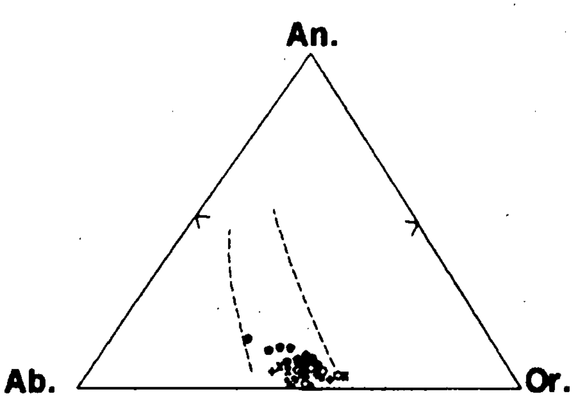

Fig. 7. An-Ab-Or Diagram (IRVINE and BARAGAR 1971)

O-Ab-Or diagram: The studied rocks are plotted on TUTTLE and BOWEN (1958) ternary diagram whereby most of the granitoids fall within the range 0.5 to 7 Kb water vapour pressure while some samples were mostly formed under higher water vapour pressure (10 Kb) and in turn deeper level (*Fig. 8.*).

Chemical Classification: Such classification follows two ways, the first depends on the major oxides or molecular values, the second depends on the calculated molecular norms.

O'CONNOR (1965) classification: This diagram is based on the norm proportions of An, Ab, and Or. Abu El-Hasan granitoids are classified as granites. (*Fig. 9.*)

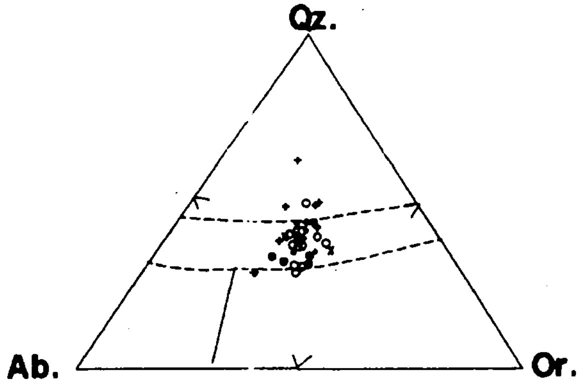

Fig. 8. Qz-Ab-Or Diagram (TUTTLE and BOWEN 1958)

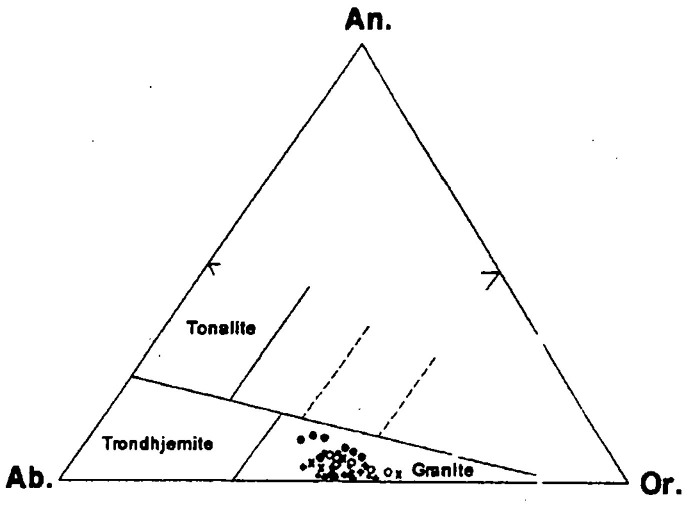

Fig. 9. An-Ab-Or Diagram (O'CONNOR, 1965)

STRECKEISEN (1976b): This diagram is based on the proportions of Or, Ab and An. Most of the studied granitoids plot in the alkali feldspar granite and the alkali granite fields, while some samples plot in the fields of syenogranite and monzogranite (*Fig. 10.*).

MIDDLEMOST (1985) classification: This diagram shows the relation of Na_2O+K_2O against SiO_2, where by Abu El-Hasan granitoids plot in the alkali feldspar granite and the granite fields (*Fig. 11.*).

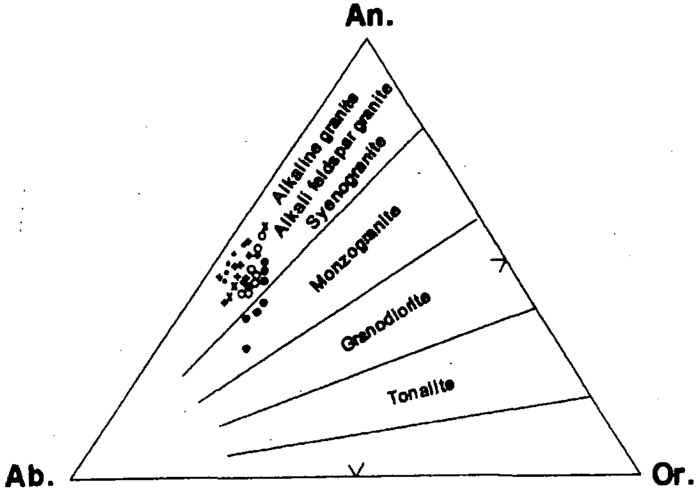

Fig. 10. An-Ab-Or Diagram (STRECKEISEN, 1976b)

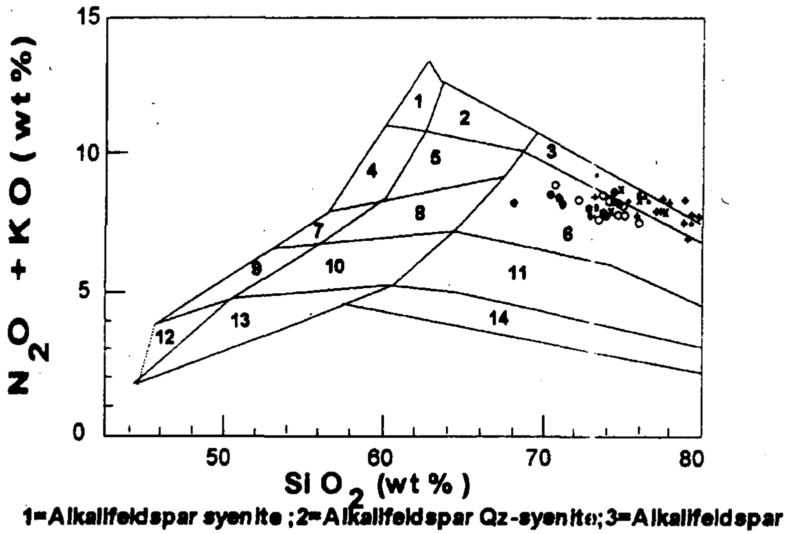

Fig. 11. MIDDLEMOST's (1985) Classification

In the present study, some trace elements are analyzed using XRD and some REE using NAA techniques. Analyses were carried out at the Institute für Mineralogie, Salzburg University, Austria. Results are given in Table 3.

TABLE 3

Trace And REE (PPM)

S. No.	1	2	3	4	5	6	7	8	9	10	11
Sc	1	1	0	2	2	0	0	0	0	0	1
Rb	146	133	153	142	150	111	151	118	114	138	231
Cs	0.77	0.72	0.00	2.65	0.00	0.00	0.00	0.00	0.65	0.00	1.47
Ba	192	192	224	377	122	157	226	162	180	179	75
Sr	40	45	55	78	34	40	51	43	51	64	15
Ga	24	25	25	22	24	22	25	25	24	25	31
Ta	2.29	3.10	0.00	2.42	4.10	0.00	0.00	0.00	0.00	0.00	5.30
Nb	41.0	42.0	36.0	34.0	50.0	36.0	35.0	38.0	30.0	45.0	54.0
Hf	7.19	8.93	0.00	8.26	7.62	0.00	0.00	0.00	0.00	0.00	7.30
Zr	148	160	110	192	137	146	138	138	148	204	98
Y	36	42	27	35	47	23	27	27	25	40	46
Th	24.00	19.00	24.00	26.00	20.00	19.00	16.00	16.00	16.00	29.00	26.00
U	7.00	6.00	8.00	7.00	8.00	5.00	5.00	5.00	5.00	8.00	8.00
La	47.71	37.42	0.00	75.21	35.79	0.00	0.00	0.00	0.00	0.00	26.38
Ce	99.86	86.44	63.00	143.43	92.40	75.00	42.00	42.00	47.00	94.00	37.00
Nd	56.06	54.80	0.00	63.62	66.00	0.00	0.00	0.00	0.00	0.00	40.80
Sm	23.16	23.94	0.00	22.09	21.91	0.00	0.00	0.00	0.00	0.00	19.66
Eu	0.54	0.49	0.00	0.94	1.00	0.00	0.00	0.00	0.00	0.00	0.92
Gd	11.59	10.26	0.00	10.91	6.86	0.00	0.00	0.00	0.00	0.00	10.68
Tb	1.98	2.26	0.00	1.88	1.42	0.00	0.00	0.00	0.00	0.00	1.16
Yb	5.82	7.91	0.00	6.10	6.27	0.00	0.00	0.00	0.00	0.00	5.45
Lu	0.75	1.03	0.00	0.87	0.94	0.00	0.00	0.00	0.00	0.00	0.97

S. No.	12	13	14	15	16	17	18	19	20	21	22
Sc	1	0	0	0	1	1	0	1	0	2	1
Rb	205	192	208	113	120	151	138	122	113	163	190
Cs	1.94	0.00	1.41	0.00	1.02	1.69	0.00	0.83	0.00	1.50	0.76
Ba	146	174	55	74	155	262	251	92	439	388	250
Sr	24	46	15	31	31	70	69	19	64	110	34
Ga	28	22	31	27	25	26	24	24	18	22	17
Ta	5.70	0.00	6.30	0.00	1.20	3.40	0.00	1.43	0.00	3.00	3.11
Nb	56.0	35.0	100.0	44.0	23.0	31.0	40.0	35.0	34.0	26.0	40.0
Hf	7.10	0.00	9.89	0.00	4.69	5.62	0.00	6.47	0.00	5.49	3.35
Zr	116	238	157	68	108	139	137	160	116	150	51
Y	48	43	55	20	23	35	31	25	20	26	36
Th	26.00	20.00	44.00	28.00	11.00	23.00	19.00	20.00	22.00	24.00	30.00
U	10.00	6.00	11.00	6.00	5.00	10.00	7.00	7.00	6.00	6.00	6.00
La	27.72	0.00	16.49	0.00	27.75	29.00	0.00	14.76	0.00	26.90	10.73
Ce	58.74	102.00	18.34	0.00	57.13	57.90	53.00	84.48	32.00	71.80	22.90
Nd	35.81	0.00	35.18	0.00	29.19	34.29	0.00	20.94	0.00	34.60	10.56
Sm	23.17	0.00	20.86	0.00	13.29	18.96	0.00	9.24	0.00	11.07	6.53
Eu	0.24	0.00	0.09	0.00	0.43	0.16	0.00	0.28	0.00	0.82	0.30
Gd	11.41	0.00	15.95	0.00	3.97	6.11	0.00	4.44	0.00	8.94	7.75
Tb	2.00	0.00	2.19	0.00	0.99	1.04	0.00	0.93	0.00	0.71	0.99
Yb	7.69	0.00	13.46	0.00	3.03	4.64	0.00	3.51	0.00	3.29	4.15
Lu	1.04	0.00									

S. No.	23	24	25	26	27	28	29	30	31	32	33
Sc	0	0	0	0	0	1	0	0	3	0	0
Rb	169	191	282	242	153	189	138	147	146	116	172
Cs	0.00	1.29	0.00	0.00	0.00	1.22	0.00	0.00	1.73	0.00	0.00
Ba	135	86	47	107	103	80	72	547	749	172	145
Sr	23	23	6	30	26	18	23	84	106	61	66
Ga	22	28	35	28	24	30	27	14	15	23	28
Ta	0.00	2.94	0.00	0.00	0.00	4.25	0.00	0.00	1.85	0.00	0.00
Nb	76.0	55.0	106.0	68.0	31.0	81.0	91.0	31.0	22.0	30.0	50.0
Hf	0.00	2.81	0.00	0.00	0.00	8.38	0.00	0.00	5.69	0.00	0.00
Zr	80	99	103	77	110	123	91.0	137	177	151	136
Y	46	43	100	66	30	66	94	26	23	26	35
Th	22.00	22.00	59.00	28.00	14.00	36.00	37.00	28.00	26.00	20.00	22.00
U	10.00	6.00	17.00	6.00	5.00	12.00	12.00	6.00	8.00	6.00	8.00
La	0.00	6.10	0.00	0.00	0.00	14.54	0.00	0.00	43.14	0.00	0.00
Ce	20.00	14.95	3.00	9.00	30.00	49.88	53.00	45.00	74.19	83.00	31.00
Nd	0.00	13.67	0.00	0.00	0.00	33.37	0.00	0.00	29.62	0.00	0.00
Sm	0.00	9.26	0.00	0.00	0.00	24.41	0.00	0.00	12.21	0.00	0.00
Eu	0.00	0.10	0.00	0.00	0.00	0.19	0.00	0.00	0.73	0.00	0.00
Gd	0.00	6.12	0.00	0.00	0.00	9.52	0.00	0.00	10.57	0.00	0.00
Tb	0.00	1.38	0.00	0.00	0.00	3.62	0.00	0.00	0.87	0.00	0.00
Yb	0.00	6.75	0.00	0.00	0.00	10.11	0.00	0.00	3.01	0.00	0.00
Lu					0.00	1.30	0.00	0.00	0.39	0.00	0.00

S. No.	34	35	36	37	38	39	40	41	42	43	44
Sc	0	2	0	0	3	0	0	2	0	0	0
Rb	165	164	133	170	166	168	173	175	176	144	174
Cs	0.00	1.91	0.00	0.00	4.65	0.00	0.00	3.30	0.00	0.00	0.00
Ba	117	400	281	610	398	439	317	359	348	379	444
Sr	54	113	73	121	89	98	78	93	86	93	98
Ga	27	25	25	22	22	24	22	20	23	22	23
Ta	0.00	3.20	0.00	0.00	2.30	0.00	0.00	3.07	0.00	0.00	0.00
Nb	49.0	37.0	45.0	22.0	37.0	28.0	35.0	44.0	39.0	25.0	25.0
Hf	0.00	5.89	0.00	0.00	5.88	0.00	0.00	6.88	0.00	0.00	0.00
Zr	114	134	204	143	142	161	52	168	137	152	136
Y	42	23	42	23	31	30	25	35	34	27	31
Th	24.00	20.00	20.00	24.00	24.00	18.00	22.00	26.00	22.00	23.00	23.00
U	11.00	8.00	7.00	7.00	7.00	6.00	7.00	8.00	7.00	8.00	12.00
La	0.00	12.56	0.00	0.00	35.02	0.00	0.00	36.81	0.00	0.00	0.00
Ce	25.00	90.30	66.00	51.00	68.04	47.00	11.00	78.41	66.00	45.00	76.00
Nd	0.00	11.20	0.00	0.00	35.11	0.00	0.00	40.58	0.00	0.00	0.00
Sm	0.00	15.56	0.00	0.00	14.73	0.00	0.00	15.23	0.00	0.00	0.00
Eu	0.00	0.80	0.00	0.00	0.72	0.00	0.00	0.76	0.00	0.00	0.00
Gd	0.00	8.16	0.00	0.00	9.37	0.00	0.00	9.50	0.00	0.00	0.00
Tb	0.00	0.67	0.00	0.00	1.44	0.00	0.00	1.60	0.00	0.00	0.00
Yb	0.00	3.93	0.00	0.00	5.00	0.00	0.00	5.70	0.00	0.00	0.00
Lu	0.00	0.64	0.00	0.00	0.70	0.00	0.00	0.81	0.00	0.00	0.00

S. No.	45	46	47	48	49	50	51	52	53	54	55	56
Sc	3	2	2	6	4	6	6	0	0	0	0	3
Rb	178	168	157	90	113	120	72	157	165	173	183	173
Cs	3.44	2.82	2.92	1.12	1.90	2.50	1.31	0.00	0.00	0.00	0.00	2.67
Ba	588	428	456	846	955	701	766	702	723	844	601	614
Sr	131	89	110	258	328	273	356	169	164	209	166	140
Ga	21	21	24	21	18	19	21	21	21	20	21	21
Ta	3.10	2.98	2.20	3.77	1.50	0.70	1.29	0.00	0.00	0.00	0.00	2.30
Nb	30.0	36.0	26.0	24.0	16.0	19.0	27.0	25.0	23.0	24.0	18.0	31.0
Hf	5.70	5.65	6.38	9.50	6.44	5.87	8.52	0.00	0.00	0.00	0.00	5.92
Zr	151	128	159	374	234	204	355	182	184	197	225	159
Y	29	30	27	26	21	18	25	29	27	21	30	26
Th	25.00	22.00	20.00	16.00	19.00	22.00	13.00	26.00	24.00	28.00	36.00	25.00
U	12.00	7.00	7.00	4.00	5.00	7.00	4.00	7.00	5.00	4.00	5.00	8.00
La	49.74	42.11	76.43	52.80	43.45	48.68	45.76	0.00	0.00	0.00	0.00	50.75
Ce	81.40	78.12	122.90	103.00	73.70	73.90	96.90	74.00	73.00	80.00	53.00	87.20
Nd	46.00	35.74	60.60	56.31	32.00	30.80	46.25	0.00	0.00	0.00	0.00	47.49
Sm	13.16	13.95	15.55	14.40	8.78	5.69	12.36	0.00	0.00	0.00	0.00	10.95
Eu	1.13	0.71	0.99	1.10	1.20	1.04	1.15	0.00	0.00	0.00	0.00	1.01
Gd	8.45	7.98	7.45	10.15	3.52	2.51	5.81	0.00	0.00	0.00	0.00	3.98
Tb	0.91	1.25	0.78	1.97	0.70	0.57	1.24	0.00	0.00	0.00	0.00	0.80
Yb	4.10	4.66	3.50	4.45	2.85	2.20	3.71	0.00	0.00	0.00	0.00	3.71
Lu	0.69	0.68	0.51	0.58	0.38	0.34	0.51	0.00	0.00	0.00	0.00	0.53

N.b. Zero in trace elements means not determined.

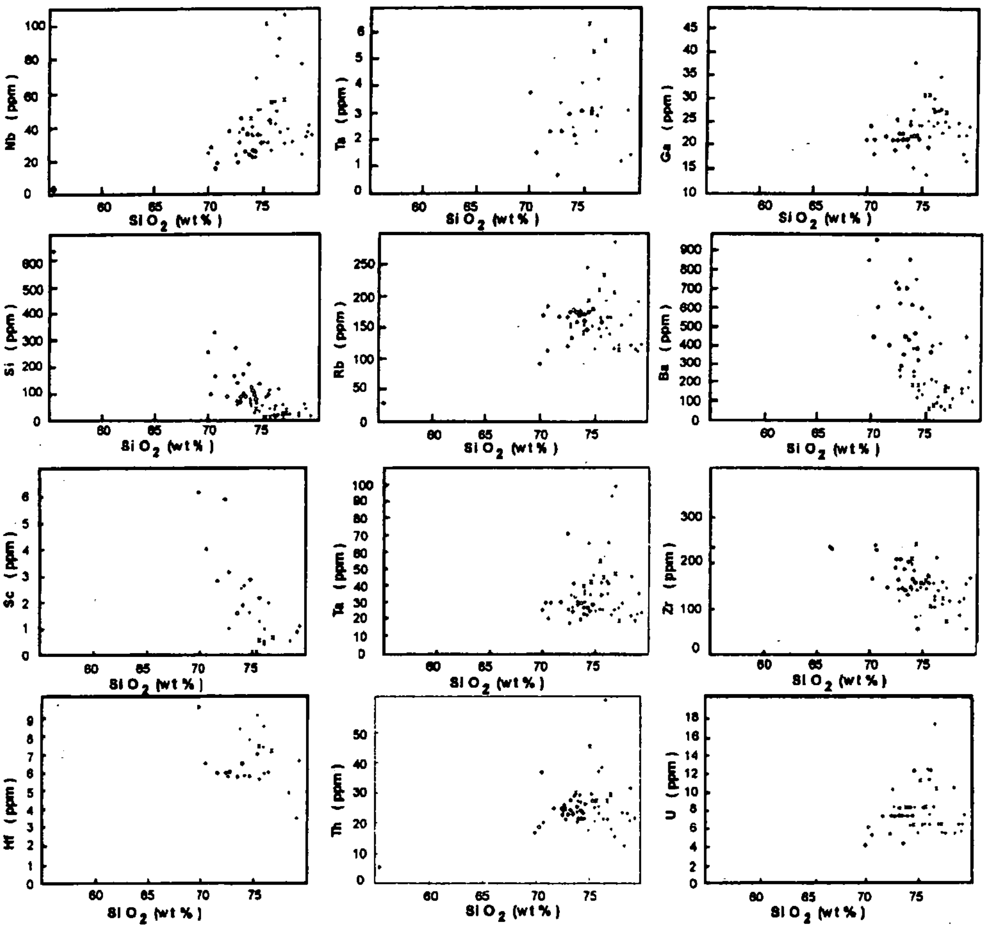

Fig. 12. Trace elements vs. SiO_2% variation diagram

Variation diagrams: The analyzed trace elements are routinely plotted against silica to reveal their evolution during the infered fractional crystallization path (*Fig. 12.*). Some elements show more or less defined trends, while others do not show and sometimes have complicated and ambiguous geochemical behaviour such as Rb which shows curvilinear increment, and then increases dramatically at almost constant silica. It seems that Rb behaves as incompatible element during all the magmatic stages and that biotite does not capture all the Rb in the melt.

Ba shows generally defined negative relation. Sr shows well defined negative relation with silica which indicates that Sr behaviour is controlled by feldspar (mainly plagioclase) fractionation which starts early during magma consolidation.

Zr and Sc show negative correlation, while Ga and Y show positive relations with drastic increase at high silica values.

The gradual increment of Y does not imply considerable fractionation of Y-bearing minerals especially garnet, where the drastic decrease in Sc involves fractionation of minerals as magnetite and ilmenite.

Rb-Ba-Sr diagram: EL-BOUSEILY and EL-SOKKARY (1975) proposed a diagram for magmatic differentiation and classification based on the ternary relation Rb-Ba-Sr. According to their classification the studied granitoids plot in the field of anomalous granites close to the boundary between anomalous and normal granites. The majority plot in the strongly differentiated granites field (*Fig. 13.*).

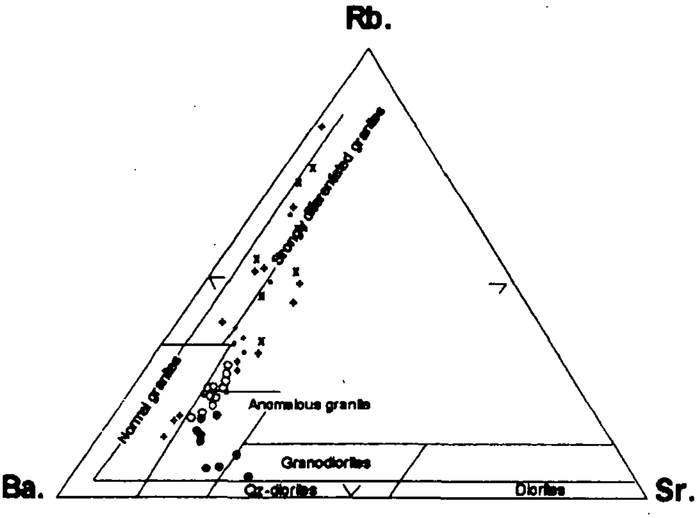

Fig. 13. Rb-Ba-Sr diagram

Normalized trace elements patterns: The trace elements are normalized to MORB and plotted in spider patterns. Fine-grained granites and red granites of the late to post-orogenic suite show three main negative anomalies for Ba, Sr and Ti in addition to a small negative anomaly for Zr. These anomalies gradually decrease in the leucocratic granite and the biotite granite of the same granite suite. In the syn-orogenic suite, only Ti anomaly is recorded, while very minor anomalies of Ba and Sr still remain, Zr anomaly disappeared (*Fig. 14.*).

REE patterns: The analyzed REE are plotted in normalized patterns for the studied granitoids (*Fig. 15.*). All types show negative europium anomaly which gradually increases from the syn-orogenic suites. The syn-orogenic granitoids have a small anomaly with Eu/Eu* ranging from 0.85 to 0.28, while in the late and post-orogenic suite, the anomaly ranges from 0.903 to 0.176 in the biotite granite, from 0.244 to 0.032 in the lecocratic granite, from 0.197 to 0.082 in the red granite and reaches its maximum from 0.176 to 0.015 in the fine-grained granite. There are also differences between these rock groups with respect to the degree of fractionation of the normalized patterns with Ce_N/Yb_N as criterion, thus the red granites, leucocratic granites with Ce_N/Yb_N as a criterion, thus the red granites, leucocratic granites and biotite granites have relatively highly fractionated patterns with Ca_N/Yb_N intervals of 6.09-2.83, 6.39-1.27 and 9.1-3.53 respectively, while the fine-grained granites and the syn-orogenic granites show moderately fractionated normalized patterns, Ce_N/Yb_N ranges are 1.98 0.35 and 8.7-6 respectively.

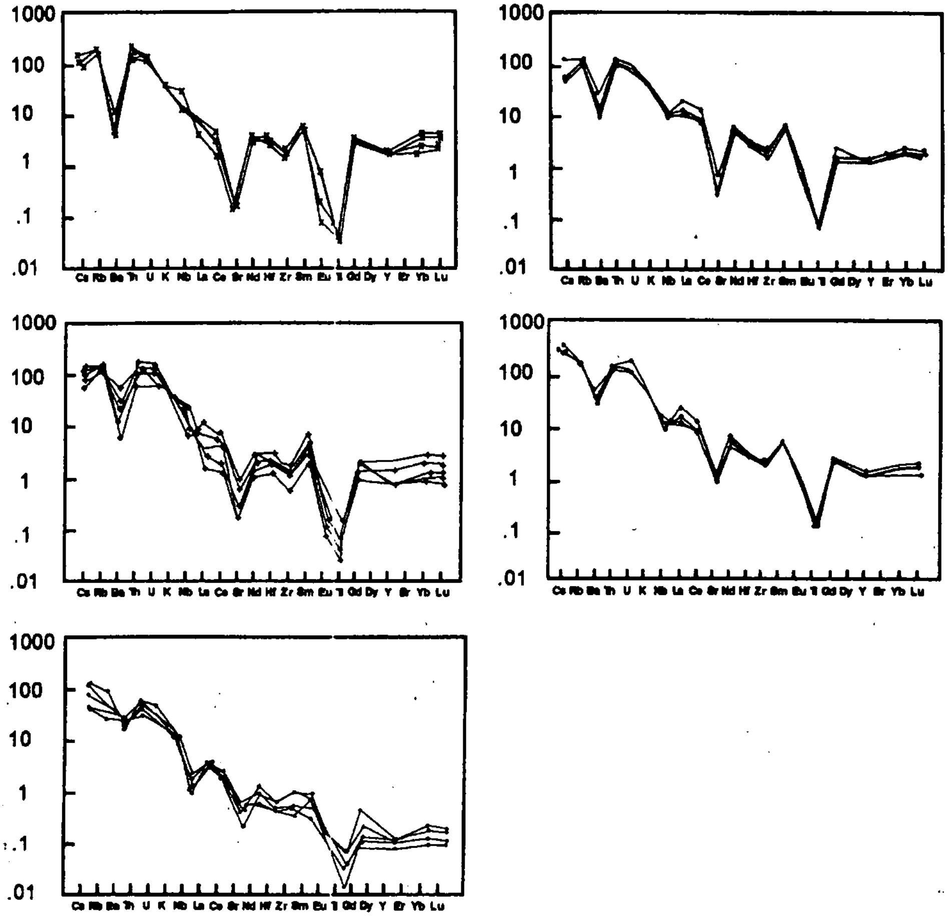

Fig. 14. Normalized trace element pattern

GENETIC CLASSIFICATION AND MAGMA TYPE

CHAPPELL and WHITE (1974) proposed a genetic subdivision of the granitic rocks into those derived from sedimentary protolith (S-type) and those derived from igneous protolith (I-type). Subgroups of I-type granites include those derived from recycled continental crust (A-type: LOISELLE and WONES 1979, COLLINS et al., 1982, WHALEN et al., 1987) and those derived directly from melting of subducted oceanic crust or overlying mantle (M-type: WHITE 1979, COLLINS et al., 1982, WHALEN et al., 1986) and those derived directly from melting of subducted oceanic crust or overlying mantle (M-type: WHITE 1979, PITCHER 1983, WHALEN 1985).

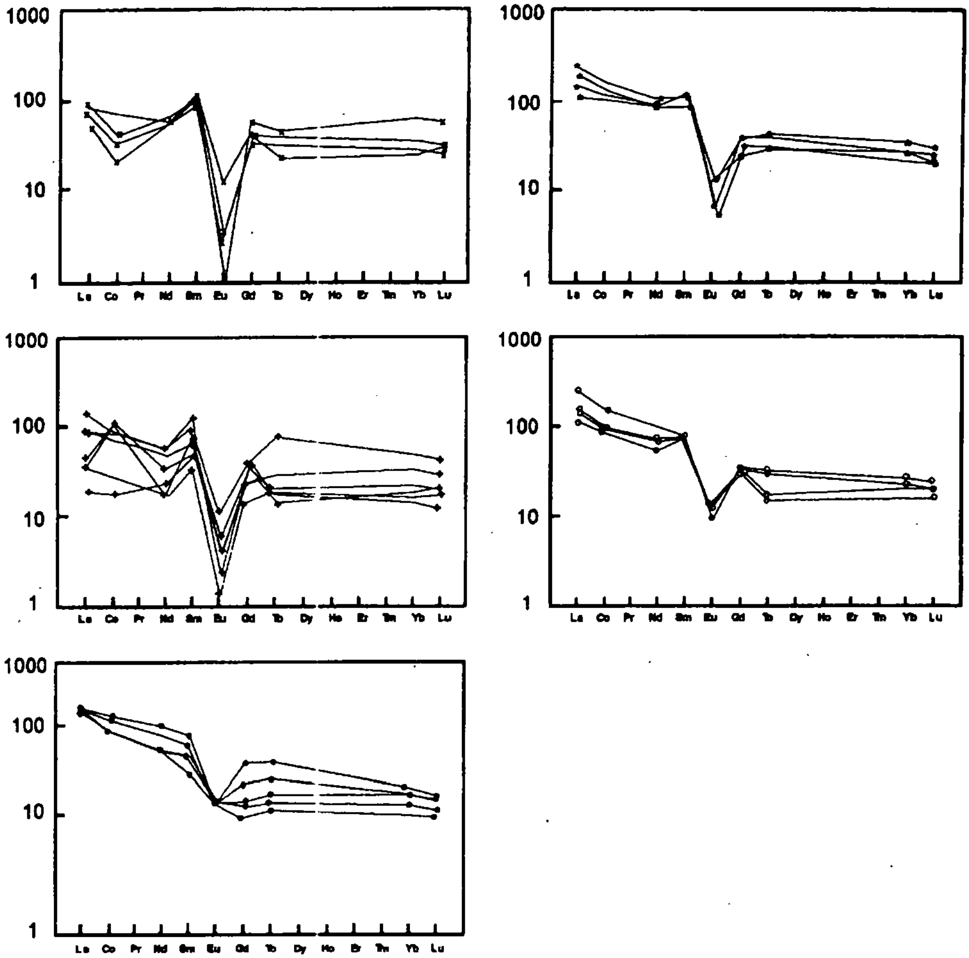

Fig. 15. Normalized REE pattern

The data are plotted on some standard diagrams: on the diagram of SYLVESTER (1989). The syn-orogenic granitoids plot in the field of calc-alkaline I-type, while the late to post orogenic granitoids plot mostly in the field of highly fractioned I-type and alkaline granite (*Fig. 16*). On the diagram of HINE et al. (1979), the syn-orogenic granitoids plot in the I-type field, while the majority of the late to post-orogenic granitoids plot also in the I-type field, with the exception of two samples which plot close the line separating the I-and S-types (*Fig. 17*).

Tectonic setting: some reference diagrams are used to deduce the tectonic environment of Abu El-Hasan granitoids. The syn-orogenic (older) granitoid plots have a general trend roughly perpendicular to the iron magnesium oxide side (*Fig. 18*), thus comparable with the compression suite of PETRO et al., (1979). The late-to post-orogenic younger granitoids plot parallel to the AF side which means that they are comparable with the extension suite of PETRO et al., (op. cit). On the multicationic diagram of BATCHELOR and BOWDEN (1985), it is concluded that the (older) syn-orogenic granites are syncollision, while the (younger) late to post-orogenic granites are post-orogenic (*Fig. 19*). Using the discrimination tectonic diagrams of PEARCE et al. (1984), the older granitoids plot in the volcanic arc granite field, while the younger granitods plot in the field of within plate granite and close to the line separating WPG and VAG (*Fig. 20*).

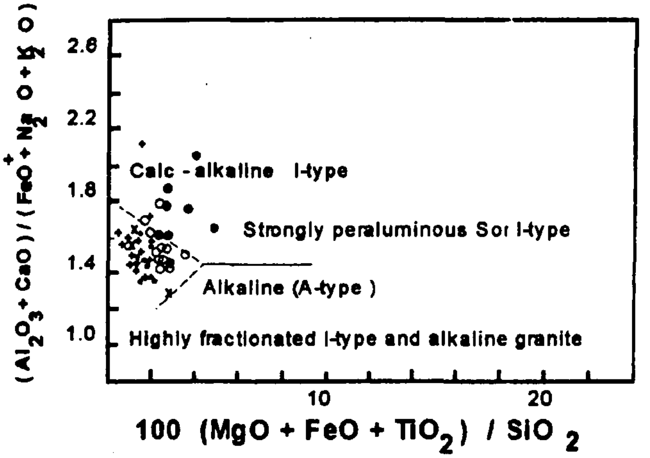

Fig. 16. SYLVESTER's (1989) diagram

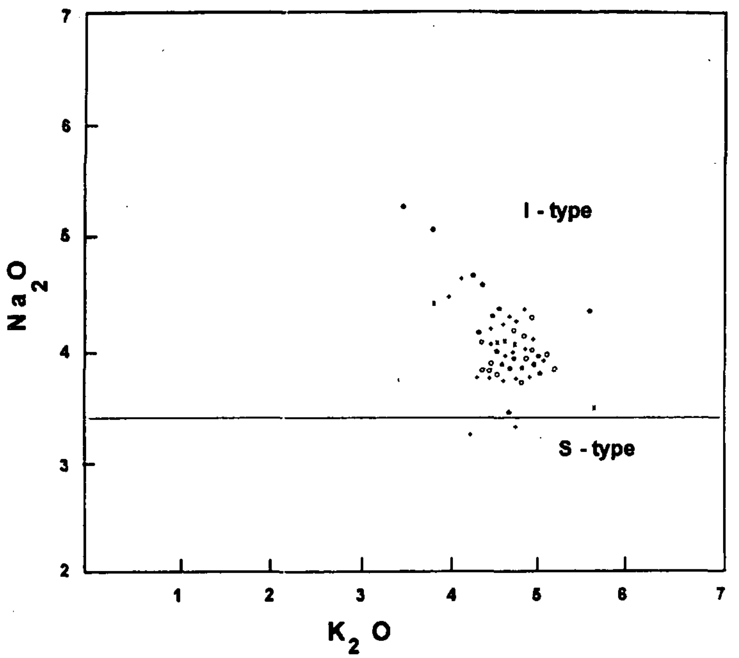

Fig. 17. Na_2O vs. K_2O diagram (HINE et al. 1978)

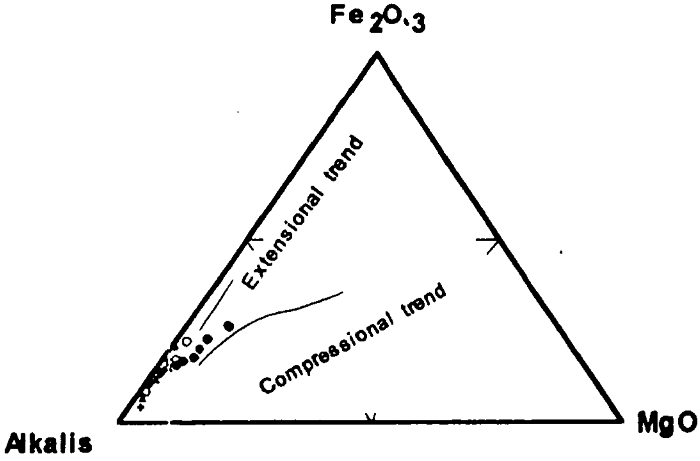

Fig. 18. PETRO et al. (1979) diagram

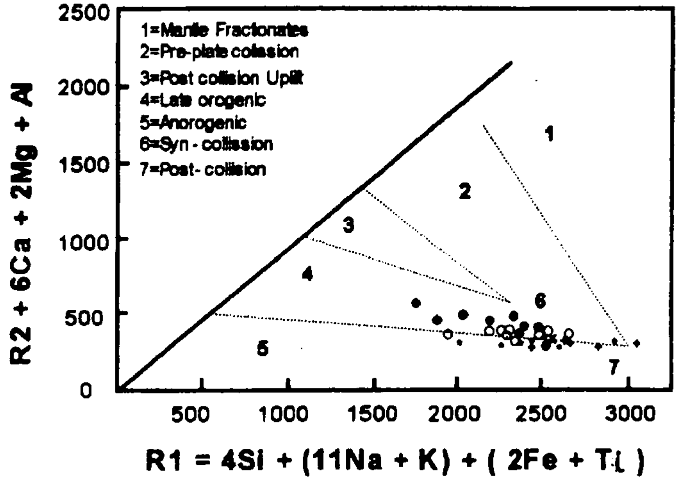

Fig. 19. Multicationic diagram (BATCHELOR and BOWDEN, 1985)

CONCLUSION

The granitic rocks of Abu El-Hasan pluton, north Eastern Desert are petrographically, geochemically and tectonically studied. The investigated rocks comprise older and younger granitoids. Petrographically, the older granitoids comprise biotite-hornblende granodiorite. The younger granitoids are represented petrographically by biotite granite, leucocratic granite, fine-granied granite and red granite.

Chemically, they are calc-alkaline to rather alkaline. They are well-differentiated with an average D.I. 95.83. These granitoids are low-calcium, somewhat potassic rather than sodic and peraluminous.

Chemical classification of Abu El-Hassan granitoids reveals that they comprise granite, alkali-granite, alkali-feldspar granite, syenogranite and monzogranite. Geochemically, Abu-El-Hasan granitoids show low Rb, very-low Sr and moderate Ba. The majority of there rocks fall withing the range 0.5 to 7 Kb water vapour pressure, while some samples were mostly formed under higher water vapour pressure (10 Kb) and in turn deeper levels.

Data for tectonic setting suggest that the older (syn-orogenic) granitoids are comparable with the compression suite of PETRO et al. (1979), while the younger (late to post-orogenic) granitoids are comparable with the extension suite. It is argued that Abu El-Hasan granitoids were derived from partial melting of the upper mantle with some lower crust contribution. The older granitoids are syn-collision and plot in the volcanio arc field, the younger granitoids are post-orogenic and plot in the within plate field and close to the line separating WPG and VAG.

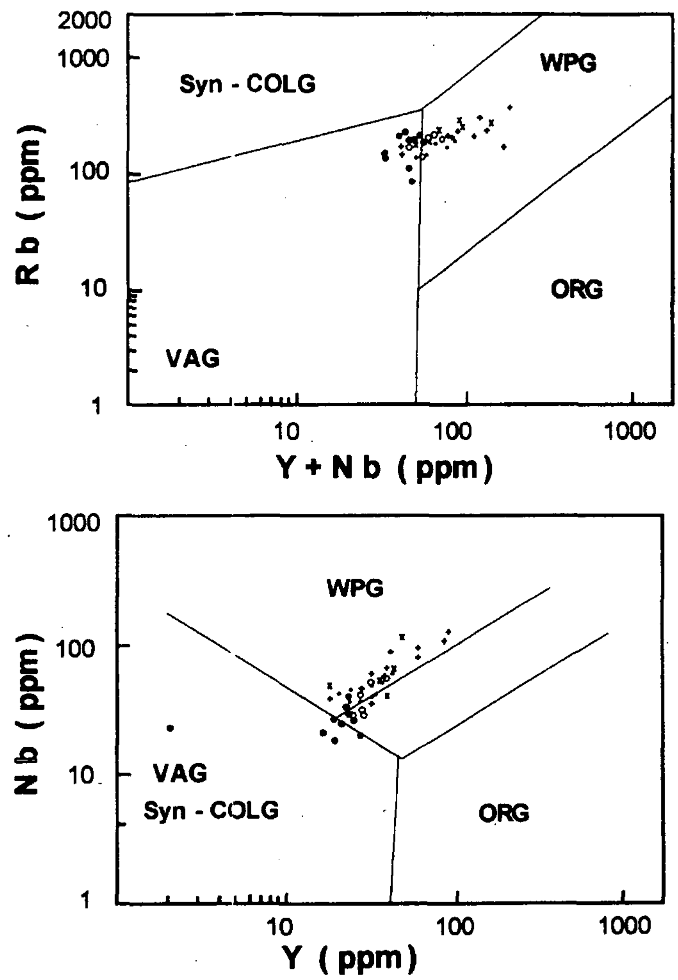

Fig. 20. Tectonic discrimination diagrams (PEARCE et al. 1984)

ACKNOWLEDGEMENT

The authors wish to express their thanks to Prof. Dr. F. FINGER, Salzburg University, Austria for useful suggestions and for facilities offered during the analytical work. The authors are grateful to Prof. M. F. EL-RAMLY, Ain Shams University for useful remarks and fruitful discussion.

REFERENCES

BATCHELOR, R. and P. BOWDEN (1985): Petrogenetic interpretation of granitoid rocks series using multicationic parameters. Chem. Geol. V, 48, 43-55.

CHAPPEL, B. W. and A. J. A. WHITE (1974): Two contrasting granite types. Pac. Geol. 80, 173-174.

DAWOUD, M. (1995): Petrography, geochemistry and tectonic environment of the granitic rocks of Gebel Abu El-Hasan Gebel Abu Samyuk, Northern Eastern Desert, Egypt. Ph.D. Thesis, Menoufia Uni. Egypt, 157.

EL BOUSEILY, A. M. and A. A. EL SOKKARY (1975): The relationship between Rb, Ba and Sr in granitic rocks. Chem. Geol. 16, 207-219.

EL-GABY, S. (1975): Petrochemistry and Geochemistry of some granites from Egypt. N. Jb. Miner. Alt. V. 124, 147-199.

EL-GABY, S., LIST, K. F. and TEHRANI, R. (1988): Geology, evolution and metallogenesis of the Pan-African belt in Egypt. Andreas Vogel, Berlin.

EL RAMLY, M. F. (1972): A new geological map for the basement rocks in the Eastern Desert and Southern Western Desert of Egypt, Scale 1:1.000.000. Annal. Geol. Surv. Egypt. 2, 1-18.

EL-SHAZLY, E. M. (1964): On the classificationof the Precambrian and other rocks of magmatic affiliation in Egypt. U. A. R. Geol. Congress, India. Sect. 10.

Geological map (1978). The Qena quadrangle. Geological survey of Egypt, Scale 1:500.000. Edited by EL RAMLY, M. F. and M. H. HERMINA.

HASHAD, A. H. (1980): Present status of geochemical data of the Egyptian Basement Complex. Symp. on the Evolution and Mineralization of the Arabian-Nubian Shield, King Abdulaziz. Univ., Jeddah. V. 3., 31-46.

HASAN, M. A. and HASHAD, A. H. (1990): Precambrian of Egypt. In: R. Said (ed.) Geology of Egypt. A. A. Balkemaa, Rotterdam, Netherlands. 201-245.

HILMY, M. E., ABDEL-MAKSOUD, M. A., AZER, H. W. (1994-1995): Close Examination of Two Phases of The Anorogenic Granite, Abu El-Hasan Area, Norhern Eastern Desert, Egypt. Annals Geol. Surv. Egypt. V. XX. 143-162.

HINE, I. S., CHAPPELL, B. W., WHITE, J. R. (1978): Contrasts between I- and S-Type granitoids of the Kosciusko batholith. J. Geol. Soc. Aust. V. 25, 4, 219–234.

HUSSEIN, A. A., ALI, M. M. and EL-RAMLY, M. F. (1982): A proposed new classification of the granites of Egypt J. Volc. and Geoth. Research. 14, 187–198.

IRVINE, T. N. and W. R. A. BARAGAR (1971): A guide to the chemical classification of the common volcanic rocks. Can. J. Earth Sci. 88, 523–549.

LOISELLE, M. C. and D. P. WONES (1979): Characteristics of anorogenic granites. Geol. Soc. Am. AGM. Abst. with Prog. 539.

MIDDLEMOST, E. A. K. (1985): Magmas and Magmatic Rocks. An introduction to igneous petrology. Longman, London and New York, 266.

O'CONNOR, J. T. (1965): A classification of quartz rich igneous rocks based on feldspar ratios, U. S. Geol. Surv., Prof. Pap. 525-B: 79–84.

PEARCE, J. A. B. W. NIGEL and G. T. ANDREW (1984): Trace element discrimination diagrams for tectonic interpretation of granitic rocks. J. Petrol. V. 25, 956–983.

PETRO, W. L., T. A. VOGEL and J. T. WILHAND (1979): Major element chemistry of plutonic rocks suites from compressional and tensional plate boundaries. Chem. Geol. 26, 217–235.

PITCHER, W. S. (1983): Granite types and tectonic environment, Ch. 1-3, pp. 19–40. In HSU, K. J. (ed.), Mountain building processes, Academic press, London.

SABET, A. H., S. EL GABY and ZALATA (1972): Geology of the basement rocks in the northern parts of El Shayib and Safaga sheets, Eastern Desert. Ann. Geol. Surv. Egypt 2, 111–128.

SABET, A. H. (1972): On the stratigraphy of the basement rocks of Egypt. Annals Geol. Surv. Egypt. V. II, 79–101.

SCHURMANN, H. M. E. (1966): The Precambrian along the Gulf of Suez and the northern part of the Red Sea. G. J. BRILL, Leiden, 404.
SHAND, S. J. (1951): The Eruptive Rocks. Wiley, New York.
STERN, R. J. (1979): Late Precambrian ensimatic volcanism in the Central Eastern Desert of Egypt. PhD. Thesis Univ. of California, San Diego, U.S.A.
STERN, R. J., GOTTFRIED, D. and HEDGE, C. E. (1984): Late Precambrian rifting and crustal evolution in the North Eastern Desert of Egypt. Geology, V. 12, 168–172.
STRECKEISEN, A. L. (1976b): Classification of the common igneous rocks by means of their chemical composition. A provisional attempt. N. Jb. Min. Mh., H. 1, 1–15.
SYLVESTER, P. J. (1989): Post-collisional alkaline granite. J. Geol., 97, 261–280.
TAKLA, M. A., KHALAF, I. M. HELMERS, H. and AL-BOGHDADY, A. A. (1997): The Sield Rocks Of Wadi Safaga Area, Central Eastern Desert, Egyp. The Third Conference On Geochemistry, Alexandria Univ., Fac., Sci, Geology Dept. September (1997). 17–31.
THORNTON, C. P. and TUTTLE, O. F. (1960): Chemistry of igneous rocks. Differentiation Index. Amer. J. Sci. V. 258, 644–684.
TUTTLE, O. F. and N. BOWEN (1958): Origin of granite in the light of experimental studies in the system $NaAlSi_3O_8$-SiO_2-H_2O. Geol. Soc. Am. Mem. 74, 1–53.
WRIGHT, J. B. (1969a): A simple alkalinity ratio and its application to questions of non-orogenic granite genesis. Geol. Mag. 106, 370–384.
WHALEN, J. B., K. L. CURRIE and B. W. CHAPPELL (1987a): A-type granites: geochemical characteristics, discrimination and petrogenesis. Contrib. Min. Petrol. V. 95, 407–419.
WHALEN, J. B. (1985): Geochemistry of an island-arc plutonic suite: the Vasilau-Yau, Yau intrusive complex, New Britain, PNG, J. Petrol. 26, 603–632.
WHITE, A. J. R. (1979): Sources of granite magmas. Geol. Soc. Am. Abst. Prog. 11, 539.
WHITE, A. J. R. and B. W. CHAPPELL (1983): Granitoid types and their distribution in the Lachlan Fold Belt, Southern Australia. Geol. Soc. Am. Mem. 159, 21–35.
ZALATA, A. A. (1972): Geology of the area around Gabal El-Shayib, Eastern Desert, Egypt. Ph.D. Thesis, Ain Shams Univ. Cairo, Egypt.

Manuscript received 16 April, 1998.

Acta Mineralogica-Petrographica, Szeged, XXXIX, 77–86, 1998

RARE ALKALI ELEMENTS IN THE HUNGARIAN GEOLOGICAL FORMATIONS: A COMPREHENSIVE STUDY.

PUSKÁS, Z., NAGY-BALOGH, J., KUBOVICS, I.*, NAGY, B.**, HOFFMANN, L.*

* Department of Petrology and Geochemistry, Eötvös University
** Hungarian Academy of Sciences

ABSTRACT

The authors of the scientific report "Comparative study of rare alkali elements (Li, Rb, Cs) distribution in magmatic, metamorphic, and volcano-sedimentary formations in Hungary" (Kubovics et al. 1992a) prepared within the framework of NSRF (OTKA) No. 728/87 intended to answer the questions raised for more than 40 years ago by SZÁDECZKY-KARDOSS (1955).

The rare alkali element contents of geological formations in Hungary were systematically studied.

It has been established that the highest Li-concentrations in Hungary are linked to lithiophorites found in bauxites and Mn-ores.

The differentiation products of the granites in the Velence Mts namely aplites and orthoclase from pegmatitic nests are most enriched in Rb.

The enrichments of Cs in various rock types - independently of their origin, e.g. in lamprophyres, basalts, andesites, rhyolites, and their pyroclastics - proved to be the result of postmagmatic alteration that resulted in zeolitisation which is the principal host of Cs.

INTRODUCTION

The alkali metals form a group of extremely reactive elements with simple electronic configurations ns^1. They have large atomic (and ionic) radii and low ionization energies compared with other elements. These properties lead to low melting point, boiling point, density and low heats of sublimation, vaporization and dissociation. The alkali metal compounds are generally characterized by high solubility in water, their hydroxides are the most basic of all ones. Their oxidation state in compounds never exceed +1.

Their chemical properties are quite similar, except for lithium in some respects, which is the smallest element in the group and has the highest ionization energy, melting point and the lowest density.

The small size of lithium ion frequently causes special properties in its compounds as well. It shows many geochemical similarities to Mg because of the similarity in ionic size of the two elements: $r(Li^+)$76pm, $r(Mg^{2+})$72pm (SHANNON-PREWIT-type ionic size in 6 coordination number, in: GREENWOOD and EARNSHAW 1984). These "anomalous" properties are for example: lower solubility of some of its compounds, and occurrence in natural ferromagnesian minerals where it partly replaces magnesium.

The distribution of alkali elements in the various geological formations has been well studied. It is particularly true for the two common alkali metals, Na and K. The distributional

* 1088 Budapest, Múzeum krt. 4/A, Hoffman, L: Geofil Kft., 2800 Tatabánya, Alugyári út 1.
** 1051 Budapest, Nádor u. 7.

charasteristics of the rare alkalis - considering that these elements have become important industrial raw materials in the recent decades - are also relatively well-known.

PREVIOUS STUDIES

The first comprehensive results on the rare alkali concentrations of geological formations in Hungary were published by SZÁDECZKY-KARDOSS (1955). He emphasized that Li was most probably enriched in the Velence and Mórágy Mts granitoids and especially pegmatites (pegmatitic mica). He also underlined the possibility of a secondary enrichment of Li-bearing mica in the surrounding sedimentary deposits. Beside these he stressed some possible Li-enrichment in the marine iron ore deposit in the Mecsek Mts as well as the glauconite-bearing sandstones in Nógrád.

In connection with Rb and Cs he emphasized that both elements were expected to be enriched in high-K rocks, like Mórágy Mts granitoids and especially pegmatites, Mecsek Mts phonolites /$K_2O \approx 4\%$/, and Telkibánya K-metasomatites ($K_2O \approx 10$-12%).

The preliminary results of the Nation-wide Rare Element Research Program co-ordinated by the Hungarian Geological Institute (1966-1970) were summarized by FÖLDVÁRI-VOGL (1970). No significant Li-deposit was found during this regional study, however, this element was relatively enriched in the hydrothermally altered slate around the Velence Mts granite. There were also no significant enrichments in coal ashes, only some minor elevated concentrations were found in the coals of Tatabánya and Pusztavám.

As to Rb, this element was found to show no enrichments of economic importance in the formations of Hungary.

According to the results of this study there was Cs-enrichment in the range of about 80 ppm in the grey granite porphyry out of the granitic rocks in the Velence Mts. The principal Cs-bearing mineral was biotite, while a small proportion was in the feldspar. The informations on the Cs-distribution in the geological formations of Hungary, however, remained scarce after the study because of methodological difficulties.

Among the previous works it is important to mention the results of VARGA et al. (1975) on the Rb-contents of some volcanic rocks in the Mátra Mts. The rocks studied were all K-enriched with high adularia and sericite. The spectral analyses yielded K/Rb-ratios, on the basis of which the Rb-content could be calculated. The highest values obtained are summarized in Table 1.

TABLE 1

Calculated Rb content of some K-rich rock in the Mátra Mts. (VARGA et al. 1975)

	K_2O %	Rb %
Bányabérc road cut	10.78	0.34
Bányabérc shaft	11.13	0.37
Korlát-hill	12.85	0.46
Korlát-hill, south edge	13.08	0.47
Kőmorzsás-peak	11.71	0.30
Felsőállás-peak	9.91	0.32
Fekete-leak	12.00	0.52

AIMS OF THE STUDY

New types of Li, Rb and Cs enrichments were found during the recent years mainly in volcano-sediments (e.g. in Usbekistan and Kazakhstan) but in perlites as well (YANEV 1994). So we also considered timely the evaluation of the Hungarian geological formations from this point of view.

Within the framework of the survey we studied the distribution of Li, Rb and Cs in the wide range of magmatic, metamorphic and volcano-sedimentary formations in Hungary using optical emission and atomic absorption methods considering foreign analogies.

METHODS OF INVESTIGATIONS

Atomic emission spectroscopy (AES)

More than 300 selected samples were analysed by emission spectrographic method. Because of Li, Rb and Cs concentration values are commonly below detection limits of conventional AES methods, one author developed a special AES technique for determining rare alkali elements concentration that is more sensitive than has been previously used (HOFFMANN and NAGY-BALOGH 1990, NAGY-BALOGH and HOFFMANN 1991, NAGY-BALOGH 1992a,b).

Li, Rb and Cs were determined using alternating current arc excitation. Matrix effects were minimized by buffering the sample with high purity NaCl. 25 mg of a 1:1 homogeneous mixture of powdered sample and NaCl were loaded into high purity aluminium electrode, dropped with 2 drops phenol-formaldehid rezin and heated at 160^{0}C for 30 minutes. The loaded and heated electrodes were excited by arc at 5 amps for 100 seconds. International standard samples were treated in the same manner.

Spectra were detected by grating spectrograph PGS-2 (Zeiss, Jena) on type 1-N (Kodak-Pathe) infrared sensitive photoemulsion. The wavelengths used for analysis were: Li 812,6; Rb 780,0 and 794,7; Cs 852,1 nm; reference lines Na 818,3 and

819,4 nm. The Na lines had extremely high intensity and it was out of the range suitable for densitometry. Decrease of Na line intensity was accomplished by a neutral filter in front of Na wavelength position. Less than 3% Na-content of rock samples does not disturb the use of Na as reference element.

Quantitative evaluation was made by digital microphotometer connected to a microcomputer.

Detection limit for Li is 4 g/t, Rb 1g/t, Cs 1 g/t, 8-10% relative standard deviation.

Neutron activation analysis (INAA)

In the course of earlier studies more than 100 samples were analysed for rare elements, inclusive Cs, by INAA.

INAA method was used also for control analyses in the low, medium and anomalously high Cs-concentration ranges. The results of AES and INAA were in a good agreement, systematic error was not noticed. The INAA analyses were made at the Nuclear Technical Institute of Technical University, Budapest.

Flame atomic absorption and emission spectrometry was the control method for Li and Rb analysis. After acidic ($HF+HClO_4$) digestion Varian AA-475 instrument, Y-capillar and standard addition technique was used for Li and Rb determination.

RESULTS AND DISCUSSION

Beside our new analyses rare alkali determinations found in theses prepared in the Department of Petrology and Geochemistry, Eötvös University as well as the results of the above mentioned Nation-wide Rare Element Research Program were also used for evaluation.

The location of sampling points is displayed in *Fig. 1.*

Our results have been summarized according to the rock types studied (Table 2).

The contents of the rare alkali elements in *ultramafic and lamprophyric rocks* correspond to their average clarke values except for those samples that suffered some kind of postmagmatic alteration.

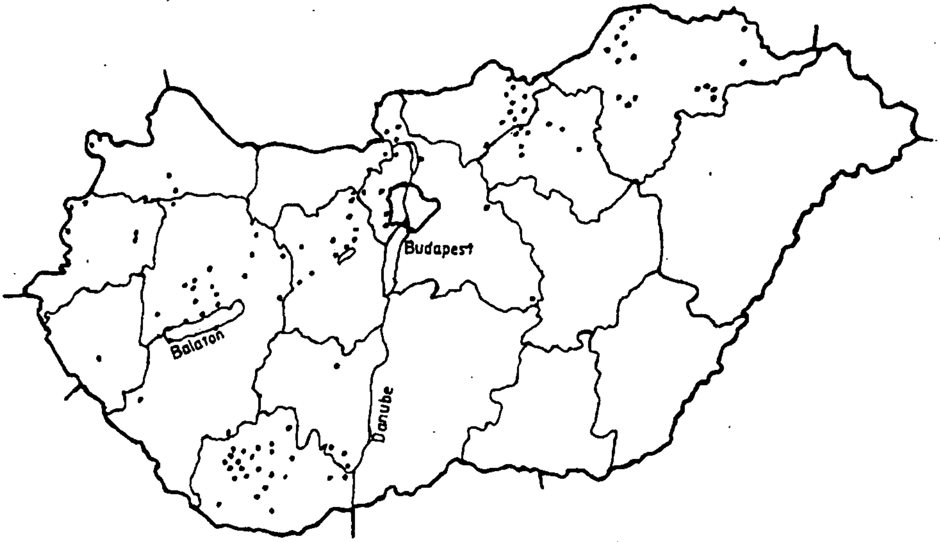

Fig. 1. Sampling points for rare alkali elements determinations in Hungary

TABLE 2

Formations measured for rare alkali element concentrations

– lamprophyres – basaltic rocks – andesite, dacite, trachyte, rhyolite and their pyroclastics – intrusive magmatic rocks – metamorphic rocks – sedimentary rocks (bauxite, Mn-ore, glauconitic sandstone, limestone, gypsum containing aleurolite, alginite, etc. – rocks of hydrothermal origin (zeolitised rhyolitic tuffs, clinoptilolite, mordenite, analcime (Csódi-hill), hydromuscovite, fluorite, barite – monomineral fractions – soils – mineral and medicinal waters

TABLE 3

Alkali element contents of Hungarian basalt samples

	Na %	K %	Li g/t	Rb g/t	Cs g/t	K/Rb	K/Cs	Rb/Li	Na/K	Rb/Cs
Somoskõ	4.21	2.01	8.4	52	0.28	390	72500	6.6	2.1	186
Salgó	3.66	1.87	9.3	45	0.56	416	33393	4.8	2.0	80
Salgó	3.97	1.89	8.8	44	0.66	430	28623	4.8	2.1	67
Kis-Salgó	4.08	1.84	9.3	45	0.85	409	21647	5.0	2.2	53
Tóti-hill	3.05	1.64	10.7	42	1.00	390	16400	3.9	1.9	42
Halyagos SW quarry	3.81	1.36	9.3	45	0.94	302	14468	4.8	2.8	48
Gulács	2.77	2.05	9.75	41	1.22	500	16803	4.2	1.4	34
Mindszentkálla	3.11	2.24	8.4	46.6	0.94	481	23830	5.5	1.4	50
Halyagos Lukács-mine	3.58	2.01	9.3	47.5	1.32	423	15227	5.1	1.8	36
Badacsony Lábdi hill	3.53	2.01	9.3	51.2	1.13	392	17780	5.5	1.8	45
Nógrád average of 4 samples	3.98	1.91	9.0	46.5	0.59	410	32300	5.2	2.09	78.8
Balatonfelvidék average of 6 samples	3.31	1.88	9.5	45.6	1.19	413	18851	4.8	1.76	38.3
average of 10 samples	3.58	1.89	9.3	46	0.9	413	26068	5	1.89	64.1

Out of the *basic volcanic rocks* those of Pannonian age are characterized with Li, Rb and Cs contents typical for continental alkaline basalts (Table 3). Basaltic rocks with older age contain more Rb and Cs than their average clarke-values for this rock type because of postmagmatic alteration to clay minerals and/or zeolites. Exceptionally high Cs-content of average 150 ppm was detected in both the outcrop and drill core samples from the leucitic lamproitic rock (PUSKÁS et al. 1993) near Bár, South Hungary. This can be explained by the loose framework crystal structure of leucite that may host the large Cs-ion.

In the *intermediate volcanic rocks* (andesite, dacite and their pyroclastics) rare alkali concentrations corresponding to their average clarke values were found, i.e. a little higher values than in the basic rocks. Specific geochemical significance can be attributed to the relatively high Cs-contents of neogene volcanics: this appear to exclude their island arc origin (STAVROV 1978). Island arc andesites and dacites, similarly to basalts, contain Cs under the 1 ppm level, while in our case the average measured values were around 5 ppm, corresponding to continental margin position of the volcanics. In the case of hydrothermally altered rocks the Cs-content may even attain 30 ppm, e.g. in the analcime containing andesite-dacite of Csódi hill, Visegrádi Mts.

According to the lithophile geochemical behaviour of alkali elements their concentrations in *acidic volcanic rocks* are higher than in the basic and intermediate volcanics. Outstanding enrichments, however, were found in the acidic pyroclastics altered by postvolcanic processes, namely Li=30-40 ppm, Rb=100-350 ppm, Cs=2,5-145 ppm.

Among the *intrusive magmatic rocks* basic ones contain rare alkali elements in low concentrations in accordance with their low clarke values in these rock types. In the granitoids of the Mecsek Mts the concentrations of rare alkali elements are higher as a consequence of their higher mica-content. The highest concentrations, however, were detected in the more evolved and differentiated Velence Mts granite. Conspicuously high Rb content was characteristic for their aplite (464-514 ppm) and pegmatitic orthoclase (797 ppm).

The rare alkali element contents in *metamorphic rocks* are principally constrained by their concentration in the pre-metamorphic protolith. We found elevated rare alkali concentrations in the amphibolite facies metamorphic rocks in the Mecsek Mts, the reason of which, however, needs further clarification.

Out of the *sedimentary rocks* only those have been involved into the scope of our measurements, in which some enrichments of any of the rare alkali elements were expected on theoretical or practical considerations.

Considerable Li enrichments were found in some bauxite samples. We supposed that Li was contained in the lithiophorite identified by BÁRDOSSY (1977).

Numerous measurements were carried out from the Mn-oxide crusts underlying bauxite bodies as well as the samples from the Úrkút Mn-ore body that were previously identified as lithiophorite. Comparing our results with those of VARENTSOV and GRASSELLY (1980) we found that the samples studied belong to the low-Li lithiophorite varieties. Their highest Li-content was 968 ppm.

Glauconite-containing sandstone and monomineral fractiones of glauconite thereof that SZÁDECKY-KARDOSS (1955) considered as most promising in view of their possible elevated rare alkali element contents proved to be not enriched in these elements. That is their higher K content was not followed by elevated Rb and Cs contents.

Out of the evaporites, we have analysed some gypsum-and anhidrite-containing aleurolite samples. Their rare alkali element contents corresponded to the average clarke values in these rocks.

TABLE 3

Alkali element contents of Hungarian basalt samples

	Na %	K %	Li g/t	Rb g/t	Cs g/t	K/Rb	K/Cs	Rb/Li	Na/K	Rb/Cs
Somoskõ	4.21	2.01	8.4	52	0.28	390	72500	6.6	2.1	186
Salgó	3.66	1.87	9.3	45	0.56	416	33393	4.8	2.0	80
Salgó	3.97	1.89	8.8	44	0.66	430	28623	4.8	2.1	67
Kis-Salgó	4.08	1.84	9.3	45	0.85	409	21647	5.0	2.2	53
Tóti-hill	3.05	1.64	10.7	42	1.00	390	16400	3.9	1.9	42
Halyagos SW quarry	3.81	1.36	9.3	45	0.94	302	14468	4.8	2.8	48
Gulács	2.77	2.05	9.75	41	1.22	500	16803	4.2	1.4	34
Mindszentkálla	3.11	2.24	8.4	46.6	0.94	481	23830	5.5	1.4	50
Halyagos Lukács-mine	3.58	2.01	9.3	47.5	1.32	423	15227	5.1	1.8	36
Badacsony Lábdi hill	3.53	2.01	9.3	51.2	1.13	392	17780	5.5	1.8	45
Nógrád average of 4 samples	3.98	1.91	9.0	46.5	0.59	410	32300	5.2	2.09	78.8
Balatonfelvidék average of 6 samples	3.31	1.88	9.5	45.6	1.19	413	18851	4.8	1.76	38.3
average of 10 samples	3.58	1.89	9.3	46	0.9	413	26068	5	1.89	64.1

Out of the *basic volcanic rocks* those of Pannonian age are characterized with Li, Rb and Cs contents typical for continental alkaline basalts (Table 3). Basaltic rocks with older age contain more Rb and Cs than their average clarke-values for this rock type because of postmagmatic alteration to clay minerals and/or zeolites. Exceptionally high Cs-content of average 150 ppm was detected in both the outcrop and drill core samples from the leucitic lamproitic rock (PUSKÁS et al. 1993) near Bár, South Hungary. This can be explained by the loose framework crystal structure of leucite that may host the large Cs-ion.

In the *intermediate volcanic rocks* (andesite, dacite and their pyroclastics) rare alkali concentrations corresponding to their average clarke values were found, i.e. a little higher values than in the basic rocks. Specific geochemical significance can be attributed to the relatively high Cs-contents of neogene volcanics: this appear to exclude their island arc origin (STAVROV 1978). Island arc andesites and dacites, similarly to basalts, contain Cs under the 1 ppm level, while in our case the average measured values were around 5 ppm, corresponding to continental margin position of the volcanics. In the case of hydrothermally altered rocks the Cs-content may even attain 30 ppm, e.g. in the analcime containing andesite-dacite of Csódi hill, Visegrádi Mts.

According to the lithophile geochemical behaviour of alkali elements their concentrations in *acidic volcanic rocks* are higher than in the basic and intermediate volcanics. Outstanding enrichments, however, were found in the acidic pyroclastics altered by postvolcanic processes, namely Li=30-40 ppm, Rb=100-350 ppm, Cs=2,5-145 ppm.

Among the *intrusive magmatic rocks* basic ones contain rare alkali elements in low concentrations in accordance with their low clarke values in these rock types. In the granitoids of the Mecsek Mts the concentrations of rare alkali elements are higher as a consequence of their higher mica-content. The highest concentrations, however, were detected in the more evolved and differentiated Velence Mts granite. Conspicuously high Rb content was characteristic for their aplite (464-514 ppm) and pegmatitic orthoclase (797 ppm).

The rare alkali element contents in *metamorphic rocks* are principally constrained by their concentration in the pre-metamorphic protolith. We found elevated rare alkali concentrations in the amphibolite facies metamorphic rocks in the Mecsek Mts, the reason of which, however, needs further clarification.

Out of the *sedimentary rocks* only those have been involved into the scope of our measurements, in which some enrichments of any of the rare alkali elements were expected on theoretical or practical considerations.

Considerable Li enrichments were found in some bauxite samples. We supposed that Li was contained in the lithiophorite identified by BÁRDOSSY (1977).

Numerous measurements were carried out from the Mn-oxide crusts underlying bauxite bodies as well as the samples from the Úrkút Mn-ore body that were previously identified as lithiophorite. Comparing our results with those of VARENTSOV and GRASSELLY (1980) we found that the samples studied belong to the low-Li lithiophorite varieties. Their highest Li-content was 968 ppm.

Glauconite-containing sandstone and monomineral fractiones of glauconite thereof that SZÁDECKY-KARDOSS (1955) considered as most promising in view of their possible elevated rare alkali element contents proved to be not enriched in these elements. That is their higher K content was not followed by elevated Rb and Cs contents.

Out of the evaporites, we have analysed some gypsum-and anhidrite-containing aleurolite samples. Their rare alkali element contents corresponded to the average clarke values in these rocks.

Our studies pointed to the importance of *post-volcanic processes* in the enrichment of rare alkali elements, so this problem has been dealt with in more detail. K-enriched volcanics originated by K-metasomatism have shown some Rb enrichment (to a max of 486 ppm), but this is far below the values supposed by VARGA et al. (1975). It has been established that there is no Rb enrichment concomitant with increasing K-content during the metasomatic process. This is also true in that case when K-mica predominates K-feldspar as is the case in Nagybörzsöny, Börzsöny Mts where the K-content of hidromica is 3%, whereas its Rb-content is merely 72 ppm.

The most significant Cs enrichments were discovered in zeolitised rocks (KUBOVICS et al. 1993).

The clinoptilolite and mordenite from Mád, Tokaj Mts contained 34 and 55 ppm Cs, respectively. The highest Cs-concentration in Hungary was found in the analcime from Dunabogdány Csódi hill, Visegrádi Mts (1153-1556 ppm).

The halloysite from the Gyöngyösoroszi ore field, Mátra Mts, contains 85-95 ppm Li in average. The clay minerals of the ore-containing dykes in Gyöngyösoroszi consist of illite, montmorillonite and halloysite. There is a max Li-content of 132 ppm, Rb-content of 218 ppm and Cs-content of 18 ppm in these vein-filling clay minerals. Rb and Cs are most probably fixed there by adsorption.

Studies on monomineral fractions

The monomineral fractions of some well-separable rock types (granite, granodiorite, gabbro, glauconitic sandstone) have also been analysed for rare alkali elements. In agreement with the previous data, biotites from granites and granodiorites were found to be enriched in Li, Rb and Cs as compared to K-feldspar. Out of our measurements we find worth of mentioning the Rb and Cs distribution inside the zoned microcline porphyroblasts from the granitoide near Pörböly, Mecsek Mts. The porphyroblasts there have a reddish core shifting towards a pinkish intermediate zone and then to a colourless outer rim. The Rb and Cs contents are 204 ppm and < 2 ppm in the core, while 213 ppm and 3 ppm in the intermediate zone and 306 ppm and 5,5 ppm in the rim. This change represents a certain shift in the rare alkali content of the crystallizing medium during porphyroblast formation.

Soils

The investigation of representative soil samples from various parts of the country has confirmed the widely accepted experience that the rare alkali element contents of soils mainly depend upon its mineral composition. However rare alkali elements can also be enriched by adsorption in clay minerals and humus. The highest Rb and Cs concentrations in soil, however, are linked to zeolites, too. Exceptionally high Cs-contents of 67 to 81 ppm were measured in the soil formed on zeolitised rhyolitic tuff at Gerendásrét, Tokaj Mts (KUBOVICS et al. 1992b).

Waters

The Li-concentrations of mineral and medicinal waters in Hungary is known for 40 years (SCHULHOFF 1957). These measurements have been completed by the National Public Health Institute (OKI) with data referring to Rb and Cs contents of mineral and medicinal waters. Out of these data the Li, Rb, and Cs concentrations of the thermal water at Mezőkövesd are conspicuous (1880, 336 and 430 ppm, respectively). It is presumed that these high concentrations are genetically connected to the rhyolitic tuffs in Bükkalja (South Bükk Mts).

TABLE 4

Average cesium concentrations in the major hungarian geological formations (g/t)

	fresh rocks	*rocks altered by post-volcanic fluids*
Volcanic and sub-volcanic rocks		Transdanubian Mid-Mts:
ultramafic rocks and lamprophyres	< 1	7-37 Alcsútdoboz 2.1-3.2 Vál-borehole No. 3. max. 230 Budaörs-borehole No. 1.
mafic rocks		
Mesozoic basalt	< 1	1.4-13.1 (max. 36) Mecsek Mts (max. 80) W-Hungary
Neogene basalt	0.9-1.9 anomaly: K-rich basaltoid from Bar (150 g/t)	
intermediate rocks (andesite, dacite)	5-16 Balatonmária, Börzsöny Mts, Mátra Mts	30 analcim andesite Dunabogdány, Csódi hill
acid-rocks (rhyolite, rhyolitic tuffs)		
Paleozoic (Permian)	6 Mecsek Mts	110-147 zeolitised rhyolite tuffs
Mesozoic	14 Bükk Mts	23 uraniferous phosphatised rhyolitic tuffs, Bükkszentkereszt, Bükk Mts.
Neogene	10 Mátra Mts, Tokaj Mts	
Intrusive rocks		
gabbro (Mesozoic, Triassic)	< 1 Recsk, Mátra Mts	3 Mecsek Mts: Kurd-borehole No. 2.
granodiorite (Paleozoic)	3.3. Mecsek Mts	
granite (Paleozoic)	4.6 Velence Mts	
Metamorphic rocks		
shale	< 1 N-Hungary, Rudabánya	
mica schist	4.6 Mecsek Mts; W-Hungary	
amphibolite	3.4 Mecsek Mts	
Volcano-sedimentary rocks		
Neogene basalt-bentonite	3.2 Balaton Highland	
alginite	1.5 Balaton Highland	
Neogene tuffites	5 Mecsek Mts	
glauconite Schlier	10 Mecsek Mts	
glauconitic sandstone	5.6 N-Hungary; Rudabánya, Diósgyőr	
gypsic shale	<1-2 N-Hungary	
arkosa	24 Mecsek Mts	
Soils	1.1-81 different places in Hungary	
Mineral and Medicinal waters	2-23 µg/l (max. 430 µg/l Mezőkövesd)	
Monomineral fractions		
biotite from granite	2.7 Velence Mts 24-43 Mecsek Mts	
fluorite	<1 Velence Mts	
Cr-illite	7.5-20 Mecsem Mts from uraniferous ore	
hydromuscovite	5.1 Börzsöny Mts: Nagybörzsöny	
halloysite	4 Mátra Mts: Gyöngyösoroszi	
zeolites: clinoptilolite	34 Tokaj Mts: Mád	
mordenite	55 Tokaj Mts: Mezőzombor	
analcime	1153-1556 Visegrád Mts, Dunabogdány, Csódi hill	

As an example, the distribution characteristics of Cs, the most variable rare alkali element in the major Hungarian geological formations is displayed in Table 4.

Suggestions for further studies

On the basis of informations obtained during our comprehensive survey it is deemed advisable to carry out the following studies:

– to delineate regions with anomalously high Cs-concentrations, e.g. in the case of Cs-rich zeolitic rocks. It is presumed that even industrially important Cs-rich zeolitic deposits could thus be found.

– to investigate the possibilities of Cs-extraction from zeolites during their preparation for technical purposes.

– to carry out biogeochemical studies on areas with higher-than-average clarke values for Li, Rb, and Cs, as these data are practically absent for Rb and Cs, and even the biochemical role of Li is not unanimous. This kind of interdisciplinary studies would need the involvement of experts from different fields of science.

ACKNOWLEDGEMENTS

This work has been supported by the National Science Research Foundation (OTKA) No. 728/87.

REFERENCES

BÁRDOSSY GY. (1977): Karszbauxitok (Karst bauxites). Akadémiai Kiadó, Budapest

FÖLDVÁRINÉ VOGL M. (1970): Összefoglaló értékelő jelentés a területi ritkaelemkutatás tájékozódó jellegű kutatási fázisának eredményeiről (Summary report on the results of preliminary research phase of regional rare element prospection). Magyar Állami Földtani Intézet. pp. 1-95.

GREENWOOD, N.N., EARNSHAW, A.(1984): Chemistry of the Elements. Pergamon, Oxford.

HOFFMANN L., NAGY BNÉ (1990): Ritkaalkálifémek vizsgálata atomspektroszkópiai módszerekkel (Investigation of rare alkali elements by atomic spectroscopical methods). XXXIII. MSzV. előadásai Szekszárd, pp. 193-196.

KUBOVICS I., NAGY B., NAGY BNÉ, PUSKÁS Z., HOFFMANN L. (1992a): A ritkaalkálifémek (Li, Rb, Cs) eloszlásának összehasonlító vizsgálata a hazai magmás, metamorf és vulkanoszediment képződményekben (Comparative study of rare alkali elements (Li, Rb, Cs) distribution in magmatic, metamorphic, and volcano-sedimentary formations in Hungary). Kézirat. OTKA Iroda Kézirattára.

KUBOVICS I., NAGY B., NAGY BNÉ (1992b): Cézium előfordulása a különböző geoszférákban (Occurance of cesium in various geospheres). A Magyar Tudományos Akadémia Agrártudományok Osztályának Tájékoztatója. pp. 93-96.

KUBOVICS, I., NAGY, B., NAGY-BALOGH, J., PUSKÁS, Z. (1993): Hungarian data on the geochemistry of Cs. Terra Abstracts, Vol. 5. pp. 560-561.

NAGY BNÉ, HOFFMANN L. (1991): Ritkaalkálifémek meghatározásának problémái az ásvány- és kőzetanalitikában (Problems of determination of rare alkali elements in the analysis of minerals and rocks). Analitikai Napok, Budapest

NAGY BNÉ (1992a): A Churchill-féle előgörbe alkalmazása a fotográfiás kiértékelés hibájának csökkentésére (Application of the Churchill-curve for the error-diminution of photographic evaluation). XXXV. MSzV előadásai, Székesfehérvár pp. 201-204.

NAGY BNÉ (1992b): Fényszűrő alkalmazása előre kiválasztott színképvonal intenzitásának gyengítésére (Application of light filter for weakening of pre-chosen spectral lines). XXXV. MSzV előadásai, Székesfehérvár. pp. 197-200.

PUSKÁS, Z., GÁL-SÓLYMOS, K., KUBOVICS, I., NAGY, B. (1993): Potassium rich volcanics with lamproitic character from Hungary. Terra nova, Vol. 5. No. 1. pp. 431-432.

SCHULHOFF Ö. /1957/: Magyarország ásvány- és gyógyvizei (Mineral and medicinal waters in Hungary). Akadémiai Kiadó, Budapest

STAVROV, O. D. (1978): Geohimija litija, rubidija, cezija v magmaticseszkom processze (Geochemistry of Li, Rb and Cs in igneous processes). Moscow, Nedra. pp. 1-214.

SZÁDECZKY-KARDOSS E. (1955): Geokémia (Geochemistry). Akadémiai Kiadó, Budapest

VARENTSOV, I. M., GRASSELLY, GY. (1980): Geology and geochemistry of manganese. Akadémiai Kiadó, Budapest

VARGA GY., CSILLAGNÉ TEPLÁNSZKY E., FÉLEGYHÁZI ZS. (1975): A Mátra hegység földtana (Geology of the Mátra Mts). A Magyar Állami Földtani Intézet Évkönyve. LVII., 1. pp. 1-575.

YANEV, Y. (1994): Cesium-bearing perlites from the Borovitza Caldera in the Eastern Rhodopes, Bulgaria. Petrology, Vol. 2. No. 1. pp. 82-97.

Manuscript received 10 December, 1997.

Acta Mineralogica-Petrographica, Szeged, XXXIX, 87–106, 1998

FROM FeO REDUCTION TO PERCOLATION AND OUTFLOW OF IRON: THERMAL EVOLUTION OF CHONDRITE PARENT BODIES

SZ. BÉRCZI[1,2], B. LUKÁCS[3], A. HOLBA[3], A. KISS[2] & É. PAPP[4]

[1] Dean's Office, R. Eötvös Univ., Fac. Sci., H-1088 Budapest, Rákóczi út 5., Hungary
[2] Dept. of Petrology, R. Eötvös University, H-1088 Budapest, Múzeum krt. 4/a., Hungary
[3] Central Research Institute for Physics RMKI, H-1525 Bp. 114. Pf. 49., Budapest, Hungary
[4] Dept. of Geology, Univ. of Western Australia, Nedlands, WA 6009, Australia

Key words: Thermal evolution, Chondrites, FeO reduction, Diffusion, Heat impact, Iron grains.

ABSTRACT

Some high petrologic class (6 & 7) members of the NIPR Antarctic Meteorite collection show signals indicating iron outflow. Meteorites are endpoints of heat-driven evolutions at various temperatures, and probably higher petrologic class corresponds to higher heat impact. At high enough temperature one expects liquidification of iron, resulting in iron loss from the texture. Compositional data suggest that the iron loss starts at petrologic class 6; at classes 6 and 7 of any chondrite type metallic iron (and maybe FeS) is less than for 1-5.

So petrologic class 6 exhibit a stage just before iron loss by flowing out: a stage of starting percolation of Fe. Percolation is a stage of phase transitions, when all the domains of the growing new phase have become interconnected but still the old phase exists. In this phase molten iron can form interconnected patches. This is the last stage before iron loss: if the percolated domain reaches a fault line, then Fe can start to flow out. This stage of thermal evolution is the link between chondrites and some achondrites, because at this stage the temperature is already high enough, so diffusion is so strong that chondrules start to be obliterated.

In order to see if this scheme is viable, it is necessary to give an overview of heat-induced evolution; afterwards we give measurements for the differences of iron grain distribution throughout the type LL, according to PC's.

INTRODUCTION

Thermal metamorphism is an important and well known process in terrestrial geology, which is there mainly surface process. In contrast, for meteorites this metamorphism mostly went inside the *original* parent body, so it can be used for tracing back the thermal history of that body. With as many meteorites, samples of the parent bodies, now available from Antarctic searches, it starts to be possible to distinguish different mechanisms and evolutionary stages among them. Textural evidences of such processes were recognised and studied as early as in the 60's (DODD & al., 1967; van SCHMUS & WOOD, 1967; KEIL & FREDRIKSSON, 1964; HUSS & al., 1981; LUX & al., 1981; SCOTT & al., 1984). In the 80's the center of gravity of the studies had shifted to transformations in the primordial solar nebula before condensation (KRONACKY & WOOD 1984; METZLER & al. 1992; WOOD & HASHIMOTO 1993; SCOTT & al. 1996). However now, when a large amount of chemical composition data have been accumulated (YANAI, KOJIMA & HARAMURA, 1995), it is again profitable to return to metamorphism in the accreted bodies.

Here we focus on thermal history on the basis of the NIPR thin section collections. The thermodynamic evolution of the condensed and accumulated material of the Solar System is studied, mainly for the small bodies which became cold early in the history of the Solar System. We guess that the original heat impact was generated by short-living radionuclides, so the heating and transformation of these bodies depended on their size and solar distance.

THERMODYNAMICS OF THE PARENT BODIES

Meteorite parent bodies are matters of theoretical reconstructions. Eucrites probably come from Vesta, but this is an idea based on the similarity of reflection spectra, not a fact. By simple logic we can see 3 possibilities for the origin of meteorites:

1) They can be remainders of primordial condensation, i.e. rocks on individual orbits. Then the parent body was essentially the meteorite itself, except for the outer layers lost in the atmosphere.

2) They can be the stony components of an extinct comet.

3) They can be fragments of asteroidal or planetary bodies.

Most probably all 3 cases are represented among the meteorites. However all these possible parent bodies classify together from thermodynamic point of view. Namely they are all quasistationary open thermodynamic systems in vacuo with an approximately fixed volume.

Let us make this statement explicit. Consider a parent body orbiting around Sun. If it is a thermodynamic system at all (we shall see immediately this problem), then it is characterized by its extensive variables. Generally they are: the volume V, internal energy E, and quantities of some independent chemical components N^i. For *closed* systems these quantities totally characterize the final state of the system and the Second Law tells that the system is going towards this final state with growing entropy; generally via decreasing inhomogeneities.

However now the system is not closed: there are fluxes through its boundary. These fluxes can be classified into 3 groups:

1) Irradiation comes in with solar (high temperature) spectrum, heats up the body, and leaves the body in infrared.

2) The internal energy production (i.e. by radionuclides) goes through the body and leaves it at the boundary.

3) Volatiles evaporate from the body: that is an outward particle flux. There is no incoming particle flux being in vacuo.

Now, the formalism of the thermodynamics of open systems is still not complete, there is argumentation about the general governing principle substituting the Second Law. As far as we know, it may be the minimal production rate of some entropy-type quantity, if the fluxes are fixed. However not too far from equilibrium the evolution equations of the system are known: for each extensive there is a balance equation

$$dx^i/dt + \mathrm{div}\mathbf{J}^i = \sigma^i \qquad (2.1)$$

where x^i is the extensive density, $\mathbf{J}^i$ is its flux, which, in the conductive regime and near equilibrium reads as

$$\mathbf{J}^i = -L^{ir}\mathrm{grad}Y_r \qquad (2.2)$$

where Y_i is the conjugate intensive and L^{ik} is the conduction matrix (Einstein convention is used for summation), while σ^i is the production rate in unit volume. Near equilibrium L^{ik} and σ^i are some functions of the densities x^i. Upper and lower indices, due to the existence of a Riemannian structure in the thermodynamic state space (DIÓSI & LUKÁCS 1984), are connected by the metric tensor, which is the negative of the second derivative matrix of the entropy density or by its inverse.

By these equations one can calculate the evolution of the body from some initial stage forward. What is needed is the specification of the initial state, and the conditions just outside the boundary surface. The latter ones are well-defined: there is a constant energy flux from Sun, determined by the orbital radius r, and lack of any chemical components. As for the initial state one may try with a C1 or C2 composition.

There is a problem with thermodynamics for large bodies where self-gravitation is already essential. There is no well-founded thermodynamics for systems with self-gravitation, since it is a volume force and then there will be problems with the additivity of subsystems in equilibrium. However until no great mass movements appear, the gravity field is practically constant and then it can be substituted by a prescribed *external* field. In that case the gravity potential gives a correction to the internal energy, resulting in barometric formulae for the concentrations. However this approximation breaks down if the matter melts and starts to rearrange itself. Then convection appears and the barometric formula is no longer valid. That phase is rather hard to follow, but one expects that still the denser components will be more abundant in the neighbourhood of the center.

In this paper we give an approximate treatment. The simplified model cannot give exact results in the fine details, but the model is transparent and gives correct trends.

First, let us neglect cross effects between heat and particle fluxes. Then for a homogeneous body (correct at least for the initial state) the heat conduction equation can be integrated as

$$T(R';t) \sim T_S + (F(t)/6k)(R^2-R'^2) \qquad (2.3)$$

$$T_S(t) = T_E(t)(r_E/r) \qquad (2.4)$$

where R' is distance from the center, F is radioactive heat production rate in volume unit, k is heat conduction coefficient, T_E is equilibrium temperature at Earth's orbit; r is solar distance and R is radius (HOLBA & LUKÁCS 1994).

Now, there are two kinds of energy fluxes going through the body. The first flux belongs to this temperature field as

$$q_1 = FR'/3 \qquad (2.5)$$

the second one is the incoming, converted and reradiated solar radiation. More or less the entropy loss in the second flux balances the entropy production in the irreversible processes converting the shortwave solar radiation into planetary infrared; the first flux can keep the entropy of the planetary interior low. Namely, in a stationary process, if the energy is lost at lower temperature than received, a negative term $dE(1/T_1-1/T_2)$ appears in the entropy balance, and this flux starts in the center with temperatures higher than on the surface. Until this internal heat production is substantial, the body may remain young, far from thermodynamic equilibrium, and with fast cooling unequilibrium features may freeze in.

OBSERVATIONS AND CLASSIFICATIONS

The Antarctic meteorite collecting project is a great possibility to get a true cross section and statistics about the material composition of the (outer) solar system, because i) survival chances of fragile meteorites are somewhat better than in other terrestrial

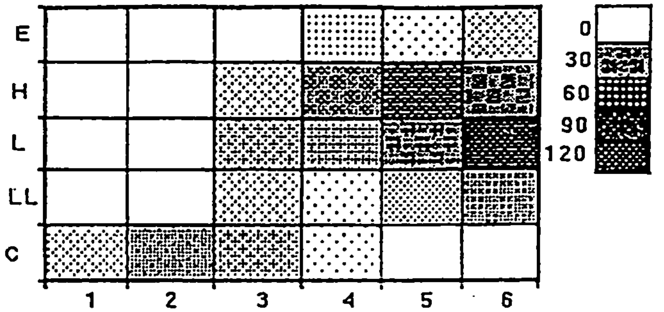

Fig. 1. Frequency of chondrite types according to the data of WASSON (1974), all types represented by a grade of gray color on their place in the Van Schmus - Wood table.

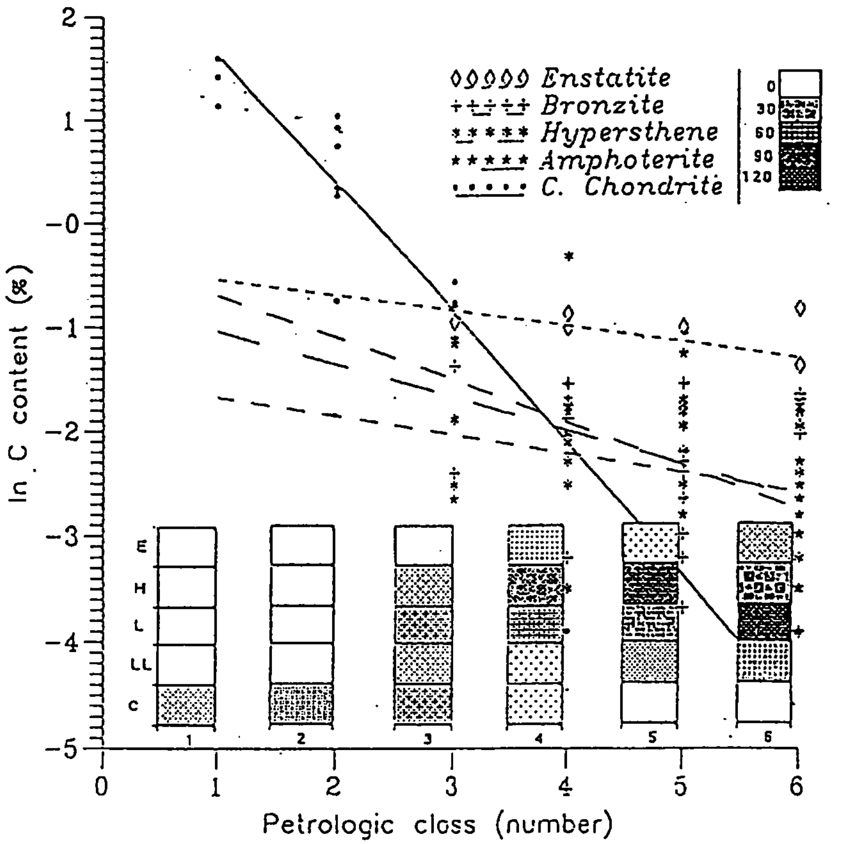

Fig. 2. Composite diagram about the carbon content of meteorite types and PC's. Columns are from *Fig. 1.* Van Schmus - Wood table with the corresponding frequencies of occurrences were added to each PC's. Therefore both carbon (from OTTING & ZÄHRINGER, 1967) and the total iron content are represented in this diagram. Lines have been fitted to the changing carbon content with PC at each meteorite types. The carbon slope corresponds to the intensity of carbon loss during thermal transformations.

localities; ii) any stony object is equally conspicuous on an ice field. However even before this project it was known that not all logically possible classes are equally abundant; what is more, some classes are absent. This suggests genetic relations among some classes.

In this paper we concentrate on the connection between the VAN SCHMUS - WOOD (1967) classification of chondrites and the Fe-FeO-C contents. This classification uses a letter and a number. The letters refer chemical composition, mainly of pyroxenes and olivines, but also oxidized iron content: E (enstatite), H (bronzite), L (hypersthene), LL (amphoterite) and C (carbonaceous), (Type, here T), while the number shows the status of chondrules (correlated with carbon and water content): 1 (absent), 2 (sharp) to 6 (very obscure) (petrologic class, here PC). (For the different C types, see OTTING & ZÄHRINGER, 1967.) *Fig. 1.* is based on the statistics of Wasson (1974). The diagonal structure of the graph is obvious: e.g. very few high numbers are seen for C and no low ones for E, H, L and LL.

Now, it is advisable to make as few assumptions as possible. However it seems natural to see some thermodynamic process behind the obscuring of chondrules; e.g. diffusion. This is faster with higher temperatures, and may freeze in with cooling. So the higher PC suggests higher and/or longer heat impact; higher PC's should be thermodynamically, and specially chemically "more evolved". To see the paths of this evolution the chemical compositions should somehow be compared to chondrite types and PC's. One may expect volatiles negatively correlated with PC if the above guess is correct, and the evolution may be different for different types.

Let us see first the C content. We use a graph of OTTING & ZÄHRINGER (1967). The vertical axis is logarithmic, and we fitted exponentials in PC number for individual T's. That is *Fig. 2.* Indeed, in general the volatile C content decreases with PC.

E2, H2, L2 and LL2 chondrites are unknown, but PC 2's may be visualized as startpoint of chondrule unsharpening via diffusion. The curves extrapolate back there. The E and H lines are clearly parallel, although mean deviation is substantial for H. The slope is smallest for E and H, then come LL, L and C. C leaves through the surface, so it is tempting to conclude that this was the size sequence from upward down for the parent bodies. Lines C and E meet at PC 3, and that is the lowest petrological class for E. This fact does not prove the C origin of E-s, but is compatible with such an idea. The original lower C content of H-s is surprising; we do not suggest any reason just now; an analogy is the difference in total Fe content between (E,H,C) and (L,LL) (WIIK, 1956).

THE ORIGIN OF CHONDRULES

The origin of chondrules may have been a process on its own right albeit somewhat connected to that of the matrix (RADOMSKY & HEWINS, 1990; SCOTT & al., 1996). One fact supporting this is the roughly spherical, droplet-like form. This suggests original melting. If so, then there was a heat-flash around the very young, non-equilibrium Sun, and somehow chondrule-free "pre-chondrites" were bombarded with the solidified droplets. In this scheme C1 "chondrites" somehow avoided the bombardment. If so, then orderly thermal evolution started in PC 2. However that is not the only viable explanation. The thermodynamics of open systems knows an interesting effect when at sufficiently high fluxes and/or entropy production rates the homogeneity of the system breaks down and some internal structure appears (PRIGOGINE, 1969). So there is no fundamental argument against chondrules differentiating from a homogeneous pre-matrix, provided that high thermodynamic fluxes were present, which is not impossible during condensation or in a large hot body. Of course this statement does not substitute an idea how the differentiation happened.

Long ago MASON (1962) suggested an evolutionary path, starting with C1. Then, with higher and higher heat effects first serpentine loses water (this process is perceptible at 400 C°), and some olivine chondrules crystallize, then the groundmass serpentine decomposes into olivine and pyroxene, finally C starts to reduce the iron oxide in olivine. Let us note that phase transitions starting from separate nucleation cores result in growing "bubbles" of the new phase, roughly spherical. If this process freezes in and the new phase cannot percolate, the general picture may be similar to matrix+chondrules in PC 2 even without melting. The scheme was

$$MgFe_2Si_4O_{10}(OH)_8 + 2C + heat \to 2(Mg,Fe)_2SiO_4 + 2(Mg,Fe)SiO_3 + 4H_2O + 2C \to$$
$$4MgSiO_3 + 2(Mg,Fe)SiO_3 + 2Fe + 4H_2O + 2CO_2$$

where water and CO_2 evaporate. In addition, C as volatile can be lost by diffusion.

One of such schemes may be proven true in the future; indeed it seems as if asteroid 3-filter colors were to suggest an evolution from something exotic in meteorites towards olivine and/or serpentine (BÉRCZI, HOLBA, & LUKÁCS 1995a). However now we want to use minimal theory. Still, no doubt, C can reduce FeO even well below melting point, and C can be lost by diffusion.

FeO REDUCTION (AND C EVAPORATION): MODEL EQUATIONS

Consider a model meteorite class whose main chemical components, according to the above Mason scheme, are silicates with some FeO in the lattice, metallic Fe and C, all others negligible. In such a system there are strong correlations between chemical composition and PC. The higher heat impact means i) more diffusion, so higher PC; ii) more diffusion, so lower C content; iii) more reduction by C, so again lower C content, less FeO in the silicates and more Fe. Two quantities are constant: Si and total Fe. Since chondrites are roughly classified into a high-Fe group of 27 % total Fe content and a low-Fe one with 20 % (WIIK, 1956), the picture is simplified but not obviously absurd. Therefore let us be investigating this model system for a while.

Let us start from PC 2, so chondrules are already in the matrix. Consider mole concentrations of only 3 independent chemical components: Fe (z), FeO (x) and C (y); the other concentrations are taken constant. The environment is oxygenfree, so the main processes are reduction of FeO by C, formation of CO and CO_2, and evaporation of C, CO and CO_2 through the surface. In first approximation we neglect the internal inhomogeneities. Then, assuming that gases vanish rapidly,

$$dx/dt \sim -2A(T)xy \tag{5.1}$$
$$dy/dt \sim -A(T)xy - R^{-1}B(T)y \tag{5.2}$$
$$dz/dt \sim -dx/dt \tag{5.3}$$

The 1/R term takes into account that C loss is through the surface. The temperature-dependent factors have the structure

$$A(T) \sim A_0 \exp(-Q_A/T);\ B(T) \sim B_0 \exp(-Q_B/T) \tag{5.4}$$

Assume that we know A_0, Q_A, B_0 and Q_B from solid-state experiments or metallurgy; for the actual temperatures take eqs. (2.3-4). Then in a parent body of radius R, at R' from the center and on an orbit of radius r one can integrate (5.1-3) from some initial conditions.

Note that for anything in asteroid range the early higher temperatures could not be maintained by anything else than the short-living radioisotopes. If we represent them mainly by Al^{26}, then F is high for times comparable to its half-life, 700000 y. The temperature dependence of A(T) and B(t) is serious, so in first approximation one can solve the equations until $t=t_c$, somewhere in the order of a million years, and then stop.

The solutions have the form

$$y_f = y_i - x_i + x_f + (B/2AR)\ln(x_f/x_i) \qquad (5.5)$$

$$z_f = z_i + x_i - x_f \qquad (5.6)$$

and x_f is the solution of the implicit equation

$$2At_c = \int_{x^f}^{x_i} w^{-1}(y_i - x_i + w + (B/2AR)\ln(w/x_i))^{-1} dw \qquad (5.7)$$

Therefore the final concentrations depend on the initial ones, on the radius, and on the temperature (which again depends on radius if the heating is internal). Reduction and C loss together goes up with temperature, but C loss is sensitive on R too.

A(T) is fairly calculable from iron productive technics below melting point (mainly belonging to ancient ages, however cf. the Höganäs method), but for free iron oxides, not for silicates; and C diffusion coefficient B(T) is well known in iron (where it is remarkably high, see KITTEL (1961)), but not in all meteoritic matrices.

DIFFUSION

Diffusion transforms the texture inside the parent body, not only the chondrules. Note that during heat impact various diffusion processes go on, each with its own diffusion coefficient D(t), and for order of magnitude the final diffusion length a_f will be

$$a_f \sim (D(T)t_c)^{½};\ D(T) \sim D_0\exp(-Q_D/T) \qquad (6.1)$$

Concentrate first on chondrules. They are "sharpest" in PC 2 and "most obscure" in 6, while cannot be seen in 7. So, with chondrules of radius a_0 the PC is 2 if $a_f<<a_0$, and 6 if $a_f a_0$. Being t_c fixed, this ratio depends on T, and if A(T), B(T) and D(T) are known, by inverting the formulae A and B will depend on a_f/a_0. So concentrations must (more or less) depend on the PC and size.

At even higher temperatures the diffusion length becomes macroscopic. Line C is where the C diffusiion during the hot million years becomes macroscopic, i.e. cca. 1 cm. Such diffusion may have produced e.g. ureilites. On the line

$$D_0\exp(-Q/T)*t_c \sim 1\ cm^2 \qquad (6.2)$$

where Q is some characteristic activation energy. The corresponding diffusion coefficient is $D=3*10^{-14}$ cm^2/s. There are measurements for at least some volatile gases in augite, and for them 1000 C° would be needed for this value of D (FECHTIG, GENTNER & ZÄHRINGER, 1960).

As for the chondrule diffusion, matrices and chondrule compositions vary, and we do not have even olivine self-diffusion coefficient at reach. So here we try to guess only from the previous date. If volatiles can diffuse 1 cm in a million years in augite at 1000 C°, then maybe olivine could diffuse that distance at 1200 C°. Then the PC 7 is created in parent bodies above cca. line D.

Consider a stage of high enough temperature. This is the situation on orbits very near to Sun (e.g. at perihelia of Earth-crossers) or in parent bodies of substantial size when the short-living radioisotopes were still present.

The short-living radioisotopes, Al^{26} and Pu^{244}, are extinct now. So their original concentration is unknown. Astronomers generally believe that Al^{26} was the more important. Now, an estimation is possible for the initial radio-Al concentration, if we assume that F/k of the parent bodies did not differ too much. Consider eqs. (2.3-4) at the center R'=0. One gets:

$$T = T_E(r_E/r)^{1/2}(1-R/R_{cr})^2 + T_{cr}(R/R_{cr})^2 \qquad (7.1)$$

where T_{cr} is some important temperature and R_{cr} is the radius of the body in which $T=T_{cr}$ in the center. Now, global differentiation starts with melting of iron, because molten iron can flow out from the silicates. The corresponding temperature is cca. 1800 K for FeNi and ·1400 K for FeC.

The only free parameter is R_{cr}. Now, observations seem to suggest that the bigger asteroids are differentiated. The picture is not clear because it seems that 349 Dembowska is only partly differentiated, but 44 Nysa is completely so. A popular explanation is that 44 Nysa *was* a part of the mantle of an asteroid, whose iron core might have been 135 Hertha. If so, then differentiation started from $R_{cr} \sim 65$ km; this value may have to be revised in the future but now will do. By writing T_{cr}=1800 K one now gets the initial central temperatures in the function of R and r; and this initial temperature is declining with the extinction of radioisotopes. If they are dominantly Al^{26}, then the characteristic time is t_c~1 My. Then the initial central temperatures are shown in Fig. 3. We decline to discuss whence came the original Al^{26} concentration; the differentiated asteroids must have been melted anyways.

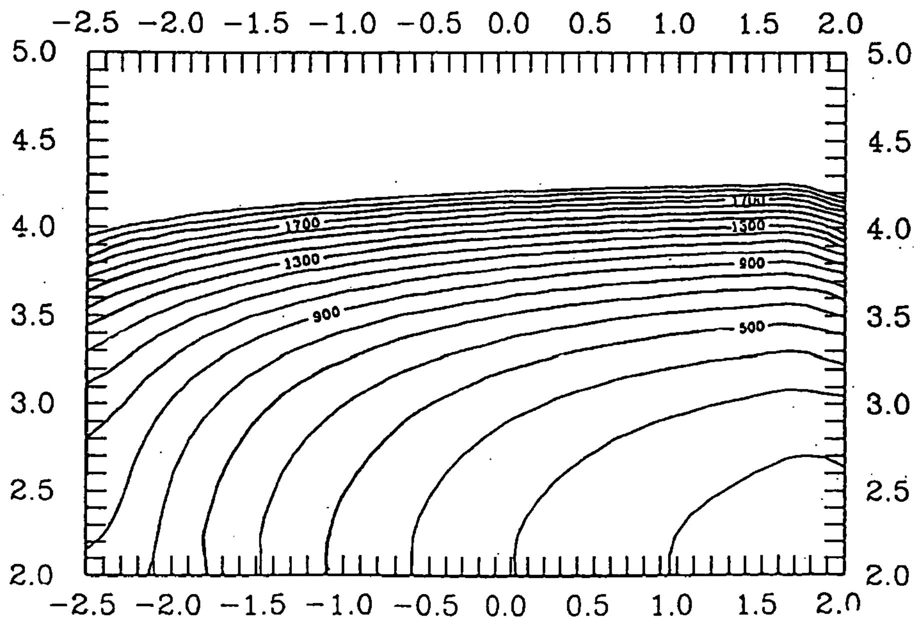

Fig. 3. Post-condensation central temperatures for bodies with different initial mass and solar distance

If iron could melt in the asteroid, then it began to accumulate in the central core of the body; during a million years even weak gravity can do it. The descending iron carries down alloying components (as C and Ni) and matter of similar density and melting point (as FeS). If partial melting in mantles of smaller bodies could produce basaltic type fluids, and they migrated to the surface, Vesta-like volcanic surfaces could develop on asteroids.

C diffuses in iron very easily in Fe; just below the melting point of carbonized iron D(T) seems to be 0.001-0.01 cm^2/s (SHEWNON, 1963). Therefore C can diffuse out from the Fe core from km depths. Due to this process one expects only minor C content in iron meteorites or at the surface of iron asteroids (whence the mantle has been peeled off).

The picture seems to be coherent, but it is not necessarily true. Fortunately just recently it became possible to check it: the National Institute for Polar Research, Tokyo, Japan, has performed chemical analyses on several hundred meteorites of the NIPR collection, mainly Antarctic ones (YANAI, KOJIMA & HARAMURA, 1995). In the next Section we will see if our simplified thermodynamic model can describe chondrite evolution.

CHONDRITE EVOLUTION IN THE LIGHT OF THE RECENT NIPR ANALYSES

The NIPR collection contains cca. 8000 meteorites, mainly Antarctic ones. The most recent report from them is YANAI, KOJIMA & HARAMURA (1995). 3334 meteorites have been classified up to now, of which 3072 are chondrites. The recent report contains chemical analysis of 541 meteorites, the overwhelming majority performed by Dr. Haramura, with a homogeneous method. This huge database enables us to check evolutionary theories. Evolutionary positions of the 30 samples of the NIPR Educational Thin Section Set are shown on *Fig. 4.*; a detailed discussion will come in Sect. 11.

First let us see if the sample is representative. Fig. 1 gave a two-variable distribution of *falls* (numbers vs. type and PC). Now, the corresponding distribution for classified NIPR chondrites is *Fig. 5.* Obviously the two distributions differ. The most striking difference is the high representation of H4's in the NIPR collection. The ratio of the earlier and 1995 distributions is shown on *Fig. 6.* However for the average properties of chondrite classes these differences are irrelevant.

Fig. 7. shows the selection in analyses. It can be seen that the analyst generally tried to select relatively more samples from the rarer classes.

Let us remember that WIIK (1956) found two strips on a plot (Fe not in oxides vs. Fe in oxides): with cca. 20 % (LL & L) and 27 % (C, H, E) total Fe contents. Of course, Fe weight ratio changes with volatile loss, so the data should be somehow normalised. We normalised the composition data to Si. Namely, we practically do not know processes extracting Si. Si generally remains in the silicates, except for minor reduction in E6 (Wasson, 1974), and silicates are not volatile. Now, Fig. 8 is oxidised Fe/Si vs. other Fe/Si. Chondritic types modestly separate, but we do not see definite straight lines. Rather, two curved strips are seen, meeting at the lower part of the H region. It seems *as if* LL's and C's were the startpoints of two parallel evolutions towards H's, but, as we shall see, it cannot be so.

Since the number of the relevant chemical components is at least 3 (Fe°, FeO, C), we need a *tripolar* representation, e.g. colours, to describe the chemical evolution. Let 30 % metallic + sulphide Fe content be represented by pure red, 30 % FeO by pure green and 5 % C by pure blue. Then, going from low petrologic classes to high and finally to achondrites, E's start from brick red through strawberry red until cherry red; the E

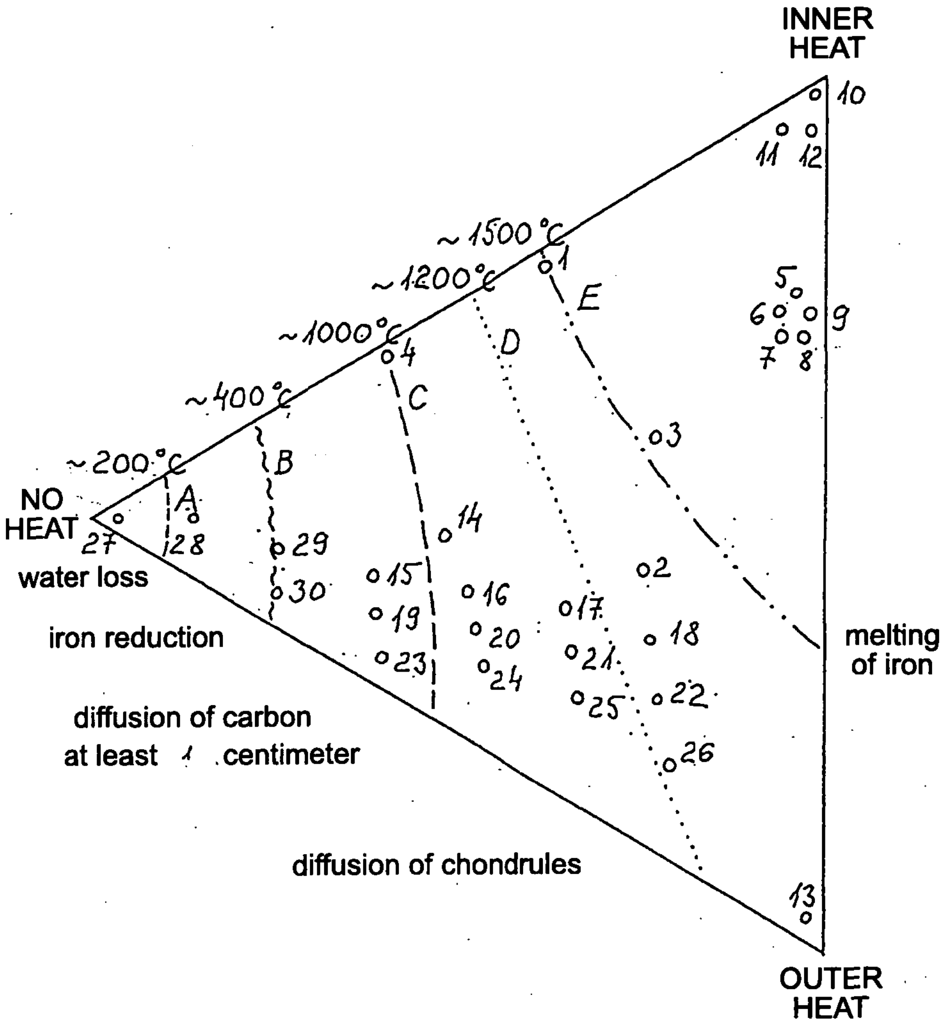

Fig. 4. The arrangement of the samples of the Japanese Antarctic Meteorite Thin Section Set in our tentative NO HEAT - INNER HEAT - OUTER HEAT triangle diagram. Detailed explanations in the text. Lines A, B, C, D, and E represent characteristical transformations in meteorites. Numbers represent meteorite types in the NIPR Thin Section Set.

achondrite is practically black. H3 is ochre yellow, H3-4 is exceptionally reddish, H4 and H5 are brownish, but H6 is greenish yellow. The H achondrite is not known. L's are oscillating between grayish green and greenish brown; the achondrite is rather green. LL's are all green, oscillating between grass green and olive green; the achondrite is deep green. Finally, C1's are bluish, C2's are grayish green, but then the colour becomes more and more green and C6 is deep green; the C achondrites are not identified, but ureilites are bluish.

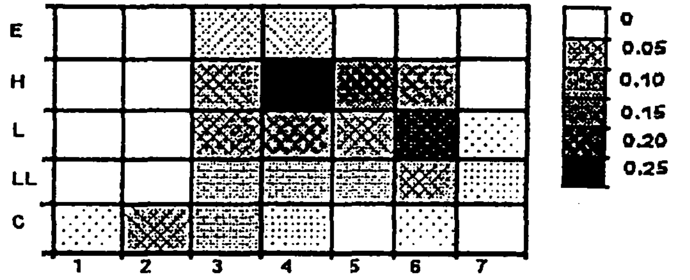

Fig. 5. Frequency of occurrence of meteorite types in that part of the NIPR Japanese Meteorite Collection where it was determined. Frequency data are transformed into a gray color grade, like as on *Fig. 1.* The two most frequent types are H4 and L6 in the NIPR Antarctic Meteorite Collection

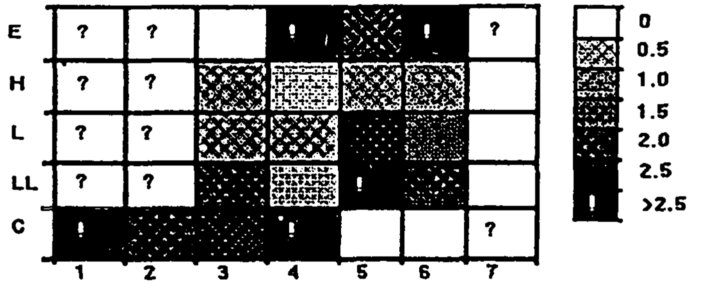

Fig. 6. Ratios of the occurrence frequencies for meteorites on *Fig. 1.* (Wasson) and *Fig. 6.* (NIPR). The "Wasson"/"NIPR" ratios show that there are considerable differences in occurence of chondritic meteorites of fall (Wasson) and found (NIPR) origin.

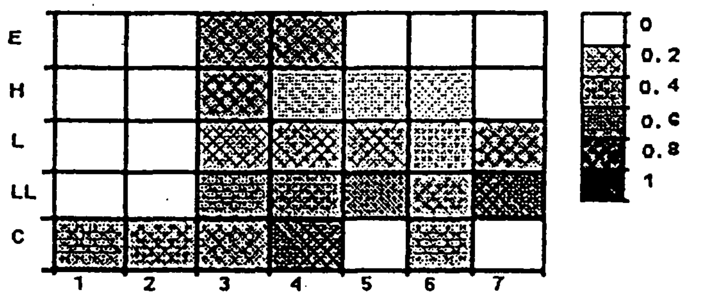

Fig. 7. This diagram shows how does the Japanese chemical analysis (Catalog of Antarctic Meteorites, NIPR, 1995 by YANAI, KOJIMA & HARAMURA) represent the various Van Schmus - Wood types.

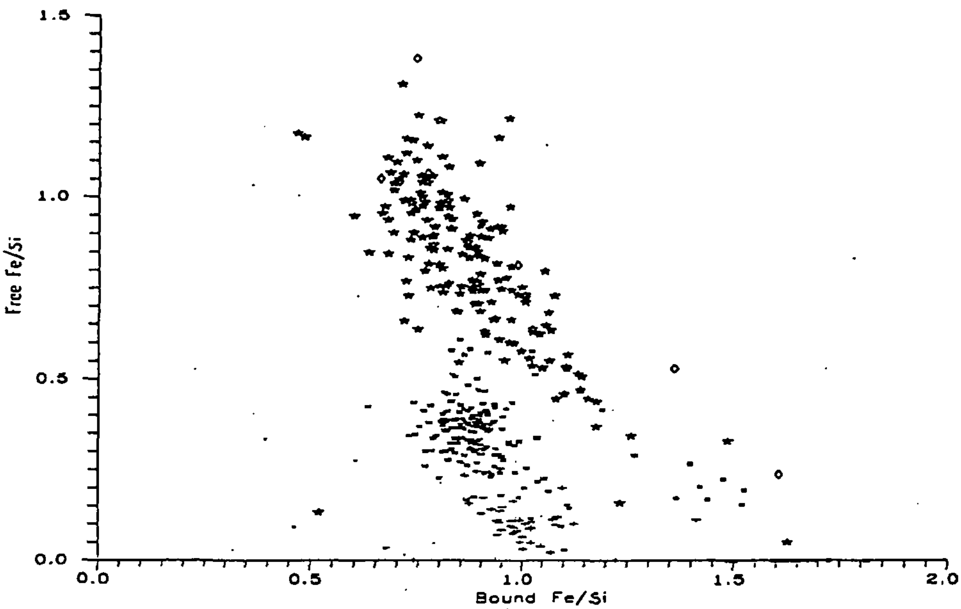

Fig. 8: NIPR Catalog Data for chondrites, arranged in the classical oxidized Fe/non-oxidised Fe diagram. The data were normalized to the Si content of the meteorites. For astronomers this diagram resembles the Hertzsprung-Russel diagram where two characteristical data of stars with different initial conditions and evolutionary paths are represented.

There are some oscillations in reduction/oxidation. *Fig. 9.* shows the five chondritic types on the Fe+FeS vs. Fe oxides map; the PC's are indicated as labels. Clearly "cycles" or "loops" are seen. This is incompatible with the evolution equations of Sect. 5. At the ends of the LL, L and E lines total Fe loss is seen; maybe there the temperature reached the melting point of carbonised Fe, so global differentiation started.

Of course the chondrites did *not* evolve through the present types, but represent final states after evolutions with the same lengths t_c but different heat impact. However, although this distinction is important, it cannot explain the oscillation if the only possible reaction is reduction.

Let us note here something from the thermodynamics of open systems. The Second Law does not imply irreversible changes in an *open* system; if the fluxes through the system are strong enough, then the system may remain stationary, may go in cycles, &c. Still, if the only possible reaction is reduction, then the process cannot go backwards. So the oscillation between reduction and oxidation needs an oxidizing agent too.

We do not have direct information about the conditions in the parent bodies of meteorites in the very youth of the Solar System. However there is a quite common material, present in meteorites, which oxidizes iron on higher temperatures. That is water. Since Fe is of more positive nature than H, Fe can take O from H_2O, liberating H. This process is seen in laboratory, but only at high temperature (cca. from 600 C°). However this temperature is quite reasonable during the early meteorite evolution, and of course the reaction goes also at lower temperatures, only imperceptibly slowly, which on million years

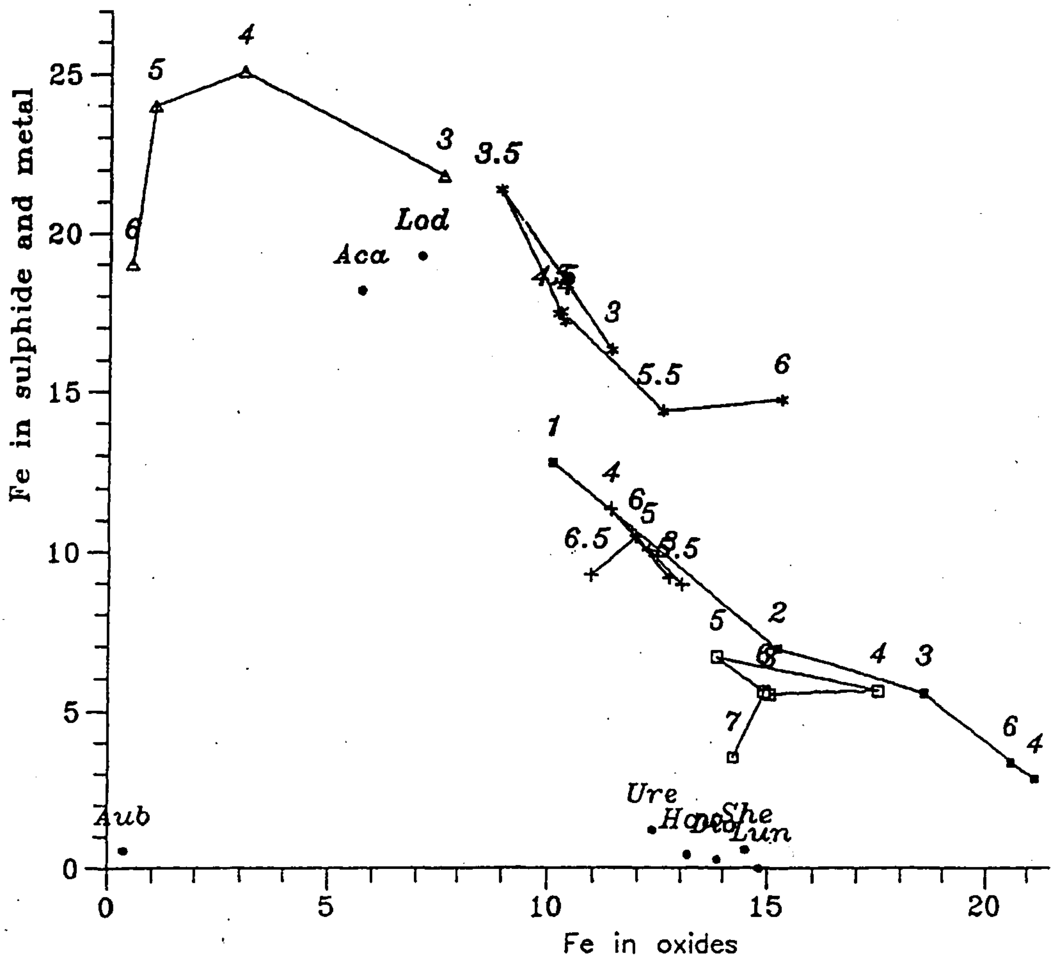

Fig. 9. Fe+FeS vs. Fe oxides data averaged from data of NIPR Catalog, connected by lines for individual T's. To and fro motions are seen. The early reduction and later oxidation can be seen for H, L, and LL groups, while the E group moves toward reduction.

scales still can be relevant. Water is a minor, but common component in LL's, L's and H's of moderate PC's, in 1 % order of magnitude (YANAI, KOJIMA & HARAMURA, 1995).

Then one could complete the system (5.1-3) by incorporating H_2O (w), as

$$dx/dt \sim -2A(T)xy + C(T)wz \quad (9.1)$$

$$dy/dt \sim -A(T)xy - R^{-1}B(T)y - Q(T)yw \quad (9.2)$$

$$dz/dt \sim -dx/dt \quad (9.3)$$

$$dw/dt \sim -2Q(T)yw - C(T)wz - R^{-1}W(T) \quad (9.4)$$

where, as far as the new terms are considered, W is a coefficient of water diffusion, C is the coefficient in the reaction rate of $Fe+H_2O \rightarrow FeO+2H$, and Q is that of $C+2H_2O \rightarrow CO_2+2H$. Then again the equations have to be integrated up to $t_c \sim 1$ Ma, obtaining the final composition.

Unfortunately the rate coefficients C(T) and Q(T) are not available for us, although the latter could be taken from the experiences of the now practically defunct industry producing artificial cooking gas ("water gas") from coal. However it is easy to see that eqs. (9.1-4) will contain oscillatory solutions if C(T) starts to rise later but more steeply in T than A(T) does. And this may be so, since a part of the water is originally bound in the silicate lattice, so it will be effective only at higher temperatures. As for quantities, characteristic values are 0.2 weight % for C and 1 weight % for H_2O. Now 1 % C can reduce 9.5 % Fe from FeO, while 1 % H_2O can oxidize 3.1 % Fe. Therefore the presence of water could explain an oscillation of amplitude about 3 %, and something similar is seen. As for the H_2O/Si ratio, it is shown on *Fig. 10.*

In order to check the genetic relations among chondrite classes, *Fig. 11.* shows the average (total Fe)/Si mass ratio vs. PC separately for E, H, L, LL and C. Since neither Fe compounds, nor Si are volatile, this ratio cannot change in evolutionary processes except for melting and global differentiation, not expected for moderate PC's. Indeed, the curves are roughly horizontal, except for the ends where the obvious explanation is partial loss of molten Fe and FeS. Now, the 5 types clearly separate to a high Fe group (E, H, C) and a low Fe one (L and LL), quite conformally with the old results of WIIK (1956) on a much less sample; but, in addition, the differences between L and LL seem significant too. This means that L's and LL's cannot be in close genetic connection with the others (as seen earlier on *Fig. 8.*).

Fig. 11. makes a problem explicit. LL2 and L2 chondrites (i.e. ones with very sharp chondrules *and* high volatile content) are unknown. They are unknown for H and E as well, but the conserved Fe/Si ratio does not rule out the common origin of the C3, H3 and E3 chondrites from a C2-like precursor. But this seems impossible for LL3 and L3. Then either the high-volatile precursors did not survive the evolution, or they never existed. The second solution is possible if LL's and L's originate from the inner System, where neither water, nor hydrated silicates condensated; but then it is difficult to understand the low iron content. We cannot solve this problem at the present stage; however *Fig. 11.* clearly shows that the so called H3-4's are well out of the H line. They cannot seem H's at all; at least for iron content they could be rather E's. So no surprise if H3-4's do not fit between H3's and H4's also for FeO, FeS and H_2O.

EVOLUTION OF IRON GRAINS: PERCOLATION AND OUTFLOWING

If the above scheme is real, then one must see some signal of thermal evolution also in the texture of chondritic meteorites, e.g. in the number and grain size distribution of iron grains. This change is the result of the oxidation-reduction chemical reactions in the system. New iron grains appear, grow or older ones shrink or disappear. We checked this on grain size distributions of LL chondrites. It seems that the statistics of the present, first, investigation should be doubled or trebled; but even now some evolutionary effects are seen.

For determining the size distribution of iron grains we used two groups of Antarctic Meteorite Samples on loan from NIPR, Tokyo. One was a sequence of LL3, LL5 and LL7 petrologic types (ALH-77304, 83-4, Y-74022, 92-2, and Y-791067, 73-1), the other one was taken from the Antarctic Meteorite Thin Section Set of NIPR, the samples of 24, 25 and 26, LL4, LL5 and LL6, (Y-74442, 83-6, ALH-78109, 88-1, and Y-75258, 97-8), respectively. Number of grains were counted in petrographic microscope (Nicon-type)

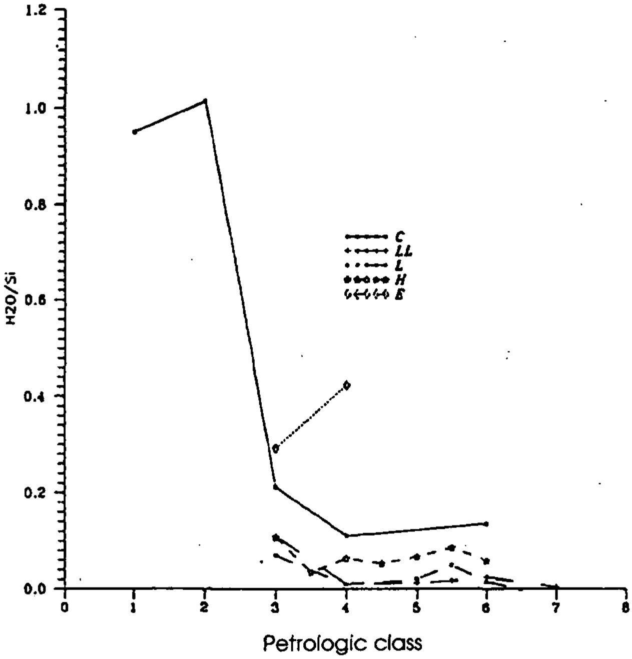

Fig. 10. H_2O data normalised to Si for chondrite types show the water loss trend for all meteorite types during thermal evolution of parent bodies.

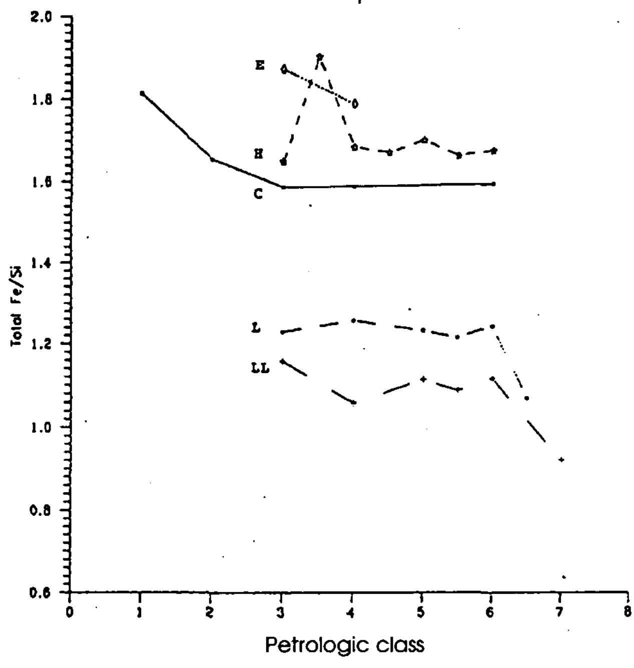

Fig. 11. Total Fe/Si versus PC for NIPR Catalog data. In first approximation we can see the two "lines" of Wiik (1956) in total Fe content.

belonging to 1: 0-25 μm, 2: 25-50 μm, ... up to 8: >175 μm size ranges. (In order to receive a more smooth averages, all 25 μm ranges were subdivided into three smaller intervals and counts were carried out for these shorter diameter ranges, then three of them were summed up.)

The measurements resulted in 6 iron grain size distributions: one for PC's LL3, LL4, LL6 and LL7 and two for LL5. The normalized distributions are shown in Figs. 12a-f. LL4 and both LL5's have "tails" at large grain sizes. It seems consistent with our observation that in the LL group at the final stage of their evolutionary path some iron loss is suspected; maybe at high temperature the substantial iron grains percolate and Fe flows out. Indeed, the "tail" is missing at LL6 and LL7.

Then we checked if there are statistically significant differences between the Fe grain distributions. In the lack of any serious theory for the shape of the distribution we used a χ^2-type test. Our first null hypothesis is that all distributions are the same, and differences come purely from statistical fluctuations. This null hypothesis is disproven on a quite satisfactory significance level.

If in size range i the actual grain size is n_i, then its statistical mean deviation is $\sim n_i^{1/2}$. Then

$$\chi^2_{12} = \Sigma_i (n_{1i}/N_1 - n_{2i}/N_2)^2/(n_{1i}/N_1^2 + n_{2i}/N_2^2) \qquad (10.1)$$

N being the total grain number. We measured at 8 points, so the degree of freedom is 7. The χ^2 values for various pairs are:

(34) = 18.5; (35) = 23.8; (36) = 31.5; (37) = 51.3
(45) = 23.2; (46) = 20.2; (47) = 47.8
(56) = 21.8; (57) = 21.2; (67) = 16.6

Here *5* stands for the united distribution of 2 LL5's. None of these values are conform with a uniform distribution considering that the expectation value is 7, and the mean deviation is $\sqrt{14}$. For more details of the test see JANOSSY (1965).

There may be moderate differences within the same van Schmus-Wood class too. We checked this possibility on the 2 LL5 samples, with the result

$$\chi^2_{55} = 12.2$$

compatible with no difference at all at slightly more than 1σ level.

Taking the numbers in face value, we can conclude that the two LL5's are undistinguishable at any fair significance level while any two samples of different classes can be; the differences are the smallest for neighbours. Our guess is that no more than 3 different thin sections for each class would suffice for settle the question if the classes are distinguishable for grain size distributions. Possibly LL5 is an exception; earlier we saw that oxidation takes over at LL5, so trends change there and the diversity may be higher.

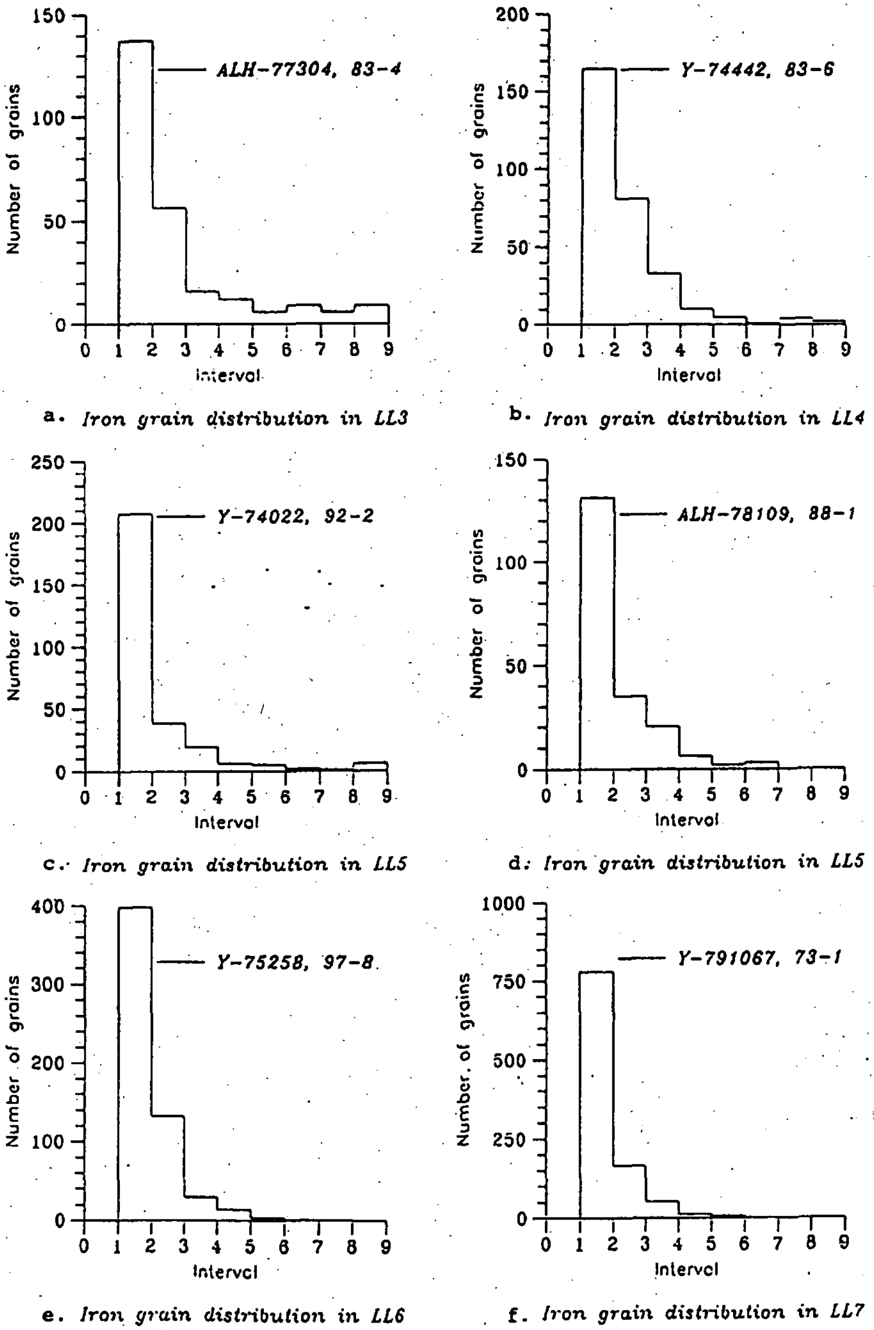

Fig. 12. Grain size statistics for NIPR LL chondrites. a: LL3, b: LL4, c & d: LL5, e: LL6, f: LL7.

SECOND DISCUSSION: SUMMARY AND PROBLEMS

Now we can return to *Fig. 4*, the thermal evolution pattern for chondrites (and closely related achondrites). Although we have found no startpoint for LL's and L's, otherwise the general structure of Fig. 4 remained unchanged. Although the samples are products of a thermal history of 4.5 billion years, this thermal history depended on size and solar distance. We sketched the main processes of the thermal history of different sized parent bodies.

Our tentative guess for genetic connections can be formulated by 5 "chains", along which the sequences fron "primitive" to "evolved" is as follows. A startpoint may be ***27*** or ***28***. After ***28*** there may seem to be a trifurcation. The "C" line goes through ***29*** & ***30*** -> C4 -> C5 -> C6 (absent in the NIPR Set) -> (maybe) ***4***. The "H" line goes via ***15*** -> ***16*** -> ***17*** -> ***18***, and may or may not end in ***13***, whose chemical analysis is not available. The "E" line goes through ***14***, continues with higher E's absent in the Set, and may end in one or more of ***1***, ***2*** and ***3***. The "LL" and "L" lines do *not* start from ***28***; the traceable part of "LL" is ***23*** -> ***24*** -> ***25*** -> ***26***, then an LL7 (absent) and it may end in pigeonite achondrites (absent), while that of the "L" seems to be ***19*** -> ***20*** -> ***21*** -> ***22*** -> L7 (absent), and it also may or may not end in ***13***. Samples ***5-12*** differentiated inside of large bodies, so their original ancestry is doubtful and they are partially out of the scope of the present paper.

The picture is transparent (and oversimplified), and the detailed numerical model calculations are impossible until the temperature-dependence of the reaction rates will be known for water dissolution by Fe and C. But this needs only simple laboratory experiments (preferably with hydrated silicates). Now come here some serious problems.

We do not see the startpoints of LL's and L's.

Although no Figure has been given here for individual Fe *compounds* (for that see BÉRCZI, HOLBA & LUKÁCS, 1995b), according to the averaged NIPR data FeS content does not depend too much on PC, except for C's, although one would expect reduction by C here too, and CS_2 is a gas at higher temperatures, similarly to CO_2. But obviously we do not know enough about the behaviour of CS_2 without free O but together with Fe and FeO. Anyway, FeS concentration seriously changes in early C's. (Sulphide Fe)/Si~0.2 for LL, L and H, but ~0.5 for E. This is again a feature connecting E's intimately to C's of low PC's (others are the C and H_2O data). A good explanation of the origin of the (rather rare) E chondrites should explain the high FeS concentration too.

Ureilites are similar to C2 for C and H_2O content (cf. *Fig. 11.*), but in the same time they are achondrites with a substantial heating. A large body could stop evaporation of C *or* H_2O, but can it completely retain CO, CO_2 and H_2 appearing in chemical reactions as well?

If we imagine that C2 resembles the common precursor of C3, H3 and E3 (which is at least not impossible according to *Figs. 10 & 11.*), then an explanation would be needed for the trifurcation. A natural idea would be the size of the body (larger ones could retain more volatiles), but PC's 3 and 6 both exist in all the 3 groups, suggesting small and large bodies as well.

And finally: what has prohibited the formation of proto-meteorites with intermediate initial Fe/Si ratio? The gap on Fig. 11 is not decisive, being a gap in averages; but *Fig. 8.* clearly shows "forbideen regions". Does this dichotomy show something about the primordial condensation, or did bodies of "intermediate" Fe/Si ratios evolved so differently that they now are not considered chondrites?

ACKNOWLEDGEMENTS

Partly supported by OTKA T/026660, MKM 694/96 & OMFB-MÜI-TP-055/96. Authors thank the illuminating discussions with Dr. Kojima, and the lending of a sample of the NIPR Antarctic Thin Section Set to Drs. YANAI and KOJIMA.

REFERENCES

BARSHAY S. S., & LEWIS J. S. 1975: In : The Dusty Universe, eds. Field G. B. & Cameron A. G. W., Neale Watson Acad. Publ., New York
BÉRCZI SZ., HOLBA AGNES, & LUKÁCS B. 1995a: KFKI-1995-10
BÉRCZI SZ., HOLBA AGNES & LUKÁCS B. 1995b: Acta Miner. Petrog. Szeged, **XXXI**, 53
BÉRCZI SZ. & LUKÁCS B. 1994: KFKI-1994-11
DIÓSI L. & LUKÁCS B., 1984: Phys. Rev. **A29**, 3343
DODD JR. R., T., VAN SCHMUS W. R. & KOFFMAN D. N., 1967: Geochim. Cosmochim. Acta, **31**, 921
FECHTIG H., GENTNER W. & ZÄHRINGER J. 1960: Geochim. Cosmochim. Acta **19**, 70
HOLBA AGNES & LUKÁCS B. 1994: In Lukács B. & al., KFKI-1994-22, p. 81
HUSS G. R., KEIL K. & TAYLOR G. J., 1981: Geochim. Cosmochim. Acta **45**, 33
JANOSSY L. 1965: Theory and Practice of Evaluation of Measurements. Oxford University Press, Oxford
KEIL K. & FREDRIKSSON K., 1964: J. Geophys. Res. **69**, 3487
KITTEL CH. 1961: Introduction to Solid State Physics. J. Wiley, New York
KORNACKI A. S. & WOOD J. A., 1984: Geochim. Cosmochim. Acta **48**, 1663
KUBOVICS I. & al. 1994: In Lukács B. & al. KFKI-1994-22, p. 29
LUX G., KEIL K. & TAYLOR G. J., 1980: Geochim. Cosmochim. Acta **44**, 841
MASON B. 1962: Meteorites. J. Wiley & Sons, New York
METZLER K., BISCHOFF A. & STÖFFLER D., 1992: Geochim. Cosmochim. Acta **56**, 2873
OTTING W. & ZÄHRINGER J. 1967: Geochim. Cosmochim. Acta **31**, 1949
PRIGOGINE I: in: Theoretical Physics and Biology, ed. M. Marois, North-Holland, Amsterdam
RADOMSKY P. M. & HEWINS R. H., 1990: Geochim. Cosmochim. Acta **54**, 3475
SCOTT E. R. D., KROT A. N & BROWNING L. B., 1969: LPS **XXVII**, 1161
SCOTT E. R. D., RUBIN A. E., TAYLOR G. J. & KEIL K., 1984: Geochim. Cosmochim. Acta **48**, 1741
SHEWNON P. G. 1963: Diffusion in Solids, McGraw-Hill, Toronto
VAN SCHMUS W. R. & WOOD J. A. 1967: Geochim. Cosmochim. Acta **31**, 747
WASSON J. T. 1974: Meteorites. Springer, Berlin
WIIK H. B. 1956: Geochim. Cosmochim. Acta **9**, 279
WOOD J. A. & Hashimoto Akihiko, 1993: Geochim. Cosmochim. Acta **57**, 2377
YANAI K. & KOJIMA H. 1987: Photographic Catalog of the Antarctic Meteorites. NIPR, Tokyo
YANAI K. KOJIMA H. & Haramura H., 1995: Catalog of the Antarctic Meteorites. NIPR, Tokyo
YU Y. & HEWINS R. H., 1996: Geochim. Cosmochim. Acta **60**, in press

Manuscript received 10 September, 1998.

Acta Mineralogica-Petrographica, Szeged, XXXIX, 107–138, 1998

GEOCHEMICAL STUDY ON A LIMESTONE/MARLSTONE ALTERNATION, BAJOCIAN, MECSEK MOUNTAINS, SOUTHERN TRANSDANUBIA, HUNGARY

BÉLA RAUCSIK[1], GYULA SZABÓ[2], ILDIKÓ BORBÉLY-KISS[2]

ABSTRACT

A geochemical study of the Bajocian portion of the Komló Calcareous Marl Formation (Mecsek Mountains, southern Hungary) was undertaken in order to characterize the rhythmic alternations of carbonate-rich and carbonate-poor layers and to investigate their possible origin. 45 samples of Komló Calcareous Marl Formation collected from six segments of the outcrops of Püspökszentlászló II. and Kecskegyűr, road cut were examined by PIXE analysis. Concentrations some of the trace elements are higher than can be explained by a pure detrital clastic source. Excess concentrations (over detrital) of these trace elements may be derived from seawater and likely associated with the organic and clay mineral fraction as well as with the carbonate phase.

Limestone semicouplets are characterized by good oxygenation as expressed by the pervasive bioturbation, by the Fe/Mn parameter and by the lack of preserved organic matter. The abundance of silica, phosphorous and strontium in the absence of high terrigenous input suggests that during limestone deposition surface waters were rather highly fertile due to an efficient recycling of nutrients from deeper waters. The enhanced fertility was coupled with a current system at the well-oxygenated seafloor which prevented the accumulation of organic matter and of the organic matter-bound trace elements, such as Zn, Cu and V. During early diagenesis, Mn should migrated from weaker oxic parts of sediment column and precipitated as carbonate and/or as oxide, oxi-hydroxide coatings on biogenic tests resulting Mn-enrichment in the carbonate-rich semicouplets.

Marly semicouplets deposited under moderately oxic, probably dysoxic conditions (indicated by the high Fe/Mn parameter), which does not allow the preservation of abundant organic matter and the appearance of sedimentary structure as lamination. High TiO_2 an SiO_2 values indicate that marly semicouplets received a substantial contribution from a terrigenous source. Differences in the solubility of reduced iron and manganese could lead to sedimentary fractionation of these elements across redox boundaries resulting Fe-enrichment during deposition of carbonate-poor semicouplets. Trace metals (Zn, Cu, V) were carried as portions of organo-metal complexes and as adsorbed ions on clay minerals in the water column. Disoxic conditions in the sediment mass and at the seafloor were favorable to preservation and accumulation a part of these trace elements. Mainly the V, Zn and Cu abundances in the carbonate-poor layers seem to be accounted by diagenetic enrichment; Ni enrichment is affiliated with the increased terrigenous supply, although some degree of redox-controlled diagenetic modification cannot be excluded. The lower phosphorous abundance in the carbonate-poor semicouplets suggests that the depositional environment should be characterized by lower surface-water fertility and productivity during their deposition.

According to these data and results of formerly stable isotope measurements, the rhythmic organization of couplets should represent climatic changes. Palaeoceanographic conditions alternated from efficiently mixed, highly-fertile surface waters and well-oxygenated seafloor, to enhanced water runoff and/or decreased evaporation with decreased productivity and moderately oxygenated bottom waters. Moderately oxidizing (most likely dysoxic) conditions at the bottom may be caused by water mass stratification. This stratification could have resulted from the presence of a less saline, ^{18}O-depleted surface-water. The corresponding climatic conditions thus alternated from more arid to more humid.

[1] Department of Earth and Environmental Sciences, University of Veszprém, P.O. Box 158, H-8201 Veszprém, Hungary

[2] Institute of Nuclear Research of the Hungarian Academy of Sciences, P.O. Box 51, H-4001 Debrecen, Hungary

INTRODUCTION

Cyclic sedimentation recorded as lithological rhythmicity (according to the terminology of EINSELE et al., 1991) in pelagic and hemipelagic succession has been the goal of many works in the last years. In many cases, interest has been focused on Cretaceous formations, which are often characterized by cyclicity expressed as alternations of carbonate-rich and carbonate-poor layers. Diagenetic enhancement of the lithological rhythms played an important role in some sequences (RICKEN, 1991, 1994). Jurassic formations has been studied by few workers (MATTIOLI, 1997).

The possible mechanisms that may produce this kind of cyclicity have been attributed to the variation of a single palaeoenvironmental factor or to a combination of several variable factors. These factors include fluctuations in (1) the supply of fine terrigenous sediments (dilution cycles); (2) the supply of calcareous biogenic sediment produced by plankton (productivity cycles); (3) the degree of saturation of seawater with respect to calcium carbonate (dissolution cycles); (4) the availability of oxygen at the sea floor and the degree of organic matter depletion/preservation (redox cycles) (ROCC Group, 1986; FISCHER et al., 1990; DE BOER and SMITH, 1994; SETHI and LEITHOLD, 1994; BELLANCA et al., 1996; BICKERT et al., 1997). Even if Milankovitch-type cyclic patterns might be expressed by a combination of physical, chemical and geological fluctuations, many of the papers emphasized so far the palaeontological aspects in order to explain the mechanisms leading to the deposition of lithological rhythms (BOTTJER et al., 1986; SAVRDA and BOTTJER, 1994; ERBA and PREMOLI SILVA, 1994). A fairly new and less common approach focuses on the geochemical characterization of such couplets. Many recent works have been centered on isotope stratigraphy (WEISSERT and BRÉHÉRET, 1991; Jenkyns et al., 1994; BELLANCA et al., 1996; BICKERT et al., 1997), but much fewer papers used geochemical data in an attempt to understand the palaeoceanographic meaning of the alternations (MURRAY et al., 1990; SUNDARAMAN et al., 1993; BELLANCA et al., 1996). This method has been appearing just sporadically in Hungarian literature (CORNIDES et al., 1979, FOGARASI, 1995). The aim of this paper is to examine the geochemical (major and trace elements) fluctuations occurring within the couplets in the Lower Bajocian interval of Komló Calcareous Marl Formation in order to reconstruct fluctuations in oxygen content at the seafloor and to unravel the climatic significance of the lithologic alternation.

GEOLOGICAL SETTING

The studied sections are located in the Mecsek Mountains, near the town of Komló (*Fig.1.*). The Mecsek Mountains belongs to the Tisza Terrane, a structural unit of the Pannonian Basin. According to the structure of the outcrops in the Apuseni Mountains (Romania) (BLEAHU 1976; IANOVICI et al. 1976) and to borehole and seismic data from the basement of the Great Hungarian Plain (BALÁZS et al. 1986; FÜLÖP et al. 1987; GROW et al. 1994) the Tisza Terrane is made up of basement nappe systems overthrust with northern vergency during the Cretaceous Austroalpine tectogenesis.

Differentiation of the carbonate shelf - a part of the northern continental margin of the Tethys - into extensional "halbgraben" structures started during the Upper Triassic (NAGY, 1969). This process was continued in the Jurassic in connection with rifting the Penninic Ocean. The Early Liassic in the Mecsek Mountains is characterized by coal and arkose-bearing continental and shallow marine siliciclastic sequence (Gresten facies). In the

Sinemurian this facies was converted into a deeper water hemipelagic/pelagic basin facies with mixed siliciclastic-carbonate lithologies. This sedimentation was prevailing until Upper Bajocian. The bioturbated hemipelagic/pelagic marl facies ("spotted marl") is characteristic to the European margin of the Tethys (Allgäu facies) (HAAS, 1994).

Stratigraphically, the analysed two profiles represent an Early to Middle Bajocian succession, i. e. upper part of the spotted marl sequence (Komló Calcareous Marl Formation). The Ammonite *Kumatostephanus sp.* indicates the Sauzei Zone (GALÁCZ, 1997, pers. comm.) found at the base of the section Püspökszentlászló II. (*Fig. 2*).

Fig. 1. a) Tectonic position of the Mecsek Mountains (M) in the Alpine-Carpathian system after Haas (1994); b) Geological map of the area simplified after Forgó et al. (1966). 1. Neogene, 2. Lower Cretaceous volcanic rocks, 4. Lower Cretaceous sedimentary rocks, 5. Upper Jurassic, 6. Middle Jurassic, 7. Toarcian, 8. Pliensbachian, 9. Upper Sinemurian, 10. Lower Sinemurian-Hettangian, 11. Triassic, 12. Proterozoic-Early Paleozoic, 13. normal faults, 14. reversed faults, 15. strike and dip of strata, 16. axis of a syncline, 17. axis of an anticline

PETROGRAPHY

The succession consists of a fairly monotonous alternation of carbonate-poor and carbonate-rich beds. It must be emphasized that in some cases petrographically the same rock types (for example limestones) can exist within a pair of beds but according to field observations those have couplet-like appearance, too. In the *Fig. 3* the lithologies are indiced on the base of calcium carbonate content. Their couplet-like appearance is presented by the width of the bed: i. e. wide rectangles of the columns represent the massive,

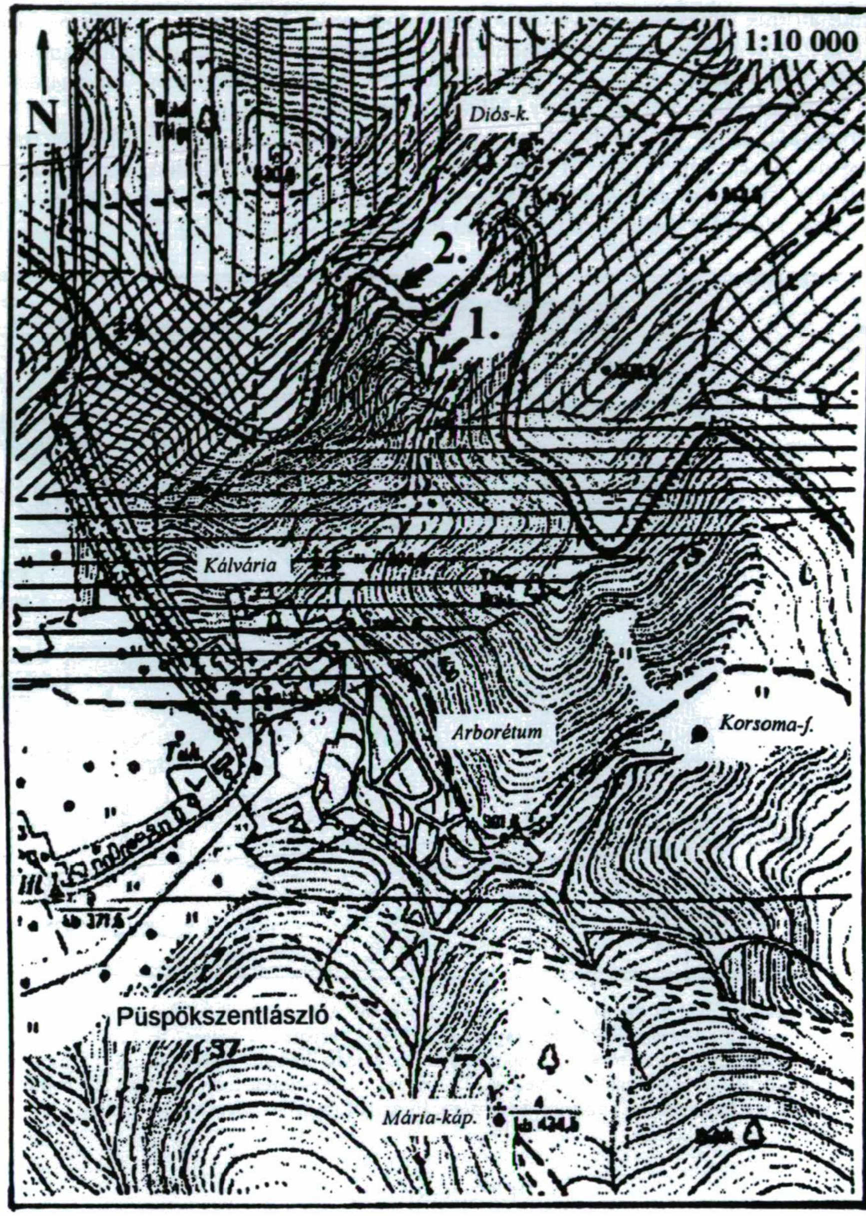

Fig. 2 Locations of the examined sections. 1. Section Püspökszentlászló II., 2. Section Kecskegyűr, road cut

Legend: Bathonian and younger formations; Komló Calcareous Marl Formation, Bajocian part

Komló Calcareous Marl Formation, Upper Toarcian-Aalenian part

Lower Toarcian and Pliensbachian sediments

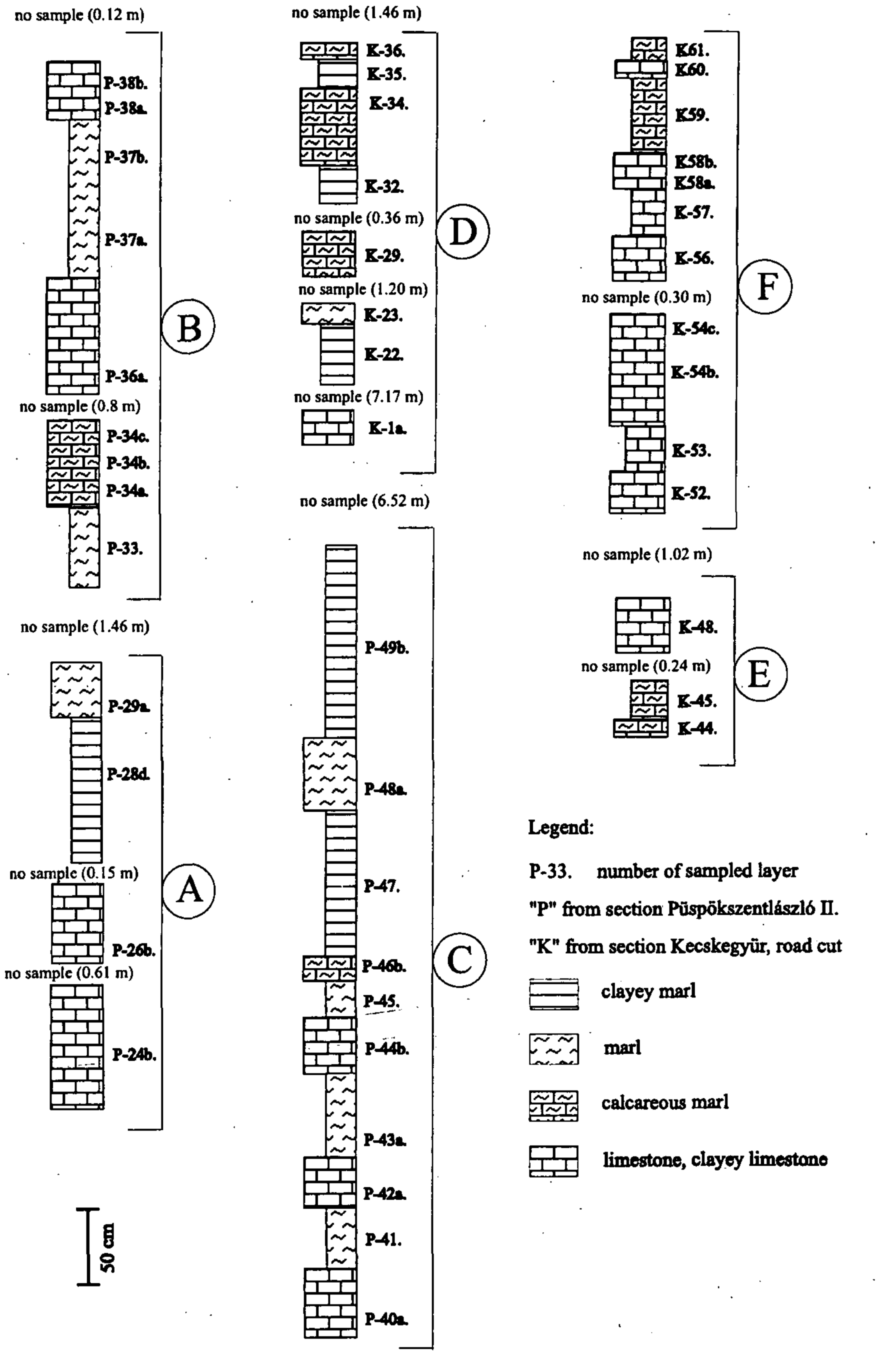

Fig. 3 Lithological column of the examined segments of the sections Püspökszentlászló II. and Kecskegyür, road cut

carbonate-rich semicouplets, whereas the narrower rectangles represent the softer, thin bedded carbonate-poor ones. All of lithology have grey, greenish grey colour, with abundant darker spots. These spots are regarded as product of intensive bioturbation. Intensity of the bioturbation and diversity of the observed ichnofossils, however, fluctuate across the sections. Carbonate-poor beds display poorer ichnofossil assemblage and shallower penetration depth than carbonate-rich layers. These phenomena are interpreted by several worker as product of changing redox conditions (and oxygenation) at the seafloor and/or in sediment mass near the sediment-water interface during sedimentation and early diagenesis (ERBA and PREMOLI SILVA, 1994; SAVRDA and BOTTJER, 1994; SAVRDA, BOTTJER, SEILACHER, 1991). The carbonate-poor beds are slightly darker than the limestones because of their higher clay content. The carbonate-poor beds with the highest clay contents are thin bedded, nevertheless all of the carbonate-rich semicouplets are massive. The $CaCO_3$ content generally fluctuates between 20-60% for the carbonate-poor beds and increases to 80-98% in the more calcareous layers. The rock types are organized in decimetre-thick couplets. The boundaries between the two dominant lithologies (within a couplet and also between the couplets) are transitional but sharp bedding contact can also be observed. All of these rocks contain quartz and muscovite silt grains with maximum 5% abundance. Rock Eval pyrolysis did not detect significant organic matter (TOC values between 0.04 and 0.17 %, HETÉNYI, 1997, pers. comm.). Because the samples were collected from a surface outcrop, this low organic matter content seems to be, at least partially, result of the oxidation during surface exposure. The above facts and the common presence of limonite pseudomorphs after pyrite besides the absence of lamination suggest that oxic to dysoxic conditions prevailed during deposition of the Komló Calcareous Marl Formation. Sharp bedding contacts may have been developed by erosive sedimentary processes, turbidity and contour current activity (TUCKER and WRIGHT, 1990; PIPER and STOW, 1991). However, another sedimentary structures indicative of redeposition by gravity mass flows (including existence of fine-grained turbidites or contourites), e.g., cross lamination, normal or inverse graded bedding, fine lamination, lenticular bedding, fine, obscure silt lenses, tool marks on underlying bedding planes, complete or incomplete Bouma-sequence were not observed.

In thin section the limestones and marls are classified as bioclastic packstones and wackestones. The most abundant biogene components are radiolarians, siliceous sponges and filaments. Echinoid fragments represent 1-2 percentage of the total bioclast assemblage. Maximum 5% unrounded terrigenous quartz sand and silt grains are present as well. Intensive bioturbation is conspicuous in all samples. Forams (*Lenticulina sp.*, *Spirillina sp.*, *Garantella sp.*) are present in some thin sections, which cannot be used for precise biostratigraphic dating, but they suggest normal marine salinity and deeper shelf area as depositional environment (RESCH, 1997, pers. comm.).

A few marlstone samples show fitted fabric structures. The partial dissolution of some of the biogenic constituents indicate carbonate dissolution and reprecipitation during diagenesis. In outcrops wavy bedding surfaces are widespread; nevertheless carbonate concretions did not form, i.e. carbonate redistribution in the sense of HALLAM (1964) probably was not significant enough to cause this alternation of carbonate-rich and carbonate-poor beds.

The studied profiles represent basinal facies dominated by hemipelagic processes. Sedimentation was presumably continuous. Consequently, this succession is a good object for geochemical analysis to study the origin of Komló Calcareous Marl Formation.

ANALYTICAL METHODS

The name PIXE (Particle Induced X-Ray Emission) refers to a process in which characteristic X-rays are generated by ion-atom collision events as the consequence of the recombination of electron vacancies appearing in the inner shells. The spectroscopy of X-rays reveals analytical information on the elemental constituents of the samples. In such a way multielemental analysis with low detection limit can be performed on thin and thick samples of small absolute mass (JOHANSSON, 1988).

The 2 MeV energy proton beam of the 5 MeV Van de Graaff accelerator of the Institute of Nuclear Research of the Hungarian Academy of Sciences, in Debrecen has been used for PIXE analysis. Details on the experimental setup and its calibration have been given in BORBÉLY-KISS et al. (1985) as well as in SZABÓ and BORBÉLY-KISS (1993). Powdered samples were pressed into pellets (1 mm thick, 10 mm in diameter). The beam current was typically between 1 and 10 nA, with a beam size of 5 mm diameter, and about 20 minutes bombardment was sufficient to detect elements in the sample. Spectra have been evaluated with the PIXYKLM programme package (SZABÓ and BORBÉLY-KISS, 1993).

Standard deviations given in Table 1a and Table 1b include the statistical errors originating from the measuring conditions and the fitting of X-ray spectra. However, do not include the error of data necessary for the determination of elemental concentrations. Those data (X-ray production cross section, respond probability of the Si(Li) detector, X-ray absorption in the sample and in the used filter and the slowing down of proton beam in the sample) are calculated theoretically. Errors of those data are systematic, depend on the atomic number and can only be estimated. They are less than 10-15 % of the value of concentrations.

RESULTS

Major and trace element data for the samples from six segments (indicated by A-F in *Fig. 3*) of sections Püspökszentlászló II. and Kecskegyűr, road cut, are listed in Table 1a and 1b. Table 2 shows the main element ratios suggested by the literature. Average values of these elements and element ratios are shown in the Tables 1a, 1b, 2. („average 1." indicates the calculated average values of the carbonate-rich, „average 2." indicates those of the carbonate-poor beds.) Values with very high standard deviation are indicated by bold numbers. Correlation matrix is presented in Table 3.

Missing values in the above tables mean that the concentrations of those elements are less than the sensitivity limits.

DISCUSSION

Major elements

SiO_2 values range from 6.63 (sample P-24b) to 62.69% (sample P-36a). Average value for the carbonate-rich layers is 29.58%, whereas for the carbonate-poor layers it is 48.47%. It is obvious that some limestone layers have higher SiO_2 content than the average value for carbonate-poor semicouplets (P-26b 59.68%, P-34c 49.80%, P-36a 62.69%, K-23 57.54%). The two main sources of Si to these sediments are biogenic opal and aluminosilicate material. Si positively correlates with Ti (r=0.700), which indicates dominant terrigenous control on Si distribution. However, according to microfacies observations, many of carbonate-rich samples contain abundant radiolarians. This fact should be the reason for higher SiO_2 content of some carbonate-rich samples.

Major and trace element composition of the measured samples

number of sample	Al_2O_3 (%)	SiO_2 (%)	CaO (%)	K_2O (ppm)	TiO_2 (ppm)	MnO (ppm)	Fe_{TOT} (ppm)
P-24b	3.63±0.7	6.63±0.3	55.25±2.2	3134±300	445±150	262±30	6910±290
P-26b	5.74±0.8	59.68±2.4	18.33±0.7	11081±500	**1269±610**	188±30	10820±450
P-28d	3.29±0.8	54.97±2.2	22.43±0.9	9359±440	1495±130	194±30	10340±430
P-29a	3.36±0.7	43.10±1.7	27.98±1.1	6138±330	1281±140	247±50	8478±360
P-33	5.63±0.8	51.08±0.5	24.69±1.0	10754±490	1676±140	214±30	12390±510
P-34a	**0.76±0.7**	18.72±0.5	45.50±1.8	4813±290	787±130	258±30	7719±320
P-34b	3.29±0.7	8.56±0.4	52.27±2.1	2944±270	754±140	235±30	7241±300
P-34c	5.63±0.7	49.80±1.9	28.06±1.1	8983±430	1349±130	203±30	6964±290
P-36a	37.79±2.0	62.69±2.5	29.02±1.1	7545±380	1274±120	141±20	5879±250
P-37a	12.89±0.9	57.62±2.3	13.64±0.5	20585±870	3521±900	250±40	16320±670
P-37b	5.48±0.9	47.83±1.9	26.06±1.0	12628±570	2082±160	216±30	12140±500
P-38a	**1.10±0.8**	19.94±0.8	46.91±1.9	4999±340	914±160	217±30	6815±280
P-38b	1.93±0.7	11.89±0.5	50.48±2.0	5307±320	1000±140	239±30	6898±290
P-40a	2.87±0.7	29.15±1.2	38.18±1.5	5594±330	1098±130	178±30	8380±350
P-41	6.61±0.9	49.00±2.0	25.21±1.0	13881±610	2345±170	221±30	12590±520
P-42a	4.61±0.7	16.17±0.7	46.89±1.9	4259±300	736±130	225±30	7227±300
P-43a	9.64±0.8	53.77±2.8	17.80±0.7	17046±730	2705±170	200±30	16390±670
P-44b	**1.70±0.8**	9.05±0.4	53.43±2.1	4331±300	1161±210	488±50	8473±350
P-45	8.50±0.9	48.11±2.0	24.92±1.0	14695±650	2562±180	234±30	13310±550
P-46b	2.76±0.7	26.59±1.1	42.39±1.7	6302±350	1106±150	214±30	8071±330
P-47	7.71±0.9	57.37±2.3	15.49±0.6	19696±830	3283±190	227±30	15380±630
P-48a	4.27±0.7	47.93±1.9	28.62±1.1	7740±400	1503±140	196±30	9801±400
P-49b	5.06±0.6	45.75±1.9	29.91±1.2	8159±410	1434±140	188±30	9088±380
K-1a	2.42±0.8	13.80±0.6	51.89±2.1	3006±280	**257±140**	638±50	5124±220
K-22	6.20±0.8	44.17±1.8	29.92±1.2	11941±550	1613±140	296±40	10630±440
K-23	13.79±1.0	57.54±2.3	16.45±0.7	23562±980	3178±190	247±40	16210±670
K-29	6.24±0.8	40.83±1.7	31.62±1.3	12838±580	1693±150	359±40	9626±400
K-32	6.92±0.9	46.84±1.9	21.03±0.8	25150±1050	3026±190	258±40	17020±700
K-34	4.35±0.7	40.28±1.6	29.67±1.2	15750±680	2115±160	332±40	11580±480
K-35	4.27±0.8	47.55±1.9	22.47±0.9	23160±970	2782±190	235±40	15270±630
K-36	**1.36±0.8**	23.57±1.0	43.33±1.7	6574±360	812±140	318±40	8543±360
K-44	3.78±0.7	37.05±1.5	29.39±1.2	18489±790	2278±170	376±40	13370±550
K-45	8.05±0.7	38.91±1.6	27.67±1.1	20956±890	2741±190	341±40	13930±570
K-48	4.16±0.7	9.15±0.4	49.65±2.0	3341±270	**350±130**	385±40	4045±170
K-52	4.16±0.9	11.74±0.5	51.65±2.1	3573±280	425±130	542±40	5904±250
K-53	9.11±0.9	45.73±1.9	22.66±0.9	23719±1000	2976±190	372±40	16400±670
K-54b	**0.76±0.8**	27.57±1.1	41.75±1.7	6798±370	652±130	528±50	6584±280
K-54c	5.18±0.8	23.14±1.0	43.15±1.7	5558±330	637±120	580±50	7669±320
K-56	5.03±0.8	31.25±1.3	37.02±1.5	7969±400	1059±120	452±40	6927±290
K-57	11.79±0.8	43.59±1.8	23.53±0.9	26740±1120	3256±200	381±40	16010±660
K-58a	**1.02±0.9**	33.20±1.4	38.58±1.6	9732±470	1178±150	553±40	8507±350
K-58b	6.20±0.8	40.21±1.6	29.63±1.2	14334±630	1908±160	520±50	15830±650
K-59	12.40±0.9	47.10±1.9	20.45±0.8	34280±1420	4078±240	435±40	20160±820
K-60	3.67±0.9	28.92±1.2	40.33±1.6	9583±470	1291±150	600±50	8860±370
K-61	11.71±0.9	40.71±1.7	27.06±1.1	24138±1010	2757±190	524±50	14970±610
average 1.	5.06±0.8	29.58±1.2	39.20±1.6	8010±400	1124±160	347±40	8516±350
average 2.	7.94±0.8	48.47±1.9	23.24±0.9	17550±800	2607±220	288±40	14255±560

TABLE 1B

Major and trace element composition of the measured samples

number of sample	Rb (ppm)	Sr (ppm)	V (ppm)	P (ppm)	Ni (ppm)	Cu (ppm)	Zn (ppm)
P-24b	-	735±50	-	6303±410	-	-	14±6
P-26b	44±13	424±40	-	-	-	22±6	43±6
P-28d	45±17	500±50	-	-	-	20±7	36±7
P-29a	35±16	589±50	-	1966±520	-	-	27±10
P-33	**26±13**	468±40	-	**1012±550**	-	17±6	53±7
P-34a	31±14	721±50	-	5924±410	-	11±5	50±7
P-34b	40±15	862±50	-	5593±370	-	14±5	22±6
P-34c	29±13	464±40	98±45	3323±600	-	16±6	35±6
P-36a	**19±12**	449±40	**76±43**	3584±650	-	23±6	30±6
P-37a	47±13	190±30	-	1730±640	**31±16**	30±7	55±8
P-37b	36±14	420±40	104±54	2705±590	-	20±6	50±7
P-38a	44±14	692±50	-	5452±490	-	**12±6**	24±6
P-38b	37±14	700±50	-	6618±440	-	15±6	28±6
P-40a	41±14	563±40	-	3464±480	-	16±6	34±6
P-41	41±14	390±40	144±55	1750±570	-	17±6	51±8
P-42a	54±15	742±50	**90±53**	5126±420	-	**12±6**	21±6
P-43a	41±13	308±30	-	2278±580	**24±16**	24±6	67±8
P-44b	43±14	724±50	-	8739±550	**20±12**	14±6	24±6
P-45	40±13	335±30	-	2169±560	-	22±7	54±8
P-46b	43±12	586±40	-	4788±500	-	11±5	28±6
P-47	51±13	247±30	157±56	-	-	16±6	68±8
P-48a	40±14	534±40	137±45	2103±560	-	21±6	29±6
P-49b	35±14	471±40	-	2927±560	-	20±6	44±7
K-1a	25±11	377±30	-	8027±500	-	**11±6**	15±5
K-22	46±15	420±40	-	1914±540	-	20±7	46±8
K-23	52±15	225±30	121±53	-	**26±16**	23±7	62±8
K-29	52±14	376±40	-	2723±550	**24±13**	19±7	42±7
K-32	56±15	261±30	131±59	-	-	25±7	75±9
K-34	41±15	368±40	-	2762±530	**29±15**	19±7	52±8
K-35	38±14	259±30	-	2144±580	**28±16**	21±7	69±9
K-36	44±15	534±40	-	5404±490	**22±12**	15±6	37±7
K-44	55±15	284±30	**107±57**	3123±500	31±15	25±7	58±8
K-45	57±16	269±30	**107±59**	1883±510	31±15	23±7	68±8
K-48	**22±13**	488±40	-	7083±430	-	**10±6**	14±6
K-52	**19±13**	491±40	-	6880±460	-	14±6	20±6
K-53	56±15	263±30	176±60	1334±600	**30±16**	16±7	87±9
K-54b	40±12	378±30	-	6536±520	-	-	17±6
K-54c	28±13	447±40	-	6919±490	**19±11**	**10±6**	33±6
K-56	**25±12**	383±30	84±41	5025±490	**20±11**	14±5	27±6
K-57	58±15	281±30	141±60	3877±540	32±16	25±7	83±9
K-58a	34±12	397±30	-	5720±560	23±11	13±6	29±6
K-58b	37±13	306±30	**102±55**	4722±550	**26±15**	15±6	53±7
K-59	54±15	197±30	137±67	3363±550	41±18	26±7	102±10
K-60	36±12	373±30	-	5984±530	**19±12**	**12±6**	35±6
K-61	54±15	277±30	-	4904±540	32±15	21±7	62±8
average 1.	36±13	508±40	102±50	5150±500	**24±13**	15±6	32±6
average 2.	45±14	321±30	137±60	2428±560	**31±16**	21±7	63±8

TABLE 2

The applied element-ratios

number of sample	Si/Al	Al/ (Al+Fe+Mn)	Fe/Ti	Fe/Mn	Mn/Ti	P/Ti	Sr/Ti
P-24b	3.24	0.15	25.87	34.09	0.76	23.60	2.75
P-26b	18.40	0.30	14.21	73.96	0.19	-	0.56
P-28d	29.64	0.27	11.54	69.12	0.17	-	0.56
P-29a	22.69	0.23	11.04	44.41	0.25	2.56	0.77
P-33	16!05	0.26	12.33	74.82	0.16	1.01	0.47
P-34a	44.37	0.20	16.34	38.63	0.42	12.54	1.53
P-34b	4.60	0.14	16.02	39.90	0.40	12.38	1.91
P-34c	15.66	0.34	8.61	44.30	0.19	4.11	0.57
P-36a	2.93	0.34	7.70	54.13	0.14	4.69	0.59
P-37a	7.91	0.05	7.73	84.04	0.09	0.82	0.09
P-37b	15.38	0.30	9.73	72.52	0.13	2.17	0.34
P-38a	32.28	0.23	12.44	40.61	0.31	9.95	1.26
P-38b	10.81	0.24	11.51	37.31	0.31	11.05	1.17
P-40a	17.90	0.21	12.73	60.81	0.21	5.26	0.86
P-41	13.12	0.31	8.95	73.67	0.12	1.24	0.28
P-42a	6.19	0.19	16.39	41.53	0.39	11.62	1.68
P-43a	9.86	0.30	10.10	105.47	0.06	1.40	0.19
P-44b	9.36	0.17	12.17	22.41	0.54	12.55	1.04
P-45	9.98	0.31	8.67	73.50	0.18	1.41	0.22
P-46b	17.04	0.24	12.18	48.68	0.25	7.22	0.88
P-47	13.17	0.34	7.82	87.64	0.09	-	0.13
P-48a	19.87	0.24	10.88	64.65	0.17	2.34	0.59
P-49b	16.02	0.27	10.57	62.33	0.17	3.41	0.55
K-1a	10.04	0.18	33.25	10.37	3.21	52.09	2.45
K-22	12.61	0.31	10.99	46.46	0.24	1.98	0.44
K-23	7.37	0.37	8.51	84.69	0.10	-	0.12
K-29	11.59	0.35	9.48	34.65	0.27	2.68	0.37
K-32	11.94	0.38	9.38	85.06	0.11	-	0.14
K-34	16.40	0.36	9.13	45.06	0.20	2.17	0.29
K-35	19.62	0.38	9.15	58.87	0.16	1.26	0.16
K-36	30.62	0.24	17.56	34.69	0.51	11.11	1.10
K-44	17.36	0.36	9.79	46.15	0.21	2.29	0.21
K-45	8.52	0.38	8.48	52.73	0.16	1.15	0.16
K-48	3.91	0.24	19.24	13.57	1.42	33.70	2.32
K-52	5.00	0.19	23.11	14.07	1.64	26.94	1.92
K-53	8.87	0.37	9.19	57.00	0.16	0.75	0.15
K-54b	63.59	0.29	16.86	16.11	1.05	16.73	0.99
K-54c	7.87	0.22	20.10	17.08	1.18	18.13	1.17
K-56	10.96	0.31	10.91	19.80	0.55	7.92	0.60
K-57	6.54	0.41	8.20	54.22	0.15	1.99	0.14
K-58a	57.57	0.31	12.05	19.86	0.61	8.10	0.56
K-58b	11.46	0.27	13.84	39.31	0.35	4.13	0.27
K-59	6.71	0.41	8.25	59.89	0.14	1.38	0.08
K-60	13.96	0.30	11.45	19.06	0.60	7.73	0.48
K-61	6.14	0.39	9.06	36.87	0.25	2.97	0.17
average 1.	17.61	0.26	26.24	35.92	1.21	25.60	2.13
average 2.	12.48	0.32	9.42	67.89	0.15	1.35	0.25

TABLE 3

Correlation matrix

Elements and element-ratios	Al	Si	P	K	Ca	Ti	V	Mn	Fe	Ni	Cu	Zn	Rb	Sr	Si/Al	Al/(Al+Fe+Mn)	Fe/Ti	Fe/Mn	Mn/Ti	P/Ti	Sr/Ti	$\delta^{13}C$	$\delta^{18}O$
Al	1	0.544	-0.326	0.384	-0.449	0.414	-0.233	-0.213	0.290	0.615	0.523	0.332	0.009	-0.383	-0.429	0.337	-0.387	0.346	-0.266	-0.279	-0.351	-0.729	-0.485
Si		1	-0.851	0.625	-0.959	0.700	0.301	-0.397	0.645	0.587	0.734	0.617	0.269	-0.670	-0.042	0.546	-0.702	0.762	-0.589	-0.730	-0.830	-0.806	-0.819
P			1	-0.567	0.870	-0.679	-0.659	-0.552	-0.623	-0.619	-0.695	-0.616	-0.344	0.470	0.121	-0.424	0.686	-0.806	0.672	0.768	0.720	0.604	0.848
K				1	-0.773	0.956	0.610	0.024	0.935	0.912	0.725	0.940	0.664	-0.809	-0.185	0.853	-0.613	0.457	-0.459	-0.572	-0.755	-0.772	-0.406
Ca					1	-0.835	-0.654	0.338	-0.801	-0.686	-0.786	-0.761	-0.433	0.751	0.097	-0.572	0.721	-0.806	0.608	0.751	0.864	0.857	0.764
Ti						1	0.707	-0.144	0.952	0.870	0.769	0.920	0.652	-0.755	-0.261	0.580	-0.713	0.690	-0.569	-0.680	-0.805	-0.801	-0.520
V							1	0.061	0.676	0.512	0.103	0.685	0.599	-0.473	0.138	0.357	-0.227	0.57	-0.551	-0.656	-0.524	-0.633	-0.322
Mn								1	-0.076	-0.314	-0.332	-0.082	-0.113	-0.256	0.089	0.048	0.401	-0.706	0.625	0.450	0.156	-0.022	0.483
Fe									1	0.830	0.709	0.932	-0.628	-0.725	-0.219	0.530	-0.592	0.683	-0.530	-0.634	-0.763	-0.826	-0.496
Ni										1	0.772	0.871	0.725	-0.694	-0.274	0.433	-0.645	0.476	-0.715	-0.750	-0.745	-0.600	0.015
Cu											1	0.654	0.494	-0.608	-0.234	0.405	-0.621	0.681	-0.360	-0.612	-0.711	-0.624	-0.545
Zn												1	0.614	-0.708	-0.203	0.662	-0.609	0.607	-0.532	-0.617	-0.747	-0.732	-0.472
Rb													1	-0.325	-0.081	0.383	-0.483	0.370	-0.497	-0.496	-0.525	-0.504	-0.390
Sr														1	0.113	-0.643	0.148	-0.366	0.130	0.313	0.708	0.830	0.311
Si/Al															1	-0.022	0.036	-0.181	0.013	-0.023	-0.020	0.066	0.055
Al/(Al+Fe+Mn)																1	-0.573	0.253	-0.377	-0.476	-0.666	-0.711	-0.469
Fe/Ti																	1	-0.586	0.875	0.925	0.879	0.552	0.626
Fe/Mn																		1	-0.657	-0.667	-0.605	-0.632	-0.700
Mn/Ti																			1	0.949	0.704	0.378	0.622
P/Ti																				1	0.864	0.510	0.758
Sr/Ti																					1	0.783	0.698
$\delta^{13}C$																						1	0.560
$\delta^{18}O$																							1

Al_2O_3 values fluctuate from 0.76 (samples P-34a and K-54b) to 37.79% (sample P-36a). The average for the carbonate-rich semicouplets is 5.06%, for the carbonate-poor semicouplets is 7.94%, correlating with the clay mineral abundance of the given samples. Two carbonate-rich samples show obviously high Al_2O_3 content (P-36a 37.79%, K-23 13.79%). It must be emphasized, that six Al_2O_3 values of the 45 are not accurate enough to use. Therefore these values must be use with caution. TiO_2 values vary between 257 ppm (K-1a) and 4078 ppm (K-59). Average values are 1124 and 2607 ppm for the carbonate-rich and the carbonate-poor semicouplets, respectively. Three TiO_2 values are not available.

Aluminium or titanium normalizations are generally used to correct for the terrestrial influences in marine sediments (MURRAY et al., 1991, 1993, MURRAY and LEINEN, 1996, NATH et al., 1992). In $CaCO_3$-rich biogenic sediments, a portion of Al may be affiliated by adsorption processes to biogenic fraction (MURRAY et al., 1993, MURRAY and LEINEN, 1996, SCHROEDER et al., 1997), thus Al normalization does not seem to be optimal in this case. Similarly, the Al/(Al+Fe+Mn) ratio (proposed by BELLANCA et al., 1996) must be used with caution for estimating the terrigenous supply. Unlike Al, no proven biological affiliation is reported for Ti, therefore this element is used for normalization and to represent the terrigenous siliciclastic component of bulk sediment.

CaO values depend strictly on calcite content of the samples. The highest value is 55.25% (P-24b), the lowest is 13.64% (P-37a). Average value for the carbonate-rich semicouplets is 39.20%, for the carbonate-poor semicouplets is 23.24%.

K_2O data fluctuate from 2944 (P-34b) to 34280 ppm (K-59). Main values are 8010 and 17550 ppm for the calcite-rich and the calcite-poor semicouplets, respectively. This suggests a major role of the silicate minerals in the K_2O distribution.

Fe_{TOT} values fluctuate from 4045 (K-48) to 20160 ppm (K-59). Average value for calcite-rich beds is 8516 ppm, for calcite-poor beds is 14255 ppm. Fe values show excellent correlation with Ti (r=0.952) and K (r=0.935). Fe values plotted versus Ti represent a good agreement with values characteristic of average shale, which indicates that all the three elements are derived primarily from lithogenic source. Concentrations of Fe when plotted against Ti, fall over the line representing the trend for average shale (*Fig.4*). (In *Figs. 4; 7; 8; 9; 10; 11* solid line represents the element/Ti ratios in average shale according to TUREKIAN (1972)). Nevertheless, the Fe/Ti ratio correlates with the Ca (r=0.721) and shows in many cases significant excess Fe corresponding with PAAS (Post-Archaean Australian Shale, values from TAYLOR and MCLENNAN, 1985) (*Fig.5*). The Ti-normalized enrichments with respect to PAAS indicates the presence of chemical sources in addition to the lattice-bound aluminosilicate contribution to the sediment (MURRAY and LEINEN, 1993). This suggests some amount of excess (non-detrital) Fe links to the abundant carbonate component of the examined rocks. The Fe enrichment in the marly intervals coupled with the presence of some pyrite pseudomorphs and moderate bioturbation reflect a poorly-oxigenated environment and a wide availability of reactive iron for authigenic mineral formation. The correlation of iron and titanium testifies that the amounts of Fe incorporated in sediments were largely controlled by detrital iron-bearing minerals. Moderate diagenetically-controlled Fe enrichment, however, cannot be excluded.

Trace elements

Trace elements in sediments that accumulate on the seafloor have two sources: detrital clastic detritus and seawater (KUMAR et al., 1996). The seawater-derived fraction also has two components: a portion that is incorporated into the marine organisms and a component that is scavenged from the dissolved elemental load of seawater by organic and inorganic particles settling through the water column.

Relations of trace elements to Ti defined for average shale, as stated above, seems to be available tool to estimate excess amounts (over detrital) of trace element. Ni (*Fig. 7*) shows relatively good accordance with the trend line characteristic of average shale, as well as the correlation between of Ni and Ti is good (*r*=0.870). Many workers give account of lower redox-sensitivity of Ni relative to other elements, above all to V (ODERMATT and CURIALE, 1991; HUERTA-DIAZ and MORSE, 1992). These features suggest that the main source of Ni is the terrigenous fraction; direct or biogenic-controlled seawater source of Ni are not provable on the basis of these data. Cu (*Fig. 8*), Zn (*Fig. 9*), V (*Fig. 10*) and Sr (*Fig. 11*) values, however, are much higher than in average shale. According to these patterns one should take into account significant amount of excess (over detrital) trace metal content, which probably derived (directly or indirectly) from seawater.

Vanadium fluctuates through the section exhibiting low values for limestones (mean value: 102 ppm) and slightly higher values in the marly intervals (mean value: 137 ppm). The amount of other trace metals (Cu, Zn) fluctuates in a similar manner showing an enrichment in the marly intervals (*Fig. 12*). Vanadium values correlate neither with Al (*r*= -0.233) nor with Al/(Al+Fe+Mn) ratio (*r*=0.357) but show positive correlation with Ti values (*r*=0.707). V plotted against Ti indicates excess amount of V corresponding to average shale, suggesting that the affiliation with the aluminosilicates is not exclusive control on the V concentration in marlstones of the studied sections. Vanadium solubility in natural waters, its precipitation from seawater and addition to sediments are controlled by redox conditions and by absorption and complexation processes. Dissolved vanadium can be strongly bound to metallo-organic complexes (LEWAN and MAYNARD, 1982) or absorbed on biogenic particles (PRANGE and KREMLING, 1985). Adsorption and complexation of vanadium are enhanced in anoxic environments where vanadium is present as a reduced V (IV) species. During post-depositional and diagenetic alteration of sediments, vanadium can be mobilized from degrading biogenic particles under oxic conditions, while it is less mobile in disoxic and anoxic sediments. Also V, together with Cu and Zn, is enriched under disoxic conditions, where these metals are trapped with organic material (SHAW et al., 1990; HATCH and LEVENTHAL, 1992). However, it must be emphasized, that in this case the use of the V/(V+Ni) ratio as a tool for proxy of redox conditions (LEWAN, 1984; HATCH and LEVENTHAL, 1992) is not favorable because of the limited number of accurate V (13 samples show enough amount of V) and Ni (six samples with sufficient accuracy for Ni) data. Using Zn and Cu values seems better.

The data indicate that the Zn concentration (up to 102 ppm) is about 1.5-2 times the amount can be explained from an aluminosilicate source. Organic matter derived from plankton with average concentrations of Zn is 110 ppm (DEAN et al., 1997). Excess (over detrital) concentrations of other chalcophile elements such as Cu (up to 30 ppm) may also be in sulfides, but more likely, the excess amounts are associated with the organic fraction, either as metal-organic complexes (BRULAND, 1983) or adsorbed on organic coatings in particulate organic matter (BALISTRIERI et al., 1981). The stratigraphic distribution of the Zn and Cu values shows differences in metal concentrations within each lithological couplet (*Fig. 12*). This pattern implies the occurrence of fluctuations in the redox state of the depositional environment of the studied section, therefore during more oxigenated periods of sedimentation (represented by carbonate-rich semicouplets) these organo-metal complexes oxidized then mobilized and migrated in the sediment. During periods characterized by less oxigenated and, probably, disoxic seafloor (represented by carbonate-poor semicouplets) these metal ions and organo-metal complexes could remain in reduced, consequently less mobile state. In the case of Zn it must be emphasized that this metal shows excellent correlation with Ti (r=0.920), thus its fluctuating distribution through the section can be explained, partially, by fluctuating terrigenous (also clay mineral) supply. However, the relationships between Ti and Zn abundances suggest some redox-controlled diagenetic redistribution.

Compared to PAAS all these Bajocian sediments from the Mecsek Mountains have low Rb (Rb values fluctuate between 19 and 58 ppm; averages for carbonate-rich semicouplets=36 ppm, for carbonate-poor semicouplets=45 ppm; Rb in PAAS=80 ppm) and high Sr (Sr values vary from 190 to 862 ppm; averages for carbonate rich-semicouplets=508 ppm, for carbonate-poor semicouplets=321 ppm; Sr in PAAS=160 ppm) abundances. The incorporation of Sr into the crystal structure of calcite, expressed by the Sr/Ti ratio, explains the excess concentrations of this element in carbonate-rich sediments (*Fig. 13*).

MnO values fluctuate between 141 and 638 ppm. The mean MnO value for carbonate-rich layers (347 ppm) is significantly higher than for carbonate-poor semicouplets (288 ppm). The high sensitivity of manganese to environmental redox conditions is well known (FORCE and CANNON, 1988; SAAGER et al., 1989; GOBEIL et al., 1997). In hemipelagic sediments subjected to a transition from suboxic (or anoxic) to oxic conditions, low Eh conditions can lead to a Mn enrichment in the porewater and the subsequent upward diffusion of dissolved Mn may concentrate this element in the solid phase, just above or below the redox boundary. DICKENS and OWEN (1994) have suggested that the redox-sensitive Mn oxi-hydroxide particulates dissolve upon entering an oxygen minimum zone. The resulting Mn^{2+} is subsequently redirected by advective and/or diffusive processes eventually to precipitate in more oxygenated environments. Thus, the fluctuation of Mn values may be interpreted as an indicator of rhythmic changes in sedimentary redox conditions. The record of Mn should reflect migration of the metal from weaker oxic clay-rich layers and concentrations of the same metal in more oxigenated carbonate-rich layers, where it is incorporated in the carbonate phase and/or precipitated as oxide, oxi-hydroxide coatings on biogenic tests.

The differences in the solubility of reduced iron and manganese could lead to sedimentary fractionation of these elements across redox boundaries. Large portion of iron being fixed in sulphide under low Eh conditions (SAAGER et al., 1989). The Mn/Ti profile shows fluctuations generally opposite to those of Ti (*Fig. 14a*) and parallel to those of Ca (*Fig. 14b*). The high Fe/Mn values indicate, according to MACHHOUR et al. (1994), mildly to strongly reducing conditions during deposition. The Fe/Mn index increases systematically from the carbonate-rich to the clay-rich part of each lithological couplet (*Fig. 15*) outlining variations in the redox-state of the bottom-waters in the Bajocian basin of Mecsek Mountains.

Phosphorous values have a minimum of 1012 ppm (P-33) and a maximum of 8739 ppm (P-44b). Average values are 5150 and 2428 ppm for the calcite-rich and the calcite-poor semicouplets, respectively. One result (1012±550 ppm, sample P-33) is just informative.

P, Sr and Ba in marine sediment and biogenic particulate matter are commonly affiliated with biogenic phases (FROELICH et al., 1982; FISHER et al., 1991; PINGITORE et al., 1992; MURRAY and LEINEN, 1993) and as such are commonly enriched in sediment deposited beneath productive surface waters (GOLDBERG and ARRHENIUS, 1958; FROEHLICH et al., 1982; BISHOP, 1988; FISHER et al., 1991). Efforts have capitalized on this relationship in order to assess paleoproductivity from within the marine stratigraphic record. P correlates well with Ca (r=0.870) and negatively with the terrigenous influx indicating elements (Ti: r= -0.679, Si: r= -0.851). According to P/Ti ratios (*Fig.6*) just a small part of the P in the bulk sediment may be explained by the adsorption onto terrigenous phases (clay minerals); a significant portion seems to be connected to disseminated apatite-group phases, which originally incorporated into the siliceous and carbonate skeleton of organisms (BISHOP, 1988). The transporting agents (opal and calcite) partially degraded on the seafloor, leaving behind the P record as a dissolution residue (FROELICH et al., 1982; MURRAY and LEINEN, 1993). This should indicate enhanced productivity during deposition of the carbonate-rich layers.

According to the interpretation of RAUCSIK (1997) surface seawater should be more saline and/or cooler during deposition of the carbonate-rich semicouplets corresponding to carbonate-poor semicouplets, on the base of the $\delta^{18}O$ values. The $\delta^{13}C$ values suggest enhanced productivity during deposition of carbonate-rich beds. Carbonate-poor beds seem to be deposited during periods of moderate surface water productivity. Alternating anti-estuarine and estuarine circulation in the basin was proposed as driving force on sedimentation.

SUMMARY AND CONCLUSIONS

The results of petrographical and geochemical studies coupled with data of formerly stable isotope measurements (RAUCSIK, 1997) are the following:

1. High concentrations of the trace elements such as Mn, Zn, Cu, V and Sr in the samples cannot be explained by a pure detrital clastic source. Excess concentrations (over detrital) of these trace elements may be derived from seawater and are probably associated with the organic fraction.

2. The limestone semicouplets are characterized by good oxygenation as expressed by the pervasive bioturbation, by the Fe/Mn parameter and by the lack of preserved organic matter. The abundance of silica in the absence of high terrigenous input suggests that during limestone deposition surface waters were rather highly fertile due to an efficient recycling of nutrients from deeper waters. The enhanced fertility was coupled with a current system at the well-oxygenated seafloor which prevented the accumulation of organic matter and the trace elements bound by organic matter, such Zn, Cu and V. During early diagenesis Mn should have migrated from weaker oxic parts of sediment and precipitated as carbonate and/or as oxide, oxi-hydroxide coatings on biogenic tests resulting Mn-enrichment in the carbonate-rich semicouplets. Highly fertile conditions are expressed by $\delta^{13}C$ values and Sr- and P-enrichment during deposition of carbonate-rich semicouplets. All parameters indicate high fertility in surface waters caused by increased upwelling that engendered high nutrient levels in near-surface waters.

3. The marly semicouplets deposited under moderately oxic, probably dysoxic conditions (indicated by the Fe/Mn parameter), which not allowed the preservation of abundant organic matter and the appearance of sedimentary structure such as lamination. High TiO_2 an SiO_2 values indicate that marly semicouplets received a substantial contribution from a terrigenous source. High Fe values of carbonate-poor layers seems to be affiliated to the enhanced terrigenous supply. However, the differences in the solubility

of reduced iron and manganese could lead to sedimentary fractionation of these elements across redox boundaries and could result in a slight Fe-enrichment during deposition of carbonate-poor semicouplets. Trace metals such as Zn, Cu and V were carried as organo-metal complexes and as adsorbed ions on clay minerals in the water column. Disoxic conditions in the sediment mass and at the seafloor were favorable to preservation and accumulation of these trace elements. On the base of formerly stable carbon isotope measurements, the depositional environment can be characterized by lower surface-water fertility and productivity during deposition of marly beds.

4. The rhythmic organization of couplets should represent climatic changes. Palaeoceanographic conditions alternated from efficiently mixed, highly-fertile surface waters and well-oxygenated seafloor, to enhanced water runoff and/or decreased evaporation and moderately oxygenated bottom waters. The presence of less saline, ^{18}O-depleted surface-waters may have created stratification that caused moderately oxidizing (most likely dysoxic) conditions at the bottom. The corresponding climatic conditions thus alternated from more arid to more humid.

ACKNOWLEDGEMENT

The authors are indebted to ERNŐ MÉSZÁROS, University of Veszprém, for making the measurements possible.

REFERENCES

BALÁZS, E., CSEREPES-MESZÉNA, B., NUSSZER, A., SZILI, GY., GYÉMÁNT, P. (1986): An attempt to correlate the metamorphic formations of the Great Hungarian Plain and the Transylvanian Central Mountains (Muntii Apuseni). Acta Geol. Hung. 29., 317-320.

BALISTRIERI, L., BREWER, P. G., MURRAY, J. W. (1981): Scavenging residence times of trace metals and surface chemistry of sinking particles in the deep ocean. Deep-Sea Res. 28., 101-121.

BELLANCA, A., CLAPS, M., ERBA, E., MASETTI, D., NERI, R., PREMOLI SILVA, I., VENEZIA, F. (1996): Orbitally induced limestone/marlstone rhythms in the Albian-Cenomanian Cismon section (Venetian region, northern Italy): sedimentology, calcareous and siliceous plankton distribution, elemental and isotope geochemistry. Palaeogeogr., Palaeoclim., Palaeoecol. 126., 227-260.

BICKERT, T., PÄTZOLD, J., SAMTLEBEN, C., MUNNECKE, A. (1997): Paleoenvironmental changes in the Silurian indicated by stable isotopes in brachiopod shells from Gotland, Sweden. Geochim. Cosmochim. Acta 61/13., 2717-2730.

BISHOP, J. K. B. (1988): The barite-opal-organic carbon association in oceanic particulate matter. Nature 332., 341-343.

BLEAHU, M. (1976): Structural position of the Apuseni Mountains in the Alpine system. Rev. Roum. Géol. Géophys. Géogr., Ser. Géol. 20., 7-19.

BORBÉLY-KISS, I., KOLTAY, E., LÁSZLÓ, S., SZABÓ, GY., ZOLNAI, L. (1985): Experimental and Theoretical Calibration of a PIXE Setup for K and L-Rays. Nucl. Instr. and Meth. in Phys. Res. B12., 496-504.

BOTTJER, D. J., ARTHUR, M. A., DEAN, W. E., HATTIN, D. E., SAVRDA, C. E. (1986): Rhythmic bedding produced in Cretaceous pelagic carbonate environments: sensitive recorders of climatic cycles. Paleoceanography 1., 467-481.

BRULAND, K. W. (1983): Trace elements in seawater. In: RILEY, J. P., CHESTER, R. (eds.): Chemical Oceanography, 157-220. Academic Press, New York.

CORNIDES, I., CSÁSZÁR, G., HAAS, J., JOCHA-EDELÉNYI, E. (1979): Oxigén izotópos hőmérséklet-mérések a Dunántúl mezozóos képződményeiből. (In Hungarian with English abstract. Temperature measurements of Transdanubian Mesozoic rocks by the oxygen isotope method) Földt. Közl. 109., 101-110.

DEAN, W. E., GARDNER, J. V., PIPER, D. Z. (1997): Inorganic geochemical indicators of glacial-interglacial changes in productivity and anoxia on the California continental margin. Geochim. Cosmochim. Acta 61/21., 4507-4518.

DE BOER, P. L., SMITH, D. G. (1994): Orbital forcing and cyclic sequences. In: DE BOER, P. L. and SMITH, D. G. (Eds): Orbital Forcing and Cyclic Sequences. IAS Spec. Publ. 19., 1-14.

DICKENS, G. R., OWEN, R. M. (1994): Late Miocene-Early Pliocene manganese redirection in the central Indian Ocean. Expansion of the intermediate water oxygen minimum zone. Paleoceanography 9., 161-181.

EINSELE, G., RICKEN, W., SEILACHER, A. (1991): Cycles and events in stratigraphy - basic concepts and terms. In: EINSELE, G., RICKEN, W., SEILACHER, A.(Eds): Cycles and Events in Stratigraphy. Springer, Berlin, 1-9.

ERBA, E., PREMOLI SILVA, I. (1994): Orbitally driven cycles in trace fossils distribution from the Piobbico core (late Albian, central Italy). In: DE BOER, P. L. and SMITH, D. G. (Eds): Orbital Forcing and Cyclic Sequences. IAS Spec. Publ. 19., 211-225.

FISCHER, A. G., DE BOER, P. L., PREMOLI SILVA, I. (1990): Cyclostratigraphy. In: GINSBURG, R. N. and BEAUDOIN, B. (Eds): Cretaceous Resources, Events and Rhythms - Background and Plans for Research. Kluwer, Dordrecht, 139-172.

FISHER, N. S., GUILLARD, R. R. L., BANKSTON, D. C. (1991): The accumulation of barium in marine phytoplankton grown in culture. J. Mar. Res. 49., 339-354.

FOGARASI, A. (1995): Ciklussztratigráfiai vizsgálatok a gerecsei krétában: előzetes eredmények. (In Hungarian with English abstract. Cretaceous cyclostratigraphy of Gerecse Mts. Preliminary results.) Ált. Földt. Szemle 27., 43-58.

FORCE, E. R., CANNON, W. F. (1988): Depositional model for shallow-marine manganese deposits around black shale basins. Econ. Geol. 83., 93-117.

FROELICH, P. N., BENDER, M. L., LUEDTKE, N. A., HEATH, G. R., DEVRIES, T. (1982): The marine phosphorous cycle. Amer. J. Sci. 282., 474-511.

FÜLÖP, J., BREZSNYÁNSZKY, K., HAAS, J. (1987): The new map of basin basement of Hungary. Acta Geol. Hung. 30., 1-2, 3-20.

GOBEIL, C., MACDONALD, R. W., SUNDBY, B. (1997): Diagenetic separation of cadmium and manganese in suboxic continental margin sediments. Geochim. Cosmochim. Acta 61/21., 4647-4654.

GOLDBERG, E. D., ARRHENIUS, G. O. S. (1958): Chemistry of Pacific pelagic sediments. Geochim Cosmochim. Acta 13., 153-212.

GROW, J. A., MATTICK, R. E., BÉRCZY-MAKK, A., PÉRÓ, CS., HAJDÚ, D., POGÁCSÁS, GY., VÁRNAI, P., VARGA, E. (1994): Structure of the Békés Basin Inferred from Seismic Reflection, Well and Gravity Data. In: TELEKI, P. G. et al. (Eds.): Basin Analysis in Petroleum Exploration. Kluwer, Dordrecht, 1-38

HAAS, J. (1994): Magyarország geológiája -- Mezozóikum. Egyetemi jegyzet. (Geology of Hungary - Mesozoic. Lecture notes.) Eötvös Loránd Tudományegyetem, Budapest. (University of Loránd Eötvös, Budapest) 199 p. (In Hungarian)

HALLAM, A. (1964): Origin of the limestone-shale rhythm in the Blue Lias of England: a composite theory. Jour. Geol. 72. 157-169.

HATCH, J. R., LEVENTHAL, J. S. (1992): Relationship between inferred redox potential of the depositional environment and geochemistry of the Upper Pennsylvanian (Missourian) Stark Shale Member of the Dennis Limestone, Wabaunsee County, Kansas, U.S.A.. Chem. Geol. 99., 65-82.

HUERTA-DIAZ, M. A., MORSE, J. W. (1992): Pyritization of trace metals in anoxic marine sediments. Geochim. Cosmochim. Acta 56., 2681-2702.

IANOVICI, V., BORCOS, M., BLEAHU, M., PATRULIUS, D., LUPU, M., DIMITRESCU, R., SAVU, H. (1976): Geologia Muntilor Apuseni. (Geology of Apuseni Mountains) Edit. Acad. R. S. R. 631 p. Bucuresti.

JENKYNS, H. C., GALE, A. S., CORFIELD, R. M. (1994): Carbon- and oxygen-isotope stratigraphy of the English Chalk and Italian Scaglia and its paleoclimatic significance. Geol. Mag. 131., 1-34.

JOHANSSON, S.A.E., CAMPBELL, J.L. (Eds.) (1988): PIXE: A Novel Technique for Elemental Analysis, John Wiley & Sons, Chichester.

KUMAR, N., ANDERSON, R. F., BISCAYE, P. E. (1996): Remineralization of particulate authigenic trace metals in the Middle Atlantic Bight: Implications for proxies of export production. Geochim. Cosmochim. Acta 60., 3383-3397.

LEWAN, M. D., MAYNARD, J. B. (1982): Factors controlling enrichment of vanadium and nickel in the bitumen of organic sedimentary rocks. Geochim. Cosmochim. Acta 46., 2547-2560.

MACHHOUR, L., PHILIP, J., OUDIN, J. L. (1994): Formation of laminite deposits in anaerobic-dysaerobic marine environments. Mar. Geol. 117., 287-302.

MATTIOLI, E. (1997): Nannoplankton productivity and diagenesis in the rhythmically bedded Toarcian-Aalenian Fiuminata section (Umbria-Marche Apennine, central Italy). Palaeogeog., Palaeoclim., Palaeoecol. 130., 113-133.

MURRAY, R. W., LEINEN, M. (1993): Chemical transport to the seafloor of the equatorial Pacific Ocean across a latitudinal transect at 135° W: Tracking sedimentary major, trace and rare earth element fluxes at the Equator and the Intertropical Convergence Zone. Geochim. Cosmochim. Acta 57., 4141-4163.

MURRAY, R. W., LEINEN, M. (1996): Scavenged excess aluminium and its relationship to bulk titanium in biogenic sediment from the central equatorial Pacific Ocean. Geochim. Cosmochim. Acta 60., 3869-3878.

MURRAY, R. W., BUCHHOLTZ TEN BRINK, M. R., JONES, D. L., GERLACH, D. C., RUSS G. P. III. (1990): Rare earth elements as indicators of different marine depositional environments in chert and shale. Geology 18., 268-271.

MURRAY, R. W., BUCHHOLTZ TEN BRINK, M. R., GERLACH, D. C., RUSS G. P. III., JONES, D. L. (1991): Rare earth, major, and trace elements in chert from the Franciscan Complex and Monterey Group, California, assessing REE sources to fine grained marine sediments. Geochim. Cosmochim. Acta 55., 1875-1896.

MURRAY, R. W., LEINEN, M., ISEM, A. R. (1993): Biogenic flux of Al to sediment in the central equatorial Pacific Ocean. Evidence for increased productivity during glacial periods. Paleoceanography 8., 651-670.

NAGY, E. (1969): A Mecsek hegység alsóliász kőszénösszlete. Földtan. (Lower Liassic coal formation of the Mecsek Mountains. Geology.) MÁFI Évkönyve (Annals of Hung. Inst. of Geol.) 51/2., 245-971. (In Hungarian).

NATH, B. N., ROELANDTS, I., SUDHAKAR, M., PLUEGER, W. L. (1992): Rare earth element patterns of the Central Indian Basin sediments related to their lithology. Geophys. Res. Letts. 19., 1197-1200.

ODERMATT, J. R., CURIALE, J. A. (1991): Organically bound metals and biomarkers in the Monterey Formation of the Santa Maria Basin, California. Chem. Geol. 91., 99-113.

PINGITORE, N. E. JR., LYTLE, F. W., DAVIES, B. M., EASTMAN, M. P., ELLER, P. G., LARSON, E. M. (1992): Mode of incorporation of Sr in calcite: determination by X-ray absorption spectroscopy. Geochim. Cosmochim. Acta 56., 1531-1538.

PIPER, D. J. W., STOW, D. A. V. (1991): Fine-grained turbidites. In: EINSELE, G., RICKEN, W., SEILACHER, A. (Eds): Cycles and Events in Stratigraphy. Springer, Berlin, 360-376.

PRANGE, A., KREMLING, K. (1985): Distribution of dissolved molybdenium, uranium and vanadium in Baltic Sea waters. Mar. Chem. 16., 259-274.

RAUCSIK, B. (1997): Stable isotopic composition of the Komló Calcareous Marl Formation („Spotted marl" s. str.), Mecsek Mountains, S Hungary. Acta Min.-Petr., Szeged 38., 95-109.

RICKEN, W. (1991): Variation of sedimentation rates in rhythmically bedded sediments. Distinction between depositional types. In: EINSELE, G., RICKEN, W., SEILACHER, A. (Eds): Cycles and Events in Stratigraphy. Springer, Berlin, 167-187.

RICKEN, W. (1994): Complex rhythmic sedimentation related to third order sea-level variations: Upper Cretaceous, Western Interior Basin, USA. In: DE BOER, P. L. and SMITH, D. G. (Eds): Orbital Forcing and Cyclic Sequences. IAS Spec. Publ. 19., 167-193.

ROCC Group (Research on Cretaceous Cycles Group) (1986): Rhythmic bedding in Upper Cretaceous pelagic carbonate sequences: varying sedimentary response to climatic forcing. Geology 14., 153-156.

SAAGER, P. M., DE BAAR, H. J. W., BURKILL, P. H. (1989): Manganese and iron in Indian Ocean waters. Geochim. Cosmochim. Acta 53., 2259-2267.

SAVRDA, C. E., BOTTJER, D. J. (1994): Ichnofossils and ichnofabrics in rhythmically bedded pelagic/hemi-pelagic carbonates: recognition and evaluation of benthic redox and scour cycles. In: DE BOER, P. L. and SMITH, D. G.(Eds): Orbital Forcing and Cyclic Sequences. IAS Spec. Publ. 19., 195-210.

SAVRDA, C. E., BOTTJER, D. J., SEILACHER, A. (1991): Redox-related benthic events. In: EINSELE, G., RICKEN, W., SEILACHER, A. (Eds): Cycles and Events in Stratigraphy. Springer, Berlin, 524-541.

SCHROEDER, J. O., MURRAY, R. W., LEINEN, M., PFLAUM, R. C., JANECEK, T. R. (1997): Barium in equatorial Pacific carbonate sediment: Terrigenous, oxide, and biogenic associations. Paleoceanography 12., 125-146.

SETHI, P. S, LEITHOLD, E. L. (1994): Climatic cyclicity and terrigenous sediment influx to the Early Turonian Greenhorn Sea, southern Utah. J. of Sed. Research B 64/1., 26-39.

SHAW, T. J., GIESKES, J. M., JAHNKE, R. A. (1990): Early diagenesis in differing depositional environments: The response of transition metals in pore water. Geochim. Cosmochim. Acta 54., 1233-1246.

SUNDARAMAN, P., SCHOELL, M., LITTKE, R., BAKER, D. R., LEYTHAEUSER, D., RULLKÖTTER, J. (1993): Depositional environment of Toarcian shales from northern Germany as monitored with porphyrins. Geochim. Cosmochim. Acta 57., 4213-4218.

SZABÓ, GY., BORBÉLY-KISS, I. (1993): PIXYKLM Computer Packege for PIXE Analyses. Nucl. Instr. and Meth. in Phys. Res. B75., 123-126.

TAYLOR, S. R., MCLENNAN, S. M. (1985): The Continental Crust, Its Composition and Evolution. Blackwell Scientific Publications, Oxford, London.

TUCKER, M. E., WRIGHT, V. P. (1990): Carbonate sedimentology. Blackwell Scientific Publications, Oxford, London.
TUREKIAN, K. K. (1972): Chemistry of the Earth. Holt, Rinehart, and Winston.
WEDEPOHL, K. H. (1978): Manganese: abundance in common sediments and sedimentary rocks. In: Handbook of Geochemistry. Springer, Berlin, II/3., 1-17.
WEISSERT, H., BRÉHÉRET, J. G. (1991): A carbonate carbon-isotope record from the Aptian-Albian sediments of the Vocontian trough (SE France). Bull. Soc. Géol. Fr. 162., 1133-1140.

Manuscript received 16 October, 1998.

Fig. 4: Plots of Fe vs. Ti (ppm)

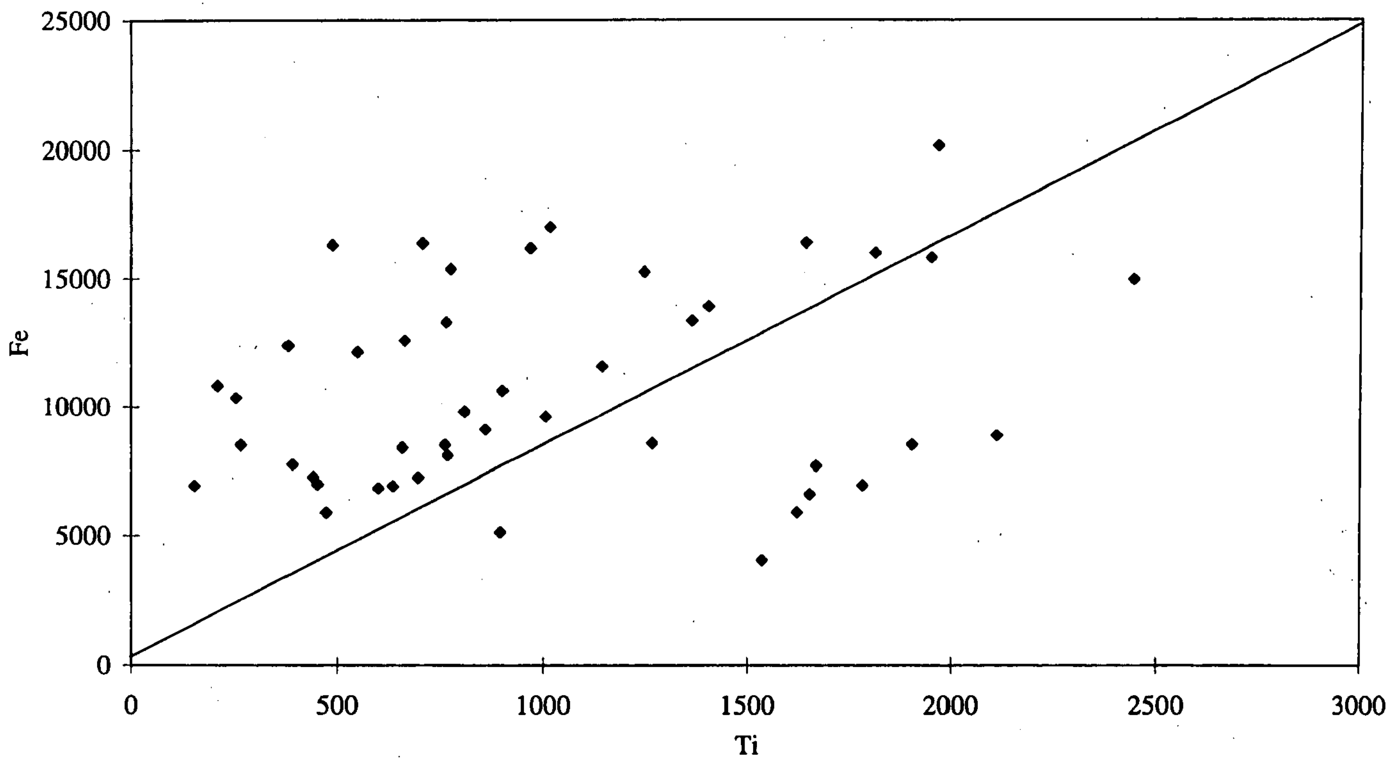

Fig. 5: Fe/Ti ratios of the measured samples

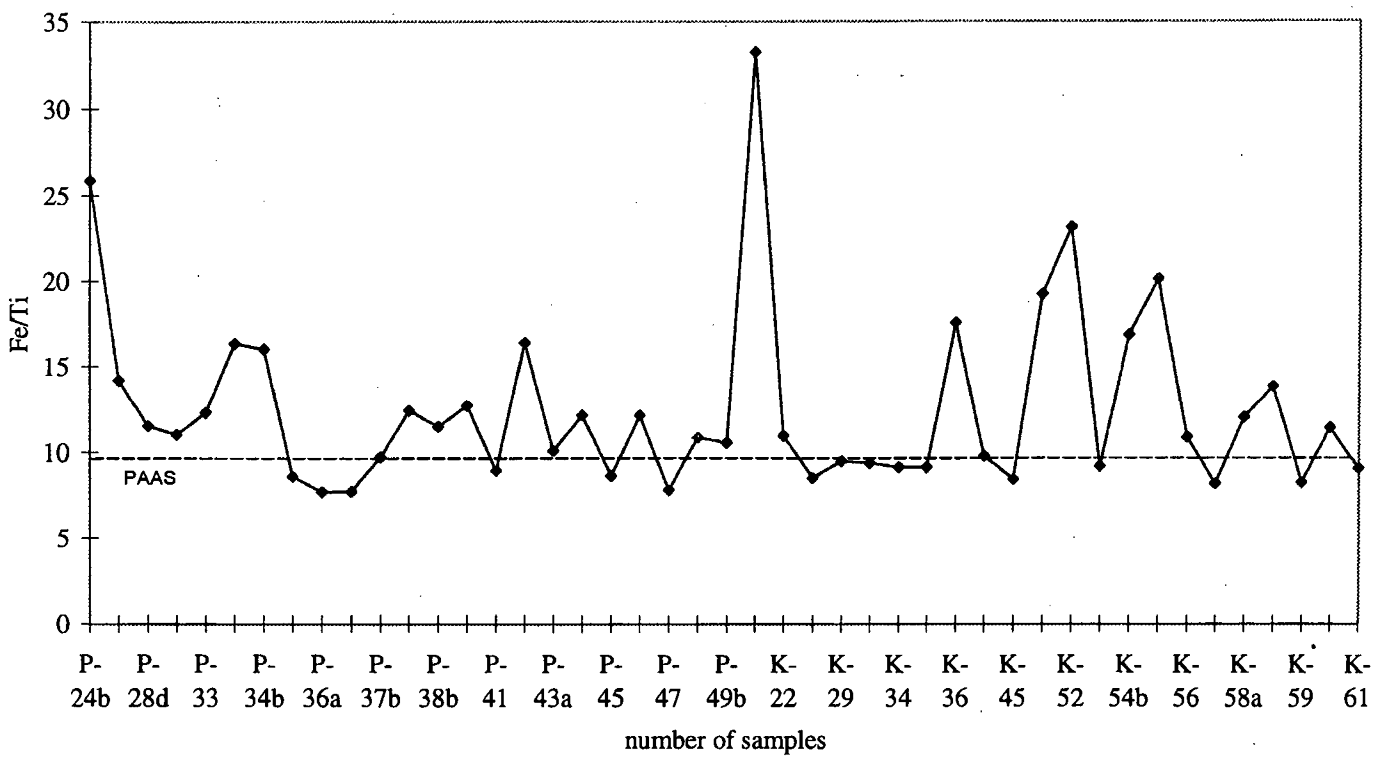

Fig. 6: P/Ti ratios of the measured samples

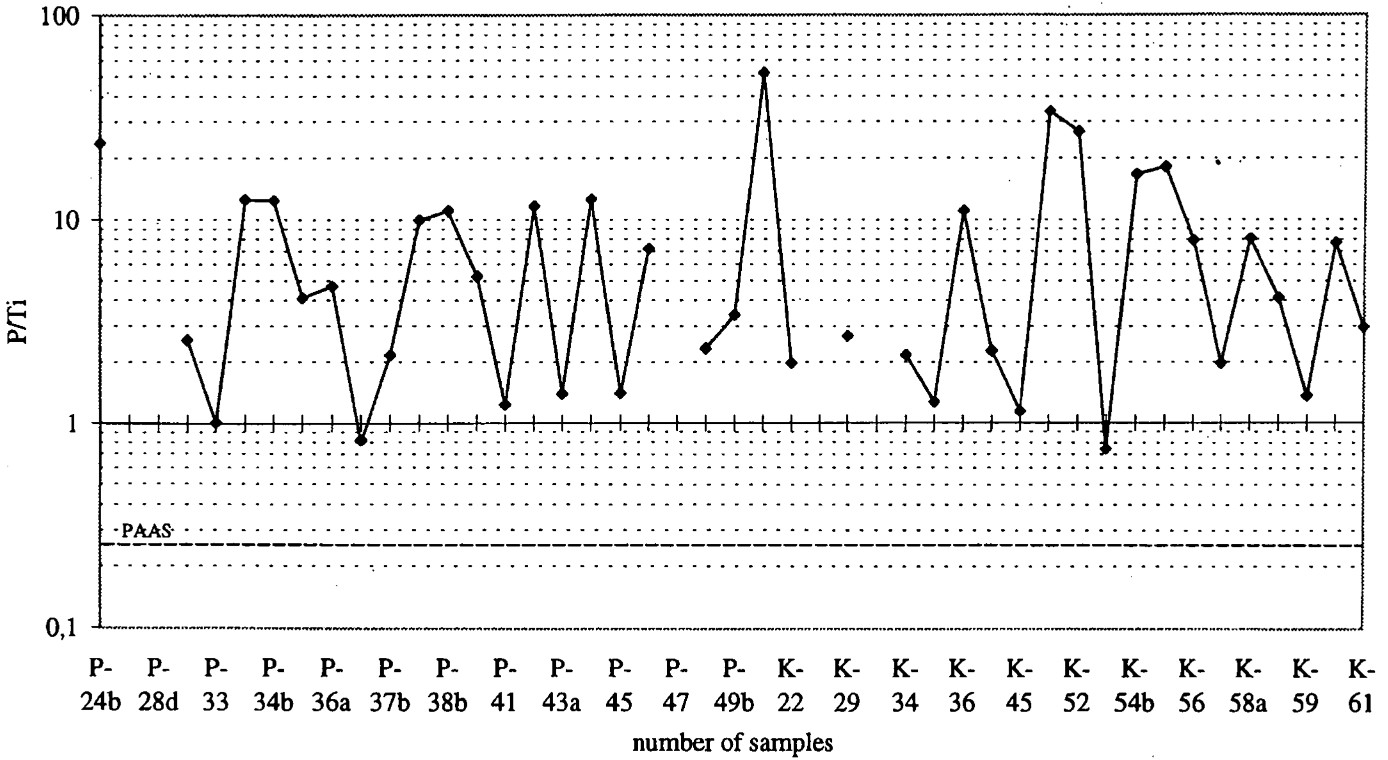

Fig. 7: Plots of Ni vs. Ti (ppm)

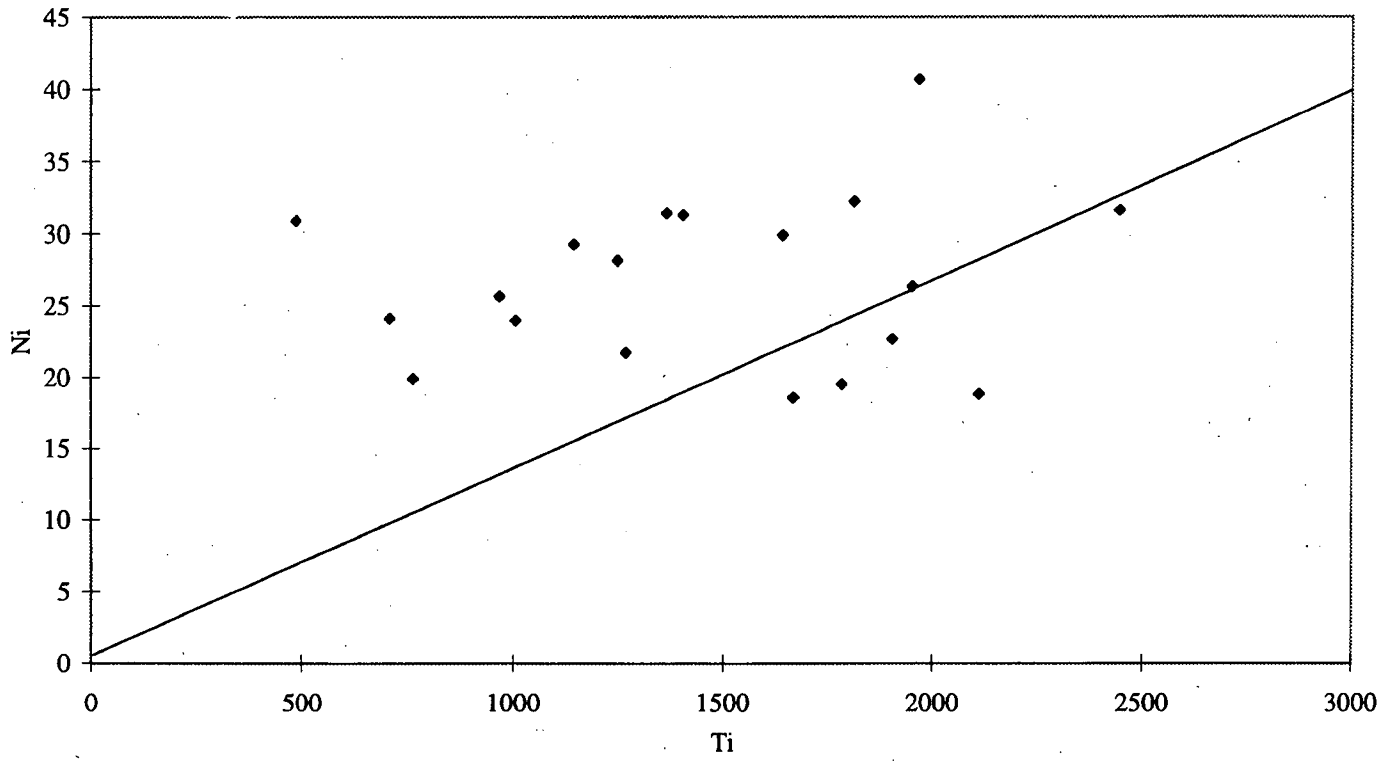

Fig. 8: Plots of Cu vs. Ti (ppm)

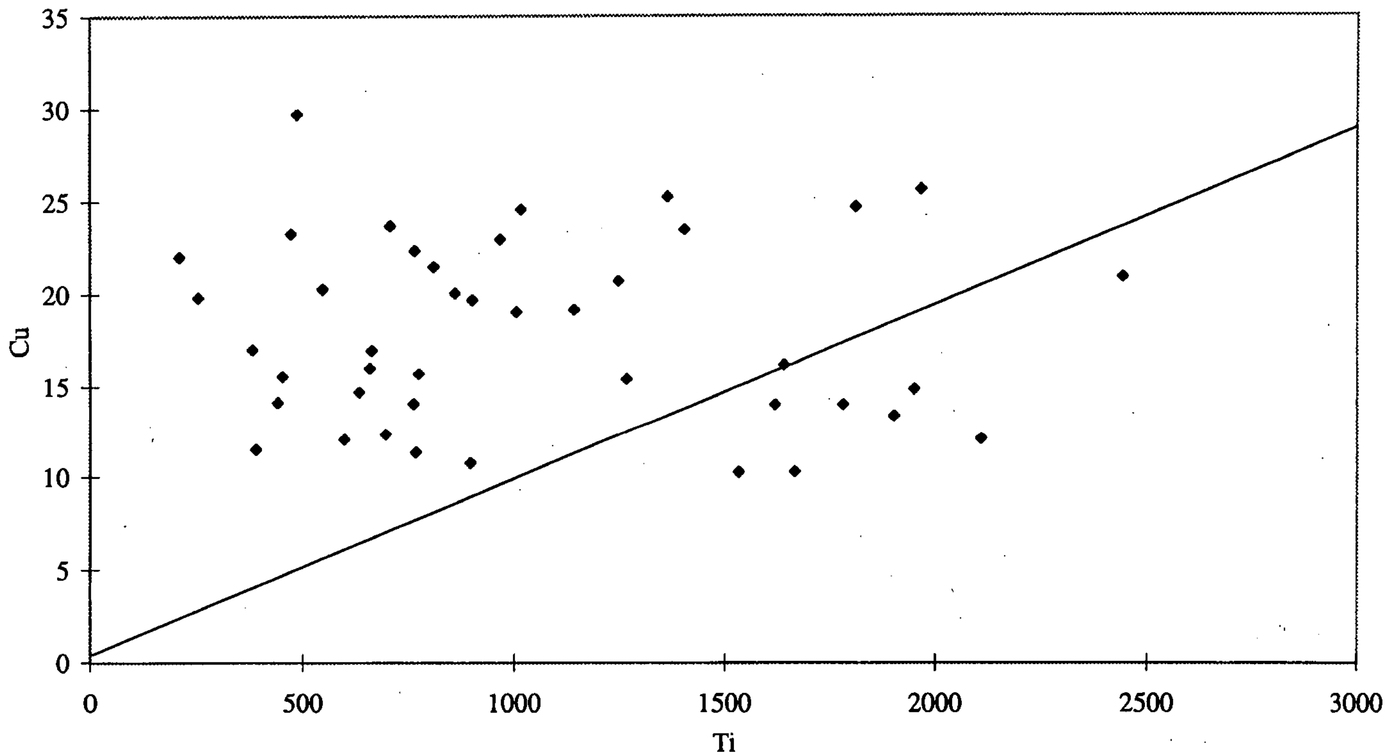

Fig. 9: Plots of Zn vs. Ti (ppm)

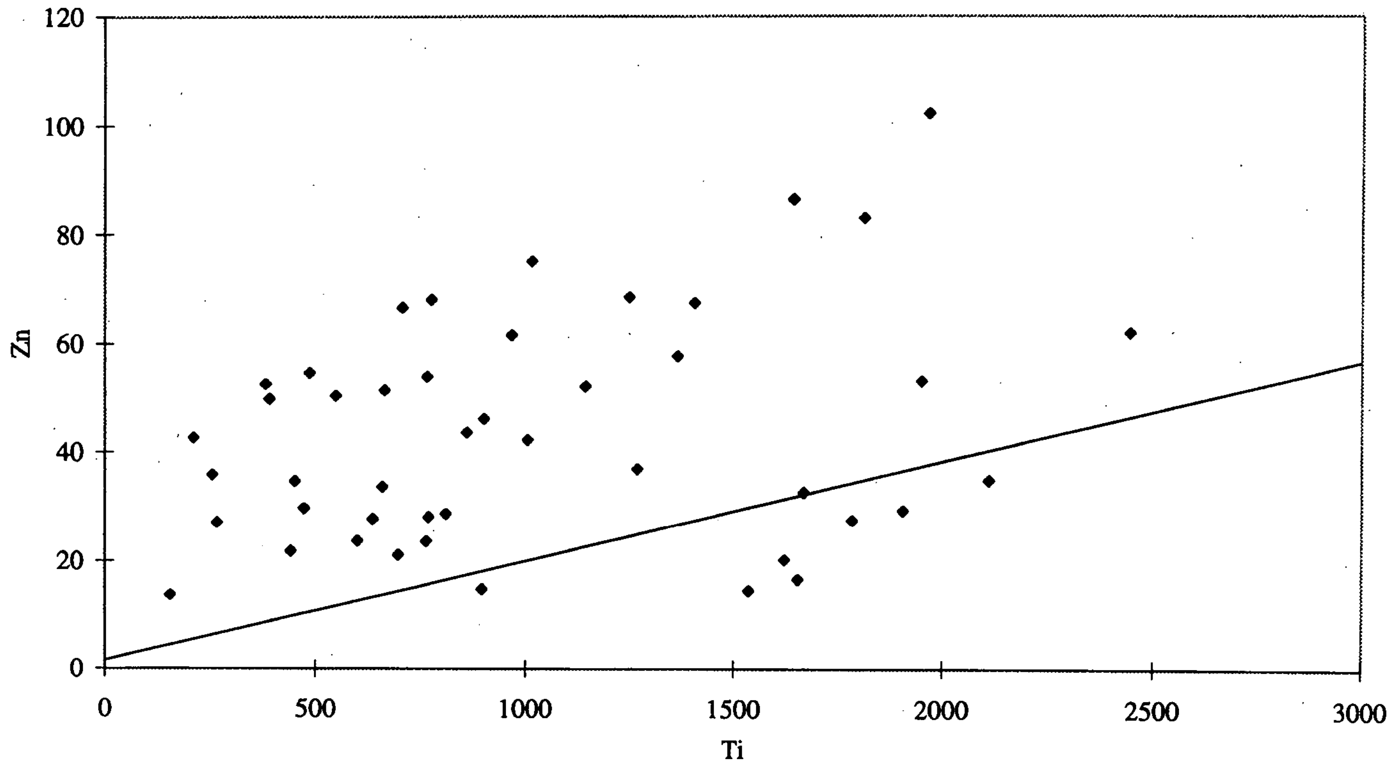

Fig. 10: Plots of V vs. Ti (ppm)

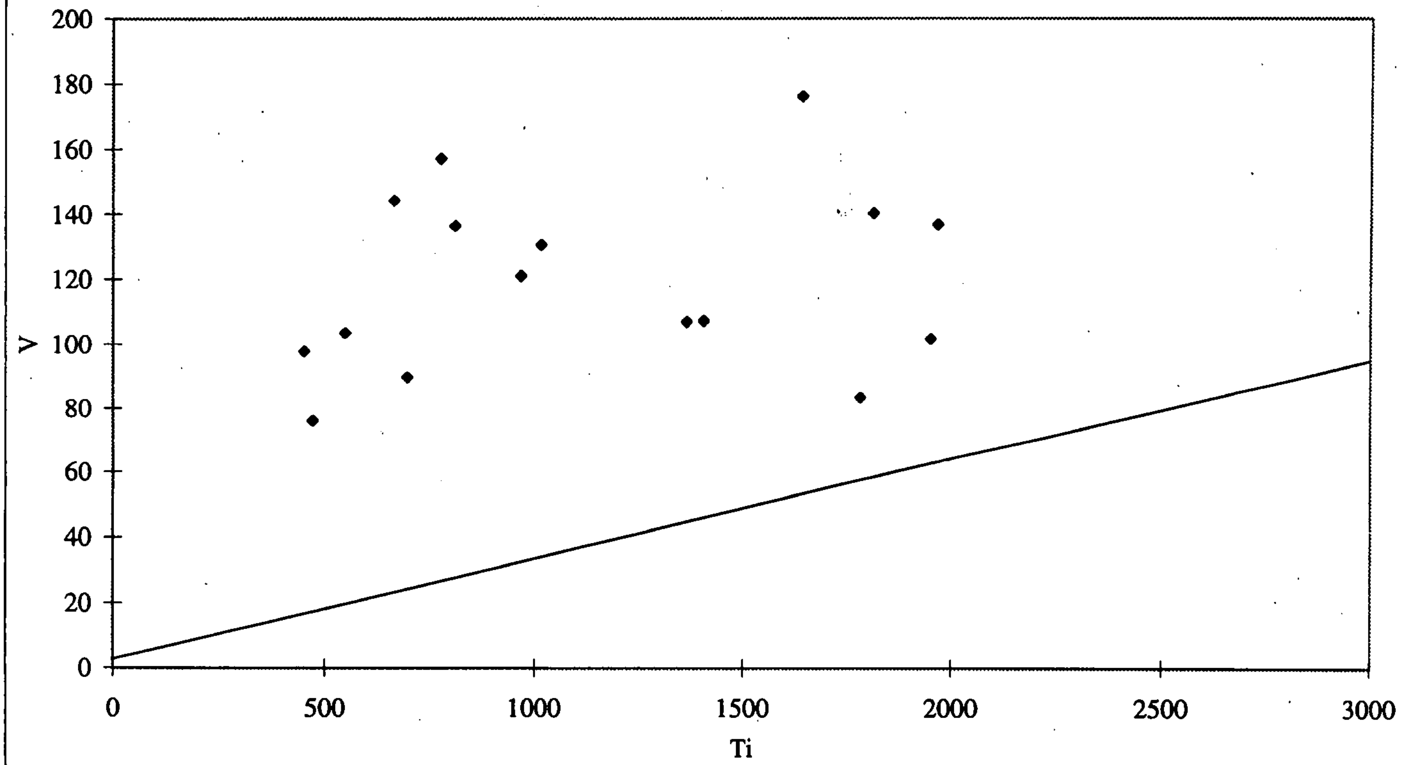

Fig. 11: Plots of Sr vs. Ti (ppm)

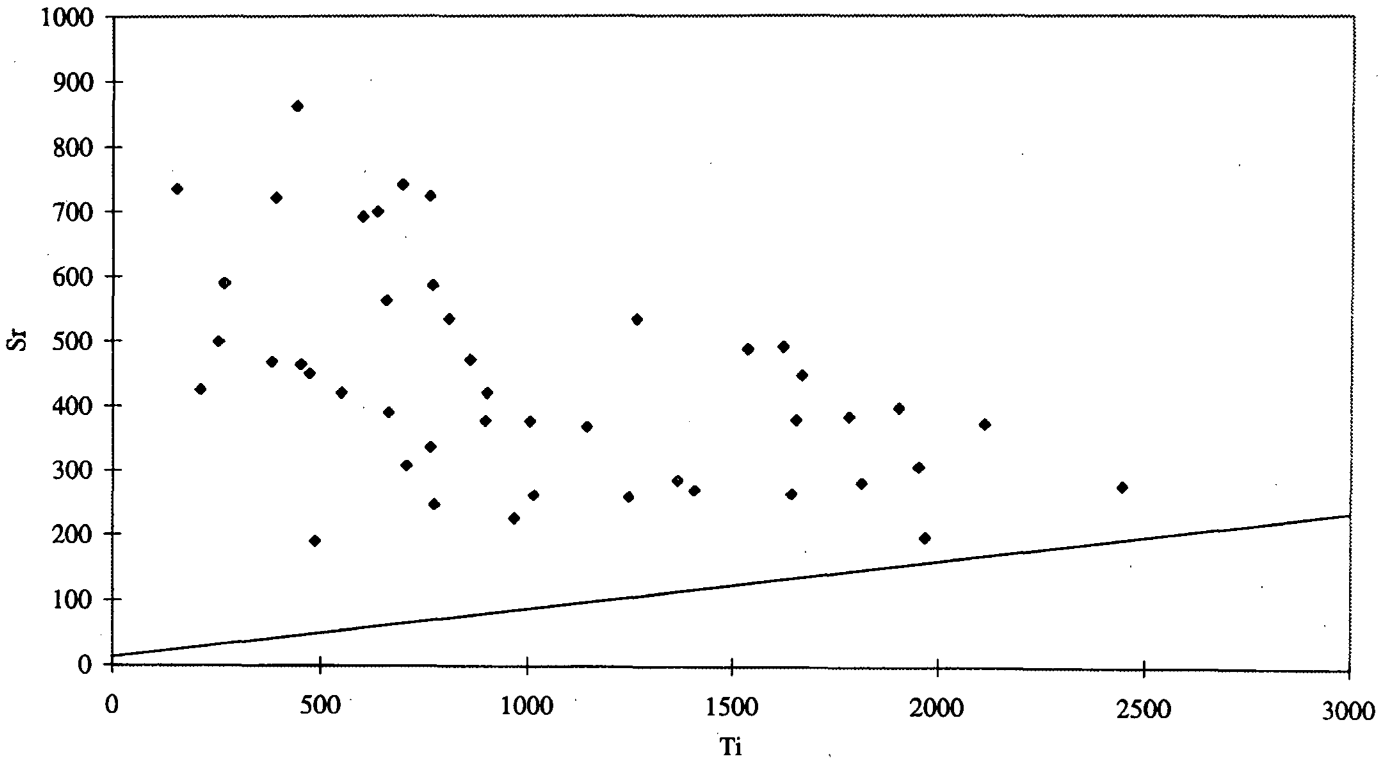

Fig. 12: Cu and Zn values of the measured samples

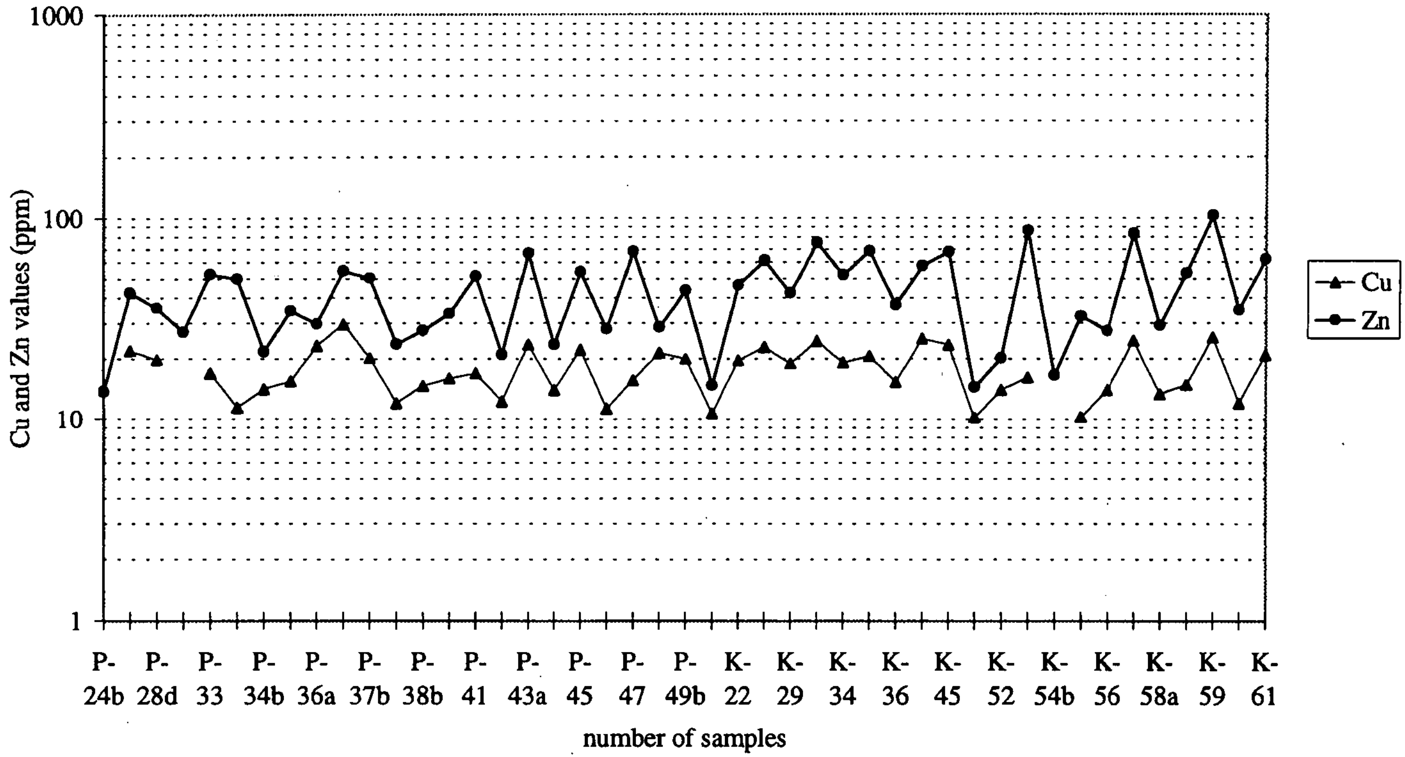

Fig. 13: Sr/Ti ratios of the measured samples

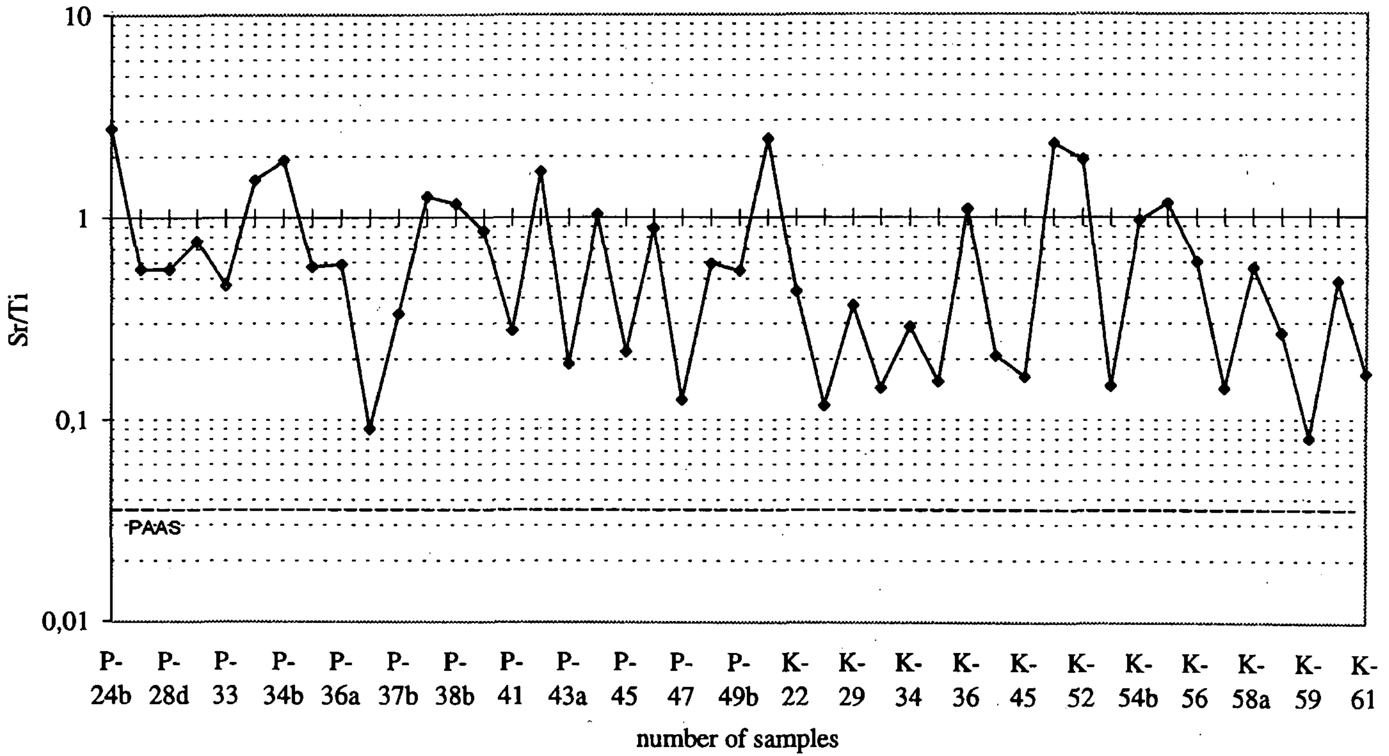

Fig. 14a: Mn/Ti ratios and Ti values of the measured samples

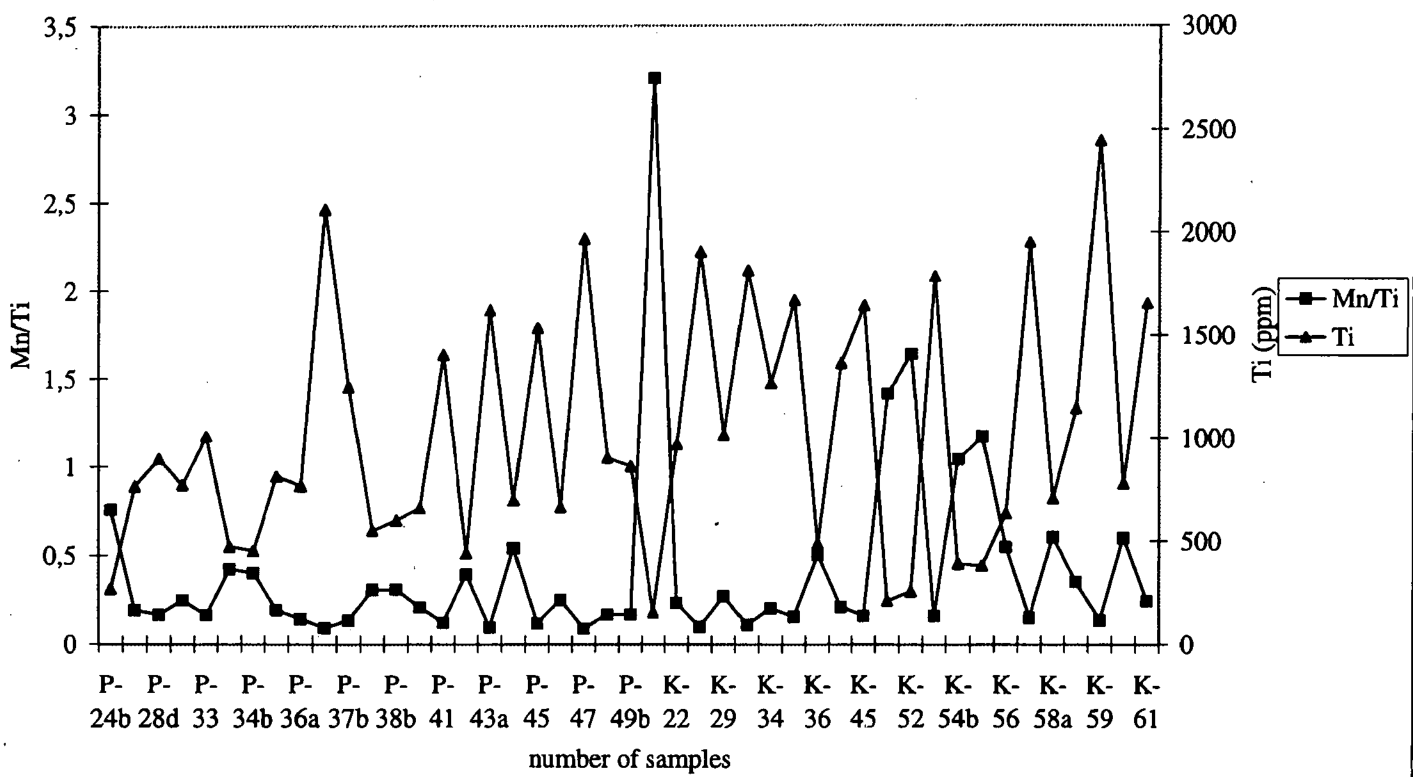

Fig. 14b: Mn/Ti ratios and Ca values of the measured samples

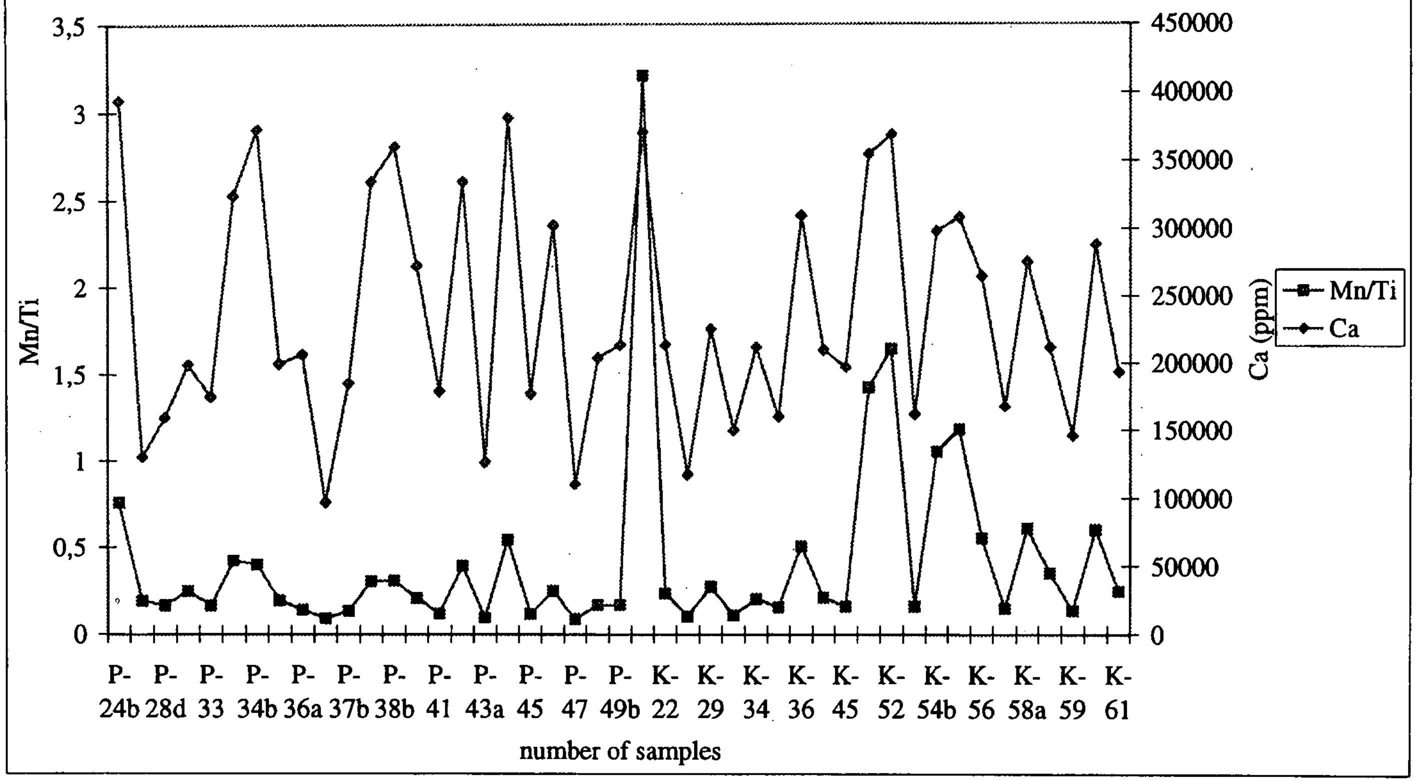

Fig. 15: Fe/Mn ratios of the measured samples

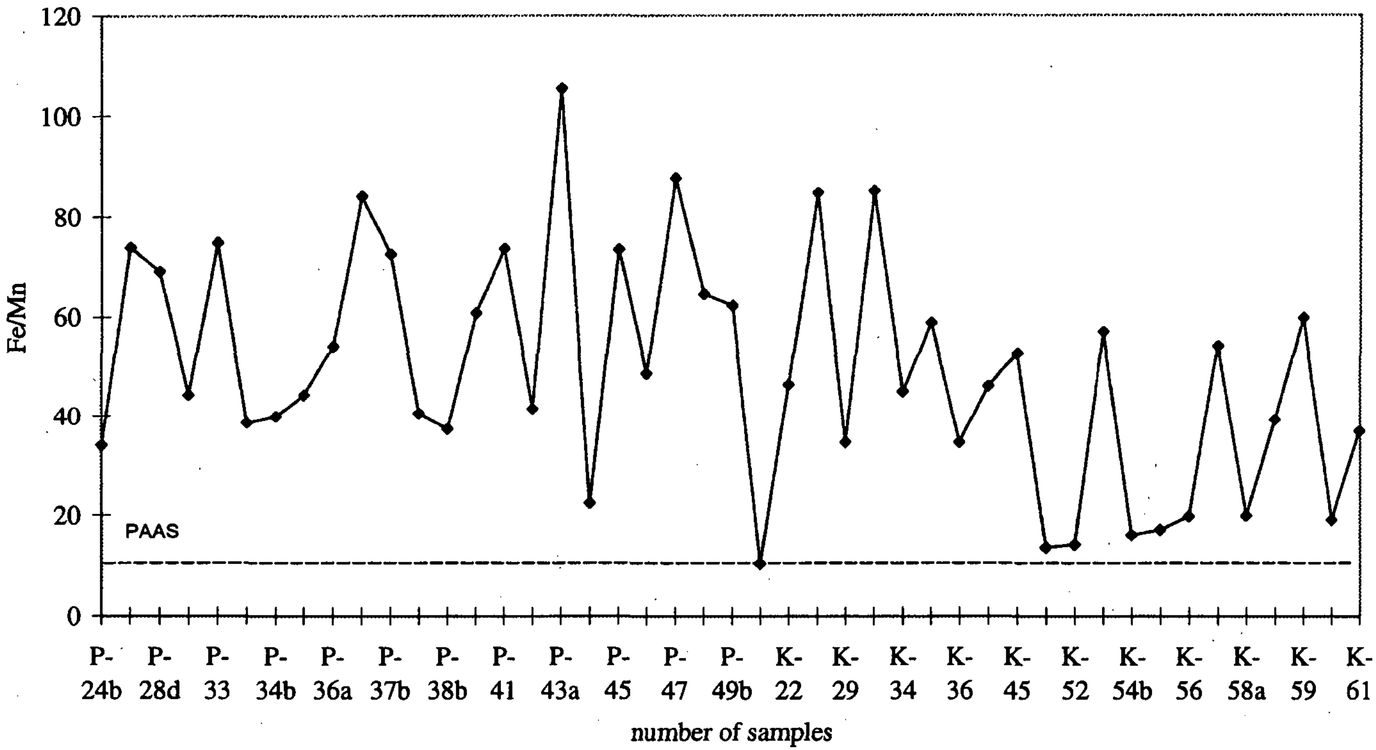

Acta Mineralogica-Petrographica, Szeged, XXXIX, 139–150, 1998

GEOCHEMICAL INVESTIGATIONS OF THE DUNASZEKCSŐ LOESS-PALEOSOL SEQUENCE, SE TRANSDANUBIA, HUNGARY

LÁSZLÓ HUM[1]

Department of Geology and Paleontology, Attila József University

ABSTRACT

The paper discusses the relation between paleoclimate and geochemical characteristics of the loess-paleosol sequence of Dunaszekcső, Hungary. Geochemical properties of the sediments reflect the intensity of weathering and pedogenesis, thus five sediment types could be distinguished upon this basis. The *weakly weathered loess* formed under cold and arid climate, while the *weathered loess* accumulated during milder, more humid periods. The *strongly weathered loess*, overlying paleosols, shows intermediate character between loess and paleosol; its geochemical analysis indicates more intense weathering than in loess, but not intensive enough for soil formation. The Mende Upper and Basaharc Double paleosols were produced by strong pedogenesis, while the Basaharc Lower paleosol underwent the most advanced weathering and pedogenesis. Analyses of the geochemical character of different stratigraphic horizons allowed the reconstruction of paleoclimatic trends.

Keywords: younger loess, paleosols, geochemistry, carbonates, major components, trace elements, paleoclimate

INTRODUCTION

Quaternary sediments reflect the environmental influences that played crucial role in their development. The paleoenvironmental conditions determined the mineralogical composition and the distribution of chemical elements in loesses and in paleosols. Consequently, the changes of the mineralogical composition and geochemistry of sediments make possible the reconstruction of the dynamic changes of paleoclimate and environment.

As the climate becomes warmer and more humid, weathering and pedogenesis intensify. In warm-humid periods the solution of the carbonates increases, and so do the development of clay minerals, the accumulation of Fe_2O_3, Al_2O_3, and the enrichment of several main components and trace elements.

On the base of their lithological features, the loesses in Hungary can be divided into two well-distinguishable units: the "young loess" and the "old loess" series. The upper part of the young loess series is designated "Dunaújváros-Tápiósüly subseries", while the lower part is known as "Mende-Basaharc subseries" (PÉCSI 1975, 1985, 1993). The Dunaújváros-Tápiósüly subseries contains two humic horizons (h_1, h_2), while the two paleosol complexes (Mende Upper I and Mende Upper II; Basaharc Double I and Basaharc Double II) and one well-developed paleosol horizon of considerable thickness (Basaharc Lower) are interlayered in the Mende-Basaharc subseries (PÉCSI-SCHWEITZER 1995).

[1] H-6722 Szeged, Egyetem u. 2-6.

Geochemistry of the loesses has been studied by a great number of scientists all over the world (GONG et al. 1987, LAUTRIDOU et al. 1984, PETROV et al. 1984, SCHNETGER 1992, TAYLOR et al. 1983). The young loess series of Hungary was investigated by PÉCSI-DONÁTH (1985). The relationship between geochemical character of loesses and paleoclimatic changes was revealed by WEN et al. (1985), LIU et al. (1995), and WEN et al. (1995).

According to previous investigations, the loesses of the area can be divided into three groups upon their geochemical and lithological composition: weakly weathered loess, weathered loess and strongly weathered loess (HUM and FÉNYES 1995, HUM 1997). As compared to weakly weathered loess, the weathered loess is characterized by higher TiO_2, Al_2O_3, Fe_2O_3, K_2O, Li, Cr, Zn, Rb, and lower CaO and Sr content, and its CaO/MgO and $(CaO+K_2O+Na_2O)/Al_2O_3$ ratios are lower, while the K_2O/Na_2O ratio is higher.

In this paper the geochemical investigation of the Dunaszekcső loess-paleosol section is discussed (*Fig. 1.*).

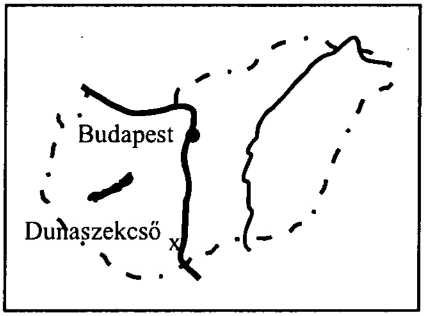

Fig. 1. Location map of the examined profile (x)

ANALYTICAL METHODS

Sampling interval was 0.25 m in the section, but thinner layers were also sampled. The color of the sediments was determined after the Rock-Color Chart (1980). After the determination of grain-size distribution and carbonate content, we selected 27 samples for mineralogical and elementary analyses. The fraction under 71 µm has been analysed. X-ray measurements were used for determination of the mineral composition. The calcite/dolomite ratios were determined by the method of TENNANT-BERGER (1957). Determination of carbonate and clay minerals was promoted by thermoanalytical examinations. Inorganic carbon was removed with HCl, and then organic carbon content was determined by using LECO Carbon-Sulphur Determinator. For the determination of trace and major elements, destructive attack was performed by using HF-$HClO_4$-HNO_3 mixture in teflon bomb under high pressure. Al, Fe (total), Mn, Mg, Ca, Na, K, Li, Zn, and Sr were analysed by flame AAS (Perkin Elmer 4100). Cr, Rb, Ni, Co, Pb and Cu were measured by graphite-tube AAS (ZEISS). Si was measured by RFA, while Ti and P were analysed by spectrophotometry (using the Tiron-method and the molybdenum yellow method). Ba was measured by ICP-AES. The AAS measurements were checked by the results of RFA and ICP-AES measurements for several elements. All methods are described in HEINRICHS-HERRMANN (1990).

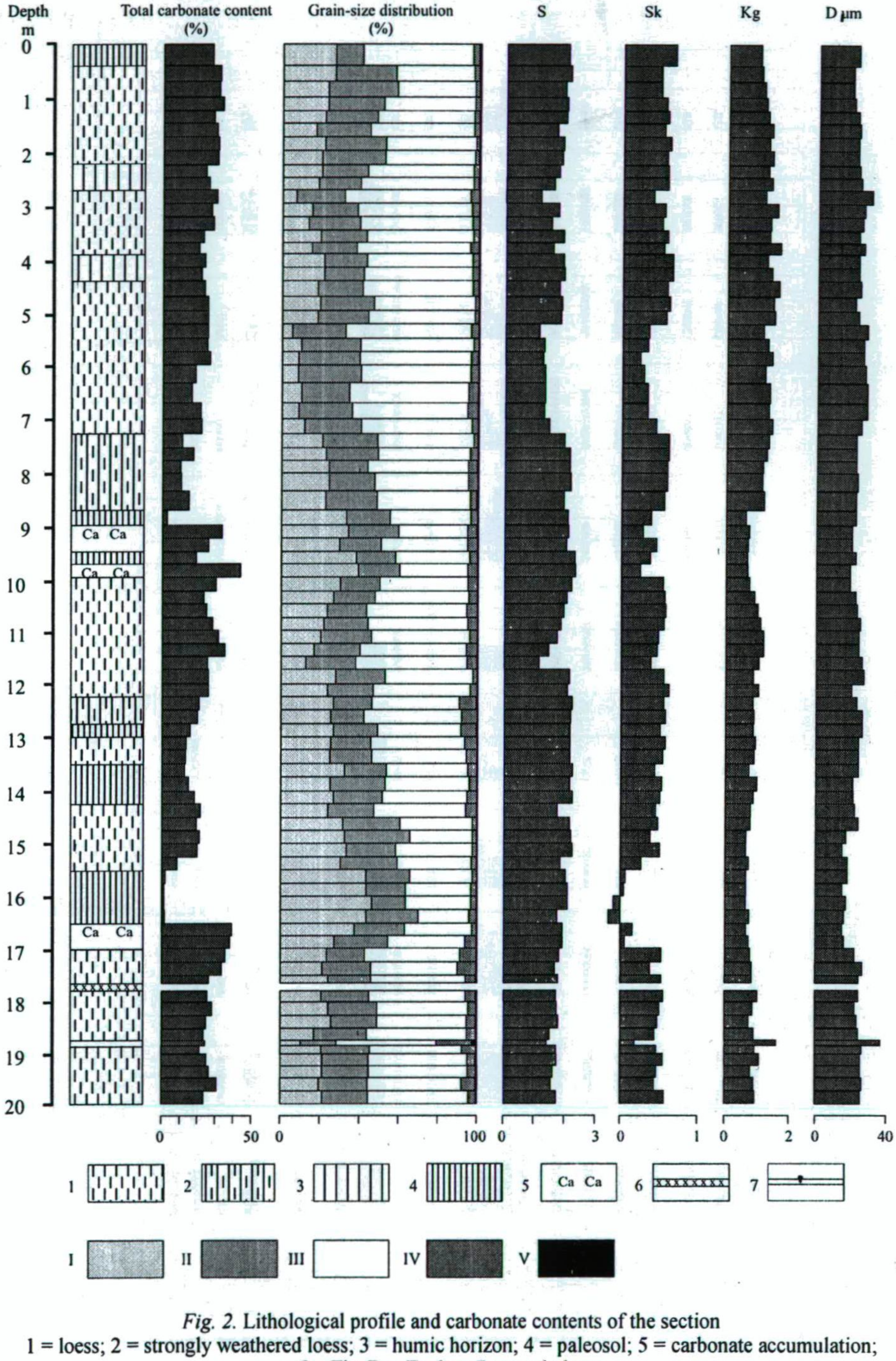

Fig. 2. Lithological profile and carbonate contents of the section
1 = loess; 2 = strongly weathered loess; 3 = humic horizon; 4 = paleosol; 5 = carbonate accumulation; 6 = The Bag Tephra; 7 = sandy layer
I = < 5 µm; II = 5 - 20 µm; III = 20 - 60 µm; IV = 60 - 100 µm; V = 100 - 200 µm; VI. = 200 < µm

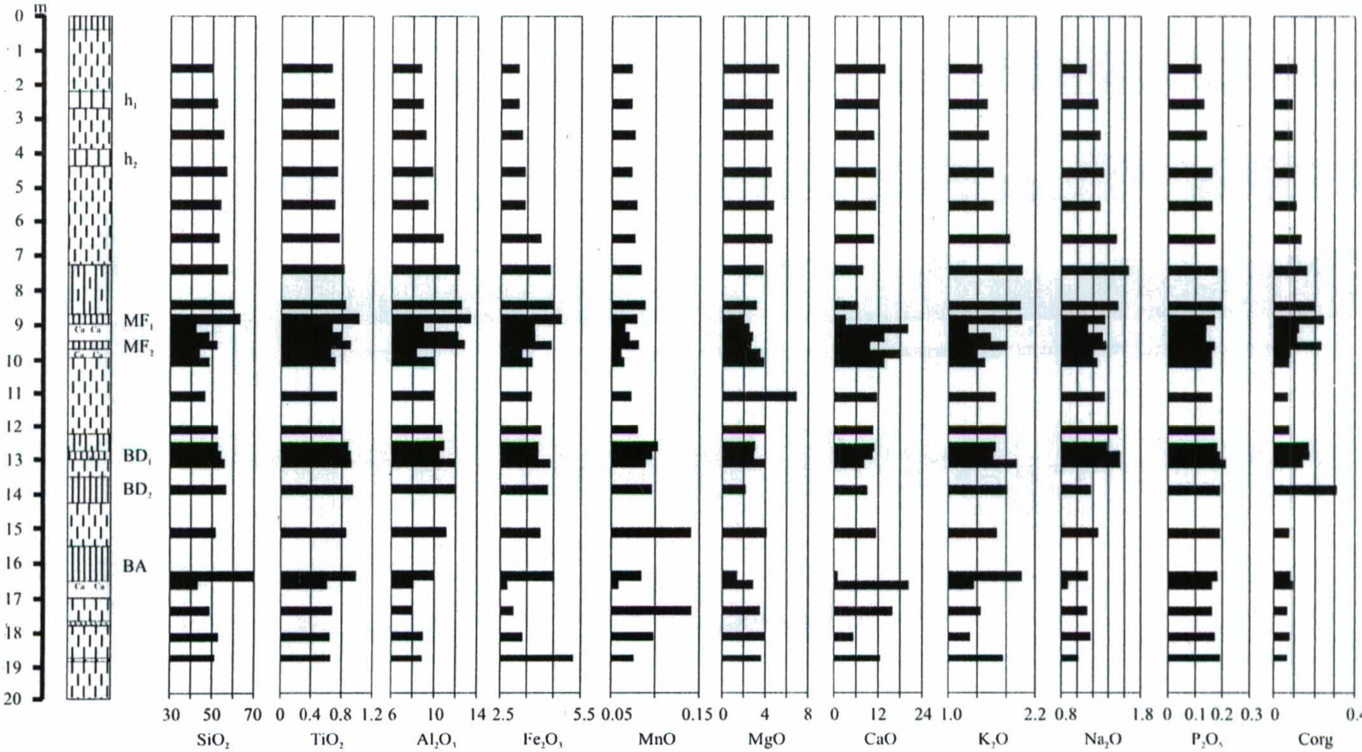

Fig. 3a. Distribution of major components (%) in the section

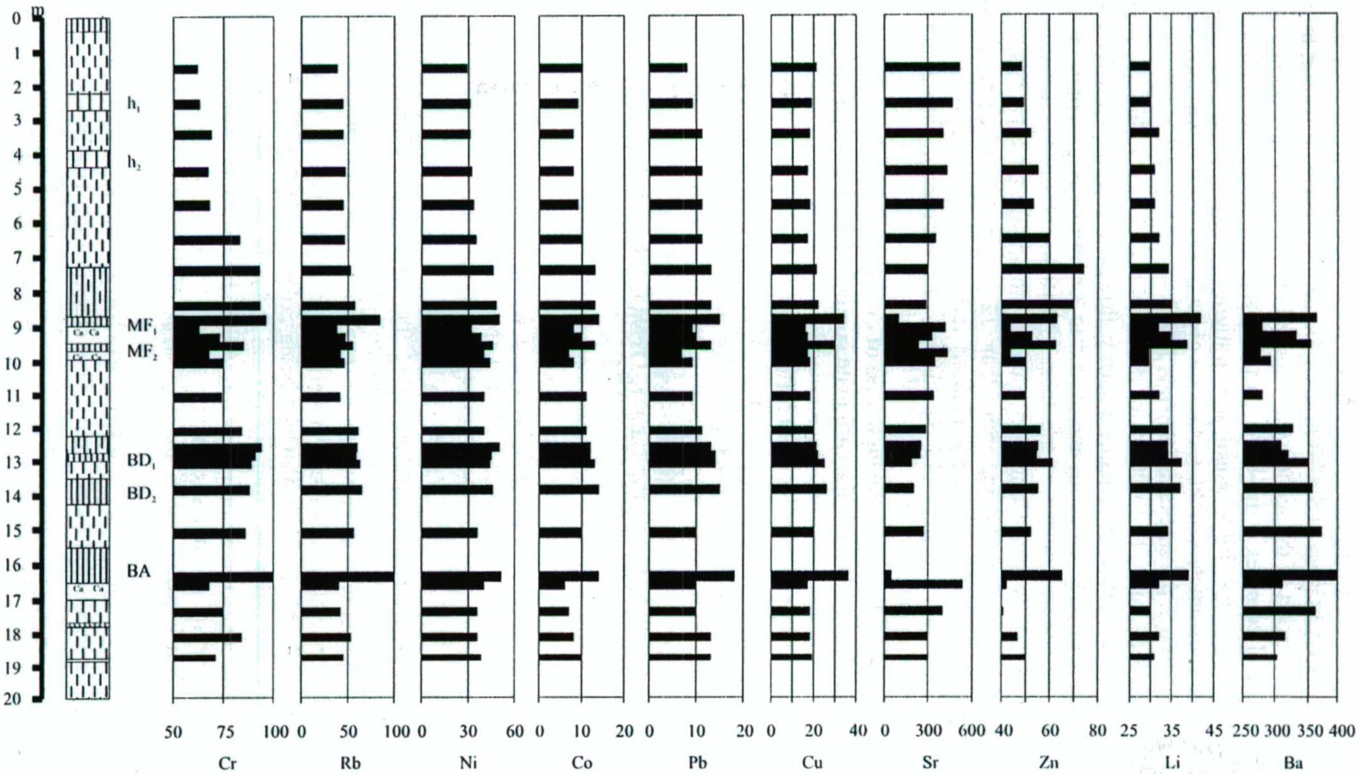

Fig. 3b. Distribution of trace elements (ppm) in the section

The nearly horizontal layers of the 20 m thick Dunaszekcső section belong to the young loess series. The upper part of the section was exposed by drilling, while – after reaching the Mende Felső paleosol complex – the lower part was sampled in the Semmelweis utca and Felszabadulás utca outcrops. Lithological and stratigraphic subdivision, carbonate content and sedimentological parameters of the section are given in *Fig. 2.* The evolutionary trends of chemical elements through the section is shown in *Fig. 3.*

The lowermost loess unit (17 to 20 m) of the section is dusky yellow (5 Y 6/4) loess with carbonate nodules. The unit contains a dark yellowish orange (10 YR 6/6) limonitic, sandy loess layer (at 18.75 to 18.80 m) and the 1.5 to 3 cm thick Bag Tephra (at 17.75 m). Within the high carbonate content of the loess (24.10 to 33.35 %), dolomite prevails (between 68 and 74 %). Several Hungarian authors, including SZILÁRD (1983) and Pécsi (1993), assign the samples containing more than 22 weight % carbonate, to loess-like formations (horizons of carbonate accumulation) rather than to real loess. Others, like FÜCHTBAUER (1988) and HÄDRICH (1975), classify the sediments with 30 or even 40 weight % carbonate content as loess.

Another conspicuous feature is the high ratio of dolomite within the carbonate content. According to FÜCHTBAUER (1988), the carbonate content of the loess consists prevailingly of calcite, while dolomite occurs exceptionally only. Literature data show that calcite/dolomite ratio of loess samples from different parts of the world falls around 2:1 or 3:1 (HÄDRICH 1975, PYE 1983, TAYLOR et al. 1983, SCHNETGER 1992). In our loess samples, however, the calcite/dolomite ratio is 1:2 in average. High dolomite content in the young loess series of Hungary was registered by PÉCSI-DONÁTH (1985) and GEREI et al. (1985) as well.

The CaO/MgO ratio (2.31) and the $CaO+K_2O+Na_2O/Al_2O_3$ ratio (1.75 to 2.33) of the sediment are high, while the K_2O/Na_2O ratio (1.28 to 1.64) is low. As its carbonate content, geochemical ratios, and distributions of major components and trace elements indicate, the loess belongs to the weakly weathered group, and formed under arid and cold climate.

The overlying Basaharc Lower (BA) soil is a well-developed moderate (yellowish) brown (10 YR 5/4, 5 YR 4/4) paleosol (between 15.5 and 16.5 m). Carbonate content of the soil horizon is 1.36 to 1.81 %. The CaO/MgO and the $CaO+K_2O+Na_2O/Al_2O_3$ ratios are extremely low (0.71 and 0.42, respectively), while the K_2O/Na_2O ratio is high. As a result of intense weathering and pedogenesis, the amount of MgO, CaO, and Sr considerably decreased, while the concentration of SiO_2, TiO_2, Fe_2O_3, and K_2O significantly increased, as well as that of Li, Cr, Co, Ni, Cu, Zn, Rb, Pb, and Ba. The 0.5 m thick carbonate accumulation horizon, underlying the soil, displays as high carbonate content as 37.5 to 39.11 %, the bulk of which being dolomite (55 %). The CaO/MgO and $CaO+K_2O+Na_2O/Al_2O_3$ ratios are high (7.18 and 2.81, respectively). This horizon is characterized by a strong decrease in SiO_2, TiO_2, Al_2O_3, Fe_2O_3, MnO, Na_2O, and K_2O, and by an extreme increase in CaO and Sr content.

The overlying unit between 14.25 and 15.5 m is dusky yellow (5 Y 6/4) loess. Its carbonate content ranges from 8.64 to 20.11 %, dominated by dolomite (72 %). Though the CaO/MgO ratio is still high, the $CaO+K_2O+Na_2O/Al_2O_3$ and K_2O/Na_2O ratios indicate that it belongs to the weathered loess group. This classification is affirmed by the TiO_2, Al_2O_3, Fe_2O_3, MnO, Na_2O, K_2O, and P_2O_5 content of the sediment, all being higher than in weakly weathered loess. The weathered loess suffered more intense weathering and formed under more humid climate.

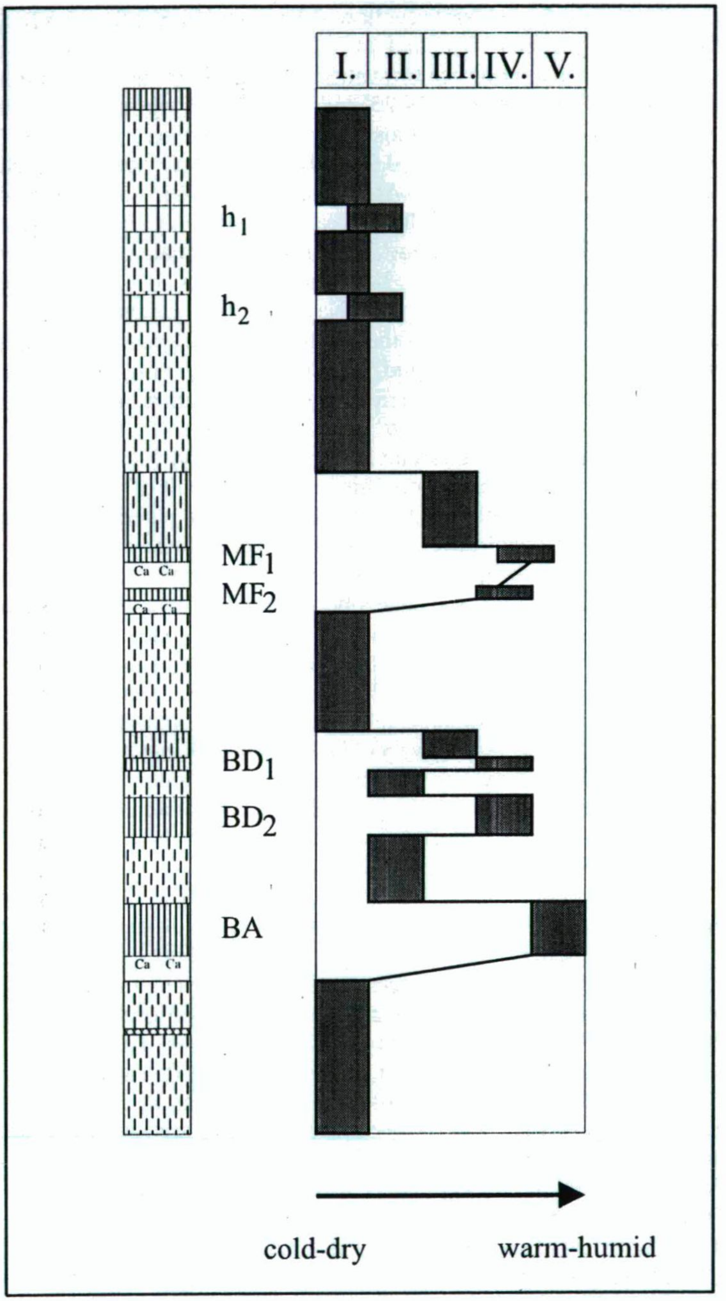

Fig. 4. The evolutionary trends of paleoclimate and intensity of weathering in the young loess series in southeastern Transdanubia as reconstructed from the geochemical analyses of the Dunaszekcső section. I. = weakly weathered loess; II. = weathered loess; III. = strongly weathered loess; IV. = MF and BD soil complexes; V. = BA soil complex

The following unit is the moderate (yellowish) brown (10 YR 5/4, 5 YR 4/4) Basaharc Double (BD) paleosol between 12.75 and 14.25 m. The lower member of the soil complex – Basaharc Double II – is a moderate brown (5 YR 4/4) chernozem-like forest steppe soil (PÉCSI-SCHWEITZER 1995) between 14.25 and 13.50 m. Carbonate content of the soil horizon is 12.73 to 17.09 %, most of which being calcite (73 %). The $CaO+K_2O+Na_2O/Al_2O_3$ ratio is low (0.98), the K_2O/Na_2O ratio is high (1.55). As compared to loess, the amount of TiO_2, Al_2O_3, Fe_2O_3, K_2O, Li, Co, Ni, Cu, and Pb shows higher values, while concentration of alkaline earthes decreases. Between BD II and BD I soils there is a loess layer (from 13.00 to 13.50 m), the carbonate content of which is 13 to 14 %, being mainly dolomite (68 %). On the base of its CaO/MgO (2.01), $CaO+K_2O+Na_2O/Al_2O_3$ (0.95), and K_2O/Na_2O (1.26) ratios and its elementary composition, this layer also belongs to the weathered loess group. Consequently, it was formed during a relatively mild period, when the weathering processes were more intensive than in typical cold and arid periods of loess formation. The moderate yellowish brown (10 YR 5/4) BD I soil (12.75 to 13.00 m) contains 16.12 % carbonate with a balanced calcite/dolomite ratio (the calcite is slightly more: 54 %). According to the oxide ratios and to the elementary composition, this soil is the result of a slightly less intensive pedogenesis than the lower member of the soil complex. The paleoclimatic conditions did not allow the formation of a well-developed soil horizons in these cases.

The next layer is a light brown (5 YR 6/5) strongly weathered loess (between 12.25 and 12.75 m). Its carbonate content changes between 20.01 and 21.37 %, 58 % of which being calcite. Both the elementary composition and the oxide ratios indicate strong weathering. The pedogenesis, however, was too weak to form a soil.

The overlying layer is a dusky yellow (5 Y 6/4) weakly weathered loess (12.25 to 9.95 m). It is characterized by high carbonate, and particularly by high dolomite content (25.92 to 31.98 % and 62 to 88 %, respectively). The CaO/MgO and $CaO+K_2O+Na_2O/Al_2O_3$ ratios are high, the K_2O/Na_2O ratio is low, and the major components as well as the trace elements indicate that this sediment belongs to the weakly weathered loess group. It was formed in a cold and arid period, offering favourable conditions for loess accumulation.

The following Mende Upper (MF) soil complex (8.75 to 9.95 m) consists of two chernozem-like forest steppe soils. The moderate brown (5 YR 5/4) lower paleosol horizon (MF II, between 9.55 and 9.75 m) contains 19.20 % carbonate, mainly calcite (61%). The CaO/MgO, $CaO+K_2O+Na_2O/Al_2O_3$, and K_2O/Na_2O ratios (3.62, 1.01, and 1.32, respectively) also indicate a low intensity pedogenesis. The highest carbonate values of the whole outcrop were measured in the carbonate accumulation horizon underlying this soil: 43.66 %, 52 % of which is calcite, the rest being dolomite. The upper member of the soil complex is the Mende Upper I horizon (8.75 to 9.05 m). Its carbonate content is low: 2.72 %. The calcite/dolomite ratio is close to 1 (46 % calcite, 54 % dolomite). The CaO/MgO ratio (1.51) and the $CaO+K_2O+Na_2O/Al_2O_3$ ratio are low, while the K_2O/Na_2O ratio is high. Beside the high content of SiO_2, TiO_2, Al_2O_3, Fe_2O_3, K_2O, Corg and low amount of MgO, CaO, and Sr, the high concentration of several trace elements, such as Li, Cr, Co, Ni, Cu, Zn, Rb, Pb, and Ba also indicates high-intensity pedogenesis. The Mende Upper I and Mende Upper II soil horizons are separated by a carbonate accumulation zone (9.05 to 9.55 m), with a carbonate content of 25.92 to 33.65 %. Within the carbonate content, the ratio of calcite ranges from 65 to 68 %.

The unit overlying the Mende Upper soil complex is a 1.5 m thick, strongly weathered, clayey, moderate yellowish brown (10 YR 5/4) loess. Its carbonate content changes between 10.00 and 17.73 %, with a dolomite ratio of 74 to 77 %. The CaO/MgO ratio of the sediment is low (1.96 to 1.99), as well as the $CaO+K_2O+Na_2O/Al_2O_3$ ratio (0.77 to 0.90), while its content of Al_2O_3, Fe_2O_3, MnO, K_2O, and P_2O_5 is high. The overall geochemical character of this layer indicates intense weathering and relatively mild paleoclimate, though paleosol formation did not take place.

The overlying layer, between 4.40 and 7.25 m, is dusky yellow (5 Y 6/4) loess. Its carbonate content ranges from 16.37 to 26.83 %, the dolomite being 63 to 80 % of the total. The CaO/MgO and the $CaO+K_2O+Na_2O/Al_2O_3$ ratios are high (2.31 to 2.52 and 1.27 to 1.49, respectively), while the K_2O/Na_2O ratio is low. According to these ratios and to the amount of major components as well as that of the trace elements, this layer belongs to the weakly weathered loess group, thus it formed under cold and arid paleoclimate.

Between 3.95 and 4.40 m, the 2nd humic loess horizon (h_2) of the Dunaújváros-Tápiósüly subseries was identified. Since this horizon is a result of very weak pedogenesis, its carbonate content (23.64 to 21.83 %) and other geochemical features are not unlike those of loesses. Another dusky yellow (5 Y 6/4) weakly weathered loess follows between 0.40 and 3.95 m. The loess is characterized by high (20.46 to 33.65 %) carbonate content, dominated by dolomite (61-72 %). The CaO/MgO and $CaO+K_2O+Na_2O/Al_2O_3$ ratios are high (2.61 and 1.83, respectively), while the K_2O/Na_2O ratio is low (1.31).

Between 2.15 and 2.65 m, the loess unit contains the 1st humic loess horizon (h_1), resulting from weak weathering processes.

CONCLUSIONS

On the base of their mineralogical and chemical composition, determined by paleoclimatic conditions, it is possible to make distinction between loess and paleosol types that suffered different degree of weathering and pedogenesis.

As weathering and pedogenesis intensify, the grain size distribution significantly shifts towards the finer fractions at the expense of the silt fraction. At the same time the carbonate content decreases; it is high in weakly weathered loess, but has been nearly entirely dissolved from well-developed paleosols. Along with the decrease in carbonate content, the originally low calcite/dolomite ratio (1:2) of the loess significantly changes and increases to 2:1 to 3:1 in paleosols, the overall carbonate content of which being very low.

Due to weathering and pedogenesis, the CaO, MgO, and Sr content of the sediments decreases, while the amount of SiO_2, TiO_2, Al_2O_3, Fe_2O_3, MnO, Na_2O, K_2O, P_2O_5, and Li, Cr, Co, Ni, Cu, Zn, Rb, Pb, and Ba increases. When weathering intensifies, the CaO/MgO and $CaO+K_2O+Na_2O/Al_2O_3$ ratios fall, and the K_2O/Na_2O ratio keeps growing. On the base of geochemical properties, groups of different origin can be established.

The *weakly weathered loess* formed under cold and arid climate. This is the group the least affected by weathering. The *weathered loess* was deposited under milder and more humid conditions, thus weathering did influence its formation. More intense weathering, however, led to the formation of *strongly weathered loess*, which can be interpreted as humic loess or embryonary soil as well. In these cases, however, pedogenesis was not strong enough to develop real soil horizon. The strongly weathered loess displays intermediate geochemical and developmental character between loess and paleosol. The Mende Upper and Basaharc Double soil complexes were formed by strong pedogenesis under mild and humid climate. The Basaharc Lower paleosol witnesses the most intense pedogenesis and weathering, and is associated with even warmer and more humid paleoclimate than the Mende Upper and Basaharc Double soil complexes.

Geochemical investigation of loess-paleosol series renders reconstruction of paleoclimatic trends possible. The loess underlying the Basaharc Lower paleosol represents the weakly weathered loess group. The cold period, favourable for loess accumulation, was interrupted by a warm, humid period, resulting in the formation of the Basaharc Lower soil horizon. The overlying weathered loess was deposited during a period characterized by cooling down. Geochemical data from the two chernozem-like forest steppe soil horizons of the following Basaharc Double soil complex argue for the same degree of pedogenesis. The weathered loess interlayered between the Basaharc Double I and Basaharc Double II soil horizons indicates that the cooling down between the two mild and humid periods forming the soils was not significant. The soil complex is overlain by strongly weathered loess, indicating graduate cooling in the profile. When the climate became cold and dry again, weakly weathered loess accumulated. During the following mild and humid period, two chernozem-like forest steppe soil horizons formed (Mende Upper soil complex). The upper horizon of the complex (Mende Upper I) suffered more intense weathering than the lower one (Mende Upper II). Again, the paleosol complex is overlain by strongly weathered loess, formed under cooler, still mild climate. The overlying weakly weathered loess hallmarks the last cold and arid period, which was interrupted by two milder intervals, as indicated by two humic loess horizons (h_1 and h_2) (*Fig. 4.*).

ACKNOWLEDGEMENT

The author thanks Prof. Dr. GERMAN MÜLLER for the opportunity to carry out the geochemical analyses at the Institut für Sedimentforschung, Heidelberg. The study trip to Heidelberg was supported by Magyar Ösztöndíj Bizottság. Research in Hungary was financed by OTKA Project No. T 014 895.

REFERENCES

FÜCHTBAUER, H. (ed.) (1988): Sedimente und Sedimentgesteine. Schweitzerbart'sche Verlagsbuchhandlung, Stuttgart. 228-231.

GEREI, L., PÉCSI-DONÁTH, É., REMÉNYI, M., SCHWEITZER, F. AND SZEBÉNYI, E. (1985): Mineralogical observations on the Paks-Dunakömlőd loess plateau (profiles sampled in 1978,1979). In: PÉCSI, M. (ed.): Loess and the Quaternary 83-91., Akadémiai, Budapest.

GONG, Z., CHEN, H., WANG, Z., CAI, F. AND LUO, G. (1987): The epigenetic geochemical types of loess in China. In : LIU, T. (ed.): Aspects of loess research. 328-340., China Ocean Press, Beijing.

HADRICH, F. (1975): Zur Methodik der Lössdifferenzierung auf der Grundlage der Carbonatverteilung. Eiszeitalter und Gegenwart, **26**, 95-117.

HEINRICHS, H.-HERRMANN, A. G. (1990): Praktikum der analytischen Geochemie. 669 p., Springer, Berlin.

HUM, L. (......): Paleoenvironmental changes and geochemistry of loesses and paleosols in Southeastern Transdanubia (Hungary). Z. Geomorph. N. F., Suppl.-Bd. **110**, pp. 69-83., Berlin-Stuttgart

HUM, L.-FÉNYES, J. (1995): The geochemical characteristics of loesses and paleosols in the South-Eastern Transdanube (Hungary). Acta Mineralogica-Petrographica, Szeged, XXXVI. 89-100.

LAUTRIDOU, J. P., SOMME, J. and JAMAGNE, M. (1984): Sedimentological, mineralogical and geochemical characteristics of the loess of North-West France. In: PÉCSI, M. (ed.): Lithology and stratigraphy of loess and paleosols. 121-132., Geogr. Research Institute, Budapest.

LIU, T.-WEN, Q. (1995): Discussion on paleoenvironment information by spectrum-geochemistry of loess in Weinan profile in the South Shanxi province. Scientia Geologica Sinica, Supplementary Issue (1). 63-71., China

PETROV, A. G., KRIGER, N. I., GOUNESHIAN, O. G., KOZHEVNIKOV, A. D., MIRONUK, S. G. AND ZIMINA G. A. (1984): Geochemical loess history. In : PÉCSI, M. (ed.):Lithology and stratigraphy of loess and paleosols. 133-138. Geogr. Research Institute, Budapest.

PÉCSI, M., (1975): A magyarországi löszszelvények litosztratigráfiai tagolása. Földr. Közl.**23/3-4**., 217-230.

PÉCSI, M., (1985): Chronostratigraphy of Hungarian loesses and the underlying subaerial formation. In: PÉCSI, M. (ed.): Loess and the Quaternary., 33-49., Akadémiai, Budapest.

PÉCSI, M. (1993): Negyedkor és löszkutatás. Akadémiai, Budapest. 375.

PÉCSI-DONÁTH, É.(1985): On the mineralogical and petrological properties of the younger loess in Hungary. In : PÉCSI, M. (ed.): Loess and Quaternary., 93-104., Akadémiai, Budapest.

PYE, K. (1983): Grain surface textures and carbonate content of late pleistocene loess from West Germany and Poland. Journal of Sedimentary Petrology, **53/3,** 973-980.

PÉCSI, M.-SCHWEITZER, F. (eds.) (1995): Concept of loess, loess-paleosol stratigraphy. Geographical Research Institute, Budapest. 94.

ROCK-COLOR CHART (1980), Prepared by the ROCK-COLOR CHART COMMITTEE, Huyskes-Enschede, Netherlands

SCHNETGER, B. (1992): Chemical composition of loess from a local and worldwide view. N. Jb. Miner. Mh., **1992,** H. 1, 29-47.

SZILÁRD, J. (1983): Dunántúli és Duna-Tisza közi löszfeltárások új szempontú litológiai értékelése és tipizálása. Földrajzi Értesítő, **32/1,** 109-166.

TAYLOR, S. R., MCLENNAN, S. M., MCCULLOCH, M. T. (1983): Geochemistry of loess, continental crustal composition and crustal model ages. Geochimica et Cosmochimica Acta, **47,** 1897-1905.

TENNANT, C. B., BERGER, R. W. (1957): X-ray determination of dolomite-calcite ratio of a carbonate rock. American Mineralogist , **42,** 23-29.

WEN, Q., DIAO, G. AND FUQING, S. (1985): Geochemical characteristics of loess in Luochuan section, Shaanxi province. In : PÉCSI, M. (ed.): Loess and the Quaternary 65-77., Akadémiai, Budapest.

WEN, Q., DIAO, G., JIA, R. AND ZHOU, H. (1995): Geochemical indicators of paleoclimatic changes in loess section. Scientia Geologica Sinica, Supplementary Issue (1). 43-51., China

Manuscript received 12 June, 1998.

paleoclimate than the Mende Upper and Basaharc Double soil complexes.

Geochemical investigation of loess-paleosol series renders reconstruction of paleoclimatic trends possible. The [illegible] loess [illegible] represents the weakly weathered loess group [illegible] loess accumulation, was interrupted by a warm, humid period resulting in the formation of the Basaharc Lower soil horizon. The overlying weakly weathered loess was deposited during a period characterized by cooling [illegible] same degree of pedogenesis. The [illegible] loess interlayered between the Basaharc Double I and Basaharc Double II soil horizons indicates that the cooling period between the two mild and humid periods [illegible]. The soil complex is overlain by strongly weathered loess, indicating graduate cooling [illegible]. [illegible] following mild and humid period, two chernozem-like forest steppe soil horizons formed (Mende Upper soil complex). The upper horizon of the complex (Mende Upper I) suffered more intense weathering than the lower one (Mende Upper II). [illegible] complex is overlain by strongly weathered loess, formed [illegible] climate. The overlying weakly weathered loess marks the last cold and arid period, which was interrupted by two milder phases indicated by two humic loess horizons (h_1 and h_2) (*Fig. 4.*).

The author thanks Prof. Dr. GERMAN MÜLLER for the opportunity to carry out the geochemical analyses at the Institut für Sedimentforschung, Heidelberg. The study trip to Heidelberg was supported by Magyar Ösztöndíj Bizottság. Research in Hungary was financed by OTKA Project No. T 014 895.

REFERENCES

FÜCHTBAUER, H. (ed.) (1988): Sedimente und Sedimentgesteine. Schweitzerbart'sche Verlagsbuchhandlung, Stuttgart 228-233.

GEREI, L., PÉCSINÉ DONÁTH, É., REMÉNYI, M., SCHWEITZER, F. AND SZEBÉNYI, E. (1985): Mineralogical observations on the Paks-Dunakömlőd loess plateau (profiles sampled in 1978,1979). In: PÉCSI, M. (ed.): Loess and the Quaternary, 83-91., Akadémiai, Budapest.

GONG, Z., CHEN, H., WANG, Z., CAI, F. AND LUO, G. (1987): The epigenetic geochemical types of loess in China. In: LIU, T. (ed.): Aspects of loess research. 328-340., China Ocean Press, Beijing.

HÄDRICH, F. (1975): Zur Methodik der Lössdifferenzierung auf der Grundlage der Carbonatverteilung. Eiszeitalter und Gegenwart, 26, 95-117.

HEINRICHS, H. HERRMANN, A. G. (1990): Praktikum der analytischen Geochemie. 669 p., Springer, Berlin.

HUM, L. ([illegible]): Paleoenvironmental changes and geochemistry of loesses and paleosols in Southeastern Transdanubia (Hungary). Z. Geomorph. N. F., Suppl.-Bd. 110, pp. 69-83., Berlin-Stuttgart.

HUM, L.-FÉNYES, J. (1995): The geochemical characteristics of loesses and paleosols in the South-Eastern Transdanubia (Hungary). Acta Mineralogica-Petrographica, Szeged, XXXVI. 89-100.

LAUTRIDOU, J. P., SOMMÉ, J. AND JAMAGNE, M. (1984): Sedimentological, mineralogical and geochemical characteristics of the loess of North-West France. In: PÉCSI, M. (ed.): Lithology and stratigraphy of loess and paleosols. 121-132., Geogr. Research Institute, Budapest.

Acta Mineralogica-Petrographica, Szeged, XXXIX, 151–167, 1998

MAIN AND TRACE ELEMENTS IN GROUNDWATER FROM THE QUATERNARY SEDIMENTS IN THE SOUTHERN GREAT PLAIN, HUNGARY

ERIKA HRABOVSZKI and IRÉN VARSÁNYI

Department of Mineralogy, Geochemistry and Petrology,
Attila József University, Szeged, Hungary

ABSTRACT

Chemical composition of groundwater samples from the southern part of the Great Hungarian Plain was determined. Cluster analysis based on major elements, and based on minor and trace elements resulted in similar separation of the study area. The units correspond to three hydrogeological regions: the River Körös basin, the River Maros alluvial fan and the River Danube deposits. Processes controlling both major and trace element concentrations are dissolution of carbonate minerals, ion exchange, oxidation-reduction, albite weathering and formation of secondary minerals. In the Körös basin water movements is restricted. In the River Maros alluvial fan the direction of water flow is from south-southeast to north-northwest, and in the River Danube deposits it is from west to east.

INTRODUCTION

In the Quaternary sediments of the Great Hungarian Plain there are two chemically distinct types of groundwater: Ca-Mg-HCO_3 type and Na-HCO_3 type. In the Ca-Mg-HCO_3 type waters the concentration of total dissolved solids is low while in the Na-HCO_3 type waters it is much higher. The processes controlling major and trace element concentrations in groundwater are dissolution and precipitation of carbonate minerals, feldspar weathering (PACES 1973, CHOU and WOLLAST 1984, BERNER 1981, MURPHY and HELGESON 1987), redox reactions and ion exchange (CHAPELLE and KNOBEL 1983, APPELO et al. 1989).

Carbonate minerals are much more soluble in waters than silicates. Dynamic interfaces between aqueous solutions and carbonate minerals lead to reversible dissolution-precipitation reactions. Thermodynamic control of equilibrium can be applied to carbonates if they react rapidly on the time scale of a hydrological system. According to HOCHELLA (1990), during dissolution the near surface of calcite remains ordered. Sr, Ba and Mn are often built in carbonate minerals. Magnesium is partially replaces by Mn in dolomite, while Sr and Ba can substitute for Ca in the structure of calcite. As precipitation of dolomite from most natural waters does not control Mg concentration in fresh water (HEM 1985), equilibrium can be reached only from undersaturation. According to STUMM and MORGAN (1981) calcite has a tendency to accommodate Mg^{2+} in its structure to form magnesian calcite. So precipitation of Ca and Mg as magnesian calcite may be a more likely process than dolomite precipitation.

The surface of feldspar is covered by leached layer and secondary minerals (DAVIS and KENT 1990). The feldspar dissolution is an irreversible process. CO_2 plays an important role both in carbonate and silicate dissolution reactions. The solubility of albite depends on the partial pressure of CO_2. If albite dissolves under the influence of CO_2 the resulting solution is characterized by HCO_3^-, Na and H_4SiO_4 (STUMM AND MORGAN 1981). Na concentration derived from the hydrolysis of albite increases with the relative surface area of albite (HELGESON 1971). The first process to occur when albite interacts with water is a rapid exchange of H^+ for Na^+ (HELLMANN et al. 1989, HELGESON et al. 1984, ALTHAUS and TIRTADINATA 1989). This initial reaction of feldspar is accompanied by increasing pH (BUSENBERG and CLEMENCY 1976), and it proceeds even at neutral and slightly basic pH conditions (CASEY and BUNKER 1990). However feldspar weathering is an irreversible process (HELGESON 1971) the composition of the resulting solution is controlled by the equilibrium among highly disordered reaction products and the aqueous phase. In silicate minerals Mn replaces Fe and Mg, Sr substitutes for Ca and Ba, and K is often replaced by Ba. A possible diadochy can occur between Li and Al, Fe(II) and especially Mg (WEDEPOHL et al. 1964, FAURE et al. 1967). In the groundwater the concentration of these metal ions are influenced by ion exchange processes on the cation-specific surface sites of calcite. Metal ion sorption depends on aqueous Ca concentration (DAVIS et al. 1987, COMANS and MIDDELBURG 1987, WERSIN et al. 1989, ZACHARA et al. 1991). The concentration of Li is primary controlled by incorporation into clay minerals (HEIER and ADAMS 1964, BILLINGS et al. 1964). The coprecipitation of Li with calcium carbonate can play an important role in the distribution of Li in groundwater (OKUMURA and KITANI 1985). Wheathering of silicate minerals can be considered as a main source of Si and Al. The solubility of silicate minerals is pH dependent. Aluminium is insoluble at neutral pH, it precipitates as gibbsit, or enters the clay minerals forming in the aqueous system (APPELO 1993).

Manganese and iron oxyhydroxides of sediments have an importance in the distribution and mobility of trace elements. Trace elements associated with Mn and Fe oxyhydroxides are released during reductive dissolution of the oxides, while the oxidation of metal oxyhydroxides can remove trace elements from solution by adsorption or coprecipitation (BALLISTRIERI and MURRAY 1994). In the trace metal adsorption significant role is played also by calcite, clay minerals and organic matter (TESSIER et al. 1980, LION et al. 1982, ZACHARA et al. 1991).Humic substances influence the complexation of trace elements with metal oxides, especially at low pH values (DAVIS and LECKIE 1978, LAXEN 1985).

The aim of this work is to separate the aquifer systems in the Pleistocene sediments of the southern part of the Great Hungarian Plain on the basis of the major and trace chemical components in groundwater, and to establish the processes controlling the chemical features of groundwater in the different aquifers.

LOCATION AND GEOLOGY

The study area is located in the southern part of the Great Hungarian Plain (*Fig.1.*) which is the biggest sedimentary basin in Europe that is filled with Neogene and Quaternary sediments of great thickness. The geological evolution of the Pannonian Basin started in the Miocene with the uplift of the Carpathian mountains and the subsidence of the enclosed area (RÓNAI 1985). Tectonic activity continued at different rates throughout the area; therefore, the thicknesses of the sediments are variable. The deepest part of the study area is the Makó-Hódmezővásárhely depression where the thickness of the sediments is more than 5000 m, of which 2000-3000 m are marine sediments, and 1000-2000 m are lake sediments which were deposited after the outlet of the basin to the Mediterranean sea had closed. The hydrogeological features are controlled by structures active in the Tertiary and Quaternary periods. During the Pliocene 2000-3000 m thick marine sediments:

conglomerate, sandstone, marl and clay, then 1000-2000 m thick lake sediments: sand, silt and clay were deposited. Going upwards the sedimentary sequence grades into variegated clay which represents the uppermost part of the Pliocene sedimentary series.

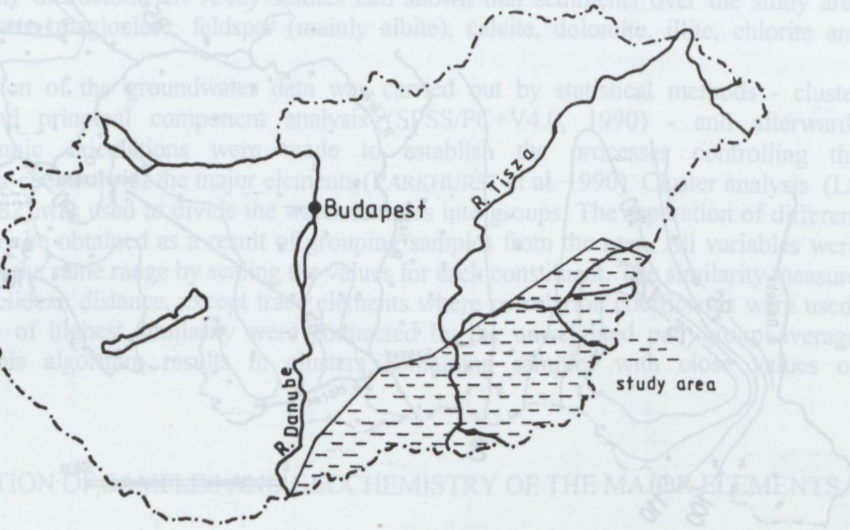

Fig. 1. Location of the study area

Towards the end of Pliocene, the basin was uplifted. Fluvial sedimentation started in the inner part of the basin about 2.4 million years ago, at the beginning of the Quaternary. Local scale tectonic events together with climatic differences determined the cyclic fluvial sedimentation during the Pleistocene. In the Early Pleistocene, 300-450 m of fluvial sediments were deposited in the deepest local sub-basins. The areas between local depressions sank as much as several tens of meters. These sediments generally consist of gravel, sand, silt and clay layers, 20-50 m in thickness. The number and the thickness of sand layers are greater than in the Middle and Upper Pleistocene. Cyclicity in grain size composition of the layers can be correlated with vertical Quaternary tectonic movements. The vertical movements produced a deep local depression in the northeastern part of the study area. This depression was filled up with fine grained material by the Rivers Körös and Berettyó: fine sand, silt and clay. These Quaternary strata are 500-550 m thick and form the lowest yielding artesian aquifer within the Southern Great Plain. In the western part of the area the River Danube deposited material during the Quaternary period. The Pleistocene formation consists of 50-70% highly permeable sand with silt and clay (ERDÉLYI 1976).).

The potentiometric contours of the Pleistocene aquifers to the depth of between 200-400 m determined by ERDÉLYI (1979) on the basis of water level elevation in drinking water wells before withdrawal, indicate that in the Pleistocene layers groundwater generally flows from west to east in the River Danube deposit, in the south-southwestern part of the study area, however no lateral water flow is supposed in the Körös basin (*Fig.2.*). The multi-layer aquifer system of the Great Hungarian Plain consists of two flow-regions. One of them is an intermediate flow-region in the upper part of the basin composed predominantly of loose clastic Quaternary sequences. The other one is in the deeper, thermal aquifer system.

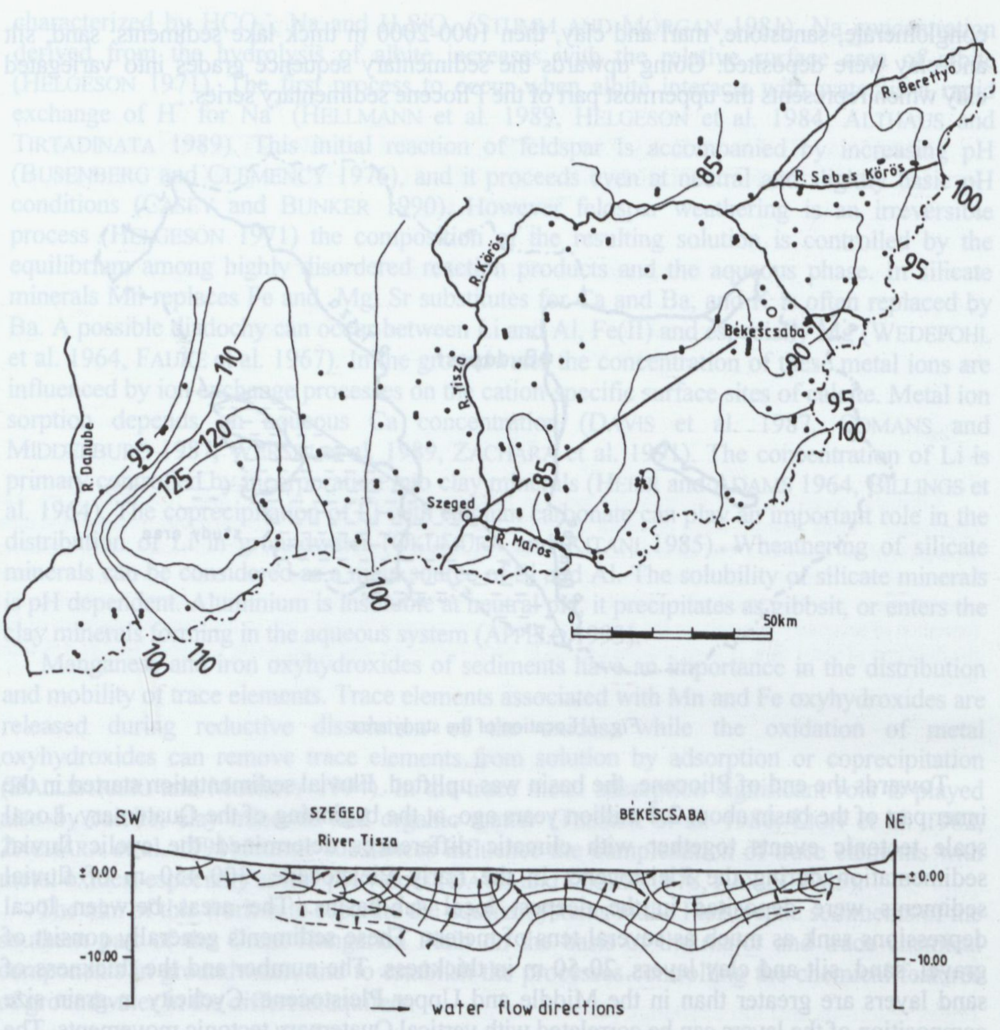

Fig. 2. The piezometric contours and water flow directions by ERDÉLYI (1976) and the location of the studied wells.

METHODS

In situ measurements and laboratory major, minor and trace element analyses were used to establish the geochemical evolution of groundwater in the studied aquifers. Groundwater samples were obtained from municipal water supplies. Field determinations of pH and temperature were made. Groundwater samples from water wells of different depths (40-600 m) were collected, cooled and analyzed within 24 hours. Conductivity, pH, hardness, alkalinity, Ca, Mg, Na, K, Fe, Mn, ammonium, chloride, and chemical oxygen demand (COD) were determined in 142 samples, and in most of them (109 samples) As, Zn, Ba, Sr, Li, Si, Al were also analysed. The analysis were performed at the Hungarian Geological Survey, Budapest, at the Horticulture University, Budapest and at the Institute of

Public Health, Szeged. Procedures for making determinations are summarized as follows: hardness, alkalinity, COD and chloride by titration; ammonium by spectrophotometry; Na, K, Ca, Mg, Fe, Mn, Zn, Ba, Sr, Li, Si, Al, and phosphate by ICP-AAS, and As by AAS-hydrid method. 22 core samples of 61-468 m depth were subjected to XRD analysis using a DRON-UM 1 X-ray diffractometer. X-ray studies had shown that sediments over the study area contain quartz, plagioclase, feldspar (mainly albite), calcite, dolomite, illite, chlorite and muscovite.

Evaluation of the groundwater data was carried out by statistical methods - cluster analysis and principal component analysis (SPSS/PC+V4.0, 1990) - and afterwards thermodynamic calculations were made to establish the processes controlling the groundwater chemistry of the major elements (PARKHURST et al. 1990). Cluster analysis (LE MAITRE 1982) was used to divide the water samples into groups. The separation of different aquifers may be obtained as a result of grouping samples from the area. All variables were brought into the same range by scaling the values for each constituent. The similarity measure was the Euclidean distance, except trace elements where correlarion coefficients were used. The groups of highest similarity were connected by the unweighted pair group average method. This algorithm results in clusters containing samples with close values of parameters.

SEPARATION OF SAMPLES AND GEOCHEMISTRY OF THE MAJOR ELEMENTS

The present study discusses the main and trace element distribution in water samples collected from the Pleistocene layers, in the southeastern part of the Great Hungarian Plain. Location of wells, the piezometric contours and the direction of groundwater flow path are given in *Fig.2.* The major cations are Ca, Mg and Na, the major anions are dominated by HCO_3. On the basis of the frequency distributions of the components it was established that groundwater quality is not uniform throughout the study area. Samples represent more than one population. This possibly means that different processes play a role in determining the chemical composition of groundwater from different depths or locations.

Separation of samples based on the distribution of the main mono- and divalent cations was performed. Flow systems were characterized by cation exchange on clay minerals. Ion exchange has fundamental importance in water-rock interactions. Along the flow path the distribution of the dissolved components may follow a chromatographic pattern because of the differences in retardation for the various cations. Along the flow path the concentration of Na increases while the concentration of divalent cations - Ca and Mg - decreases. There is a linear trend with a slope of -2 between the molar concentrations of mono- and divalent cations (VARSÁNYI and Ó. KOVÁCS, 1997). The molar concentration of Na against Ca + Mg is shown in *Fig.3.* Data appear to be scattered around two lines. It suggests that at least two ion exchange systems with different Na concentrations exist over the study area. To draw lines between water samples belonging to the different flow systems in which ion exchange takes place cluster analysis was performed with three variables. Two of them are X and Y coordinates of the location of water wells. The third variable is the distance between each point in *Fig.3.* and a line with a slope of -2. These distances are similar for the samples belonging to the same water flow system but they differ from those of the other water flow system with different ion concentration. However under natural conditions the effect of ion exchange prevails only statistically because factors other than ion exchange modify the concentration of mono- and divalent cations. These distances appear suitable variables to separate water flow or aquifer systems (VARSÁNYI and Ó. KOVÁCS, 1994). Cluster analysis resulted in three main groups which are shown in *Fig.4./a.* By their location, the groups correspond to the geological regions established by RÓNAI (1985) i.e. Group A to the River Körös basin (black diamond), Group B to the alluvial fan of the River Maros (black square) and Group C to the River Danube deposits (open symbols) located in the region between the Rivers Danube and Tisza, and the southern section of the River Tisza valley. The average water quality in the three groups is listed in Table 1.

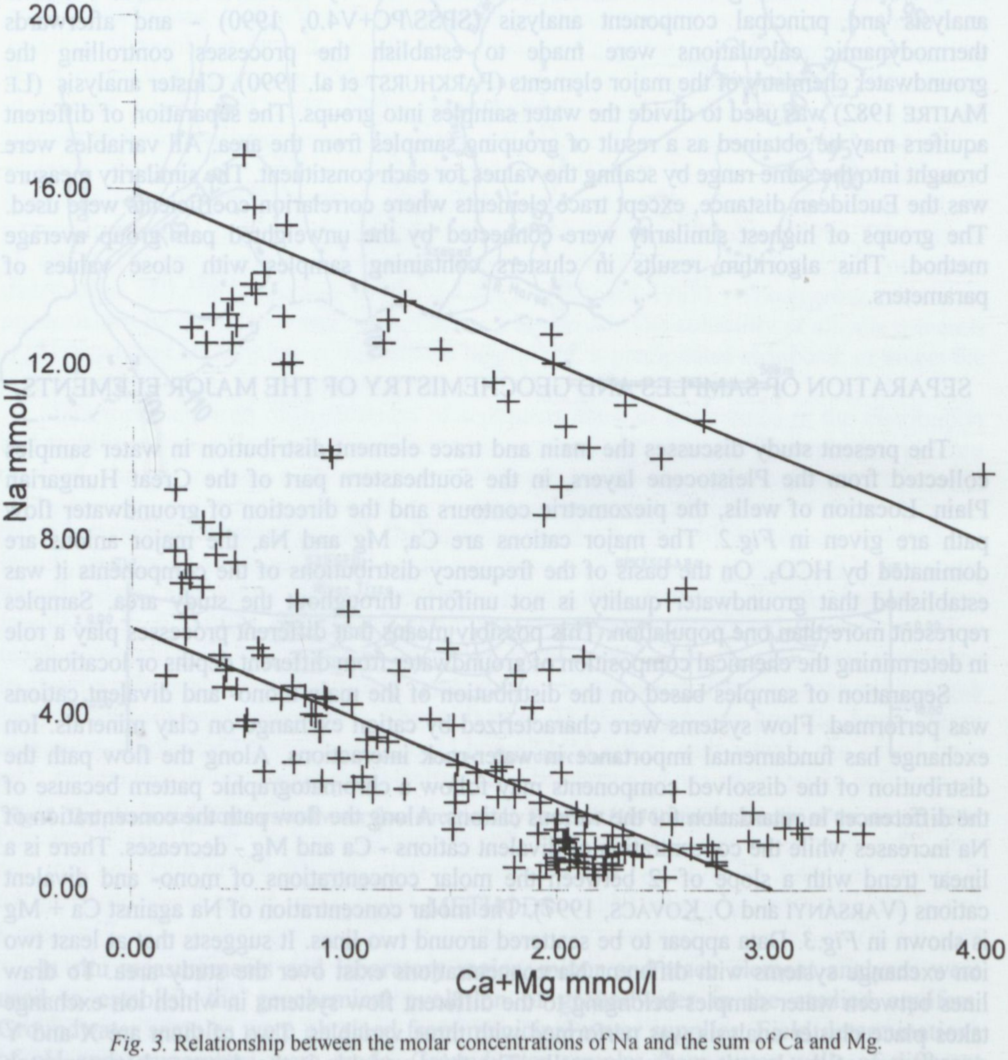

Fig. 3. Relationship between the molar concentrations of Na and the sum of Ca and Mg.

In order to understand what reactions control the major element composition of groundwater in the three geological regions, PHREEQE (PARKHURST et al. 1990) was used to perform the simulation (VARSÁNYI AND Ó. KOVÁCS, 1994). On the basis of these simulations it has been established that originally in each group the system is open for CO_2. In these systems calcite, dolomite and albite dissolve. In the River Körös basin the CO_2

TABLE 1

Mean values and standard deviations in the groups separated on the basis of major element.

Water type		Group A, River Körös			Group B, River Maros			Group C, River Danube		
Component	Unit	Mean	s.d.	No. of sample	Mean	s.d.	No of sample	Mean	s.d.	No. of sample
Electric conduct.	uS/cm	1264	202	34	550	158	31	484	93	77
pH		7,88	0,21	34	8,07	0,33	31	7,71	0,27	77
Alkalinity	mequ/l	14,4	1,9	34	6	1,8	31	6,1	1,2	77
Ca	mmol/l	0,8	0,6	34	0,9	0,5	31	1,1	0,5	77
Mg	mmol/l	0,5	0,3	34	0,4	0,2	31	0,7	0,3	77
Na	mmol/l	11,7	2,4	34	3,6	1,5	31	2,6	2,4	77
K	mmol/l	0,05	0,03	34	0,03	0,04	31	0,03	0,01	77
Ammonium	mmol/l	0,16	0,06	34	0,17	0,12	31	0,07	0,04	77
Cl	mmol/l	0,63	0,23	34	0,61	0,13	31	0,13	0,06	77
COD	mg/l	9,9	6,9	34	5,2	3,6	31	2,1	1,5	77
SI calcite		0,64	0,26	34	0,53	0,18	31	0,26	0,2	77
SIdolomite		1,12	0,48	34	0,64	0,38	31	0,34	0,43	77

TABLE 2

Mean values and standard deviations in the groups separated on the basis of minor and trace elements .

Water type		Group 1.			Group 2.			Group 3.		
Component	Unit	Mean	s.d.	No. of sample	Mean	s.d.	No of sample	Mean	s.d.	No. of sample
As	mmol/l	0,00009	0,00011	18	0,00025	0,00014	19	0,00032	0,00023	27
Fe	mmol/l	0,00492	0,00212	18	0,00316	0,00187	19	0,00265	0,00222	27
Zn	mmol/l	0,00016	0,00013	18	0,00021	0,00022	19	0,00009	0,00009	27
Mn	mmol/l	0,00079	0,00017	18	0,00085	0,00070	19	0,00063	0,00075	27
Ba	mmol/l	0,00107	0,00026	18	0,00110	0,00023	19	0,00053	0,00027	27
Li	mmol/l	0,00050	0,00025	18	0,00078	0,00037	19	0,00100	0,00055	27
Sr	mmol/l	0,00336	0,00053	18	0,00514	0,00054	19	0,00178	0,00114	27
Si	mmol/l	0,46006	0,03778	18	0,38163	0,02996	19	0,31964	0,03347	27
Al	mmol/l	0,00000	0,00000	18	0,00000	0,00000	19	0,00000	0,00000	27
Depth	m	318	08.5	18	324	115	19	335,62	129,81	27

Water type		Group 4.			Group 5.			Group 6.		
Component	Unit	Mean	s.d.	No. of sample	Mean	s.d.	No of sample	Mean	s.d.	No. of sample
As	mmol/l	0,00143	0,00066	13	0,00113	0,00034	22	0,00081	0,00040	10
Fe	mmol/l	0,01780	0,00745	13	0,00280	0,00186	22	0,00804	0,00550	10
Zn	mmol/l	0,00026	0,00026	13	0,00013	0,00011	22	0,00154	0,00203	10
Mn	mmol/l	0,00231	0,00101	13	0,00083	0,00066	22	0,00110	0,00079	10
Ba	mmol/l	0,00107	0,00024	13	0,00076	0,00031	22	0,00097	0,00046	10
Li	mmol/l	0,00112	0,00097	13	0,00185	0,00158	22	0,00267	0,00196	10
Sr	mmol/l	0,00431	0,00166	13	0,00203	0,00097	22	0,00223	0,00145	10
Si	mmol/l	0,38131	0,04614	13	0,36800	0,05413	22	0,38180	0,08821	10
Al	mmol/l	0,00000	0,00000	13	0,00000	0,00000	22	0,00258	0,00200	10
Depth	m	153,15	86,93	13	363,91	204,72	22	453,65	410,29	10

pressure remained fairly high (log pCO_2=-1,8) and due to this high CO_2 pressure a large quantity of albite dissolved. In the other two groups the CO_2 pressures were lower (log pCO_2=-2.0 and -2.3 respectively) and lower Na contents were produced. Due to the albite dissolution in the open system, water becomes oversaturated for both calcite and dolomite. The degrees of oversaturation are different in the three groups and they correspond to the Na contents of water. The equilibrium between water, calcite and dolomite seems to be reached only from undersaturation and not from oversaturation. In the River Körös basin and in the alluvial fan of the River Maros the CO_2 pressure decreases from the shallower to the deeper layers, the system becomes closed and albite dissolution proceeds. pH increases and there is not enough H^+ available for further albite dissolution.

Over the region between the Rivers Danube and Tisza and in the southern section of the River Tisza valley (in the River Danube deposits) the system was initially open. Less albite dissolved in relation to the River Körös basin. The reason for the smaller Na concentration in this group may be the lower partial pressure of CO_2, the shorter exposure of feldspar to the water in the open system and the lower ratio of the reactant mineral surface area to the volume of the aqueous phase. It was supposed that along a west-east flow path ion exchange is the main process, albite dissolution under the closed system conditions does not play an important role in controlling water quality. Within the study aquifer Na is exchanged to Ca and Mg on the clay minerals and equilibrium with calcite and dolomite is reached.

The relationship between alkalinity, calcium, magnesium and sodium concentrations suggests three sub-types of water in the River Danube deposits. Along the W-E flow path significant changes in the concentrations of the main cations occur which may be summarized as follows:

1. The samples with the highest water hardness (calcium plus magnesium concentrations are up to 2.75 mmol/l) are situated in the western part of the study area (open circles in *Fig.4./a*). The variation in alkalinity is related mainly to calcite and dolomite dissolution. This is the recharge area (ERDÉLYI, 1979) and the beginning of the groundwater flow system. Dissolved sodium content is supposed to originate from irreversible feldspar weathering. Dissolution of carbonate minerals is an equilibrium process which is controlled by CO_2 partial pressure while sodium concentration depends on the reaction rate and time.

2. From the chemical point of view this is a transitional zone between the beginning and the end of the flow path (open diamonds in *Fig.4./a*). The sum of calcium and magnesium concentrations changes between 0.5 and 2.5 mmol/l, and the sodium concentration between 5.5 and 0.3 mmol/l. The mirror image of mono and bivalent cations (*Fig.3.*) and the almost constant alkalinity show that ion exchange controls water chemistry along this part of the flow path.

3. The water samples having the lowest calcium and magnesium and the highest sodium concentrations are situated in the eastern part of the River Danube deposits, around Hódmezővásárhely (open squares in *Fig.4./a*). Ca and Mg concentrations are constant, Na concentration is increasing with alkalinity. In this group of samples the mean alkalinity is higher (7.7 meq/l) than it is in the samples from the recharge area (5.9 meq/l). The increase in alkalinity demands an additional carbon source. In spite of the availability of organic material in the sediments (TOC varies from 0.02% to 0.5%, mean value is 0.1%), the in situ CO_2 production through oxidation is limited by the availability of oxidizing agents. However, an anaerobic, microbially mediated disproportioning of organic matter may result in CO_2 (BRONS et al., 1991). Both the transformation of organic matter and the mixing of recharge water with older formation water may be the processes

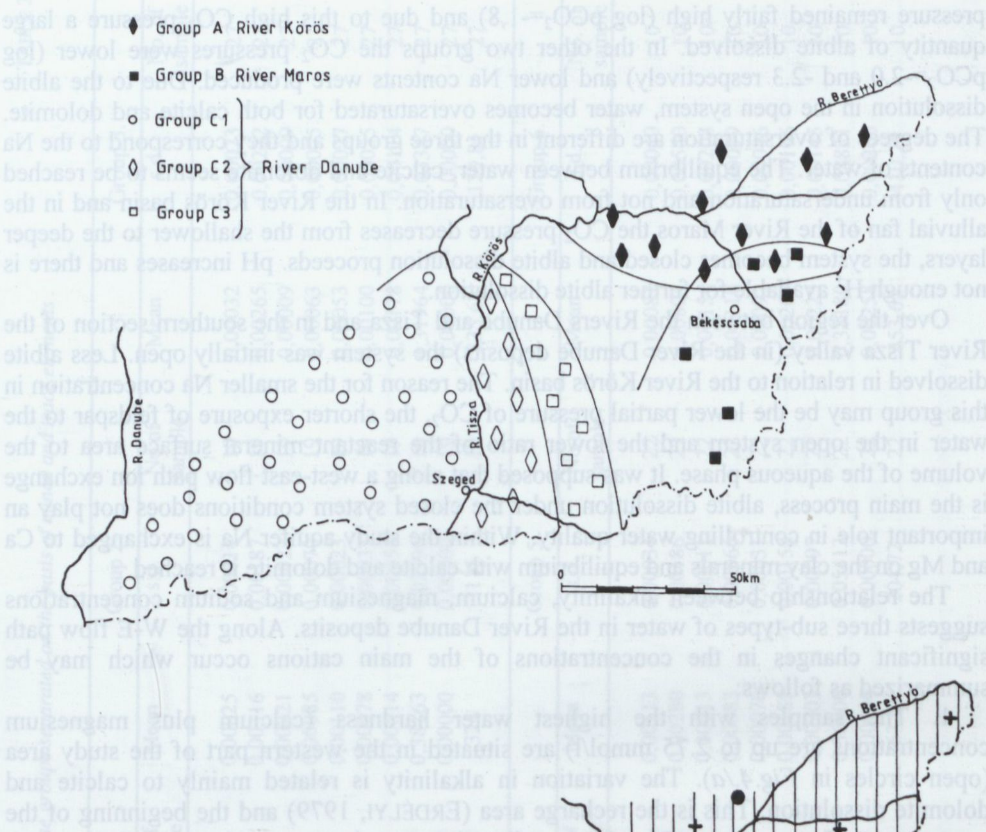

Fig. 4. Location of the groundwaters characterized by different water quality
a) separaion on the basis of major elements b) separaion on the basis of minor and trace elements

which resulted in the increase in alkalinity. This sodium-bicarbonate type water is located in the discharge area of the water flow system (ERDÉLYI, 1979).

Changes of sodium concentration from west to east and from south to north are given in *Fig.5.* and *Fig.6.* In the River Körös basin neither piezometric contours nor water chemistry show infiltration. On the basis of the piezometric contours it is a discharge area. In the River Maros alluvial fan sodium concentration is increasing from south to north, and this increase corresponds to the water flow direction. In the River Danube deposits the increase in Na concentration indicate a west-east flow direction.

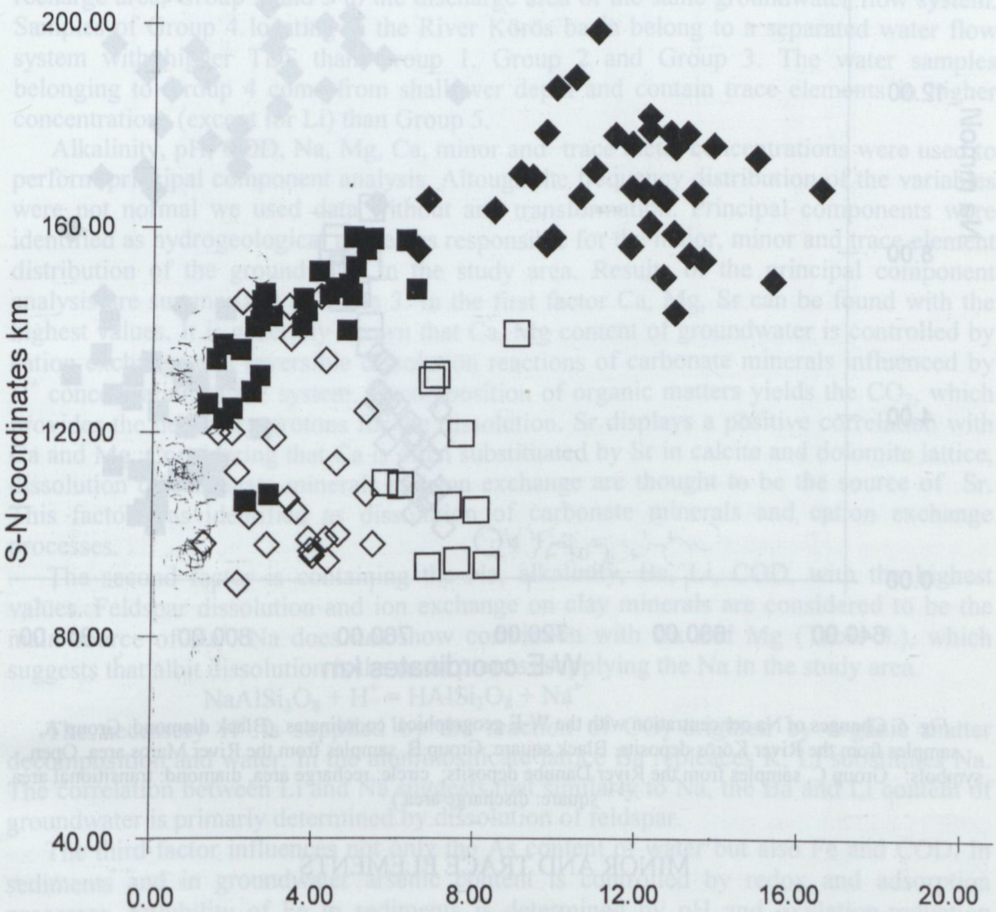

Fig. 5. Changes of Na concentration with the S-N geographical coordinates. (Black diamond: Group A, samples from the River Körös deposits. Black square: Group B, samples from the River Maros area. Open symbols: Group C, samples from the River Danube deposits; circle: recharge area, diamond: transitional area, square: discharge area.)

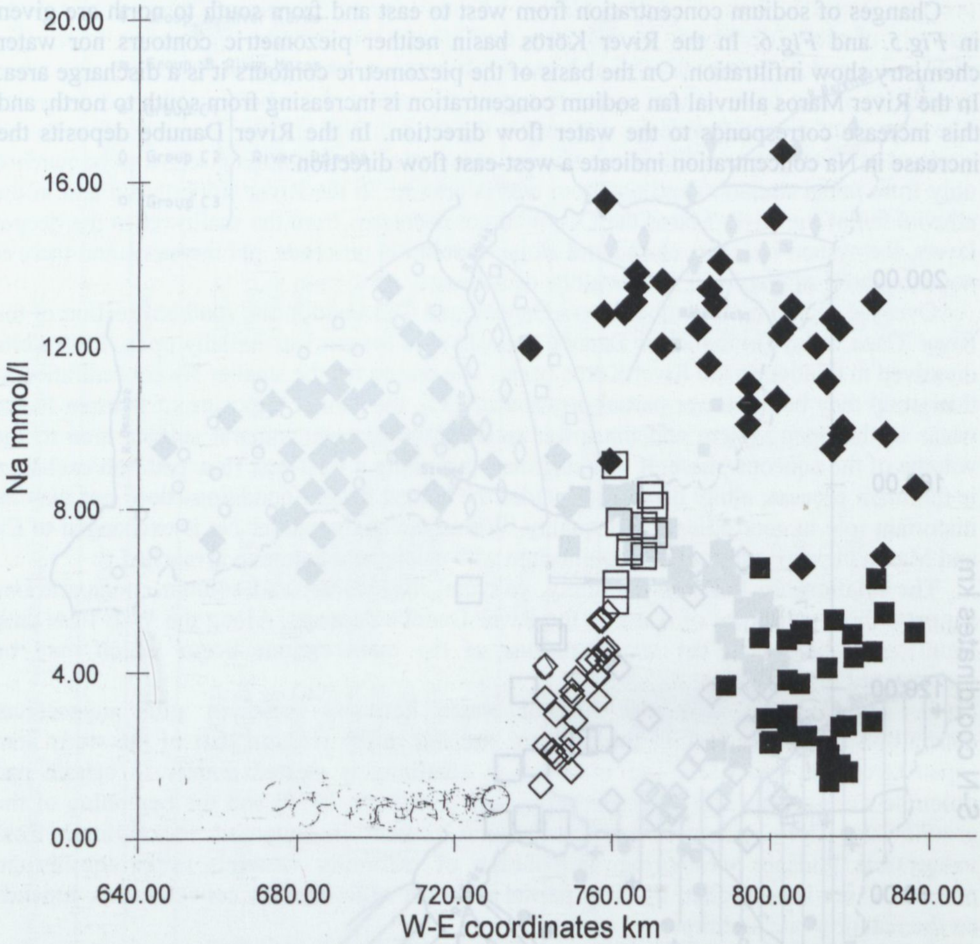

Fig. 6. Changes of Na concentration with the W-E geographical coordinates. (Black diamond: Group A, samples from the River Körös deposits. Black square: Group B, samples from the River Maros area. Open symbols: Group C, samples from the River Danube deposits; circle: recharge area, diamond: transitional area, square: discharge area.)

MINOR AND TRACE ELEMENTS

In 109 samples minor and trace element concentrations were determined, as well. Cluster analysis based on the concentrations of nine minor and trace elements resulted in six main groups which are shown in *Fig.4./b*. Mean values and standard deviations of the minor and trace elements in these groups are summarized in Table 2. Four of the six groups correspond to the geological regions: Group 1, Group 2 and Group 3 to the River Danube deposits, Group 4 to the River Körös Basin. Trace element analysis are not available from the River Maros alluvial fan. Location of Group 1, Group 2 and Group 3 in the River Danube deposits correspond to the location of the Ca-Mg bicarbonate, transitional and Na bicarbonate water type, i.e. the recharge and discharge areas. Group 5 and Group 6 are located in the River Körös basin and in the discharge area of the River Danube water flow system. Group 5 consists of samples with the highest arsenic content, and in the River Körös sediments it corresponds to the deepest samples from about 350 m depth. Group 6 consists of samples with the highest Al concentrations. Based on the similar distribution of groups separated by main and trace elements it is supposed that processes controlling the main and trace element contents are similar.

In the River Danube deposits, where the changes in the concentration of the major elements indicate a west-east water flow direction, from west to east the COD, Si and Fe desrease together with Ca and Mg, while Na, As and Li increase. Group 1 belongs to the recharge area, Group 2 and 3 to the discharge area of the same groundwater flow system. Samples of Group 4 locating in the River Körös basin belong to a separated water flow system with higher TDS than Group 1, Group 2 and Group 3. The water samples belonging to Group 4 come from shallower depth and contain trace elements in higher concentrations (except for Li) than Group 5.

Alkalinity, pH, COD, Na, Mg, Ca, minor and trace metal concentrations were used to perform principal component analysis. Altough the frequency distribution of the variables were not normal we used data without any transformation. Principal components were identified as hydrogeological processes responsible for the major, minor and trace element distribution of the groundwater in the study area. Results of the principal component analysis are summarized in Table 3. In the first factor Ca, Mg, Sr can be found with the highest values. It is generally known that Ca, Mg content of groundwater is controlled by cation exchange and reversible dissolution reactions of carbonate minerals influenced by H^+ concentration of the system. Decomposition of organic matters yields the CO_2, which provides the necessery protons for the dissolution. Sr displays a positive correlation with Ca and Mg. Considering that Ca is often substituated by Sr in calcite and dolomite lattice, dissolution of carbonate minerals and ion exchange are thought to be the source of Sr. This factor was identified as dissolution of carbonate minerals and cation exchange processes.

The second factor is containing the Na, alkalinity, Ba, Li, COD, with the highest values. Feldspar dissolution and ion exchange on clay minerals are considered to be the main source of Na^+. Na does not show correlation with Ca and Mg (Table 3.), which suggests that albit dissolution is the main process supplying the Na in the study area.

$$NaAlSi_3O_8 + H^+ = HAlSi_3O_8 + Na^+$$

The necessery H^+ is supplied by the reaction of CO_2 origined by organic matter decomposition and water. In the aluminosilicate lattice Ba repleaces K, Li substitutes Na. The correlation between Li and Na suggests that similarly to Na, the Ba and Li content of groundwater is primarly determined by dissolution of feldspar.

The third factor influences not only the As content of water but also Fe and COD. In sediments and in groundwater arsenic content is controlled by redox and adsorption processes. Solubility of Fe in sediments is determined by pH and oxidation-reduction (SAKATA 1985). Fe oxides can adsorb As on its surface (TAKAMATSU et al. 1985, NEWMAN et al. 1985). Oxidative degradation of organic matter is carried out with O_2, NO_3^-, MnO_2, Fe_2O_3 és SO_4^{2-} in consecutive steps (FROEHLICH et al. 1979). Quantity of the burried organic matters can be brought in connection with the velocity of sedimentation (WILSON 1985). At higher velocity of sedimentation the oxigen is comsumed by organic matters and NO_3^-, MnO_2, Fe_2O_3 és SO_4^{2-} become oxidising substances. Fe is reduced and ferrous iron goes into solution which results mobilisation of arsenic. According to this above, this factor was connected with oxidation and reduction.

TABLE 3

Results of the principal component analysis (λ is Eigenvalue).

factors	I.	II.	III.	IV.
Alkalinity	-0.333	0.731	0.308	-0.166
pH	-0.726	0.121	0.095	0.023
COD	-0.043	0.671	0.491	-0.003
Na	-0.418	0.760	-0.096	-0.196
Ca	0.952	0.023	0.037	0.039
Mg	0.940	0.054	-0.104	0.013
As	0.051	0.242	0.719	-0.059
Fe	0.508	0.305	0.533	-0.073
Zn	0.087	0.173	0.337	0.657
Mn	0.481	0.029	0.422	-0.103
Ba	0.409	0.702	-0.395	0.053
Li	-0.218	0.695	-0.414	0.035
Sr	0.854	0.234	-0.135	-0.025
Si	0.172	0.506	-0.597	0.213
Al	-0.245	0.043	0.140	0.679
λ	4.142	3.055	2.180	1.031
λ%	38.2	28.2	20.1	9.5

Al and Zn show the highest value in the fourth factor. Al may go into solution by weathering of silicates. Solubility of Al species depends on pH. Aluminium is insoluble at neutral pH, that it precipitates from the solution as gibbsite or other minerals. This factor, which influences the Al and Zn content of ground water in the similar way, was considered as a process of formation secondary minerals. Zn concentration of waters is influenced by adsorption on the surface of Al oxides. The pH of the system effects both the solubility of aluminium oxides and the adsorption on its surface. Factors influencing the pH also modify the concentration of Al and Zn in groundwater (COSTON et al., 1995).

CONCLUSIONS

1. The whole study area can be divided into three main parts on the basis of major components dissolved in water. The separation based on the distribution of minor and trace elements resulted in very similar location of groups. This separation corresponds to geological units established earlier: the River Körös Basin, the River Maros alluvial fan, and the River Danube deposits. Water quality is different in the three areas.

2. In the River Körös basin where the potentiometric surface does not indicate infiltration or lateral water flow, the chromatographic pattern of ion exchange cannot be pointed out. Groundwater chemistry suggests restricted water movements.

3. In the River Maros alluvial fan the changes in the concentration of Ca, Mg and Na correspond to a chromatographic pattern, indicating a SSE-NNW water flow direction.

4. In the River Danube deposits, water chemistry supports that the groundwater flow direction, in accordance with the potentiometric surface, is from west to east. Both recharge and discharge areas were identified. Recharge area is characterized by Ca-Mg bicarbonate water type, discharge area by Na bicarbonate water type. Between these two

types of groundwater there is a transitional water type, where the changes in the concentrations of chemical components are the highest.

6. Four geochemical processes were identified by principal component analysis which influence minor and trace element content in groundwater of the study area. The four processes are as follows: calcite and dolomite dissolution together with cation exchange, weathering of aluminosilicate minerals, reduction-oxidation processes, and formation of secondary minerals. Sr is primary controlled by calcite and dolomite dissolution and ion exchange on clay minerals. Ba and Li content is determined by aluminosilicate weathering. Distribution of As and Fe is influenced by oxidation and reduction, while the concentrations of Al and Zn are the result of the formation of secondary minerals.

ACKNOWLEDGEMENTS

This work has been supported by the Scientific Research Fund (Hungary), grant No. is T 026241.

REFERENCES

ALTHAUS E. and TIRTADINATA E. (1989) Dissolution of feldspar: The first step. In Water-Rock Interaction (ed. MILES D. L.), pp. 15-17. Balkema, Rotterdam.

APPELO C. A. J., PONTEN J. and BEEKMAN H. E. (1989) Natural ion-chromatography during fresh-/sea water displacements in aquifers: A hydrogeochemical model of the past. In Water-Rock Interaction (ed. MILES D. L.), pp. 23-28. Balkema, Rotterdam.

APPELO C. A. and POSTMAN D. (1993) Geochemistry, Groundwater and Pollution. A. A. Balkema.

BALISTRIERI L. S., MURRAY J. W., PAUL B. (1994) The geochemical cycling of trace elements in a biogenic meromictic lake. Gechim. Cosmoshim. Acta, Vol. 58, pp. 3993 - 4008.

BERNER R. A. (1981) Kinetics of weathering and diagenesis. Reviews in Mineralogy Vol. 8, Kinetics of geochemical processes (eds LASAGA A. C. and KIRKPATRICK R. I.), Chap. 3, pp. 111-135.

BILLINGS G. K., HITCHON B., SHOW D. R. (1964) Geochemistry and origin of formation waters in the western Canada sedimentary basin: Alkali metals. Part 2. In: The geochemistry of subsurface brines . Chem. Geol.Vol. 4, pp. 211-223.

BRONS H. J., GRIFFIOEN J., APPELO A. J. AND ZEHNDER A. J. B. (1991) (Bio)chemical reactions in aquifer material from a thermal energy storage site. Wat. Res. Vol. 25, pp. 729-736.

BUSENBERG E. and CLEMENCY CH. V. (1976) The dissolution kinetics of feldspars at 25 C° and 1 atm CO_2 partial pressure. Geochim. Cosmochim. Acta, Vol. 40, pp. 41-49.

CHASEY W.H. and BUNKER B. (1990) Leaching of mineral and glass surfaces during dissolution. Reviewes in Mineralogy. Vol.23. Eds. M.F. Hochella, A.F. White. Chapter 19. pp. 397-427.

CHAPELLE F. H. and KNOBEL L. L. (1983) Aqueous Geochemistry and the Exchangeable Cation Composition of Glauconit in the Aquia Aquifer, Mariland. Groundwater, Vol. 21, pp. 343-352.

CHOU L. and WOLLAST R. (1984) Study of the weathering of albite at room temperature and pressure with a fluidized bed reactor. Geochim. Cosmochim. Acta, Vol. 48, pp. 2205-2217.

COMANS R. N. J. and MIDDELBURG J. J. (1987) Sorption of trace metals on calcite: Applicability of the surface precipitation model. Geochim. Cosmochim. Acta, Vol. 51, pp. 2587 - 2591.

DAVIS J. A. and LECKIE J. O. (1978) Surface ionization and complexation at the oxide water interface. Surface properties of amorphous iron oxyhydroxide and adsorption of metal ions. J. Colloid interface Sci.Vol. 67, pp. 90 - 107.

DAVIS J. A., FULLER C. C. and COOK A. D. (1987) A model for trace metal sorption processes at the calcite surface: Adsorption of Cd^{2+} and subsequent solid solution formation. Geochim. Cosmochim. Acta, Vol. 51, pp. 1477 - 1490.

DAVIS J. A. and KENT D. B. (1990) Surface complexation modeling in aqueous geochemistry. Reviews in Mineralogy Vol. 23, Mineral-water interface geochemistry (eds HOCHELLA M. F. JR. and WHITE A. F.), Chap. 5, pp. 177-260.

ERDÉLYI M. (1976) Outlines of the hydrodinamics and hydrochemistry of the Pannonian Basin. Geologica Hungarica. Tom 20. pp. 287 - 309.

ERDÉLYI M. (1976) Hydrodinamics of the Hungarian Basin. In Hydrogeology of Great Sedimentary Basins, Conference, IAHS Publication No. 120, pp. 146-163.

ERDÉLYI M. (1979) Hydrodynamics of the Hungarian Basin (VITUKI), Proc. No.18, Budapest.

FAURE G., CROCKET J. H. and HURLEY M. P. (1967) Some aspects of the geochemistry of strontium and calcium in the Hudson Bay and the Great lakes. Geochim. Cosmochim. Acta, Vol. 31, pp. 451-460.

FROELICH P.N., KLINKHAMMER G.P., BENDER M.L., LUEDTKE N.A., HEATH G.R., HAMMOND D., HARIMAN B. and MAYNARD V. (1979) Early oxidation of organic matter in pelagic sediments of the eastern equatorial Atlantic: suboxic diagenesis. Geochim. Cosmochim. Acta, Vol. 43, pp. 1075-1090.

HEIER K. S. and ADAMS J. A. S. (1964) The geochemistry of the alkali metals. Phys. Chem. Earth 5. pp. 255-380.

HELGESON H. C. (1971) Kinetics of mass transfer among silicates and aqueous solutions. Geochim. Cosmochim. Acta, Vol. 35, pp. 421-469.

HELGESON H. C., MURPHY W. M. and AAGAARD P. (1984) Thermodynamic and kinetic constraints on the reaction rates among minerals and aqeous solutions. II. Rate constants, effective surface area and the hydrolysis of feldspar. Geochim. Cosmochim. Acta Vol. 48, pp. 2405-2432.

HELLMANN R., EGGLESTON C. M., HOCHELLA M. F. JR. and CRERAR D. A. (1989) Altered layers on dissolving albite - 1. Results. In Water-Rock Interaction (ed. MILES D. L.), pp. 293-296. Balkema, Rotterdam.

HEM J. D. (1985) Study and Interpretation of the Chemical Characteristics of Natural Water. U. S. Geological Survey Water-Supply Paper 2254.

HOCHELLA M. F. JR. (1990) Atomic structure, microtopography, composition, and reactivity of mineral surfaces. Reviews in Mineralogy Vol. 23, Mineral-water interface geochemistry (eds HOCHELLA M. F. JR. and WHITE A. F.), Chap. 3, pp. 87-133.

LAXEN D. P. H. (1985) Trace metal adsorption /coprecipitation of hydrous ferric oxide under realistic conditions. Wat. Res. Vol. 19, pp. 1229 - 1236.

LION L. W., ALTMANN R. S. and LECKIE J. O. (1972) Trace - metal adsorption characteristics of estaurine particulate matter: evaluation of contribution of Fe/Mn oxide and organic surface coatings. Environ. Sci. Technol. Vol. 16, pp. 660-666.

LE MAITRE R. W. (1982) Numerical petrology. Developments in Petrology 8. Elsevier.

MURPHY W. M. and HELGESON H. C. (1987) Thermodynamic and kinetic constraints on the reaction rates among minerals and aqeous solutions. III. Activated complexes and the pH-dependence of the rates of feldspar, pyroxene, wollastonite, and olivine hydrolysis. Geochim. Cosmochim. Acta, Vol. 51, pp. 3137-3153.

NEWMAN M.C., ALBERTS J.J. and GREENHUT V.A. (1985) Geochemical factors complicating the use of Aufwuchs to monitor bioaccumulation of arsenic, cadmium, chromium, copper and zink. Water Res. Vol. 19, pp. 1157-1165.

OKUMURA M. and KITANO Y. (1985) Coprecipitation of alkali metal ions with calcium carbonate. Geochim. Cosmochim. Acta, Vol. 50, pp. 49 - 58.

PACES T. (1973) Steady-state kinetics and equilibrium between groundwater and granitic rock. Geochim. Cosmochim. Acta, Vol. 37, pp. 2641-2663.

PARKHURST D. L., THORSTENSON D. C. and PLUMMER L. N. (1990) PHREEQE - A computer program for geochemical calculation. U. S. Geol. Surv. Water-Resources Investigations, 80-96.

SAKATA M. (1985) Diagenetic remobilization of manganese, iron, copper and lead in anoxic sediment of a freshwater pond. Water Res. Vol. 19, pp. 1033-1038.

STUMM W. and MORGAN J. J. (1981) Aquatic Chemistry, 2nd Ed. John Wiley and Sons.

RÓNAI A. (1985) The Quaternary of the Great Hungarian Plain. Geol. Hung. Tom. 21, Inst. Geol. Hung. Budapest.

TAKAMATSU T., KAWASHIMA M. and KOYAMA M. (1985) The role of Mn^{2+} -rich hydrous manganese oxide in the accumulation of arsenic in lake sediments. Water Res. Vol. 19, pp. 1029-1032.

TESSIER A., CAMPBELL P. G. C. and BISSON M. (1980) Trace metal speciation in the Yamaska and St Francois rivers (Québec). Can. J. Earth. Sci. Vol.17, pp. 90 - 105.

VARSÁNYI, I. and Ó.KOVÁCS, L. (1994) Combination of statistical methods with modelling mineral-water interaction: a study of groundwater in the Great Hungarian Plain. Applied Geochemistry,Vol. 9, pp. 419-430.

VARSÁNYI, I. and Ó.KOVÁCS, L. (1997) Chemical evolution of groundwater in the River Danube deposits in the southern part of the Pannonian Basin (Hungary). Applied Geochemistry, Vol. 12, pp. 625-637.

WERSIN P., CHARLET L., KARTHEIN R. and STUMM W. (1989) From adsorption to precipitation: Sorption of Mn^{2+} on $FeCO_3$ (s) . Geochim. Cosmochim. Acta, Vol. 53, pp. 2787 - 2796.

WEDEPOHL K.H. (1968) Chemical Fractionation in the sedimentary enviroment. In: AHRENS L. H., (ed) Origin and distribution of the elements. Oxford: Pergamon Press.

WILSON, T.R.S., THOMPSON J., COLLEY S., HYDES D.J., HIGGS N.C. and SORENSEN J. (1985) Early organic diagenesis: The significance of progressive subsurface oxidation fronts in pelagic sediments. Geochim. Cosmochim. Acta, Vol. 49, pp. 811-821.

ZACHARA J. M., COWAN C. E. and RESCH C. T. (1991) Sorption of divalent metals on calcite. Geochim Cosmochim. Acta, Vol. 55, pp. 1549 - 1662.

Manuscript received 4 April, 1998.

[illegible] (1976) Outlines of the hydrodynamics and hydrochemistry of the Pannonian Basin. Geologica Hungarica [illegible] pp. [illegible].

ERDÉLYI M. (1976) Hydrodinamics of the Hungarian Basin. In: Hydrogeology of Great Sedimentary Basins. Conference, [illegible] pp. [illegible].

ERDÉLYI M. (1979) Hydrodynamics of the Hungarian Basin (VITUKI, Proc. No. 18) Budapest.

FAURE G., CROCKET J. H. and HURLEY M. P. (1967) Some aspects of the geochemistry of strontium and calcium in the Hudson Bay and the Great lakes. Geochim. Cosmochim. Acta, Vol. [illegible]

FROELICH P. N., KLINKHAMMER G. P., BENDER M. L., LUEDTKE N. A., HEATH G. R., HAMMOND D., HARTMAN B. and MAYNARD V. (1979) Early oxidation of organic matter in pelagic sediments of the eastern equatorial Atlantic: suboxic diagenesis. Geochim. Cosmochim. Acta, Vol. 43, pp. 1075-1090.

HEIER K. S. and ADAMS J. A. S. (1964) The geochemistry of the alkali metals. Phys. Chem. Earth 5, pp. 255-380.

HELGESON H. C. (1971) Kinetics of mass transfer among silicates and aqueous solutions. Geochim. Cosmochim. Acta, Vol. 35, pp. 421-469.

HELGESON H. C., MURPHY W. M. and AAGAARD P. (1984) Thermodynamic and kinetic constraints on the reaction rates among minerals and aqeous solutions. II. Rate constants, effective surface area and the hydrolysis of feldspar. Geochim. Cosmochim. Acta Vol. 48, pp. 2405-2432.

HELLMANN R., EGGLESTON C. M., HOCHELLA M. F. JR. and CRERAR D. A. (1989) Altered layers on dissolving albite - I. Results. In Water-Rock Interaction (ed. MILES D. L.), pp. 293-296. Balkema, Rotterdam.

HEM J. D. (1985) Study and Interpretation of the Chemical Characteristics of Natural Water. U. S. Geological Survey Water-Supply Paper 2254.

HOCHELLA M. F. JR. (1990) Atomic structure, microtopography, composition, and reactivity of mineral surfaces. Reviews in Mineralogy Vol. 23, Mineral-water interface geochemistry (eds HOCHELLA M. F. JR. and WHITE A. F.), Chap. 3, pp. 87-133.

LAXEN D. P. H. (1985) Trace metal adsorption /coprecipitation of hydrous ferric oxide under realistic conditions. Wat. Res. Vol. 19, pp. [illegible].

LION L. W., ALTMANN R. S. and [illegible] (1972) Trace - metal adsorption characteristics of estaurine particulate matter: evaluation of contribution of Fe/Mn oxide and organic surface coatings. Environ. Sci. Technol. Vol. 16, pp. [illegible].

LE MAITRE R. W. (1982) Numerical petrology. Developments in Petrology 8. Elsevier.

MURPHY W. M. and HELGESON H. C. (1987) Thermodynamic and kinetic constraints on the reaction rates among minerals and aqeous solutions. III. Activated complexes and the pH-dependence of the rates of feldspar, pyroxene, wollastonite, and olivine hydrolysis. Geochim. Cosmochim. Acta. Vol. 51, pp. 3137-3153.

NEWMAN M.C., ALBERTS J.J. and GREENHUT V.A. (1985) Geochemical factors complicating the use of Aufwuchs to monitor bioaccumulation of arsenic, cadmium, chromium, copper and zink. Water Res. Vol. 19, pp. 1157-1165.

OHUMURA M. and KITANO Y. (1985) Coprecipitation of alkali metal ions with calcium carbonate. Geochim. Cosmochim. Acta, Vol. 50, pp. 49 - 58.

PAČES T. (1973) Steady-state kinetics and equilibrium between groundwater and granitic rock. Geochim. Cosmochim. Acta, Vol. 37, pp. 2641-2663.

PARKHURST D. L., THORSTENSON D. C. and PLUMMER L. N. (1990) PHREEQE - A computer program for geochemical calculation. U. S. Geol. Surv. Water-Resources Investigations, 80-96.

SAKATA M. (1985) Diagenetic remobilization of manganese, iron, copper and lead in anoxic sediment of a freshwater pond. Water Res. Vol. 19, pp. 1033-1038.

STUMM W. and MORGAN J. J. (1981) Aquatic Chemistry, 2nd Ed. John Wiley and Sons.

RÓNAI A. (1985) The Quaternary of the Great Hungarian Plain. Geol. Hung. Tom. 21. Inst. Geol. Hung. Budapest.

TAKAMATSU T., KAWASHIMA M. and KOYAMA M. (1985) The role of Mn^{2+} -rich hydrous manganese oxide in the accumulation of arsenic in lake sediments. Water Res. Vol. 19, pp. 1029-1032.

TESSIER A., CAMPBELL P. G. C. and BISSON M. (1980) Trace metal speciation in the Yamaska and St Francois rivers (Quebec). Can. J. Earth. Sci. Vol. 17, pp. 90 - 105.

VARSÁNYI, I. and Ó.KOVÁCS, L. (1994) Combination of statistical methods with modelling mineral-water interaction: a study of groundwater in the Great Hungarian Plain. Applied Geochemistry, Vol. 9, pp. 419-430.

[illegible] I. and Ó.KOVÁCS, L. (1997) Chemical evolution of groundwater in the River Danube deposits in the [illegible] part of the Pannonian Basin (Hungary). Applied Geochemistry, Vol. 12, pp. 625-637.

[illegible] L., ERNSTAMP R. and STUMM W. (1989) From adsorption to precipitation: Sorption of [illegible] Geochim. Cosmochim. Acta, Vol. 53, pp. 2787 - 2796.

[illegible] Geochemical Fractionation in the sedimentary environment. In: AHRENS L. H., (ed.) Origin [illegible] of the elements. Oxford. Pergamon Press.

Illustrations

Figures should be used only where they are essential to elucidate text.

The illustrations should be numbered according to their sequence in the text, and in the text references should be made to each figure.

All illustrations should be given separately, not stuck on sheets and not folded. The number of the figure and the authors name should be noted on the reverse side of the photographs and on the lower frontside of drawings, indicating at the same time the top of the figure where it necessary.

Captions for all figures should be given typewritten on a separate list at the end of the manuscript. Drawn text in the figures should be kept to a minimum.

Drawings should be made on tracing paper by Indian ink. The thickness of the lines and the size of the lettering should enough to allow a necessary reduction.

Photographs of good contract and intensity on glossy paper are only acceptable. Colour photographs or drawings cannot be accepted.

Use bar scale on all illustrations instead of numerical scales that must be changed if reductions are necessary.

References

All references to publications made in the text should be made by quoting the author's name (without initials) and year of publications in paranthesis.

The list of references at the end of the manuscript should be arranged alphabetically by author's names and chronologically per author.

If the referred publications are written by more than two authors, in the text only the name of the first author should be indicated, the other co-authors are denoted by "et al.", however, in the list of references the names of authors and all co-authors should be mentioned.

In the list of references all references should be written, e. g. Balogh, K., A. Barabás (1972): The Carboniferous and Permian of Hungary. Acta Miner. Petr. Szeged, XX/2, 191–207.

At references to books beside the author's name, year of publicaton, title and the publishing house should also be mentioned.

In the case of references for symposium volumes, special issues or multi-authors books, the following system should be used: Roser, B. P., C. W. Childs, and G. P. Glasby (1980): Manganese in New Zealand. In: I. M. Varentsov and Gy. Grassely (Editors): Geology and Geochemistry of Manganese, Vol. II. Akadémiai Kiadó, Budapest, 199–211.

Manuscripts that are not adequately prepared will be returned to the authors(s).